THE UNIVERSITY OF QUEENSLAND

AUSTRALIA

Functional network study on the wild type and *DISC1* transgenic mice

Tong Wu
Bachelor's Degree of Electronic Engineering, Master's Degree of Communication and Information System

A thesis submitted for the degree of Doctor of Philosophy at The University of Queensland in 2017

Queensland Brain Institute

Abstract

Major mental disorders such as schizophrenia (SZ), bipolar disorder and major depression create a heavy social burden and remain poorly treated. Recent reports examining the genetic and molecular structure of brain disorders discovered the gene *Disrupted-in-Schizophrenia 1 (DISC1)* to be significantly associated with these disorders and plays a substantial role in influencing a range of shared endophenotypes underlying these disorders. This has led to a powerful gateway to explore the underlying pathology and to achieve better diagnosis and treatments of major mental diseases. Characterising the phenotypes of *DISC1* in brain functions would provide valuable insights into the mechanism of how this gene influences the brain.

Resting-state fMRI (rs-fMRI) is a powerful technique being applied to more than 30 different kinds of brain disorders and different species. Findings from rs-fMRI studies on humans provide ample evidence of abnormal functional patterns in patients with mental illnesses. Specifically, altered functional connectivity (FC) and network topologies are proposed to be plausible imaging endophenotypes of psychotic disorders. However, little is known about the direct effects of gene dysfunction, such as *DISC1* mutations, on resting-state brain activations. One aim of this thesis is to investigate the impacts of *DISC1* on variations of resting-state functional networks (RSNs) in anaesthetized mouse brains using *DISC1* transgenic mice and rs-fMRI.

Before characterizing disease phenotypes in mouse models, it is necessary to understand how the mouse brain functions in normal states. Anaesthesia is currently an integrated part of most mouse rs-fMRI experiment. However, it influences blood-oxygenation-level-dependent (BOLD) fMRI signals via modulation of neurovascular coupling and brain metabolism, and therefore alters FC and topologies of RSNs. Investigating FC and its changes associated with genes therefore initially requires an understanding of the anaesthetics. Furthermore, various anaesthetic protocols are adopted by different labs leading to difficulties in result comparisons.

The brain is a complex and hierarchical system, whereby its RSN architecture can be characterised from mutiple perspectives at regional or global levels. Previous mouse rs-fMRI studies have focused on long-distance FC, however, given the non-uniform influence of anaesthesia on the brain, mapping functional activations across scales in mice under different anaesthetics remain sparsely explored. Establishing this relationahsip would provide a reliable reference to study mouse brain functions in abnormal states and facilitate comparisons across laboratories.

In the first aim of this thesis, I investigated the local connectivity in wide type (WT) mice under six commonly used anaesthetic regimens. I identified that the regional connectivity altered across the brain as a function of the expression density of receptors relative to specific agents. In addition, the depth of anaesthesia influences local synchronization.

In the second aim, I investigated how large-scale network topologies changed under different regimens. Small-worldness was observed to be different between medetomidine and a combination of medetomidine and isoflurane, which was driven by altered clustering coefficients. This indicated that local alterations played important roles on global topologies. Similar functional modules were observed under most regimens, but the anaesthetic dosage influenced module structures significantly.

In the third aim, I investigated the potential link between RSNs and the *DISC1* gene. Isoflurane was chosen based on results from the previous aims and experimental conditions available. Eleven *DISC1* transgenic mice (Tg) and ten WT littermate controls (Wt) were first sent to Y maze and fear conditioning behaviour tests before the acquisition of rs-fMRI data from all mice. Independent component analysis (ICA), regional connectivity and complex network analysis were performed to detect the link between FC and the *DISC1* gene across analytical scales. No significant differences were revealed by behaviour assays, ICA, regional analysis or global graph parameters. However, functional modules were different between the two groups. Specifically, the amygdala, a region closely related to the fear conditioning, was assigned to a different module in Tg mice compared to Wt mice. Furthermore, some discrepancies in modular structures in Wt mice in this aim and WT mice under isoflurane in the second aim were observed. This implies that there might be other factors influencing community identification using mouse rs-fMRI, for example, factors relating to experimental pipeline used.

The results from the first two aims are the first to establish regional connectivity and large-scale network topology in mice across different anaesthetics. Methods used in these aims are widely applied in human studies, therefore, the results presented here will serve as preliminary references for comparisons across labs and help translate observations from mice to humans. Results from the third aim are the first to investigate FC alterations associated with the *DISC1* gene across scales using mouse rs-fMRI. The abnormal functional modules in *DISC1* mice provide insights into how this gene may influence brain functions in amygdala-related emotional processing. Finally, differences in modular organizations of WT mice between the second and the third aims suggest that experimental pipelines and other factors may influence module identification.

Declaration by author

This thesis is composed of my original work, and contains no material previously published or written by another person except where due reference has been made in the text. I have clearly stated the contribution by others to jointly-authored works that I have included in my thesis.

I have clearly stated the contribution of others to my thesis as a whole, including statistical assistance, survey design, data analysis, significant technical procedures, professional editorial advice, and any other original research work used or reported in my thesis. The content of my thesis is the result of work I have carried out since the commencement of my research higher degree candidature and does not include a substantial part of work that has been submitted to qualify for the award of any other degree or diploma in any university or other tertiary institution. I have clearly stated which parts of my thesis, if any, have been submitted to qualify for another award.

I acknowledge that an electronic copy of my thesis must be lodged with the University Library and, subject to the policy and procedures of The University of Queensland, the thesis be made available for research and study in accordance with the Copyright Act 1968 unless a period of embargo has been approved by the Dean of the Graduate School.

I acknowledge that copyright of all material contained in my thesis resides with the copyright holder(s) of that material. Where appropriate I have obtained copyright permission from the copyright holder to reproduce material in this thesis.

Publications during candidature

Conference abstracts

1. **Tong Wu**, Joanes Grandjean, Simone C. Bosshard, Markus Rudin, David Reutens, and Tianzi Jiang, “Global-scale network analysis on the effects of different anaesthesia agents using mice rs-fMRI”, OHBM 2016, Geneva, Switzerland (Abstract accepted).

2. **Tong Wu**, Joanes Grandjean, Simone C. Bosshard, Markus Rudin, David Reutens, and Tianzi Jiang, “Multi-scale analysis on different anaesthesia protocol effects in mice using resting-state fMRI”, ISMRM 2015, Toronto, Canada. Poster presentation.

Publications included in this thesis

Wu T, Grandjean J, Bosshard SC, Rudin M, Reutens D, Jiang T (2017) Altered regional connectivity reflecting effects of different anaesthesia protocols in the mouse brain. Neuroimage 149:190-199 - incorporated as Chapter 3.

Contributor	Statement of contribution
Tong Wu (Candidate)	Planned the paper (40%); Analysed the data (70%); Wrote and edited the paper (55%).
Joanes Grandjean	Provided the data (100%); Planned the paper (40%); Analysed the data (30%); Wrote and edited paper (26%).
Simone Bosshard	Planned the paper (5%); Wrote and edited the paper (8%).
Markus Rudin	Provided the data (100%). Wrote and edited the paper (1%).
David Reutens	Planned the paper (5%); Wrote and edited the paper (5%).
Tianzi Jiang	Planned the paper (10%); Wrote and edited the paper (5%).

Contributions by others to the thesis

Chapter 1: No contributions by others.

Chapter 2: No contributions by others.

Chapter 3: Prof. Tianzi Jiang supervised the research. Dr. Joanes Grandjean performed the pre-processing, assisted the writing of the manuscript and made some of the figures. Prof. David Reutens and Dr. Simone Bosshard assisted the research plan and writing. Prof. Markus Rudin and Dr. Joanes Grandjean provided the data.

Chapter 4: Prof. Tianzi Jiang supervised the research. Prof. David Reutens and Dr. Simone Bosshard assisted the research design. Prof. Markus Rudin and Dr. Joanes Grandjean provided the data.

Chapter 5: Prof. Tianzi Jiang designed the research protocols and supervised the research. Dr. Cirong Liu designed and performed the behavioural experiment. Dr. Nyoman Kurniawan assisted in fMRI data acquisition. Prof. David Reutens and Dr. Simone Bosshard assisted the fMRI experiment design.

Chapter 6: No contributions by others.

Statement of parts of the thesis submitted to qualify for the award of another degree

None.

Acknowledgements

I would like to first thank my advisors. My principle supervisor, Prof. Tianzi Jiang, for giving me this opportunity to perform this challenging and exciting research, and study at UQ. I thank his guidance and principles, for helping me shape and polish my ideas better on the projects. I would like to thank Prof. David Reutens. I appreciate his guidance on the direction of the projects and insightful advice. I want to thank Dr. Simone Bosshard, for her down-to-earth advices on experiment design, project directions and objectivity. They provided me inspiring guidance during my PhD. I'd like to thank them for accepting me as their student.

To the chair of my milestone committee panel, Prof. Linda Richards, I'd like to thank you for your support and help during my PhD. I also want to thank you for your timely reminders during my progress throughout the PhD. For all the other milestone committee members: Dr. Marcus Gray, thank you for your professional comments on my projects and encouragement; Prof. Feng Liu, thank you for your support in my milestone; Prof. Hana Burianova, your helpful advice and support; Dr. Steven Yang and Dr. Zuyao Shan, for your support during my first year. I appreciate sincerely the valuable time, attention and constructive feedbacks you provided to me on my projects.

I want to thank Prof. Markus Rudin for your kindness and agreement on the collaboration. Dr. Joanes Grandjean, thank you for your patience, being a supportive collaborator and the friendly scientific communications. I appreciate that you shared your expertise to help me improve my projects. Dr. Nyoman Kurniawan, thank you for your patient help on the fMRI experiment.

I would like to thank my labmates, Dr. Cirong Liu, Dr. Xianfeng Yang, Dr. Yonghui Li and Xiaoqing Zhou. For all friends and nice colleagues I met here who have been so kind to me during my PhD, I want to say thank you all for your friendship, help, support and smiles. Those merry moments are valuable to me.

I would also like to express my gratitude to The University of Electronic Science and Technology of China, China Scholarship Council and Queensland Brain Institute, for providing the opportunity and financial support to study in Australia.

To my father, thank you for encouraging me keep pursuing further study abroad. And my mom, for your unending understanding and support.

Keywords

Resting-state fMRI, mouse, anaesthesia, *DISC1*, functional brain network

Australian and New Zealand Standard Research Classifications (ANZSRC)

ANZSRC code: 090399 Biomedical Engineering not elsewhere classified, 40%
ANZSRC code: 110999 Neurosciences not elsewhere classified, 60%

Fields of Research (FoR) Classification

Allows for categorisation of the thesis according to the field of research.

FOR code: 0903 Biomedical Engineering, 40%
FOR code: 1109 Neurosciences, 60%

Table of Contents

List of figures

List of tables

List of Abbreviations used in the thesis

AMBMCA	Australian Mouse Brain Mapping Consortium
AuD	Auditory cortex
BOLD	Blood-oxygenation-level-dependent
Cg	Cingulate cortex
CryoProbe	Cryogenic radiofrequency probe
CSF	Cerebrospinal fluid signal
DISC1	*Disrupted-in-Schizophrenia 1*
DMN	Default mode network
EPI	Echo-planar imaging
FC	Functional connectivity
FDR	False Discovery Rate
FWE	Family-wise error rate
fMRI	Functional magnetic resonance imaging
FOV	Field of view
GABA(A)	γ-aminobutyric acid type A
GE-EPI	Gradient-echo echo-planar imaging
GSR	Global mean signal regression
Hipp	Hippocampus
HypoTh	Hypothalamus
IC	Independent component
ICA	Independent component analysis
LCN	Lateral cortical network
LFF	Low frequency fluctuations
Limbic	Limbic area
M1/M2	Primary and secondary motor cortex
MV	Motion and ventricle signal regressed
MVG	Motion, ventricle and global signal regressed
NA	Number of averages
pCO_2	Carbon dioxide
pO_2	Blood gas partial pressure of oxygen

ReHo	Regional homogeneity
TR	Repetition time
Tg	*DISC1* transgenic mice
ROI	Region-of-interest
RSD	Retrosplenial dysgranular cortex
rs-fMRI	Resting-state fMRI
RSN	Resting-state network
S1/S2	Primary and secondary somatosensory
SBA	Seed-based analysis
SN	Salience network
SNR	Signal-to-noise ratio
SZ	Schizophrenia
TFCE	Threshold-free cluster enhancement correction
Th	Thalamus
tSNR	Temporal SNR
V1/V2	Primary and secondary visual cortex
WM	White matter signal
WT	Wild type
Wt	Wild type littermate control of *DISC1* transgenic mice
αCaMKII-DN-DISC1	Dominant-negative *DISC1* under control of the αCaMKII promoter

Chapter 1 Introduction

Overview

Functional magnetic resonance imaging (fMRI) is a quickly growing field that provides rich information on how the brain functions. Resting-state fMRI (rs-fMRI) is one core fMRI technique mapping the brain activity in the absence of tasks. Given the simple data acquisition, non-invasiveness and insightful signals from spontaneous neural activity, rs-fMRI is gaining popularity and is applied to different human diseases and age populations as well as animal species (Biswal, 2012; Shen, 2015). The brain is a complex network where anatomically distinct brain regions with specialized functions cooperate with each other to support various cognitive processes (Park and Friston, 2013). Therefore, understanding the brain from a network perspective is of high importance. Functional brain networks encompassing regions that are functionally correlated are usually measured by functional connectivity (FC) (Sporns, 2013). Particularly, FC analysis on rs-fMRI data has revealed a large amount of information and knowledge on spontaneous brain functions in humans, such as several intrinsic resting-state networks (RSNs) and evidence for abnormal network structures of patients suffering from psychiatric brain disorders (van den Heuvel and Pol, 2010). However, the evidence from human studies alone is not enough for researchers to further investigate and understand the underlying mechanisms of these brain disorders.

It is well established that the risk of mental illness is due to heredity. Some genes may play critical roles in the transmission of risk (Hyman, 2000). One direction of searching for the mechanisms of mental illness is therefore led by understanding the dysfunction of suspicious genes. Given the wide use of transgenic mouse models of human brain diseases and the availability of small animal scanners, characterizing brain functions of these models using rs-fMRI opens a new and promising avenue to investigate how gene dysfunctions influence functional networks.

As a relatively new research field, FC patterns mapped by mouse rs-fMRI remains largely unexplored. The gap of FC characteristics in both normal wild type mice and disease models is yet to be filled. One major feature of mouse rs-fMRI is the use of anaesthesia. While anaesthesia facilitates animal preparations and scanning procedures, it impacts on blood-oxygenation-level-dependent (BOLD) fMRI signals via modulation of neurovascular coupling and brain metabolism (Pan et al., 2015). Hence, anaesthesia influences FC patterns and network topologies (Peltier et al., 2005; Boveroux et al., 2010). Investigating FC changes associated with genes initially requires an understanding of how anaesthetic agents affect mouse RSNs.

The existence of some RSNs and characteristics of some network topologies of healthy mouse brains have been investigated. Although there are similarities, many discordant results are observed between studies. One reason for this may be that different labs adopted different anaesthetic regimens (Jonckers et al., 2011; Grandjean et al., 2014b; Jonckers et al., 2014; Mechling et al., 2014; Sforazzini et al., 2014; Liska et al., 2015; Zerbi et al., 2015). For example, comparative studies on rodents reported agent-specific characteristics of long-distance FC patterns (Williams et al., 2010; Grandjean et al., 2014b; Jonckers et al., 2014). However, characteristics of local connectivity and network topologies in mice across commonly used anaesthetics remain unknown. One aim of this thesis is to investigate how different and commonly used anaesthetic regimens influence the regional connectivity and network topologies in mice using rs-fMRI. The two analytical methods were chosen for their wide application in human fMRI studies, hence can provide preliminary references to bridge studies on mouse disease models and human brain disorders.

Major mental illnesses, such as schizophrenia (SZ), bipolar disorder, major depression and autism remain poorly understood and treated causing heavy burdens to society and patients' families (Brandon and Sawa, 2011). A gene named *Disrupted-in-Schizophrenia 1 (DISC1)* is a well-known candidate gene for involvement in these psychiatric illnesses leading to the generation of several *DISC1* mouse models (Ishizuka et al., 2006; Hikida et al., 2007; Soares et al., 2011; Niwa et al., 2013a). Another aim of this thesis is to investigate how *DISC1* modulates FC and network topologies in one mouse model using rs-fMRI (Hikida et al., 2007). Based on the first aim of understanding the effects of different anaesthetics on the mouse brain and the available experimental conditions, isoflurane was used for the study of this transgenic mouse model. Characterizing FC changes associated with dysfunctions of the *DISC1* gene may shed light on the link between this gene and potential FC endophenotypes using rs-fMRI, and hence may help translate findings from mouse disease models to ongoing human studies of major mental illnesses.

The following chapter will review some basics of fMRI and rs-fMRI signals, with a brief review of the analysis of functional brain networks and their applications to mental illness. The mouse rs-fMRI data acquisition is very challenging. Because there were no mouse rs-fMRI protocols established and used at the University of Queensland, an important part of this PhD candidature was to set up and optimize an experimental pipeline including animal preparation and MRI parameters for data acquisition on *DISC1* transgenic mice. Rs-fMRI data acquisition will be reviewed and discussed. In particular, application of general anaesthesia on mouse rs-fMRI and recent advances in mouse RSNs will be discussed.

Finally, current knowledge regarding the *DISC1* mouse model used in this thesis will be reviewed.

1.1 Functional magnetic resonance imaging (fMRI)

1.1.1 Blood-Oxygen-Level-Dependent (BOLD) functional MRI

FMRI is 25 years old and still growing fast as a successful and popular imaging tool for investigating brain function (Bandettini, 2012). It indirectly measures neural activity by measuring the blood oxygenation level, i.e. one of the metabolic correlates of neural activity whose changes in the vascular system of the brain respond to the metabolic demands of active neurons. Traditionally, it was presumed that hemodynamics were triggered by activated neurons because of energy consumption and oxidative metabolism. A more recent theory proposes that increased cerebral blood flow to an activated region is mainly driven by neurovascular signaling for functional hyperaemia instead of energy demand. Although hypotheses for the underlying physiology of how neuronal activity controls the supply of glucose and O_2 via vascular system have shifted, the coupling between neuronal activity and brain blood flow is a well-known phenomenon forming the basis of fMRI imaging (Attwell et al., 2010; Fox, 2012).

This basis relies on two facts. The first is the different magnetic properties of hemoglobin with and without attached oxygen discovered by (Pauling and Coryell, 1936). They reported that oxygenated hemoglobin is diamagnetic and has little effect on the nearby magnetic field, whereas deoxygenated hemoglobin is paramagnetic and distorts the surrounding magnetic field by making it less uniform. The second can be measured using the T_2^* contrast method. T_2^* describes the time constant of tissues measuring the decay of transverse magnetization caused by a combined effects of spin-spin relaxation and local magnetic field inhomogeneity. Because paramagnetic substances, such as deoxyhemoglobin, distort the nearby magnetic field causing more rapid decay of transverse magnetization, i.e. shorter T_2^*, MR images based on T_2^* contrast provide information on the concentration of deoxyhemoglobin present in a region. More specifically, images generated by MR pulse sequences sensitive to T_2^* would show stronger signal where blood is rich in oxygenated hemoglobin and weaker signal where blood is rich in deoxygenated hemoglobin (Huettel et al., 2009). This is the blood-oxygen-level-dependent (BOLD) contrast of T_2^* -weighted images reflecting the concentration of deoxyhemoglobin.

In 1990, Ogawa and colleagues first demonstrated using BOLD contrast to map brain oxygenation level changes (Ogawa et al., 1990). They inferred from their experimental results that the BOLD contrast depends on the balance of oxygen supply via blood flow and oxygen consumption extracted by tissue, hence this endogenous contrast could be used to study the brain function non-invasively. Their work opened the avenue for investigating neuronal activity using BOLD-based MR techniques based on the coupling between neuronal activity and brain blood flow. Studies examining neuronal metabolism and blood flow showed that if the neurons become active and consume more oxygen, the vascular system supplies more oxygen to the activated region via increasing cerebral blood flow and volume flushing away the deoxygenated hemoglobin. Therefore, the strength of BOLD signals increases in the activated regions (Huettel et al., 2009). Because the vascular system changes (blood flow and volume) more slowly than neuronal events (Ogawa, 2012), BOLD fMRI non-invasively takes snapshots of the changing vascular response to estimate the faster changes of related neuronal activity. The information of these variations is recorded in the time series of each voxel in fMRI images. By analyzing time courses of voxels with different methods, researchers can infer the neural events related to various brain functions causing these fluctuations.

After Ogawa's work, early pioneering research on human brains using BOLD fMRI demonstrated the power and feasibility of this technique for widening the scope of brain science. Since then, developments in hardware, pulse sequence, imaging methods and analytical approaches of fMRI have continued to advance (Bandettini, 2012). Particularly, a very fast imaging sequence, echo-planar imaging (EPI), became the most commonly used technique to rapidly and efficiently acquire data for fMRI. Compared to conventional gradient-echo acquisition and fast spin-echo acquisition techniques, EPI yields decreased motion and physiological artefacts, increased signal-to-noise ratio (SNR) and BOLD sensitivity (Nair and Duong, 2004). Its inventor shared the Nobel Prize in Physiology or Medicine in 2003 (Huettel et al., 2009). Discovered in rats (Ogawa et al., 1990), the application areas of BOLD fMRI have been expanded not only to humans (Kwong et al., 1992), but also monkeys (Vincent et al., 2007) and now mice (Jonckers et al., 2011). Its contributions to both clinical and scientific research are still growing steadily. Apart from stimulation-based fMRI, new paradigms have been developed, one of which is resting-state fMRI, which records spontaneous signal fluctuations without inducing tasks (Bandettini, 2012). Advantages of rs-fMRI, such as the easy acquisition procedures and rich information of spontaneous brain activity itself, have made it increasingly accepted by researchers in this field. It will be further reviewed in the next section.

In summary, the discovery of the intrinsic BOLD contrast widened the scope of brain function research. Changes in one voxel over time in the total quantity of deoxygenated hemoglobin shapes the BOLD hemodynamic response. Oxygen consumption by active neurons and compensatory oxygen supply by the cerebral blood flow and blood volume contribute to the changes in the amount of deoxygenated hemoglobin. Even though some healthy dosages of skepticism and debate still remain regarding to the underlying complex relationships between neuronal activity and vascular system, rich information of the brain functions evidenced by a large amount of fMRI studies and increasing clinical applications show that BOLD fMRI is a sensitive and reliable tool for understanding brain activity non-invasively (Bandettini, 2012; Fox, 2012).

1.1.2 Resting-state fMRI

1.1.2.a A brief overview

"Resting-state" refers to spontaneous neuronal activity intrinsically generated by the brain. Resting state is not related to specific inputs or outputs (Fox and Raichle, 2007). Therefore, it is also described as "baseline", "spontaneous BOLD activity" and "task-free" state. Subjects are usually instructed simply to lie still in the scanner without falling asleep and to think about "nothing". The human brain represents 2% of total body weight. In resting state, the brain consumes 20% of the total oxygen needed by the body. Most of this energy consumption is used to support constant neuronal firing. Stimuli-related increases induced by tasks in neural metabolism and changes in fMRI signals are usually small (Gusnard et al., 2001; Shulman et al., 2004). All of this evidence suggests significant ongoing functionality of the brain while appearing to do nothing. To better understand how the brain performs, it is therefore important to study this functional component consuming most of the brain's energy.

In 1995, Biswal et al. (1995) first observed significant functional connectivity between left and right motor areas during rest (Biswal et al., 1995). All time courses were band pass filtered to remove some physiological noise leaving only the low frequency components (< 0.1Hz). Correlations were calculated between the time course from one motor region and the time course in the rest of the brain. The most significant FC patterns were found to be within bilateral motor cortices with small portions of extension to regions related to sensorimotor function. This phenomenon revealed that low frequency fluctuations of the resting brain were not random, but may arise from blood oxygenation or flow. Hence the resting-state FC may manifest intrinsic properties of the functioning brain during rest. The

whole scanning procedure was simple and fast, i.e. it took only several minutes, showing that it is efficient. There was no task or stimulation involved implying that it can be applied to special populations who cannot follow complex instructions during scanning, such as some clinical patients, very young children and animals. Therefore, rs-fMRI drew wide attention.

Multiple robust resting-state neural networks were observed in humans following the motor network discovered by Biswal et al. (1995). These most frequently reported networks showed consistency across different groups of subjects, analysis methods and data acquisition protocols. They are: the motor network (Biswal et al., 1995; Xiong et al., 1999; Beckmann et al., 2005; Damoiseaux et al., 2006), visual network (Lowe et al., 1998; Cordes et al., 2000; Hampson et al., 2004), default mode network (DMN) (Beckmann et al., 2005; Damoiseaux et al., 2006; van den Heuvel et al., 2008), left and right parietal-frontal network (De Luca et al., 2006; van den Heuvel et al., 2008), insular-temporal network (Beckmann et al., 2005; De Luca et al., 2006) and a network composed of one superior frontal region (van den Heuvel and Pol, 2010). The lower sensory networks include primary and secondary cortical regions, and are organized bilaterally. The DMN encompasses the posterior cingulate cortex, the precuneus, the medial frontal lobes and the medial temporal lobes. These RSNs (coherent spatiotemporal patterns) suggest that: 1) anatomically distributed brain areas are constantly communicating with each other and forming different functional sub-systems; 2) brain regions within one RSN yielded similar time series to each other, but not to structures in other RSNs; 3) these distinct functional networks coexist within the brain and may form the basis for supporting cognitive functions. The “resting brain” is not truly resting. Therefore, findings of rs-fMRI may shed light on important and intrinsic mechanisms of how the brain operates. It has now been applied to more than 30 different kinds of brain diseases, across species and received a rapid increase in clinical applications (Biswal, 2012).

One particular point worth mentioning is the importance of analysis of rs-fMRI data, since the rich information cannot usually be extracted from the raw signal without proper processing. The analytical pipeline of rs-fMRI data includes pre-processing and post-processing. After acquiring raw data, pre-processing needs to be performed to minimize noise in the signal and to prepare the data for further analysis. Then post-processing methods are applied to map the characteristics of brain activations. From pre-processing to post-processing, each step may influence the final results and the conclusions that are drawn. Therefore, a well-designed and precise processing pipeline is essential for rs-fMRI studies.

1.1.2.b Pre-processing in rs-fMRI

During data acquisition in scanners, the fMRI signal is unavoidably corrupted by noise from many sources, including scanner hardware imperfection, the subject's head and body motion, subject's physiology (e.g., breathing and heart beats), and non-task and task related undesirable variability. This noise introduces unwanted BOLD signal fluctuations. Meaningful changes in the BOLD signal are very small compared to noise variability. Task-related increase of the signal intensity is only about 5% compared to resting-state fluctuations (Huettel et al., 2009).. At 1.5T, signal changes induced by neuronal activity are around 1-2% (Parrish et al., 2000). The signal-to-noise ratio (SNR) of BOLD signals is hence usually low. Pre-processing algorithms are designed to increase SNR by minimizing non-neuronal noise and are incorporated into almost all fMRI studies in a similar manner. It is independent of experiment design and other analytical procedures (Huettel et al., 2009). Understanding the source of the noise and strategies for reducing and/or compensating for the confounds is important for data quality improvement. In humans, standard pre-processing steps include: slice-timing correction, head motion correction/realignment, co-registration, spatial normalization, spatial smoothing, temporal filtering and nuisance covariates regression.

Slice timing

Most fMRI 3D volumes are acquired using 2D imaging techniques. This means that each slice is scanned at a slightly different time point. However, the majority of fMRI statistical models assume that there is no temporal offset between different slices. Slice-timing correction aims to adjust the time course of a given voxel to make them appear to be sampled at the same time. Though the debate on the effectiveness and necessity of slice-timing correction still exists, one study reported that slice-timing effects can remarkably bias fMRI analysis and slice-timing correction approaches based on temporal interpolation can successfully compensate for these effects (Sladky et al., 2011). This study suggests that slice-timing correction should be considered in fMRI pre-processing. However, this is usually applied to data acquired by repetition time (TR) longer than 2s. Slice timing may be skipped if the data is acquired by using shorter TR (TR <2s), since the delay between slices of the 3D volumes is negligible within a shorter TR duration compared to the slow BOLD response.

Subjects can easily move their heads during scanning. MRI scanners acquire image volumes at absolute spatial positions. Thus head motion can cause a given voxel to represent different spatial points in the brain across volumes. This results in mixed signals

from very different tissues in some voxels, especially those located in tissue boundaries. Spurious activations caused by head motion may be the most damaging problem for fMRI studies (Huettel et al., 2009). A study on motion-related artefacts reported that head motion causes significant spurious but systematic connectivity patterns across the whole brain (Power et al., 2012). This suggests that motion correction should be carefully applied and examined. Realignment attempts to guarantee that each voxel contains the signal from a single brain region so that the brain appears to be unmoved, i.e. the brain is maintained in the same position across different image volumes. It is a necessary and well-accepted pre-processing approach in humans.

Head motion correction

FMRI images contain little anatomical contrast. They normally have low spatial resolution and are often distorted. It is therefore difficult to gain enough information on the relationship between neuroanatomy and functional activation in the brain (Huettel et al., 2009). To better locate functional activity within an individual brain, researchers use functional-structural co-registration to link functional images to higher resolution and undistorted structural images, which also benefits fMRI spatial normalization. Human brains show substantial variability in size and shape across different individuals, so well-located activation in one individual using co-registration is not sufficient for group analysis and comparisons between different studies (reporting results derived from common coordinates). Spatial normalization aligns subjects' brains to each other by warping them into a standard stereotaxic space, i.e. a common template.

Spatial and temporal filtering

In order to increase SNR, filtering attenuates uninteresting components in fMRI data while preserving informative components. Spatial filtering applies a smoothing kernel to average intensities of local voxels. During this averaging process, random noise is likely to be cancelled out. According to the matched filter theory, if the smoothing kernel is designed to match the frequency shape of signals, i.e. the extent of interested activations in space, SNR will be maximized (Huettel et al., 2009). Spatial filtering also aids many statistical analyses by introducing more spatial correlation into adjacent voxels and making noise more normally distributed, however it is only desirable for voxel-based analyses (Huettel et al., 2009). The most commonly used smoothing widths for fMRI are about two to three voxels.

Temporal filtering is applied to reduce unwanted fluctuations within certain frequency bands. Slow variability such as scanner drift can be removed by high-pass filtering. High

frequency variability such as those from particular physiological processes in the subject can be removed by low-pass filtering. For rs-fMRI, signals are low frequency fluctuations (LFF) from 0.01 to 0.08 Hz.

Nuisance covariates regression

There are several nuisance variables observed to influence the robustness of fMRI analysis. They are the white matter (WM) signal, cerebrospinal fluid (CSF) signal, linear detrending, head motion traces and global mean signal regression (GSR). Removing them can further reduce the effects of non-neuronal BOLD fluctuations. It is known that fMRI signals are largely related to postsynaptic potential occurring mostly in grey matter, so fMRI studies mainly focus on this kind of tissue (Friston, 2012). As a consequence, signals from other tissues (e.g., WM and CSF) are generally considered as uninteresting artefacts. In human fMRI analysis, reduction of these artefacts is optional but well-accepted. Low frequency drift has often been observed in BOLD signals. Two known sources are scanner instabilities and physiological pulsations (Tanabe et al., 2002). Since BOLD signal fluctuations are relatively small compared with noise, removing this gradual drift is an important and standard analytical step. During realignment, information on how the head moves is estimated and stored in parameters (typically six parameters). However, movement-related noise still exists after head motion correction. To further remove these artefacts, motion-related noise is later modeled and regressed out as nuisance signals according to information in the parameters (Power et al., 2012).

Global signal is defined as the mean signal of all the voxels in the brain. It is considered to include nuisance fluctuations without neuronal origin and is usually removed by regressing it out from the time series of each voxel using general linear model (GLM). Global signal regression (GSR) has been repeatedly observed to significantly influence some functional connectivity patterns (Greicius et al., 2003; Fox et al., 2005). However, ongoing controversies remain regarding this pre-processing step. Murphy et al. casted doubts on the interpretation of GSR arguing that it may introduce artefacts in both negative and positive correlations. Several other studies reported that GSR caused false group-level differences (Murphy et al., 2009; Gotts et al., 2013; Saad et al., 2013). One study on anaesthetized monkeys, however, reported that GSR is related to neuronal activity (Scholvinck et al., 2010). GSR now remains an optional pre-processing step in rs-fMRI studies.

One main challenge of analyzing fMRI and rs-fMRI data is to detect the meaningful signal among the variability of noise signals. Understanding the sources of the uninteresting variability and commonly used methods used to reduce their effects in human rs-fMRI data

helps pre-process animal rs-fMRI data. Because several pre-processing approaches encompass interpolation algorithms and spatial smoothing, improper applications can introduce artefacts or distort meaningful signals too. Reasonable selection of the pipeline is also necessary to keep the data from being over-processed.

1.1.2.c Post-processing

After data preparation, post-processing aims at detecting informative features in the data. Many analytical approaches have been developed to analyze rs-fMRI signals via looking at the brain from different perspectives. The brain is an organ with complex and hierarchical organizations, hence there are methods to extract information from regional to global scales, i.e. extract information yielded by small clusters of voxels to large-scale distributed networks. Over the twenty-years of rs-fMRI studies, several analytical approaches have been proven to be robust and effective in characterizing both normal and abnormal brains. In this thesis, I chose three widely used methods to study the mouse brain which will be reviewed and discussed as follows.

Regional homogeneity (ReHo)

ReHo hypothesizes that a given voxel and its nearest neighbours form a functional cluster, thus their time series are similar to each other, i.e. they are homogeneous voxels in a functional sense (Zang et al., 2004). This method uses Kendall's coefficient of concordance (KCC) as an index of temporal homogeneity. ReHo is highly sensitive to the number of voxels in a neighbourhood and the spatial smoothing magnitude used in pre-processing. But it is easy to be implemented and explained. ReHo analysis has been applied to many studies of brain diseases, such as schizophrenia (Liu et al., 2006), remitted geriatric depression (Yuan et al., 2008), autism spectrum disorder (Paakki et al., 2010), attention deficit hyperactivity disorder (Cao et al., 2006), Alzheimer's disease (He et al., 2007), and Parkinson's disease (Wu et al., 2009). These studies reported that abnormal activation patterns revealed by ReHo are similar to abnormal changes in the brain observed in other studies using different methods. Activation patterns in normal adults generated by ReHo also show consistency with DMN (Long et al., 2008).

With the above evidence, ReHo may serve as an indicator to measure local activity in resting-state brains. While the majority of analytical approaches focus on large-scale functional connectivity, ReHo provides us a complementary way to examine local brain functions and was used to characterize local activations in mice in this PhD project.

Independent component analysis (ICA)

As previously described in the pre-processing section, there are various sources (components) contributing to BOLD signal fluctuations in an unknown mixing way. ICA attempts to decompose fMRI data into as statistically independent components as possible across the whole brain simultaneously. This technique assumes that different functional brain networks behave independently. If functional networks behave independently, their signals should be independent of each other. Noise sources should be independent of RSNs and each other as well (Calhoun et al., 2009; Lee et al., 2013). ICA is very suitable for rs-fMRI where little information is given prior to brain activations. It revealed a couple of reliable RSNs in human and animal brains (Damoiseaux et al., 2006; Hutchison et al., 2010; Hutchison et al., 2011; Sforazzini et al., 2014) and is becoming a popular method for detecting abnormal functional networks in patients suffering from brain disorders (Cocchi et al., 2012a; Li et al., 2012b; Ambrosino et al., 2014). Some researchers use ICA to identify noise components for pre-processing (Tohka et al., 2008; Kundu et al., 2012; Salimi-Khorshidi et al., 2014). Like seed-based analysis (SBA), ICA focuses on interhemispheric FC in the brain, i.e. large-scale functional networks. Results from ICA and SBA on rs-fMRI data were shown to be very similar in one study (Rosazza et al., 2012). However, another study reported that significant differences between ICA and SBA were observed and results are sensitive to the selection of seed positions. Hence, ICA is proposed to be a superior method to SBA (Ma et al., 2007).

This technique also has some disadvantages. First, there seems to be no criterion for the choice of the optimum component number. Second, how to select meaningful components remains a relatively subjective process. Third, the complexity of the method introduces some complexity in interpretations of the final results. Nevertheless, the explorative power of ICA, successful applications in previous studies and the rich information it can provide have made it one of the most popular analytical approaches for rs-fMRI (Fox and Raichle, 2007; van den Heuvel and Pol, 2010).

Graph theory analysis

The brain is a network. The idea that neuronal elements of the brain constitute a complex anatomical network began in the nineteenth century. The notion that anatomical substrate supports multiple functional organizations/networks distributed across spatially distinct brain regions started in the twentieth century (Bullmore and Sporns, 2009b). Functional and anatomical brain networks are proposed to be important for us to understand the “brain’s many-to-one function-structure relationships” supporting consciousness and behaviors

(Park and Friston, 2013). Particularly, topological analysis using graph theory has revealed several organizational properties of the brain network based on functional and structural connectivity. Graph analysis has been successfully applied to many fields of science (Bullmore and Sporns, 2009b). Networks bind neurons and other cells into functional clusters, organize clusters into functionally specialized brain regions and integrate regions into a whole and cooperative neuronal architecture. Understanding the network hierarchy provides insights into the principles of how basic elements are organized and interact with each other (Sporns, 2011).

Topological analysis starts at defining proper nodes and edges. For large-scale networks constructed from rs-fMRI data, nodes can be defined as each single voxel in the 3D volume or each brain region parcellated by a brain atlas. Edges can be defined by functional connectivity between the time course of each voxel or the mean time course of all the voxels within each brain region. The FC can be calculated by Pearson's correlation coefficient or partial correlation (Zhen et al., 2007; Fornito et al., 2016). Functional connectivity is usually undirected statistical dependencies. The connectivity/edge strength between each pair of nodes of the brain is represented in a 2D matrix, i.e. the connectivity matrix or adjacency matrix. In graph theory, there are measurements to quantify the topology of networks via both the binarized and weighted connectivity matrix. Traditionally, researchers use a wide range of arbitrary thresholds before measuring the network to remove weak or spurious edges between nodes for functional networks, including removal of negative links and self links. All edges above the thresholds are set to unity indicating the existence of link between the two nodes, otherwise to zero. Analysis is advised to be performed across all thresholds. Recent studies suggest that the negative and positive values before binarization may contain information to further understand the brain. Therefore, analyses of weighted adjacency matrices are proposed to be one future direction. Since many network measurements are very sensitive to some basic properties, such as the number of nodes (degree) and edges, as well as the degree distribution within one network, it is important to compare these measurements to their correspondents drawn from null-network models. This helps establish the significance of the network statistics (Rubinov and Sporns, 2010).

Many measurements have been developed to describe the graph topology quantitatively. Some of them are used in this thesis to characterize the functional network of the mouse brain. Small-worldness is a ubiquitous phenomenon observed in a wide variety of complex systems, such as computer networks, social networks, protein interaction networks and brain networks of humans and animals (Bullmore and Sporns, 2009b; Telesford et al., 2011). Small-world networks have both highly clustered nodes supporting specialized processing

at local scales, and a simultaneously very short average path length supporting efficient and distributed communications between all connected nodes. Networks with this property are assumed to possess an optimum balance between specialized and distributed parallel information processing. A single numerical number as a ratio between nodal clustering coefficient and mean shortest path length summarizes this global characteristic of a network (Watts and Strogatz, 1998). However, this single number is only a rough estimation. Some nodal/local measurements are developed in graph theory to gain detailed information on the network structures, for example, the nodal clustering coefficient and node global efficiency. Nodal clustering coefficient is a metric measuring how cliquish a given node and its neighbours are, hence serves as an indicator of functional specialization of local node groups; node global efficiency quantifies how efficient the communications between a given node and all other nodes in the graph are (Achard and Bullmore, 2007; Rubinov and Sporns, 2010). Together, they extract information on single node performance. Brain function has been described as global integration of local functional segregation. The functional module is a graph metric revealing the hierarchiical aspect of neuronal systems. Brain networks are observed to be divided into several modules with specialized functional roles. Nodes within one module are closely connected to each other, but only sparsely connected to nodes within other modules. The degree to which the network is divided into distinct sub-groups is usually measured by a single-number called modularity (Newman, 2006).

Since the first study used graph topology to describe the whole brain network using rs-fMRI ten years ago (Salvador et al., 2005), this analytical tool has gained wide popularity as an alternative to ICA and SBA. Altered structures of functional networks are observed in normal developmental processes, aging, different mental illness and anaesthetized states (Wang et al., 2010a; Liang et al., 2012b). Graph topology provides abundant insightful evidence for researchers to understand brain functions. It may also advance treatments of brain disorders as brain network organizations are proposed to be plausible endophenotypes of psychiatric disorders (Bullmore, 2012).

1.1.2.d Summary

As a specific fMRI paradigm, rs-fMRI has gained wide attention and applications due to the simple and fast data acquisition, no task requirement for subjects and power of revealing intrinsic characteristics of brain function in various states. Detecting meaningful signals in rs-fMRI data is challenging because of multiple noise sources during scanning. The noise may arise from hardware imperfection, thermal noise, head motion and physiological noise.

The uninteresting variability may mask meaningful BOLD fluctuations, hence pre-processing is applied in almost all fMRI studies to minimize noise effects. Several steps remain selective because of ongoing disputes. Over-processing may cause more artefacts influencing final result interpretations. Therefore, reasonable selection of the pre-processing pipelines requires understanding the source of the noise and processing strategies. Following improved data quality, mapping brain activations is usually performed by post-processing approaches. The hierarchical nature of the brain drives multiple analysis methods aiming at describing its function from multi-scale perspectives, i.e. from regional/local to global levels. In this thesis, methods which are widely used in human brain studies were applied to map brain activation in mice: regional homogeneity to characterize the mouse brain at local level, ICA to detect RSNs in mice, and graph topological analysis to describe the structure of functional networks in mice. Results presented in this thesis may provide initial reference to parallel comparisons between research on mice and humans.

1.2 Mouse rs-fMRI

1.2.1 Introduction

As mentioned above, BOLD-based rs-fMRI is a powerful, non-invasive and widely applied technique in human brain studies and clinical applications. It has been used to demonstrate robust and repeatable FC changes of many brain disorders. However, the biological origins of the changed FC remain poorly understood. Experimental studies on humans are limited to non-invasive approaches and suffer from several other limitations hampering the establishment of early diagnosis, tracing disease progress and development of new therapies, such as the latency of disease development, complex disease expressions because of the coexistence of multiple risk factors, and experimentation not possible in patients. Animal models of human brain diseases are developed in this context to help researchers understand the molecular and cellular mechanisms of the brain under these pathological conditions and test new treatments. Particularly, the mouse is an ideal model organism for human disease research, not only because this species is physiologically, genetically and pathologically similar to humans, but it is also cheap, easy to maintain, relatively fast to breed and amenable to genetic engineering (Rosenthal and Brown, 2007; Harper, 2010).

The availability of a large reservoir of genetically modified mouse models, the majority of which exhibit phenotypes close to those of human diseases, provide valuable resources for investigating the mechanisms of corresponding human diseases and new prevention and

treatment strategies (Bedell et al., 1997). Specifically, mouse models of human brain disorders have been used as a major tool in neuroscience to study the function of disease-related genes in both normal and abnormal brains (Leung and Jia, 2016). The studies of these models commonly focus on behavioral tests, structural imaging and post-mortem analysis. Non-invasive *in vivo* rs-fMRI in mice would offer other significant advantages: longitudinal research aiming at monitoring disease progress in the mouse models, paralleled comparisons with rich information from other species using rs-fMRI, and combination with the aforementioned assessing approaches of mouse models. Furthermore, functional readouts, such as fMRI, generally provide more subtle information on pathological tissues than morphological parameters (Mueggler et al., 2012; Leung and Jia, 2016).

Experimental applications of rs-fMRI have been developed on animals from non-human primates to rodents (Vincent et al., 2007; Jonckers et al., 2011; Lu et al., 2012). “Resting-state” is also used in studies involving animals under different anaesthesia (Biswal, 2012). Due to several challenging issues, mouse rs-fMRI has only begun to progress quickly in the past six years (Jonckers et al., 2011), and remains a largely unexplored field. The reasons are mainly due to technical and physiological issues, including low SNR because of the high magnetic field of small animal scanners, application of anaesthesia and tight control of physiological states of the mouse during scanning (Benveniste and Blackband, 2006; Guilfoyle et al., 2013; Nasrallah et al., 2014a). Recent progress in mouse rs-fMRI includes studies on the detectable RSNs in healthy mice under anaesthesia (Jonckers et al., 2011; Guilfoyle et al., 2013; Grandjean et al., 2014b; Mechling et al., 2014; Nasrallah et al., 2014a; Sforazzini et al., 2014; Stafford et al., 2014; Zerbi et al., 2015), some network topological properties observed in mice (Mechling et al., 2014; Liska et al., 2015), comparative studies on different anaesthetic protocols (Grandjean et al., 2014b; Jonckers et al., 2014), and studies on mouse models of some brain disorders (Shah et al., 2013; Grandjean et al., 2014c; Zerbi et al., 2014; Haberl et al., 2015; Grandjean et al., 2016; Sforazzini et al., 2016). These studies advanced our knowledge in mapping mouse brain functions, but discrepancies are reported across studies. Reasons may lie in different coils, MRI protocols, animal handling and analytical methods being used. Another reason may be the different anaesthetic regimens applied by different labs, because anaesthesia is reported to influence FC and induce anaesthetic-specific effects on some RSNs (Williams et al., 2010; Grandjean et al., 2014b).

In the following sections, data acquisition on mice using rs-fMRI, anaesthesia and functional brain network analysis in mice will be reviewed and discussed.

1.2.2 Data acquisition of mouse rs-fMRI

Reliable data acquisition is the first and crucial step for fMRI studies involving experimental work. High-quality images (e.g., little distortion and signal loss) and high SNR are factors important to achieve robust brain activation using BOLD-based fMRI. However, fMRI of small rodents, especially mice, is very challenging due to several technical and physiological issues.

There are three reasons that mouse rs-fMRI demands high SNR. Firstly, the small brain size of mice requires high spatial resolution to resolve brain structures and functional brain organization. Secondly, high temporal resolution is required for the analysis of BOLD time series. Thirdly, high enough sensitivity has to be achieved to detect BOLD signals at rest given the small changes of signal intensity compared to noise. One solution is to increase the main magnetic field of the small animal scanners. However, higher fields and small brain size cause other issues (Baltes et al., 2011). For example, more severe image distortions due to increased susceptibility artifacts at larger tissue-bone and tissue-air interfaces of the mouse brain, lower local field homogeneity due to generally poorer shimming capability at high fields, and reduced detection sensitivity (Nair and Duong, 2004; Baltes et al., 2011; Guilfoyle et al., 2013; Nasrallah et al., 2014a). A cryogenic radiofrequency probe (CryoProbe) is one strategy to address these problems, which has been shown to achieve enhanced sensitivity to the mouse BOLD-based fMRI signal (Baltes et al., 2011).

Another important technical indicator of measuring the quality of BOLD signal is temporal SNR (tSNR). For BOLD-based fMRI, tSNR is probably the most important quality indicator evaluating signal levels of a time course. It measures the amount of signal present in the data across time and could be estimated as the mean time series divided by the standard deviation within a ROI in the gray matter (Parrish et al., 2000; Triantafyllou et al., 2005; Bennett and Miller, 2010; Welvaert and Rosseel, 2013).

Physiological issues arise from the fact that most *in vivo* mouse fMRI experiments require the maintenance of the animal's normal and stable physiology under anaesthesia. Rs-fMRI studies on humans take for granted that the subjects are under normal and stable physiological conditions throughout the experiment. Given the rs-fMRI experiment on mice during awake resting-state condition remains impractical (Jonckers et al., 2014), anaesthesia is still a necessary step. Therefore, achieving a reliable and normal physiological condition through the entire scanning session of mouse rs-fMRI studies becomes more complicated. Maintaining the normal and stable physiological condition is critical for obtaining robust BOLD fMRI signals (Nair and Duong, 2004). Fluctuations of

physiological noise, such as cardiac and respiratory motion, head motion and metabolic rates, could mask fluctuations of BOLD signals originated from neuronal activities. The first step to minimize physiological noise originating from motion and hemodynamic conditions is the proper and stable preparation of the small animals. The second step is to maintain the normal physiological conditions. Tight control of several physiological parameters within limits is necessary for fMRI studies on mice. Basic parameters to be monitored are breathing rate, heart rate, blood gas partial pressure of oxygen (pO_2) and carbon dioxide (pCO_2), and body temperature. PO_2 and pCO_2 influence BOLD signals per se. Body temperature is an important parameter to monitor and maintain, since it drops fast when mice are under anaesthesia and substantially influences the metabolic oxygen consumption rate and the hemodynamic system which are all critical for BOLD-fMRI. Due to the application of anaesthesia and the small total blood volume of mice, physiological control and monitoring are demanding (Baltes et al., 2011; Mueggler et al., 2012), but facilitated by advanced MRI-compatible physiological maintenance and monitoring equipment. Another critical point to acquire images with minimum distortions is the head positioning of the animals, given the fact that the size of the radio-frequency coil should be matched to the size of the scanned object to achieve the best SNR. Stereotaxic fixation can facilitate not only the control of head motion, but head positioning (Mueggler et al., 2012).

While anaesthesia helps to restrain the animals and minimize stress-related physiological confounds, it affects neurovascular coupling and neuronal activity, which introduces confounds into the measured BOLD signals. In the next section, some commonly used anaesthetic regimens will be reviewed.

1.2.3 General anaesthesia and commonly used anaesthetic regimens for rodent fMRI

General anaesthesia is a drug-induced, temporary and reversible state with some of the following components: amnesia, analgesia, loss of consciousness and immobility (Brown et al., 2010). Anaesthesia is applied to assist animal handling, keep the animal immobilized, as well as to prevent discomfort, anxiety and pain (Benveniste and Blackband, 2006). Therefore, anaesthesia reduces artefacts introduced by motion or physiological noise related to stress during fMRI scanning. However, it also induces adverse effects, such as the reduction of neuronal activity, disruption of the neurovascular coupling mechanism, respiratory suppression, disturbance of the cardiovascular system and regulation of the animal's body temperature (Tremoleda et al., 2012; Pan et al., 2015). These factors influence BOLD signals and confound the interpretations of fMRI experimental results.

Fortunately, published studies proved that functional connectivity and brain networks are preserved in mice under light to moderate anaesthesia (Pan et al., 2015).

The most commonly used anaesthetics in preclinical rodent experiment are alpha-chloralose, isoflurane or halothane, medetomidine, propofol and urethane. Various anaesthetics have their own advantages and disadvantages, and differentially influence the animal's normal homeostasis and brain activity (Mueggler et al., 2012; Haensel et al., 2015). Alpha-chloralose induces minimal impacts on the cardiopulmonary system, basal physiology, brain activity and neurovascular coupling, but is not suitable for longitudinal studies due to its depressive effects on respiration and toxicity (Haensel et al., 2015; Pan et al., 2015; Petrinovic et al., 2016). One recent study reported that this agent led to unstable physiological maintenance of mice for fMRI studies when compared to isoflurane (Low et al., 2016a). It is hence an agent unsuitable for longitudinal mouse rs-fMRI experiment. Halothane and isoflurane are inhalation anaesthetics commonly used in studies involving animals, among which isoflurane is the mostly used anaesthetic in laboratory animals (Tremoleda et al., 2012; Haensel et al., 2015). Therefore, isoflurane, medetomidine, propofol and urethane will be further reviewed in this section.

Due to the ease of application during both induction and maintenance stages, fast reversibility of its anaesthetic effect, high safety, minimal depression of the cardiovascular system and reduced adverse impacts on the animals after long experiments (if not overdosed), isoflurane is an extensively used general anaesthetic agent for various animal studies (Tremoleda et al., 2012). However, it is a well-known vasodilatory agent that increases the baseline cerebral blood flow in a dose-dependent way, and hence may influence neurovascular interactions that could be detected by fMRI technique. Isoflurane also suppresses neural activity which confounds rs-fMRI results (Haensel et al., 2015; Pan et al., 2015). Like other general anaesthetics, the precise molecular mechanism of action of isoflurane is not clearly understood. Although it targets multiple receptor systems, the major component of its mode of action is modulation of γ-aminobutyric acid type A (GABA(A)) receptors (Richards, 2002; Ballesteros et al., 2012; Haensel et al., 2015). Despite its disadvantages, isoflurane is still a very useful agent. For example, its vasodilatory effects can be effectively reduced at a relatively low dosage level (~1%) (Bosshard et al., 2010). Studies on monkey and rat brains demonstrate that though FC decreased when dosage levels of isoflurane increased, many resting-state networks are still detectable in spontaneous BOLD signals (Vincent et al., 2007; Hutchison et al., 2010). Hutchison et al. further reported that there was no prominent difference in RSNs under isoflurane and ketamine/xylazine anaesthesia (Hutchison et al., 2010). FC studies using mouse rs-fMRI

showed that long-range connectivity in the striatum was suppressed, but other resting-state networks were detectable at a low dosage level under isoflurane anaesthesia (Grandjean et al., 2014b). Moreover, effective electrical stimulation, pharmacological stimulation and resting-state studies all prove it to be a very useful anaesthetic agent on mouse fMRI studies (Mueggler et al., 2002; Bosshard et al., 2010; Guilfoyle et al., 2013).

Medetomidine is a sedative agent with several beneficial properties. It induces reliable sedation, anxiolysis, analgesia and muscle relaxation. Using sedatives is preferable for small animal fMRI studies, because sedation allows minimal physiological monitoring and free breathing, especially compared to alpha-chloralose, which causes unstable physiological conditions in animals (Nasrallah et al., 2014a; Pan et al., 2015). Medetomidine is suitable for longitudinal animal experiments and its effects can be reversed by atipamezole (Weber et al., 2006; Jonckers et al., 2015). However, it induces negative effects on cardiovascular functions and causes dose-dependent vasoconstriction (Sinclair, 2003; Jonckers et al., 2015). Medetomidine is the most potent α2-agonist, i.e. it shows strong affinity to α2-adrenoceptors with high specificity and selectivity (Scheinin et al., 1989). Studies on rats and mice revealed that it influences FC differently from some other anaesthetics, such as isoflurane and propofol (Williams et al., 2010; Grandjean et al., 2014b). Decreased FC in several RSNs under higher dosage level of medetomidine anaesthesia was reported, except for FC in the striatum. Propofol is an intravenous anaesthetic widely used in clinical application and laboratory animals (Fulton and Goa, 1996; Fodale and La Monaca, 2008; Richard, 2008). Its main advantages are rapid onset as well as rapid and complete recovery even after prolonged anaesthesia. Its dosage-effect relationships are well-established in humans and hold good potential for rodent fMRI research (Fiset et al., 1999; Fodale and La Monaca, 2008; Tremoleda et al., 2012). The disadvantages include common incidence of apnea, decreased blood pressure and respiratory suppression. Propofol does not induce analgesia, which should be taken into consideration for experiments involving painful procedures. Like isoflurane, propofol mainly targets GABA(A) receptors to induce its sedative and hypnotic effects (Trapani et al., 2000; Tremoleda et al., 2012). One study on rats under propofol anaesthesia revealed that thalamocortical FC was suppressed at high surgical dosages (Tu et al., 2011). Another study investigated the dosage-dependent effects of this agent on rats reported complex FC changes in cortical and subcortical areas as anaesthetic level increased (Liu et al., 2013b). Comparative studies on anaesthetics using mouse rs-fMRI showed that long-range FC patterns in mice under propofol were similar to those observed in mice under isoflurane (Grandjean et al., 2014b).

Urethane is also widely used for animal research. It is well-known for inducing long-lasting and stable anaesthesia with minimal effects on the cardiovascular system, blood pressure and respiration. Due to its carcinogenicity, cytotoxicity and immunosuppression, urethane is not used as a human anaesthetic and should be applied very carefully to laboratory animals. It is not suitable for longitudinal studies (Hara and Harris, 2002; Tremoleda et al., 2012). Unlike the previously described agents markedly targeting one receptor system, urethane has modest effects on multiple receptor systems (Hara and Harris, 2002). This agent suppresses thalamocortical neuronal activities as revealed in one study on rats (Huh and Cho, 2013). Urethane is reported to uniquely induce sleep-like brain states in rats, and hence may be suitable for studies on FC changes across sleep-like states using rodent models (Zhurakovskaya et al., 2016).

In summary, different agents induce anaesthesia through different mechanisms, influence basal physiological conditions of the animals differently, and alter FC patterns in complex ways. It is therefore important to choose appropriate anaesthetic regimens for rodent rs-fMRI studies. The availability and wide usage of the above mentioned anaesthetics provide flexible choices for labs, but their unique characteristics also introduce discrepancies across studies. Understanding how they modulate FC patterns and brain network topology using mouse rs-fMRI would provide important references for ongoing research.

Besides the bias of anaesthesia, some analytical considerations of mouse rs-fMRI data are also important to achieve more parallel comparisons to human rs-fMRI research. The pre-processing, the mouse brain atlases and current functional network studies in mice will be reviewed as follows.

1.2.4 Functional brain network analysis in mice

1.2.4.a Pre-processing of mouse rs-fMRI

The pre-processing pipelines are well-established for human rs-fMRI studies, often with different software/strategies available for each step. Due to different brain size, brain structures and physiology, the pre-processing tools used in humans usually need to be adapted to mouse data analysis. Furthermore, experimental and scanning conditions for mouse fMRI are not the same across different labs. For example, breathing modality (ventilation or free breathing), signal detectors (room temprature probe or CryoProbe), scanning protocols, animal handling procedures and anaesthetic regimens differ between labs. These factors may all contribute to BOLD fluctuations, and therefore influce the final results and result interpretations.

Each lab usually choses their own pre-processing pipelines which vary widely across groups (Jonckers et al., 2011; Grandjean et al., 2014b; Nasrallah et al., 2014a; Sforazzini et al., 2014; Liska et al., 2015; Zerbi et al., 2015). Specifically, slice timing correction is not always performed which may be due to the relatively short repetition time (TR) typically used in mouse rs-fMRI studies (<2s). Realignment was applied in most studies. One study chose to omit this step to avoid artefacts introduced by realigning algorithms, given the small motions they observed during experiment and estimated using the realigning tool (Nasrallah et al., 2014a). Reference image spaces for realignment and spatial normalization varied from single animal's EPI images (Jonckers et al., 2011; Mechling et al., 2014), group-mean EPI template (Grandjean et al., 2014b) , in-house anatomical template (Sforazzini et al., 2014) or anatomical templates that are publically available (Zerbi et al., 2015). One group did not mention normalization in the pre-processing step (Nasrallah et al., 2014a). Low frequency thresholds for mouse rs-fMRI studies were typically set as the same as thresholds used for humans <0.1Hz. But upper band threshold was recommended as 0.3Hz for data acquired under medetomidine anaesthesia (Grandjean et al., 2014b). Spatial smoothing was applied in most studies. Not all studies performed nuisance covariates regression. Because of the abscence of tissue masks in rodent brains, removing noise from white matter and cerebrospinal fluid is not widely used in mouse data processing. Efforts towards exploring optimized pre-processing procedures have been made recently by one research group (Zerbi et al., 2015). The pre-processing pipelines applied in this thesis were designed to provide optimal datasets for the type of analysis to be performed..

1.2.4.b The mouse brain atlas for functional network construction

Choosing the appropriate representations of functional brain networks requires proper definitions of nodes and edges, whose nature greatly determines the neurobiological meanings of the modeled interactive topology (Butts, 2009). At macroscale, however, there is no gold standard for the precise definition of nodes due to the coase spatial resolutions given by macroscale techniques, such as fMRI. Researchers usually define nodes as anatomically continous and functionally specialized neuron populations or cell assemblies based on cytoarchitecture and anatomical landmarks. One commonly used and widely accepted approach is to rely on stereotactic anatomical atlases made with validated parcellation schemes (Fornito et al., 2016).

For mice, there are several mouse brain templates available (Ma et al., 2005; Chen et al., 2006; Dorr et al., 2008). However, the cortex areas of these templates are coarsely

segmented. From previous studies on rodent rs-fMRI using ICA and seed-based analysis, it is known that cortex areas contain several functional clusters suggesting that poorly segmented cortical regions may introduce significant bias in functional correlation analysis. Very fine segmented cortex, hippocampus, cerebellum and basal ganglia templates are provided by the Australian Mouse Brain Mapping Consortium, though the thalamus is not yet available at the moment (AMBMC, http://www.imaging.org.au/AMBMC/AMBMC). Another whole brain mouse atlas is available from the Allen Brain Atlas (http://mouse.brain-map.org). The AMBMC and Allen Brain Atlas provide refined anatomical segmentation for mouse brain network analysis. Before their availability and completion, some studies defined nodes based on the in-house template or functional clusters identified by ICA (Grandjean et al., 2014c; Mechling et al., 2014). One group performed functional module analysis on the mouse brain using individual voxels as nodes to construct the functional network (Liska et al., 2015). The disadvantages of using single voxel as each node in MRI are from the partial volume effects that may spuriously amplify connectivity between neighbouring voxels (Fornito et al., 2016) and the expensive computational time. AMBMC and Allen Mouse Brain Atlas are used in this thesis to define nodes.

1.2.4.c Current knowledge of functional networks and network properties in mice

Recent advances have been achieved in this burgeoning area. Evidence of detectable RSNs has been provided by different labs. The most commonly observed cortical RSNs are the somatosensory cortex, motor cortex, cingulate/retrosplenial cortex, and piriform cortex, while the most commonly observed subcortical RSNs are the hippocampus, striatum (espcially caudate-putamen), thalamus and hypothalamus (Jonckers et al., 2011; Grandjean et al., 2014b; Mechling et al., 2014; Nasrallah et al., 2014a; Sforazzini et al., 2014; Zerbi et al., 2015). The presence of a default-mode like network was reported by some studies using different anaesthetic regimens (Guilfoyle et al., 2013; Sforazzini et al., 2014; Stafford et al., 2014; Liska et al., 2015; Zerbi et al., 2015). Topological analysis of the functional brain network in mice revealed that the mouse brain is organized into segregated modules and preserves small-worldness under anaesthesia. However, modular structures were not completely consistent between studies which might be due to the application of different node definitions , modular detection algorithms applied and different anaesthetics (Mechling et al., 2014; Liska et al., 2015; Bardella et al., 2016).

Explorations on some mouse models of brain disorders using established experimental protocols have been reported. Disease models being studied include mouse models of

amyloidosis and Alzheimer's disease (Shah et al., 2013; Grandjean et al., 2014c; Zerbi et al., 2014; Grandjean et al., 2016; Shah et al., 2016b), and models of autism (Zhan et al., 2014; Haberl et al., 2015; Sforazzini et al., 2016). Findings from wild type and transgenic mouse models confirmed that mouse rs-fMRI is an invaluable tool for researchers to understand system-level brain function and functional alterations associated with risk genes of brain disorders, and influence clinical research and applications. However, mouse models resembling features of major mental illnesses have not been investigated by far.

1.3 *Disrupted-in-Schizophrenia 1 (DISC1)* mouse model

1.3.1 *DISC1* is a well-known risk gene for major mental illness

Like Alzheimer's disease and autism, there are many other mental disorders that remain poorly understood and undertreated. According to the World Health Organization (WHO), metal disorders include: depression (affects approximately 350 million people globally), bipolar affective disorder (affects approximately 60 million people affected worldwide), Schizophrenia (affects about 21 million people globally), developmental disorders including autism, dementia including Alzheimer's disease and other psychoses. Global burdens caused by metal disorders are heavy and keep growing. Understanding the mechanisms of these illnesses is the necessary avenue to cure affected people and prevent disease onsets. However, our knowledge and understandings of causes of mental disorders are still very limited.

Major mental illnesses include Schizophrenia (SZ), major depression and bipolar disorders. These illnesses are complex brain disorders driven by a combination of genetic and environmental factors (Tsuang et al., 2004; Dean and Murray, 2005; Brandon and Sawa, 2011). One gene named *DISC1* is a well-established risk gene for these disorders and a potential risk factor for autism (Chubb et al., 2008; Soares et al., 2011). It was first identified in a Scottish pedigree possessing a high loading of major mental illnesses (Muir et al., 2008). *DISC1* has crucial roles in both the developing and the mature brain, and is proposed as a key lead to explore human cortex development which is critical for the normal cognition (Narayan et al., 2013). Accumulating evidence shows a link between *DISC1* and specific endophenotypes commonly associated with Schizophrenia and affective disorders (Brandon and Sawa, 2011).

Correlations between variants in *DISC1* and human brain structural imaging, functional imaging and neurochemistry have been examined by several studies (Duff et al., 2013). Volumetric studies reported some common variants of *DISC1* show association with frontal

and hippocampal regions in both healthy controls and SZ patients. Thickness and width of the frontal, temporal and parietal cortices are reported to be associated with several variants in *DISC1* in healthy cohorts. The cortical thinning effects are observed during a key time in neurodevelopment. FMRI studies reported an association between prefrontal function and *DISC1* in the health. These results indicate that common missense variants in *DISC1* may influence cortical development, brain function and structure, as well as neurochemistry. But findings from human imaging research are not sufficient to understand the underlying mechanisms associated with DISC1.

DISC1 genetic mouse models are created for modelling major psychiatric disorders. Observations from these mouse models show that decreased cortical thickness, enlarged lateral ventricles and partial agenesis of corpus callosum are associated with altered *DISC1* expression (Shen et al., 2008). Enlarged lateral ventricles in mutant *DISC1* mice and altered dendritic arborization have also been reported by one study (Pletnikov et al., 2008; Johnstone et al., 2011). Behaviourally, *DISC1* manipulation in genetic mouse models results in phenotypes that are plausibly consistent with findings in psychiatric patients. Neurochemical deficits resembling findings from human patients are also reported (Hikida et al., 2007; Shen et al., 2008; Johnstone et al., 2011; Jaaro-Peled et al., 2013; Niwa et al., 2013b). One study reported that a mouse strain with natural *DISC1* mutation displayed behavioural abnormalities associated to mental disorders (Gomez-Sintes et al., 2014). This evidence shows a relationship between *DISC1* animal models and major mental illnesses, supporting the feasibility of studying *DISC1* associated effects using mice.

In this thesis, one published transgenic mouse model, i.e. dominant-negative *DISC1* under control of the αCaMKII promoter mouse model (Hikida et al., 2007), was used to investigate effects of *DISC1* on functional brain network using mouse rs-fMRI.

1.3.2 Dominant-negative *DISC1* under control of the αCaMKII promoter (*αCaMKII-DN-DISC1*) mouse model

This mouse model was generated by inserting a C-terminal truncated human DISC1 under the αCaMKII promoter in a pure C57BL/6 background (Hikida et al., 2007). The *αCaMKII-DN-DISC1* mice display several abnormalities that resemble findings from at least a subset of human schizophrenia patients. Enlargement of lateral ventricles, especially on the left side, were observed in juveniles (at 6-week old). But this abnormality disappeared when the mouse models reached 3-months old. Behavioural analysis performed between 3 to 8 months revealed altered behavioural characteristics in *αCaMKII-DN-DISC1* mice

compared to wild type control: hyperactivity, disturbance in sensorimotor gating, abnormal olfactory-associated behaviour and an anhedonia/depression-like deficit. These observations suggest a link between the genetic mutation and associated phenotypic changes. Therefore, *αCaMKII-DN-DISC1* mice are promising models for understanding the functional roles of *DISC1* and major mental illness. One potential issue of this model is that the observed differences between it and the wild type control were significant but subtle. Hikida et al. (2007) explained that effects of one single genetic factor may not cause the full manifestation of disease phenotypes in mouse models, since schizophrenia is a complex and multifactorial disorder caused by several susceptible genetic factors, environmental factors and gene-environment interactions.

To the authors best knowledge, the regulation of system-level functional connectivity by *DISC1* characterized by mouse rs-fMRI remains uninvestigated. Given the above listed translatable markers, filling this gap using *αCaMKII-DN-DISC1* mice will advance our understanding of the function of this specific and important risk gene.

1.4 Summary and specific aims

This introduction has outlined how the findings from resting-state functional network analysis in humans, the availability of high-field small animal scanner and transgenic mouse models of human brain disorders have been driving the increasing need of translating functional brain network analysis in mice using mouse rs-fMRI. Specifically, this chapter highlighted the challenges of mapping brain activity in mice using this technique. In particular, confounds from different anaesthetics on functional brain networks in mice require caution in interpreting final results. Studies in this field have revealed the existence of several networks and some preserved network topological properties. However, most analysis was performed under only one single anaesthetic regimen. Although anaesthetic-specific FC patterns in mice were reported by one study using long-distance FC analysis, our understandings on how various anaesthetics impact on local FC as well as network topologies in mice remain unknown. Filling this gap not only will greatly facilitate comparisons between different labs, but will also help interpretation of findings from mouse disease models anaesthetized with these regimens. Furthermore, understanding functional patterns in the mouse brain revealed by widely used analytical methods in humans also facilitate more parallel comparisons between the two species. One main purpose of mouse rs-fMRI is to investigate the brain function of transgenic mouse models of human brain disorders, but only very limited mouse models have been examined in this new field so far.

In particular, mouse models of major mental illness, such as *DISC1* transgenic mice, have not yet been examined by fMRI. Filling this gap will advance our understanding of this important gene, and facilitate the identification of potential functional phenotypes associated with its dysfunction. The major goals of this thesis were therefore to investigate the effects of different anaesthetic regimens on functional networks in mice and how *DISC1* regulates the functional networks in a mouse model under one anaesthetic regimen using rs-fMRI. Wild type mice (C57BL/6) and *αCaMKII-DN-DISC1* mice were used for the goals by addressing the following specific aims:

Aim 1: To investigate effects of different anaesthetic regimens on regional functional connectivity in mice (Chapter 3)

Aim 2: To investigate effects of different anaesthetic regimens on network topologies in mice (Chapter 4)

Aim 3: To investigate effects of *DISC1* on the functional brain network in mice using rs-fMRI (Chapter 5)

Chapter 2 Materials and Methods

In this chapter, general materials and methods used in this thesis are described. For Aim 1 and Aim 2, I used publicly available data. For Aim 3, as the first PhD student working on mouse rs-fMRI projects at the University of Queensland, I set up and optimized the experimental pipeline for animal preparation and MRI scanning. After experimental pipeline validation, I acquired data from *DISC1* transgenic mice. Pre-processing used in different studies in the thesis will be described. Detailed post-analysis approaches will be included.

2.1 Data for investigating effects of different anaesthetic regimens on the wild type mouse brain

2.1.1 Data acquisition

Data were collected by (Grandjean et al., 2014b), who provided a detailed protocol in their paper. Briefly, female C57BL/6 mice were mechanically ventilated, paralysed with pancuronium bromide (0.5mg/kg bolus, 0.5 mg/kg/h continuous infusion), and either anaesthetized with propofol (30 mg/kg bolus, *Propofol30*), isoflurane (1% maintenance, *Isoflurane1*), urethane (1.5g/kg, *Urethane1.5*), medetomidine (0.1 mg/kg bolus, 0.2 mg/kg/h continuous infusion or 0.05 mg/kg bolus, 0.1 mg/kg/h continuous infusion, *Medetomidine0.1* or *Medetomidine0.05*, respectively) or a medetomidine (0.05mg/kg bolus, 0.1 mg/kg/h continuous infusion) and isoflurane (0.5%) combination (*Mediso*). Rs-fMRI was acquired on a small animal 9.4T MR system (Bruker BioSpin MRI, Ettlingen, Germany) equipped with a receiver only 2x2 phased array cryogenic coil. Gradient-echo echo-planar imaging (GE-EPI) data were acquired with repetition time /echo time /flip angle = 1000 ms/10 ms/90°, 360 repetitions, matrix dimension = 90 x 60, in-plane voxel dimension 263 x 233 μm. The complete dataset is available on XNAT online repository (http://central.xnat.org, project ID: fMRI_ane_mouse). Animal numbers for each group were 6 in *Propofol30*, 11 in *Isoflurane1*, 13 in *Urethane1.5*, 13 in *Medetomidine0.1*, 6 in *Medetomidine0.05*, 8 in *Mediso*.

2.1.2 Systemic physiological measurement

Systemic physiological measurement was performed to monitor each animal's physiological conditions under anaesthesia. Values for every animal were averaged over recordings during a period of 15 min starting from 45 min after the anaesthetic induction. All animals were under normal physiological states as shown in Table 2 in (Grandjean et al., 2014b).

2.2 Experimental pipeline set-up and validation

2.2.1 Experimental pipeline set-up

The first crucial and fundamental step for study on functional brain network in *DISC1* transgenic mouse models was to acquire reliable data with publication-level quality. As reviewed in Chapter 1, data acquisition on mouse using rs-fMRI is very challenging. My task was to set up an experimental pipeline for data acquisition including design and optimization of procedures on the following components: animal preparation, MRI parameters and pipeline verification. In pilot studies, I established animal preparation procedures aiming at reproducible and tight physiological control during scanning, achieved reproducible and good head positioning for using CyroProbe and tested proper fMRI parameters acquiring data with minimum geometric distortions.

Animal preparation was performed under isoflurane. Reasons for the choice of this anaesthetic agent were: 1) the limitation of the experiment condition; 2) the beneficial reasons reviewed in Chapter 1, such as it is the most widely used inhalation agent for laboratory animals and preserved functional brain networks in mice reported by previous studies; 3) current research on effects of different regimens on the mouse brain using local connectivity and graph analysis. Dosage levels during induction and maintenance were tested in pilot studies according to the following considerations: stable physiology of the animals throughout the entire experiment period, smooth changes of breathing and body temperature during the preparation, normal recovery after the experiment and detectable signals caused by electrical stimulation. Physiological control includes maintenance and monitoring of body temperature, monitoring of breathing rate, heartbeat, and SpO_2 (peripheral capillary oxygen saturation, an estimate of the amount of oxygen in the blood and a surrogate of pCO_2). Details on the equipment used will be described in the following section. Figure 2-1 shows a representative picture of the experiment setup of the animal preparation for mouse rs-fMRI. Figure 2-2 shows a representative figure of the stable physiological monitoring during one experiment.

Gradient-echo echo-planar (GE-EPI) sequence and FLASH sequence were used for functional and anatomical images, respectively. The GE-EPI sequence was selected with the following considerations: high tSNR, minimum geometric distortions, no severe noise induced by artefacts such as Nyquist ghost (Giannelli et al., 2010) and reliable signals/reproducible RSNs. Details of the MRI will be listed in the following experimental pipeline verification section.

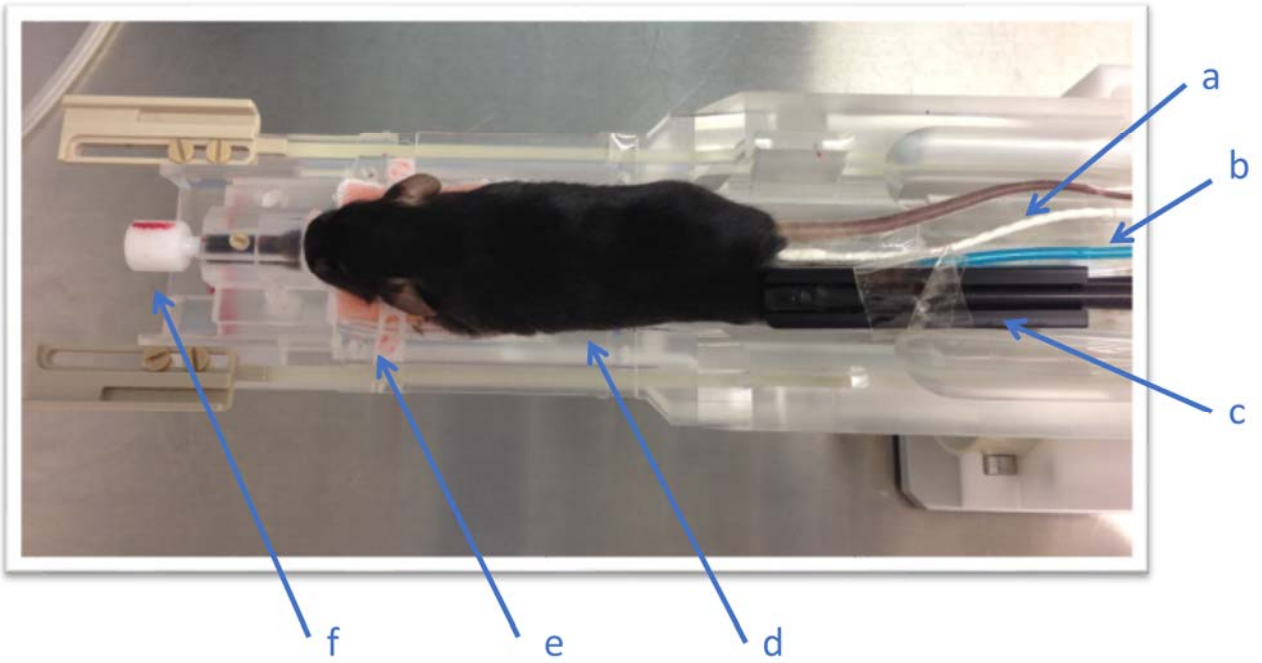

Figure 2-1 Representative picture of the experiment setup of the animal preparation for mouse rs-fMRI. The anaesthetized (1.2%) mouse is positioned prone on a cradle designed for CryoProbe, with in-built warm water circulation to keep the animal's body temperature. Ear bars and bite bars help to fix the animal's head position properly. MR compatible infrared sensor clipped on the shaved upper hind limb (left) monitors SpO_2 and heartbeats. Breathing rate is monitored with a sensor pad placed under the animal. A MR compatible rectal temperature probe monitors the animal's body temperature. (a) rectal temperature probe; (b) breathing rate sensor pad; (c) infrared sensor; (d) animal cradle with in-built warm water circulation; (e) ear bars; (f) bite bars.

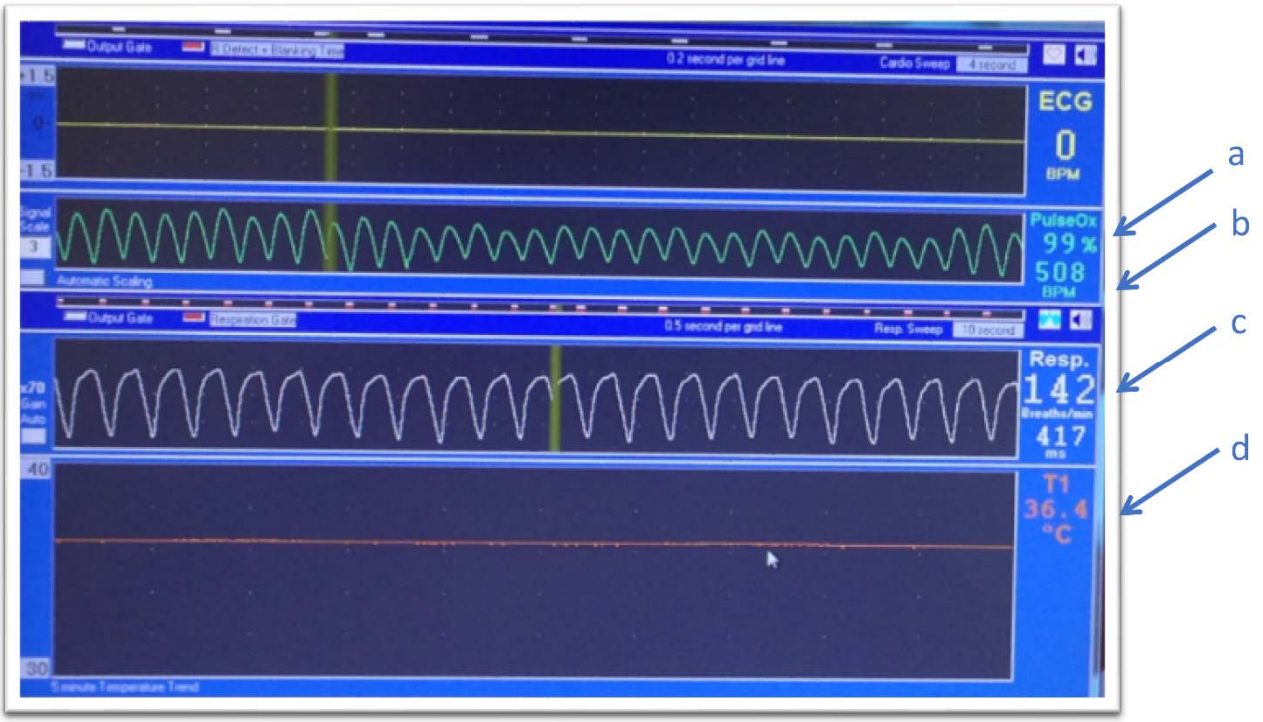

Figure 2-2 Stable recordings of each physiological parameter. After proper animal handling and preparation, physiological parameters usually produce stable readings reflecting the

normal state of animals during the rs-fMRI experiment. (a) SpO_2; (b) heartbeat; (c) respiration rate; (d) body temperature.

2.2.2 Experimental pipeline validation

To verify the optimized experimental pipeline, one group analysis was performed. After data acquisition, tSNR and group ICA were applied for signal analysis.

2.2.2.a Materials and methods for experimental pipeline validation

Animal preparation

All experiment were performed in accordance with the University of Queensland Animal Ethics. Seven WT male C57Bl/6J mice with an average age of 5 months weighing 30.4±2.8 g were anaesthetized with isoflurane (induction 2-3%, maintenance 1.2%; Biomac Pty Ltd, Australia) and were placed prone on a cradle. Body temperature was maintained with an in-built warm water circulation. A rectal temperature probe (MR-compatible rectal temperature probe, SA Instruments, Inc. USA) was inserted to keep the animal at 36.6±0.7 ^{o}C. Breathing rate was monitored with a sensor pad (MR-compatible sensor, SA Instruments, Inc. USA) with an average breathing rate of 113.3±16.8 Resp/min. To measure SpO2 and heart rate, a MR-compatible infrared sensor (MR-compatible optical fiber, pulse oximeter sensor, SA Instruments, Inc. USA) was placed on the shaved left upper hind limb on five of the animals, with an average SpO2 of 96.5±2.4 and an average heartbeat of 472.0±60.9 bpm. For accurate and reproducible positioning, the head of the mouse was fixed with a bite bar and a pair of stereotactic ear bars. Eye cream was applied to protect the animal's eyes from becoming dry.

MRI

MRI experiment were performed on a Bruker BioSpec 94/30 small animal MR system (Bruker BioSpin MRI, Germany) operating at 400 MHz (9.4 Tesla). For signal transmission and reception, a commercially available Cryogenic Probe operating at a temperature of 30 K was used (Bruker BioSpin MRI, Germany). Anatomical images acquired in the sagittal and horizontal directions allowed exact and reproducible positioning of 15 adjacent coronal slices used for rs-fMRI scan. The first slice was placed 2.5 mm rostrally of the bregma according to a stereotaxic mouse brain atlas (Franklin and Paxinos, 2007). An anatomical reference scan was acquired using FLASH sequence: field of view (FOV) = 23.7×14.0 mm^2, MD = 432×256, TR = 584.6 ms, TE = 4.6 ms, number of averages (NA) = 4. Subsequently, local field homogeneity was optimized using previously acquired field maps with an

implementation of MAPSHIM in ParaVision 5. BOLD fMRI data were acquired using a gradient-echo echo-planar (GE-EPI) imaging sequence adapted from (Grandjean et al., 2014b): FOV = 23.7×14.0 mm^2, MD = 90×60 yielding an in-plane resolution of 263×233 µm, slice thickness (STH) = 0.45 mm, slice gap = 0.05 mm, FA = 65º, bandwidth = 300 kHz, TR/TE = 1000/10 ms, NA = 1, with interlaced acquisition of slices, 400 volumes and a total rs-fMRI acquisition time 6.7 minutes.

Temporal SNR

Because tSNR were tested in several pilot studies with consist results, raw data from one mouse was used for this verification study. Time series were extracted from two region-of-interest (ROIs) drawn in the cortical (somatosensory cortex) and subcortical areas (striatum), respectively. The ratio of standard deviation and mean of the mean time course of each ROI was calculated as the estimation of tSNR.

Image pre-processing

Pre-processing was performed using Statistical Parametric Mapping (SPM8, Wellcome Trust Centre for Neuroimaging, UK), DPARSFA and FSL with the following pipeline. First, images were realigned with 6 rigid body parameters (correction for motion) after discarding the first ten volumes. No significant head movements were observed. The maximum translational and rotational movements of each mouse along each direction were within one voxel size and smaller than 0.01 degree, respectively. Second, functional images were normalized to an in-house EPI template using FSL's FLIRT (linear) followed by FNIRT (non-linear). Linear trends were removed. Finally, images were temporally filtered between 0.01 to 0.1Hz and spatially smoothed with a Gaussian kernel of full width at half maximum = 1.5 voxel size. Motion traces and blood vessel signals (an in-house blood vessel template) were regressed. A brain mask was created based on the EPI template and applied to all data before further processing.

Independent component analysis

Spatial Group Independent Component Analysis (ICA) (Calhoun et al., 2001) using the Group ICA of fMRI Toolbox v3.0a (GIFT) (http://mialab.mrn.org/software/gift/index.html) was performed on the rs-fMRI mice data using the Infomax algorithm. Because of the stochastic nature of most ICA algorithms, Himberg and colleagues (2004) (Himberg et al., 2004) proposed a method named ICASSO to investigate the reliability of estimated independent components (ICs) and a quality index I_q to quantify the compactness and isolation of each

IC. It performs an ICA algorithm for many times with slightly different conditions (initial conditions and/or randomly sampled data using bootstrapping) and combines the information from all runs to give the best stable estimates (Ma et al., 2011). ICASSO also provides a visual method (similarity graph) to investigate component clustering to aid component choice. In a pilot study, we investigated the number of components *N* = 15, 20, 25, 30, 40, 45, 50, 55, 60, 65, 70, 80 and 100 using ICASSO. For each number of components, Infomax was first performed for 20 times with varying initial conditions and bootstrapped data. Using a threshold of $I_q > 0.65$ (Ma et al., 2011; Mechling et al., 2014) and information from similarity graphs, reliable ICs at each run were kept. As shown in Figure 2-3, estimates from *N*=70, 80 and 100 displayed obvious decreased number of ICs with $I_q > 0.65$. These component number also showed decreased proportion of high quality component clusters with $I_q > 0.8$ compared with other dimensions. Unilateral components were observed in these high component numbers indicating potential split networks.

Although smaller *N*s such as 15, 20 and 25 generated higher percentages of stable ICs compared to 70, 80 and 100, they may underestimate the number of ICs indicating mixtures of various components, e.g. relatively larger clusters covering areas with unclear anatomical borders were observed at these lower *N*s. We observed that most anatomically meaningful ICs estimated by smaller *N*s could be detected using larger *N*s = 30, 40, 45, 50, 55, 60 and 65, while the larger *N*s also identified other ICs covering separated neuroanatomical regions as well as artefacts from plausible ventricle and blood vessel areas in mice. Therefore, we focused on $N = 30, 35, 40, 45, 50, 55, 60$ and 65 for further analysis. The final $N = 50$ was chosen based on two criterions: 1) ensuring the maximum spatial integrity and bi-laterality of rs-fMRI signals in recognizable neuroanatomical systems (Sforazzini et al., 2014); 2) the neuroanatomical systems identified by this N were able to be detected by at least more than half of the other *N*s from 30 to 65. The group maps were converted to z scores.

Statistics

Statistics were performed using FSL for each component. An EPI volume of one reference animal was used as the display bottom. Image overlays indicate p<=0.05 for one-sample t-test, with threshold-free cluster enhancement correction (TFCE). To aid anatomical identification, statistic test images were overlayed onto one normalized GE-EPI scan. Figure 2-4 shows the representative GE-EPI and anatomical template images of one mouse.

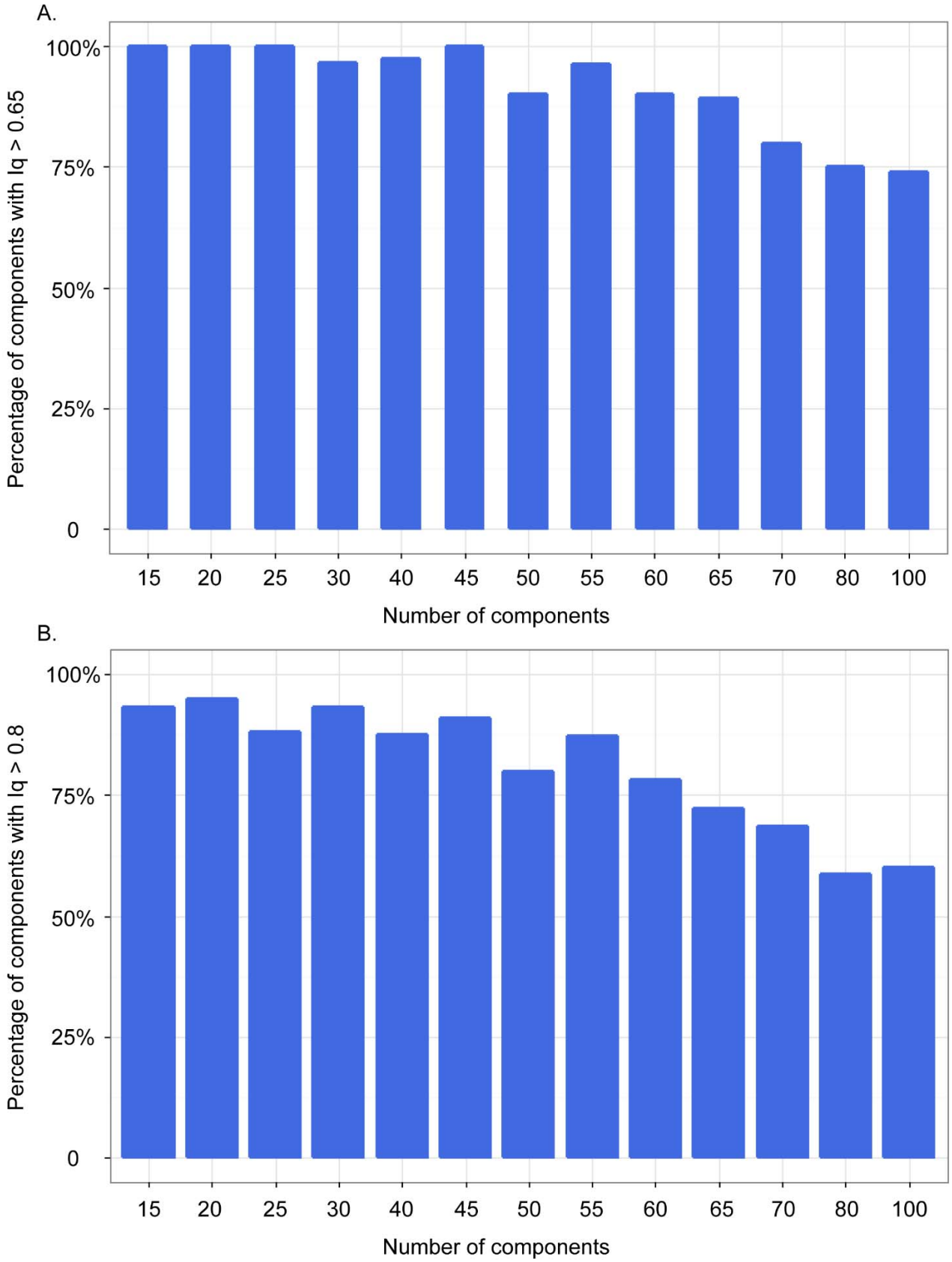

Figure 2-3 Investigations on the component stability for different user-defined component numbers. (A) Pronounced decrease of the ICs with Iq > 0.65 were seen when using *N*=70.,80,100. (B) The percentage of high quality components with *Iq* > 0.8 at each evaluated *N*. Higher *N*=65,70,80,100 showed reduced high quality components compared with other component numbers. The horizontal axis showed each unser-defined *N*. The

vertical axis showed the percentage of components with corresponding *Iq* thresholds in each graph.

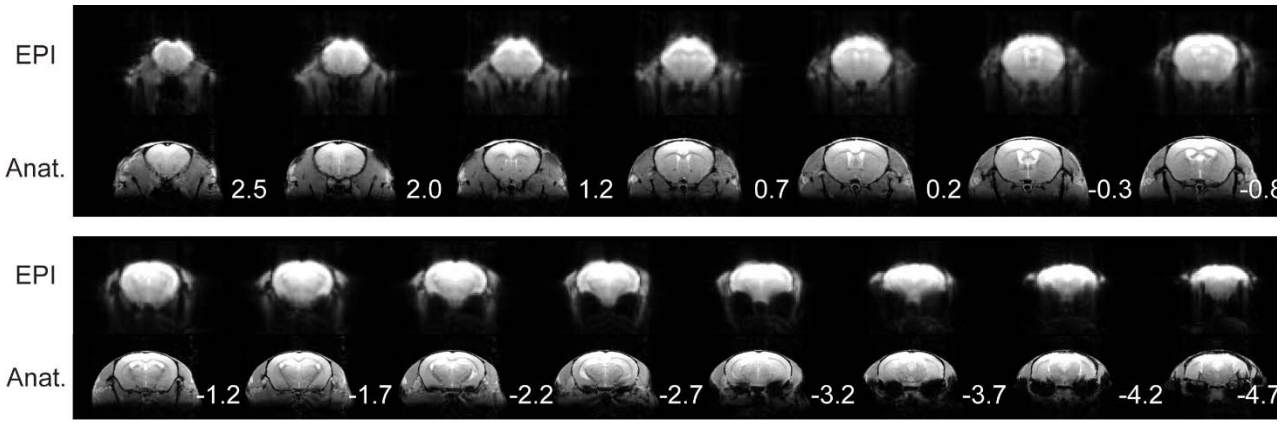

Figure 2-4 Representative anatomical template and the multi-slice GE-EPI image of one mouse. EPI images show minimum geometric distortions. The left labels of EPI and Anat. indicate image rows showing GE-EPI slices and a high resolution T2-weighted anatomical image of one representative mouse, respectively. EPI slices are the15 coronal sections through the mouse brain used to display the rs-fMRI results. Anatomical images are spatially matched with the GE-EPI images. Distances relative to bregma are shown on the right bottom of each anatomical slices. EPI: GE-EPI images. Anat.: anatomical images.

2.2.2.b Pipeline validation

Temporal SNR

Values of tSNR in the cortical and subcortical regions were 0.0123 and 0.0060, respectively. They were both smaller than 1%. The tSNR values from both cortical and subcortical areas showed enough temporal stability in the BOLD signals according to experience of experts and published results (Welvaert and Rosseel, 2013).

Physiological monitoring

Strict physiological control is critical to robust BOLD activations and reliable baseline conditions in rodent fMRI (Mueggler et al., 2012), therefore impacts on the interpretations of the results. Physiological readings reported by several previous published studies on mice rs-fMRI were listed in Table 2-1**Error! Reference source not found.**. In comparison to these reports, monitoring records from this study showed that all animals were under normal physiological states proving the reliability and reproducibility of our animal preparation procedures.

Published studies	Body temperature (°C)	Heartbeat (bpm)	SpO2 (%)	Breathing Rate (Resp/min)	Anaesthesia regimen and depth
(Jonckers et al., 2011)	37.0±0.5	Monitored	Monitored	Monitored	Medetomidine 0.6 mg/kg/h

(Guilfoyle et al., 2013)	37±0.2	500	-	50-70	Isoflurane 1.5%
(Mechling et al., 2014)	35.5±1.5	Monitored	97-99	Monitored	Medetomidine 0.6 mg/kg/ in 200 µl per hr
(Nasrallah et al., 2013)	36.9±0.1	200±27, 196±26, 206±24	98.0±0.5, 97.6±0.5, 97.0±2.0	100±10, 100±14, 124±17	Medetomidine 0.1 mg/kg/h, 0.6 mg/kg/h, 1.0 mg/kg/h

	Anaesthesia	Heart rate (bpm)	Breathing Rate (Resp/min)	O_2 saturation (%)
(Grandjean et al., 2014b)	Iso1	515.6 ± 22.3	80	95.8 ± 1.0
	Med0.1	335.0 ± 36.9	80	95.8 ± 1.0
	Med0.05	364.2 ± 14.0	80	97.0 ± 0.2
	Pro30	563.4 ± 29.5	80	97.1 ± 1.1
	Ure1.5	640.2 ± 10.5	80	95.6 ± 0.4
	Med/Iso	384.9 ± 3.8	80	96.7 ± 0.5

Table 2-1 Information on physiological parameter monitoring from several published studies on mouse using rs-fMRI. The sub-table in the last work was adapted from (Grandjean et al., 2014b).

Independent component analysis

Several functional systems in the cortical and sub-cortical areas were detected in this study as shown in Figure 2-5. In the cortical regions, we observed primary and secondary somatosensory cortex (S1/S2), motor cortex (M1/M2), cingulate cortex (Cg), retrosplenial dysgranular cortex (RSD), primary and secondary visual cortex (V1/V2), some portions of auditory cortex (AuD) and limbic areas (including some parts of insular, amygdala and piriform cortices) (Grandjean et al., 2014b). The subcortical systems were hippocampus (Hipp), thalamus (Th) and hypothalamus (HypoTh). Most networks in the cortical and sub-cortical areas showed bi-laterality across the two hemispheres.

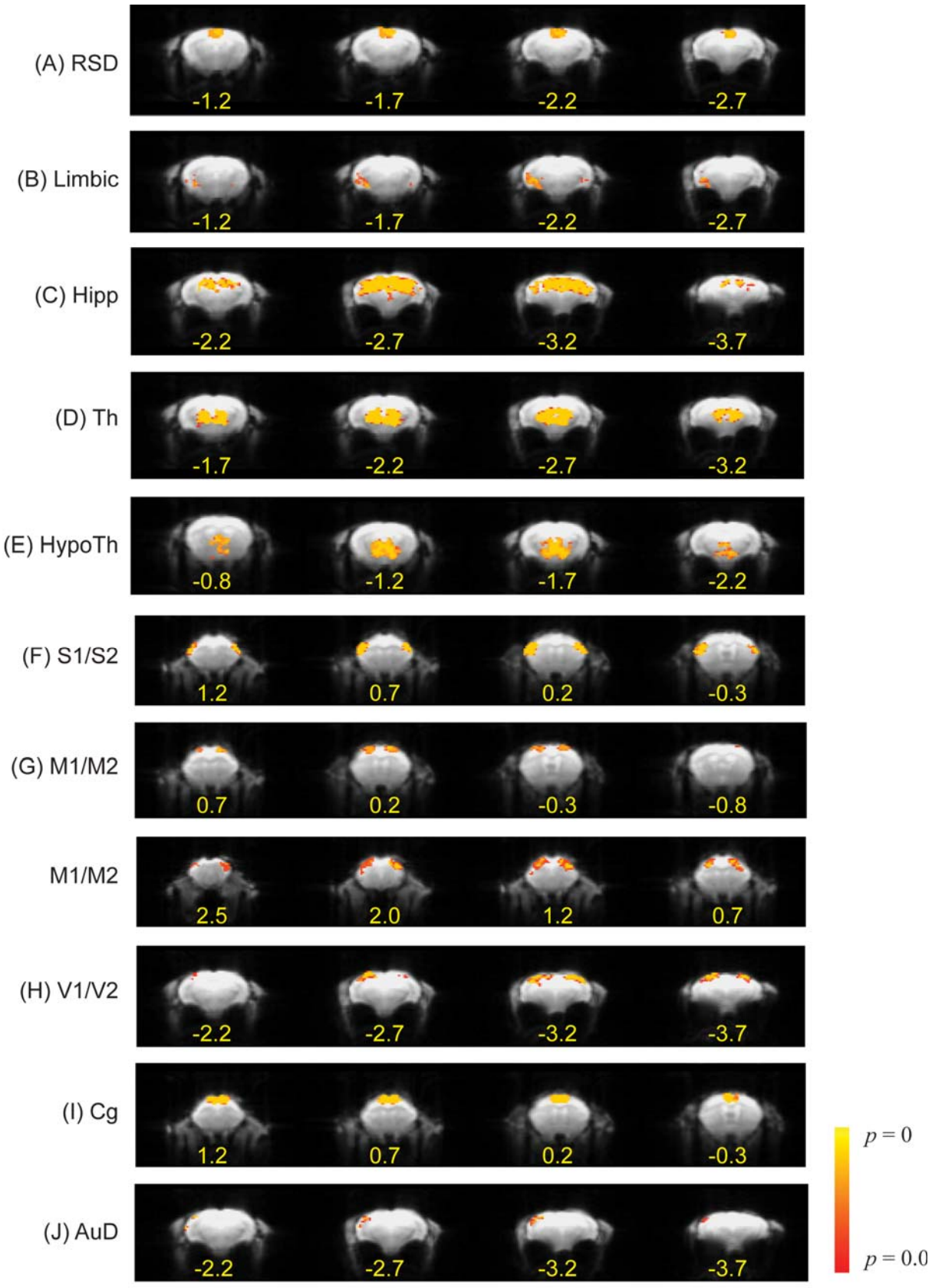

Figure 2-5 Functional systems revealed by 50-ICASSO. One-sample t test was performed with non-parametric permutation-based method. Image overlays indicate p<=0.05, with threshold-free cluster enhancement correction (TFCE) (A) Retrosplenial dysgranular cortex (RSD); (B) limbic areas (Limbic); (C) hippocampus (Hipp); (D) thalamus (Th); (E) hypothalamus (HypoTh); (F) primary and secondary somatosensory cortex (S1/S2); (G) primary and secondary motor cortex (M1/M2); (H) primary and secondary visual cortex

(V1/V2); (I) Cingulate cortex (Cg); (J) auditory cortex (AuD). Color bar shows the range of values in the maps. Distances (mm) relative to bregma are shown on the bottom of each image row.

The group ICA analysis revealed several cortical and subcortical RSNs in the mouse brain. These networks overlapped with known neuro-anatomical systems including somatosensory cortex, motor cortex, cingulate/retrosplenial cortex, limbic areas, visual cortex, auditory cortex, thalamus, hypothalamus and hippocampus. Most RSNs were bilaterally distributed across hemispheres. The unilateral limbic areas and auditory regions might be due to the relatively small sample size used in this study and the relative difficulty of the detection of them in mice, which could be supported by another thorough ICA analysis on mouse using rs-fMRI (Sforazzini et al., 2014). Under isoflurane, the unilateral limbic system encompassing some parts of amygdala and piriform cortex was also observed in (Grandjean et al., 2014b). However, both networks were observed in several animals in the pilot study with consistent bilateral distributions and anatomical boundaries (data not shown). Functional connectivity was not observed in the striatum in this study. This may be explained by the usage of isoflurane, which targets GABAergic receptors as a major component of its mode of action (Richards, 2002). The expression density of GABAergic receptors is very high in the striatum (Muller and Nistico, 1989), and this may lead to less retained activations in this region under isoflurane (Grandjean et al., 2014b). However, the other observed networks demonstrate that we were able to observe robust functional clusters from BOLD signals in mouse brains using the current experiment pipeline.

Summary

The goal of this study was to verify the newly established experiment pipeline. Rs-fMRI data from seven WT male C57Bl/6J mice were acquired with systematic physiological monitoring. High tSNR of BOLD signals was achieved. ICA was performed to investigate the existence and detectability of RSNs in the mouse brain. Stable and normal physiological parameters were observed reflecting the reliable and proper maintenance of the animal's physiological conditions. Several RSNs repeatedly reported by previous studies were revealed by both individual and group ICA analyses in this study. These results showed that the experimental pipeline for mice rs-fMRI is effective. Together with the minimum geometric distortion of the EPI images, high tSNR of the BOLD signals, we concluded that the experimental pipeline was successfully established and could be applied to further *DISC1* transgenic mouse study.

2.3 Application of the verified pipeline to *DISC1* transgenic mice

2.3.1 Animals and behavioural experiment

All experiments were performed in accordance with the University of Queensland Animal Ethics. Two heterozygous male mice of dominant-negative *DISC1* under control of the αCaMKII promoter (*αCaMKII-DN-DISC1*) were imported to the University of Queensland to set up a colony by mating with C57BL/6 mice (Hikida et al., 2007). Eleven heterozygous *αCaMKII-DN-DISC1* transgenic male mice (Tg) and ten littermate wild type male controls (Wt) were included in the experiment. All mice were normally housed in standard cages (3 or 4 litter mates per cage). Behavioral experiment design and implementation were the projects of another PhD student. Briefly, behavioral analysis was performed between 3 and 4 months of age, with intervals between different behavioral tasks of around 1 week. Both Tg and Wt mice were subjected to two behavioral tests: (1) Y maze spontaneous alternation (Dember and Fowler, 1958); (2) cue and contextual fear conditioning tests (Pattwell et al., 2011). *In vivo* rs-fMRI experiment was done after around one week including time for animals to adapt to the new environment where the 9.4T small animal MR system is located.

2.3.2 Animal preparation and physiological monitoring for rs-fMRI experiment

Rs-fMRI scanning was done on all mice weighing 29.8±2.1g (mean±std.). No statistically significant difference in body weight was detected between Tg and Wt groups. Animals were anaesthetized with isoflurane (induction 2-3%, maintenance 1.2%; Biomac Pty Ltd, Australia) and were placed prone on a cradle. Body temperature was maintained with an in-built warm water circulation. A rectal temperature probe (MR-compatible rectal temperature probe, SA Instruments, Inc. USA) was inserted to keep the animal at 36.9±0.4 ^{o}C. Breathing rate was monitored with a sensor pad (MR-compatible sensor, SA Instruments, Inc. USA) with an average breathing rate of 100.4±20.3 Resp/min. To measure SpO_2 and heartbeat, a MR-compatible infrared sensor (MR-compatible optical fiber, pulse oximeter sensor, SA Instruments, Inc. USA) was placed on the shaved left upper hind limb of the animals, with an average SpO2 of 95.7±3.4% and an average heartbeat of 416.2±65.3 bpm. One animal's physiological parameter recordings were not saved after scanning due to monitoring software problems. All parameter readings of this animal were normal and stable during rs-fMRI scanning according to hand-written records during the experiment. For accurate and reproducible positioning, the head of the mouse was fixed with a bite bar and a pair of stereotactic ear bars. Eye cream was applied to protect the animal's eyes from becoming dry.

2.3.3 MRI

MRI parameters used for data acquisition of this transgenic mouse study are the same as those described in 2.2.2.a.

2.4 Data analysis

2.4.1 Pre-processing pipelines used in this thesis

Different pre-processing pipelines were used in different chapters in this thesis. A regional connectivity study using the public data were pre-processed with pipelines based on FIX classifier (FMRIB's ICA-based Xnoiseifier v1.062 beta) (Salimi-Khorshidi et al., 2014; Zerbi et al., 2015), which were decided together with the collaborator working on the project. The study investigating network topologies across different anaesthetic regimens used traditional pre-processing pipelines, because of the network construction using the Allen Mouse Brain Atlas. Pre-processing pipelines performed on the *DISC1* mouse models in Chapter 5 also used standard pipelines. Specifically, pre-processing for ReHo and ICA studies of *DISC1* mouse models in Chapter 5 used the original spatial resolution, because of the much smaller computational time cost. Pre-processing for the functional network analysis using graph theory on *DISC1* mouse models in Chapter 5 used a higher spatial resolution to match with the resolution of the mouse brain atlas. Details of pre-processing pipeline will be further described in each study separately.

2.4.2 The mouse brain atlas

For analysis of the functional brain network using graph theory, AMBMC and the Allen Mouse Brain Atlas were used to construct the adjacency matrix in Chapter 4 and Chapter 5, respectively. Details will be described in 2.4.3.c and 2.4.3.d.

2.4.3 Post-processing analysis of the functional brain network

2.4.3.a Regional homogeneity analysis

ReHo is a local measure of the temporal similarity between a given voxel and its closest neighbours (Zang et al., 2004). It uses Kendall's coefficient of concordance (KCC) to define the ReHo value for a central voxel:

$$W = \frac{\sum (R_i)^2 - n(\bar{R})^2}{K^2 \left(n^3 - n\right)/12}, \qquad (0.1)$$

where W (ranging from 0 to 1) is the KCC of the time series of given voxels, R_i is the sum rank of the ith time point, $\bar{R}$ is the mean of all R_is, K is the number of time series in the measured neighbourhood ($K = 27$ in this study), and n is the number of ranks, or the length of the time series. No spatial smoothing was performed before ReHo calculation to reduce the introduction of artificial regional coherence influencing its reliability (Zuo et al., 2013). The KCC value was assigned to the given voxel. Individual ReHo maps were generated in a voxelwise way for all groups. A higher ReHo value implies a greater similarity within neighbouring voxel time courses. Spatial smoothing was applied with a 1.5x voxel size full-width at half-maximum (FWHM) Gaussian kernel. Mean ReHo maps were calculated for each group. ReHo was performed using the Data Processing Assistant for Resting-State fMRI (DPARSF) toolbox (Chao-Gan and Yu-Feng, 2010).

Statistical analysis of ReHo results from anaesthesia data

ReHo analysis was performed on both anaesthesia data and *DISC1* transgenic mice data for mapping the local connectivity patterns and potential variations across agents and abnormalities associated with *DISC1* gene, respectively. Therefore, details of statistical analysis will be described specifically in each relevant section of the corresponding chapters.

2.4.3.b ICA analysis on the *DISC1* transgenic mouse model

Various sources (components) contribute to BOLD signals in an unknown fashion that is not trivial to disentangle. ICA is a blind source separation tool aiming at recovering source signals in an explorative way (McKeown et al., 2003). It is data-driven with user-interaction only in the component selection stage. ICA maximizes statistical independence among the detected resting-state networks (RSNs) and has provided fruitful findings in fMRI studies. In this work, Spatial Group Independent Component Analysis (ICA) (Calhoun et al., 2001) using the Group ICA of fMRI Toolbox v3.0a (GIFT) run on MATLAB R2014a (http://mialab.mrn.org/software/gift/index.html) was performed on the rs-fMRI mice data based on Infomax algorithm. Because of the stochastic nature of most ICA algorithms, (Himberg et al., 2004) proposed a method named ICASSO to investigate the reliability of estimated independent components (ICs) and a quality index to quantify the compactness and isolation of each IC. It performs an ICA algorithm for many times with slightly different conditions (initial conditions and/or randomly sampled data using bootstrapping) and combines the information from all runs to give the best stable estimates (Ma et al., 2011). ICASSO also provides a visual method (similarity graph) to investigate component clustering to aid component choice. To search for the best estimated RSNs within each group and

maximize discrepancies of spatiotemporal properties between groups, ICA was run separately on each group. Following this approach, ICA was also run on one combined group to obtain an average statistical estimation of each RSN. Results from both approaches provided information on RSN activations potentially different between and shared by both groups (Cocchi et al., 2012a).

For the separate and combined ICA estimations on MV data, a pilot study was performed on a wide range of the number of components N = 35, 40, 45, 50, 55, 60, 65 using ICASSO. For each number of components, Infomax was first performed for 10 times with varying initial conditions and bootstrapped data. A threshold of I_q >0.65 (Ma et al., 2011; Mechling et al., 2014) and information from similarity graphs were used to identify reliable ICs at each run. All tested N showed high proportion of reliable ICs, i.e. above 90% of ICs yielded $I_q > 0.65$. Therefore, the choice of the best estimated number of component was based on the following considerations: (1) ensuring the maximum spatial integrity and bi-laterality of rs-fMRI signals in recognizable neuroanatomical systems (Sforazzini et al., 2014); (2) the neuroanatomical systems identified by this N were observed at least at more than half of the other Ns from 35 to 65. The optimum number of components for Tg and Wt groups hence were both 50. The optimum number of components for the combined group was 45. After estimations of group components, subject-wise components were obtained via back-reconstruction and scaled to empirical z-scores (Mannell et al., 2010). The identification of each neuroanatomical network was based on visual inspection and previous literatures on rodent rs-fMRI (Hutchison et al., 2010; Jonckers et al., 2011; Grandjean et al., 2014b; Mechling et al., 2014; Sforazzini et al., 2014; Zerbi et al., 2015).

The separate and combined ICA estimations on MVG data were performed in the same way as described above, except that the tested range of number of components were N=35, 40, 45, 50, 55, 60. The optimum number of components for separate Tg and Wt groups were 45 and 50, respectively. The optimum number of components for the combined group was also 40.

Statistical analysis

For MV data, within- and between-group statistical analyses were performed on results from both separate and combined groups. For each selected RSN, individual component maps were entered into FSL randomise for one-sample T-test, with threshold-free cluster enhancement (TFCE) (Smith and Nichols, 2009). Two-sample T-test was performed using randomise based on masks from one-sample T-test (Mannell et al., 2010; Luo et al., 2011).

Statistical significance was declared at $p < 0.05$, family-wise error rate (FWE) corrected. For a better visual display (Sforazzini et al., 2014; Zerbi et al., 2015), results from mean components were thresholded at $|Z| > 2$ (equivalent to $p < 0.05$, uncorrected). Components were overlaid onto the in-house EPI template to aid structural identification.

For MVG data, statistical tests were only performed on shared components revealed by the combined ICA approach.

2.4.3.c Graph analysis for investigation on the effects of different anaesthetics on the mouse brain

The whole brain atlas from Allen Brain Atlas (http://mouse.brain-map.org) was downloaded and registered to the MRI template. To reduce the number of ROIs, we merged children branches according to (Oh et al., 2014) and split merged ROIs into left and right. The final atlas contains 118 region of interest (ROI). The templates and data were multiplied by a factor of 10 in voxel spacing to adapt to human imaging software, with a final resolution 1x1x1 mm^3.

Complex network analysis

A 118 by 118 connectivity matrix was calculated for each animal. Connectivity was computed using Pearson's correlation coefficient. According to the different FC patterns detected in the brain under different anesthetics (Grandjean et al., 2014b), the connection densities of the functional brain networks might vary across groups. To keep the functional connectivity densities relatively comparable between groups, the choice of the threshold was based on correlation significance (Liang et al., 2011; Zuo et al., 2012; Mechling et al., 2014). Data without global signal regression showed higher correlation values on average. Therefore, to keep the threshold consistent across both datasets and to avoid disconnected networks, a threshold a_0 was estimated with statistical significance p=0.001 (uncorrected):

$$a_{ij} = \begin{cases} a_{ij}, & \text{if } a_{ij} > a_0 \\ 0, & \text{if } a_{ij} < a_0 \end{cases}. \qquad (0.2)$$

This yielded an undirected and weighted network for each subject (Zuo et al., 2012), and $a_{ij} = 0$ for all $i \in G$ where G is the set of nodes in a graph. To be more consistent with the modularity analysis in this study, this adjacency matrix was not binarized. It was further normalized before computing weighted network measures (Rubinov and Sporns, 2010).

A more conservative threshold a_0 estimated from p=0.0001 was also applied to construct the graph. GSR data, global and nodal attributes are similar.

Measures of global topology

The scaffold of functional brain networks could be abstracted as a sum of distributed brain regions and their functional interactions. In attempt to characterize this scaffold in mice and to understand its possible functional outcomes, the following global and nodal network measures were computed. Figure 2-6 showed a schematic illustration of the analysis pipeline.

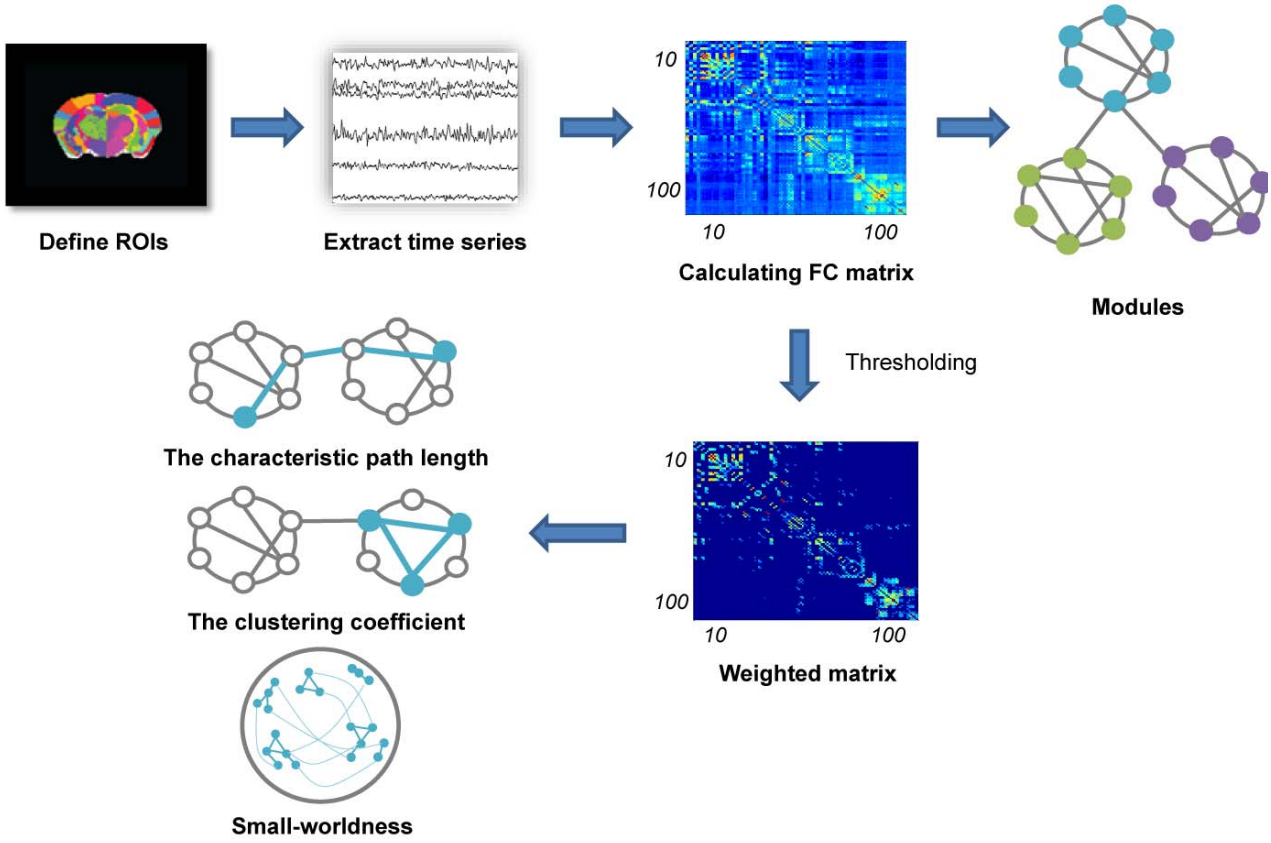

Figure 2-6 Schematic illustration of the graph analysis.

The characteristic path length is the mean of the shortest path length between all node pairs and was first introduced by (Watts and Strogatz, 1998). It provides information on the average separation between two nodes in a graph. A lower characteristic path length implies a potentially easier information combination from distributed node pairs. It characterizes the overall extent of functional integration achieved by a specific structure (Watts and Strogatz, 1998; Rubinov and Sporns, 2010). The weighted characteristic path length is defined as (Rubinov and Sporns, 2010):

$$L^w = \frac{1}{n}\sum_{i\in G}\frac{\sum_{i\neq j, j\in G} l_{ij}^w}{n-1}, \qquad (0.3)$$

where l_{ij}^w is the weighted shortest path length between node i and j, and n is the total number of nodes in the graph. Clustering coefficient is another commonly used parameter

to quantify structural properties of a network (Watts and Strogatz, 1998). If the nearest neighbors of an individual node are also nearest neighbors to each other, links between them form a triangle. Evidence suggests that in many real networks, some subgraphs formed by particular patterns of interactions are not purposeless and may reflect functional abilities. Therefore, as the simplest and most basic subgraph, triangles play an important role in the quantification of network features (Onnela et al., 2005; Saramaki et al., 2007). Nodal clustering coefficient measures the fraction of triangles attached to a node, with high nodal clustering coefficient indicating densely connected clusters, hence functional specialization at the local level. The average clustering coefficient therefore reflects the prevalence of triangles around individual nodes in the graph. Weighted clustering coefficient is defined as (Onnela et al., 2005; Saramaki et al., 2007; Rubinov and Sporns, 2010):

$$C^w = \frac{1}{n}\sum_{i\in G} C_i^w = \frac{1}{n}\sum_{i\in G} \frac{\sum_{j,g\in G}\left(w_{ij}w_{jg}w_{gi}\right)^{1/3}}{k_i\left(k_i-1\right)}, \tag{0.4}$$

where C_i^w is the weighted nodal clustering coefficient, w_{ij} is the normalized correlation weight between nodes i and j, and k_i is the degree of *ith* node. Basic network characteristics affect many network measures (Rubinov and Sporns, 2010). The two global parameters were also computed in null-hypothesis networks that contained the same node and link numbers, and degree distribution as the original networks. Ensembles of 20 random networks were generated using a network randomization algorithm proposed by (Maslov and Sneppen, 2002). The mean characteristic path length and clustering coefficient averaged over the 20 random networks were labeled as L_{rand}^w and C_{rand}^w. The normalized shortest path length and clustering coefficient were calculated as (Rubinov and Sporns, 2010):

$$lambda: \lambda^w = \frac{L^w}{L_{rand}^w}, \tag{0.5}$$

$$gamma: \gamma^w = \frac{C^w}{C_{rand}^w}, \tag{0.6}$$

The shortest path length and clustering coefficient individually measure functional integration and specialization of a network.

Small-worldness is another numeric measure of a network topology. It implies the coexistence of high clustering and short path length in the same network, hence a substrate supporting both distributed and specialized parallel information processing (Bassett and

Bullmore, 2006; Sporns and Honey, 2006). The small-worldness σ^w is a scalar defined as the ratio of γ^w and λ^w:

$$\sigma^w = \frac{\gamma^w}{\lambda^w}. \tag{0.7}$$

A network with small-world property has $\sigma^w > 1$ (Humphries and Gurney, 2008; Rubinov and Sporns, 2010).

To investigate the distribution of nodes with higher C_i^w for its potential contribution to global metrics, group-mean nodal clustering coefficients were calculated for each group. Ten nodes with the highest C_i^w were extracted for further examination.

Modules

Beyond descriptions of broadly distributed links and clusters, modules (communities) delineate a higher order structure observed in many real-world networks. They are non-overlapping subsets of networks with clear size and organization, and therefore represent meaningful partitions with specialized functions. Nodes within a module are tightly connected with each other, but sparsely linked with nodes in other modules (Girvan and Newman, 2002). Modularity is a scalar quantifying the goodness of a modularity partition. High modularity indicates reliable module divisions (Newman, 2006). Based on the traditional measure, Rubinov et al. (2011) (Rubinov and Sporns, 2011) proposed a generalized modularity for functional brain networks by using both positive and negative weights.The assumptions are that both positinve and negative weights contain meaningful information, but not equally important to community detection in functinal brain networks. This asymmetric modularity was defined as:

$$Q = Q^+ + \frac{s^-}{s^+ + s^-} Q^-, \tag{0.8}$$

where Q^+ and Q^- is the modularity, i.e. contributions to Q calculated using positive and negative weights, respectively. s^+ and s^- is the total weight summed over all positive and negative weights, respectively. In this study, we used Q as the measure of community partition quality. (Rubinov and Sporns, 2011)

Group-average networks were obtained by averaging over the z-score networks of each subject within each individual group (Power et al., 2011; Rubinov and Sporns, 2011; Power et al., 2013; Mechling et al., 2014; Liska et al., 2015). To characterize the degeneracy of modularity, community detection was performed on the group-average networks using the algorithm proposed by Rubinov et al. (Rubinov and Sporns, 2011). The degeneracy of high-

modularity partitions is the existence of distinct topological partitions with similar high modularity values (Good et al., 2010). The algorithm has two steps.

Firstly, a modularity-maximization Louvain method (Blondel et al., 2008) was used to detect seed partitions. It is a greedy optimization approach and searches for high modularity partitions in two phases. Briefly, initial partition started by assigning each node as an individual community. In the first phase, the method looked for a local maxima of modularity by moving each node to its neighbor communities sequentially and repeatedly. In the second phase, it aggregated nodes in the same community discovered during the first phase and built a new network whose nodes were the communities. The two phases were iteratively repeated until no more increase of the modularity could be achieved. I performed Louvain method for 1000 times for each network. These seed partitions were further refined with a fine-tuning algorithm (Sun et al., 2009). It iteratively refined each seed partition by randomly moving all nodes between modules and calculating the corresponding modularity changes. Node moves that resulted in increased modularity were considered and the corresponding moves were fixed for this node. At each iteration, each node was examined once. The iteration was repeated until no increase in modularity could be achieved. This step generated 1000 seed partitions representing the peak plateau in the modularity landscape of each functional network (Good et al., 2010; Rubinov and Sporns, 2011). The topology of seed partitions showed high consistency.

The second step was an effort to evenly sample and systematically search for high-modularity degenerate partitions of the network. Specifically, another iteration of fine-tuning algorithm was performed on the seed partitions with incorporated random moves of randomly chosen nodes. The range of the probability of random moves was from 0 to 0.05 with a step of 5×10^{-5}. Partitions with modularity among the top 1% of the estimated maximum value were chosen to be degenerate partition candidates (Rubinov and Sporns, 2011).

A large ensemble of high-Q candidates were discovered for each network. The number of distinct topologies, i.e. degenerate partitions, was very small in comparison to this ensemble of all discovered candidates, indicating a significant consistency of detected module structures. In light of this observation, topological information from all candidates was used to create a representative module affiliation for each functional network (Liska et al., 2015). Briefly, a node was assigned to a module if it was affiliated with this module in more than 50% of the high-Q candidates. Distances between degenerate high-modularity partitions of each network were calculated using the variation of information (VI). Corresponding null-networks were created for each group (Rubinov and Sporns, 2011). I

observed many distinct degenerate partitions in the null-networks demanding high consumption of computational time on VI. Therefore, to estimate the mean VI of all the degenerate partitions of null networks, 500 degenerate partitions were randomly selected from all partitions detected in one null network. This process was repeated five times. The averaged VI over the 2500 randomly selected partitions was then used as an estimation of the mean VI of null-network degenerate partitions.

Statistics

Statistic tests were performed using MATLAB R2014a (The MathWorks, USA). Because the distribution properties of the above graph parameters are not well-known (Bullmore and Bassett, 2011; Uehara et al., 2014), a non-parametric Kruskal-Wallis test was applied to global metrics to evaluate the differences between groups, significance was declared using $p < 0.05$. Follow-up statistics were performed with the Wilcoxon rank sum test. Significance was declared using $p < 0.05$ with False Discovery Rate (FDR) correction.

2.4.3.d Graph analysis on the *DISC1* transgenic mouse model

The whole brain atlas from Allen Brain Atlas (http://mouse.brain-map.org) was downloaded and registered to AMBMC template. To reduce the number of ROIs, we merged children branches according to (Oh et al., 2014) and split merged ROIs into left and right. The final atlas contains 152 regions of interest (ROI). The templates and data were multiplied by a factor of 10 in voxel spacing to adapt to human imaging software.

Complex network analysis

A 152 by 152 connectivity matrix was calculated for each animal. Functional connectivity (FC) was computed using Pearson's correlation coefficient. To simplify analysis, the individual connectivity matrix was thresholded with a broad range of edge densities from 5% to 40% with a step size of 5%. Connectivity values within the largest X% of values in each FC matrix were set to 1 indicating the presence of a connection, while all the other values were set to 0 indicating the absence of a connection. The binary and undirected matrix contains information on the strong and significant connections constructing the scaffold of the functional brain network. Both global and local network attributes were calculated to characterize the topological properties (Rubinov and Sporns, 2010).

Measures of global and nodal topology

The definition and meaning of the following parameters are the same as described in 2.4.3.c., but the corresponding unweighted equations are used in this section. The shortest path length L (also known as the geodesic distance) is defined as infinite between disconnected vertices, hence L is alternatively defined as the harmonic mean of geodesic distances between all nodes (Latora and Marchiori, 2001; Newman, 2003; Hayasaka and Laurienti, 2010; Uehara et al., 2014),

$$L = \frac{n(n-1)}{\sum_{i \neq j \in G} l_{ij}^{-1}}, \tag{0.9}$$

where l_{ij} is the geodesic distance between nodes i and j. G is a set of nodes in a graph, and n is the total number of nodes in the graph. The average clustering coefficient reflects the prevalence of triangles around individual nodes in the graph. The unweighted clustering coefficient is defined as (Rubinov and Sporns, 2010):

$$C = \frac{1}{n}\sum_{i \in G} C_i = \frac{1}{n}\sum_{i \in G} \frac{2\Delta_i}{k_i(k_i - 1)}, \tag{0.10}$$

where C_i is the nodal clustering coefficient of node i, Δ_i is the number of triangles around the ith node and k_i is the degree of the ith node. Basic network characteristics affect many network measures (Rubinov and Sporns, 2010). The two global parameters were also computed in null-hypothesis networks that contained the same number of nodes and preserved degree distribution as those of the original networks at the same connection densities. Ensembles of 20 random networks were generated using a network randomization algorithm proposed by (Maslov and Sneppen, 2002). The mean characteristic path length and clustering coefficient averaged over the 20 random networks were labeled as L_r and C_r. The normalized shortest path length and clustering coefficient were calculated as (Rubinov and Sporns, 2010):

$$lambda: \lambda = \frac{L}{L_r}, \tag{0.11}$$

$$gamma: \gamma = \frac{C}{C_r}, \tag{0.12}$$

The shortest path length and clustering coefficient individually measure functional integration and specialization of a network.

The small-worldness σ is a scaler defined as the ratio of γ and λ:

$$\sigma = \frac{\gamma}{\lambda}. \tag{0.13}$$

A network with small-world property has $\sigma > 1$ (Humphries and Gurney, 2008; Rubinov and Sporns, 2010).

The nodal property was investigated using nodal clustering coefficient as described above. It measured how closely a particular region and its immediate neighbors were connected to each other, hence an indicator of functional specialization at regional level. The node global efficiency is another local graph measurement investigated in this study measuring the extent of information transmission between one node to all other nodes in the network. It is defined as (Achard and Bullmore, 2007; Rubinov and Sporns, 2010):

$$E(i) = \frac{1}{n-1} \sum_{i \neq j \in G,} \frac{1}{l_{ij}}, \tag{0.14}$$

where $E(i)$ is the *i*th node's global efficiency. Shorter path lengths imply faster interactions, therefore higher $E(i)$ implies higher communicating efficacy between node *i* to the remaining nodes in the network.

Modules

Module analysis was performed as the same as described in 2.4.3.c.

Statistics

For both MV and MVG data, a two-tailed two-sample t test was carried out on each global attribute to investigate the significance of any between-group differences. A separate t test was performed on each global network measurement at each connection density. For the nodal attribute, a two-sample t test was performed for each of the 152 regions. After the multiple comparison tests, an alpha level of 1/n (p<0.01) was used to declare the significance for the local properties (Lynall et al., 2010; Cocchi et al., 2012b; Liu et al., 2014). Statistic tests were performed using MATLAB R2014a (The MathWorks, USA).

Chapter 3 Altered regional connectivity reflecting effects of different anaesthesia protocols in the mouse brain

3.1 Abstract

Studies in mice using resting-state functional magnetic resonance imaging (rs-fMRI) have provided opportunities to investigate the effects of pharmacological manipulations on brain function and map the phenotypes of mouse models of human brain disorders. Mouse rs-fMRI is typically performed under anaesthesia, which induces both regional suppression of brain activity and disruption of large-scale neural networks. Previous comparative studies using rodents investigating various drug effects on long-distance functional connectivity (FC) have reported agent-specific FC patterns, however, effects of regional suppression are sparsely explored. Here we examined changes in regional connectivity under six different anaesthesia conditions using mouse rs-fMRI with the goal of refining the framework of understanding the brain activation under anaesthesia at a local level. Regional homogeneity (ReHo) was used to map local synchronization in the brain, followed by analysis of several brain areas based on ReHo maps. The results revealed high local coherence in most brain areas. The primary somatosensory cortex and caudate-putamen showed agent-specific properties. Lower local coherence in the cingulate cortex was observed under medetomidine, particularly when compared to the combination of medetomidine and isoflurane. The thalamus was associated with retained local coherence across anaesthetic levels and multiple nuclei. These results show that anaesthesia induced by the investigated anaesthetics through different molecular targets promote agent-specific regional connectivity. In addition, ReHo is a data-driven method with minimum user interaction, easy to use and fast to compute. Given that examination of the brain at a local level is widely applied in human rs-fMRI studies, our results show its sensitivity to extract information on varied neuronal activity under six different regimens relevant to mouse functional imaging. These results, therefore, will inform future rs-fMRI studies on mice and the type of anaesthetic agent used, and will help to bridge observations between this burgeoning research field and ongoing human research across analytical scales.

3.2 Introduction

Resting-state functional magnetic resonance imaging (rs-fMRI) is a popular translational fMRI approach to characterize whole brain activity in different species (Biswal, 2012; Pan et al., 2015). Rodent fMRI has been providing an increasing contribution to neuroscience research given the use of murine models in pharmacological studies (Shah et al., 2015; Shah et al., 2016a) and the wide availability of transgenic mouse models (Shah et al., 2013; Grandjean et al., 2014c; Zhan et al., 2014; Haberl et al., 2015; Grandjean et al., 2016).

These studies further help to translate preclinical findings to research on humans, and may help to link molecular events that are known to occur in these models to specific fMRI signatures found in both the models and human diseases. A major feature of rodent functional imaging has been the use of anesthesia, which eases the restrain on the subjects, and controls stress levels, while mouse awake imaging with fMRI was reported impracticable (Jonckers et al., 2014). Previous studies repeatedly observed several resting-state functional networks (RSNs) in mice under different anaesthetic regimen (Jonckers et al., 2011; Guilfoyle et al., 2013; Grandjean et al., 2014b; Mechling et al., 2014; Nasrallah et al., 2014a; Sforazzini et al., 2014; Liska et al., 2015). Comparative studies on rodents reported agent-specific characteristics in functional connectivity (FC) patterns (Williams et al., 2010; Grandjean et al., 2014b; Jonckers et al., 2014). Although there are many points of agreements between these studies, many aspects of the anesthetic effect remain to be uncovered.

Anaesthesia is widely used in the practice of medicine and scientific research. In general, the mechanisms of actions of general anaesthetics are not yet well understood and remain an important question in medicine and neuroscience (Brown et al., 2010). Numerous findings from clinical and research applications suggest that anaesthetics do not affect the brain uniformly and do not all act in the same way. Anaesthetics cause both regionally specific suppression of brain activity and impaired interactions between distributed functional networks (Heinke and Koelsch, 2005). Many studies have examined changes of large-scale functional networks under anaesthesia, supporting the hypothesis that the anaesthetic-induced unconsciousness is a failure of information integration. The more distributed and complex a neural system is, the more vulnerable it may be to accumulated local disruptions. Although the causal relationship between regional suppression and large-scale FC changes remain unclear, alterations of local connectivity within a brain region has been proposed to be equally important for understanding unimodal and multimodal information integration (Hudetz, 2012). These notions suggest that changed functions of the brain as a whole under anaesthesia may at least partially originate from local disturbances of neuronal activity induced by drugs.

Studies investigating anaesthetic effects in human and rodents (Peltier et al., 2005; Lu et al., 2012; MacDonald et al., 2015; Song and Yu, 2015) have mainly adopted independent component analysis (ICA) and/or seed-based analysis (SBA) focusing on synchronous neural activity across the whole brain and/or brain regions that are anatomically distant from each other. However, the effects of anaesthetic agents on local neural activity driven by smaller units of neuronal organization are rarely investigated by rs-fMRI. Regional

homogeneity (ReHo) measures the temporal similarity between a given voxel and its closest neighbours (Zang et al., 2004). Whereas ICA and seed-based FC analysis provide information on inter-regional synchronization of spontaneous fMRI signals, ReHo provides information on intra-regional synchronization. It has been used in many studies investigating neurological disorders in humans (Cao et al., 2006; Liu et al., 2006; He et al., 2007; Yuan et al., 2008; Wu et al., 2009; Paakki et al., 2010). In the context of anesthesia, mapping the regional characteristics of brain activation under different anaesthesia conditions becomes relevant when investigating regional disturbances in neural activity. Furthermore, ReHo analysis presents an additional advantage over the major rs-fMRI analysis schemes, in that it requires minimal user interaction, and is therefore robust to individual bias. This is in contrast to ICA or SBA, where the user interaction is expected to provide either the number of components in the ICA decomposition, or a selection of seeds. Either approach may lead to differences between studies that made it difficult to draw direct comparisons. ReHo is also efficient in computation and very robust against noise (Jiang and Zuo, 2015). Based on voxelwise ReHo maps and motivated by the desire to gain more comprehensive information on the characteristics of regional neural activity, this study further investigated how the distribution of local connectivity among small clusters spreads within brain areas, with a specific focus on the cingulate cortex, primary somatosensory cortex (barrel field), insular cortex, caudate putamen, hippocampus and thalamus.

Anaesthetics and/or sedatives are commonly used in preclinical rodent experiments including alpha-chloralose, isoflurane or halothane, medetomidine, propofol and urethane. Alpha-chloralose is not suitable for longitudinal studies due to its depressive effects on respiration and toxicity (Haensel et al., 2015; Pan et al., 2015; Petrinovic et al., 2016). One recent study reported that this agent led to unstable physiological maintenance of mice for fMRI studies when compared to isoflurane (Low et al., 2016a). It is hence an agent unsuitable for longitudinal mouse rs-fMRI experiments. Halothane and isoflurane are inhalation anaesthetics commonly used in studies involving animals, among which isoflurane is the mostly used anaesthetic in laboratory animals (Tremoleda et al., 2012; Haensel et al., 2015). However, it is a well-known vasodilatory agent that increases the baseline cerebral blood flow in a dose-dependent way, and hence may influence neurovascular interactions that could be detected by fMRI technique. Although increasingly used in rodent studies, medetomidine induces negative effects on cardiovascular functions and causes dose-dependent vasoconstriction (Sinclair, 2003; Jonckers et al., 2015). In addition, animals under medetomidine anaesthesia were reported to show epileptic activities (Fukuda et al., 2013; Grandjean et al., 2014b). Fukuda et al. (2013) proposed a combination

of low-dose isoflurane and dexmedetomidine to suppress potential epileptic activity without sacrificing the desired effects of medetomidine. In addition, the vasodilatory effect of isoflurane and the vasoconstrictive effect of medetomidine appeared to compromise each other (Fukuda et al., 2013), showing promising effects of the combination regimen for rodent fMRI experiments. This study compared changes in regional connectivity in mice using rs-fMRI under six anaesthesia regimens relevant to rodent functional imaging studies: isoflurane, two different doses of medetomidine, propofol, urethane, and a combination of medetomidine and isoflurane. After ReHo calculation, several regions of interest (ROIs) were chosen to further investigate how local connectivity distributed within these regions and differed between them. The results shed light on the accumulative and region-specific characteristics of the brain and may help bridge imaging studies in humans and mouse models.

3.3 Materials and methods

3.3.1 Data acquisition

Please find details of the data acquisition for this study in Chapter 2 Materials and Methods, Section 2.1.1 Data acquisition.

3.3.2 Systemic physiological measurement

Please find details of the systemic physiological monitoring for this study in Chapter 2 Materials and Methods, Section 2.1.2 Systemic physiological measurement.

3.3.3 Pre-processing

Images were preprocessed using FSL (FMRIB Software Library 5.0.2, http://fsl.fmrib.ox.ac.uk*).* The image size was multiplied by 10, and the first 10 volumes in each scan were removed to allow for the T_1 relaxation effect, followed by motion correction (MCFLIRT*),* B0 field correction (FAST), and brain extraction (BET). The EPI images were co-registered to the AMBMC template (Australian Mouse Brain Mapping Consortium, http://www.imaging.org.au/AMBMC) (Janke et al., 2012) using ANTs (Advanced Normalization Tools 2.1.0, http://picsl.upenn.edu/software/ants/*)* using linear affine and non-linear greedy SyN transformation. Individual-level ICA was performed with MELODIC using automatic dimensionality estimation. Half the scans from each group were randomly assigned to the training dataset to estimate a study-specific FIX classifier encompassing each group (FMRIB's ICA-based Xnoiseifier v1.062 beta) (Salimi-Khorshidi et al., 2014; Zerbi et al., 2015). Components in the training datasets were manually labelled as 'noise' if:

i) they co-localized mostly with the boundaries of the brain and/or presented a highly repetitive temporal profile (motion artefact); ii) they co-localized with major blood vessels in the brain (vascular artefact) (Dorr et al., 2007); iii) they indicated an equipment/acquisition-related artefact such as single-slice components, spike-related components, and ripple components (alternation between positive and negative correlations in the wave form). The classifier was used to sort the individual-level components into 'signal', 'noise', and 'unknown'. The temporal profiles from 'noise' components were regressed from the EPI images. The accuracy of the classification was compared against manually sorted components. Signal-related components were labelled according to the following rules, based on (Grandjean et al., 2014b) and (Zerbi et al., 2015): i) bilateral topological organization, or ii) unilateral organization with existing matching contralateral component, iii) overlap with plausible grey matter regions, iv) predominantly low-frequency power spectra (0.01-0.3Hz), v) no seamless crossing of white matter and/or ventricle boundaries, vi) the components did not match the description of the three classes of noise (motion, vascular, or acquisition-related artefacts). Components overlapping mostly with tissues outside the brain were not included in the 'noise' component list. The majority of the components, between 39 and 91 on average in each group, could not be manually sorted in either of the categories (Appendix A). Automatic noise classification with FIX was highly specific and no component manually labelled as 'signal' was classified as 'noise' by the FIX algorithm (Appendix A). Motion and vascular artefacts were correctly sorted into the 'noise' category in 92-100% and 67-98% of the cases, respectively, while sorting of equipment/acquisition artefacts was less sensitive with 50-75% of the components automatically recognized as 'noise' (Appendix A).

3.3.4 Regional homogeneity (ReHo) analysis

Please find details of ReHo analysis in Chapter 2 Materials and Methods, Section 2.4.3.a.

3.3.5 ROI analysis

Six ROIs were selected based on anatomical relevance, the cingulate cortex, primary somatosensory cortex (barrel field), insular cortex, caudate-putamen, and hippocampus were based on the AMBMC atlas (Richards et al., 2011; Ullmann et al., 2013; Ullmann et al., 2014) and the thalamus was based on (Zerbi et al., 2015). Data extracted from left and right ROIs were combined for analysis (Figure 3-1). ReHo values were extracted using these ROIs for each animal in each group.

3.3.6 Statistics

Voxelwise statistics were performed with non-parametric F-Tests and two-sample unpaired t-tests (FSL Randomise), 500 permutations for the F-Tests to detect global differences and 1000 permutations for t-tests to compare all groups with each other. Image overlays indicate colour-coded t-values surviving threshold-free cluster enhancement correction (TFCE).

For ROI analysis, One-way ANOVA (p<0.05) was performed to test the global difference, followed by an unpaired t test with false discovery rate (FDR) correction using a significance level of p<0.05. Statistics were performed using MATLAB R2015a (The MathWorks, Natick, Massachusetts, U.S.A). Descriptive statistics are given as mean±1 standard deviation (SD). To verify the similarity of distributions of regional connectivity strengths across anaesthetics between two hemispheres, caudate-putamen and primary somatosensory cortex (barrel field) were split into left and right parts. ReHo values were extracted from the four ROIs, respectively.

3.4 Results

3.4.1 Physiological parameters

Animals were under normal physiological conditions with the complete information of the physiological parameters recorded non-invasively. Oxygen saturation was maintained at 95% or above in all anaesthesia condition (*Propofol30*: 97.1±1.1, *Isoflurane1*: 95.8±1.0, *Urethane1.5*: 95.6±0.4, *Medetomidine0.1*: 95.8±1.0, *Medetomidine0.05*: 97.0±0.2, *Mediso*: 96.7±0.5). Pulse distention was lowest for *Urethane1.5* (10.1±0.5 µm), *Isoflurane1* (12.8±0.3 µm), and *Medetomidine0.05* (16.2±2.4 µm), while *Medetomidine0.1* (21.6±7.1 µm) and *Mediso* (29.4±4.5 µm) presented intermediate values, and *Propofol30* the highest (44.2±10.1 µm). Adapted from (Grandjean et al., 2014b).

3.4.2 Voxelwise analysis of regional homogeneity

The distribution of ReHo in the brain is presented using thresholded (Figure 3-1) and unthresholded (Appendix B) group-mean maps. Thresholded maps showed the distributive characteristics of ReHo more clearly within each group. Most anaesthetic regimens were associated with high ReHo values in the cortical areas, e.g. the cingulate cortex, primary somatosensory cortex and insular cortex. Retained ReHo in the caudate-putamen was observed in the *Medetomidine0.1*, *Medetomidine0.05*, *Mediso* and *Urethane1.5* groups. *Urethane1.5* and *Propofol30* were associated with higher ReHo in the thalamus and

hippocampus compared to other groups. *Mediso* and *Isoflurane1* also yielded high ReHo in some parts of the hippocampus. Unthresholded group-mean maps revealed similar information, with cortical areas and the caudate-putamen being the most highlighted brain regions (Appendix B).

The two-sample unpaired t-test was performed to search for between-group differences in a voxelwise way across the entire brain. Regions showing changed ReHo values were mainly located in the primary somatosensory cortex (particularly the barrel field) and caudate-putamen. In cortical areas, *Isoflurane1* and *Mediso* yielded statistically significantly higher ReHo than *Medetomidine0.1* or *Urethane1.5* (Figure 3-2 A, D, E and F). *Propofol30* was associated with higher ReHo than *Medetomidine0.1* in some sections of cortical areas (Figure 3-2 G). In the caudate-putamen, *Isoflurane1* yielded significantly lower ReHo compared to *Medetomidine0.1*, *Medetomidine0.05* and *Mediso* (Figure 3-2 A, B and C). In the thalamus, *Propofol30* was associated with higher ReHo than *Medetomidine0.1* (Figure 3-2 G). Compared to *Urethane1.5*, *Isoflurane1* and *Mediso* yielded significantly lower ReHo in some areas in the caudate-putamen and hypothalamus, respectively (Figure 3-2 D and F).

Two brain areas, i.e. striatum and somatosensory cortex, in the statistical maps yielded some unilateral significant results between anaesthetics. However, further investigations of the average strength of ReHo values in the left and right part of the two regions showed very similar distributions across hemispheres. This indicated that effects of anaesthetics were presented in both sides of the brain (Appendix C).

3.4.3 ROI analysis

Selected ROI analysis based on ReHo maps further revealed how the local connectivity is distributed in several brain regions under different agents (Figure 3-3). One-way ANOVA revealed that there were significant between-group differences in the cingulate cortex ($F_{(5,51)}$=2.42, p=4.84×10^{-2}), primary somatosensory cortex (barrel field) ($F_{(5,51)}$=7.04, p=4.52×10^{-5}), caudate-putamen ($F_{(5,51)}$=2.51, p=4.15×10^{-2}) and thalamus ($F_{(5,51)}$=2.43, p=4.77×10^{-2}). No significant differences were detected in the insular cortex or hippocampus. The highest regional connectivity within cortical areas was observed in the *Mediso* group (cingulate cortex, ReHo=0.71±0.05; primary somatosensory cortex (barrel field), ReHo=0.70±0.04; insular, ReHo=0.63±0.04). Higher regional connectivity within the primary somatosensory cortex (barrel field) and insular cortex were also observed in the *Isoflurane1* group (ReHo=0.69±0.06 and ReHo=0.58±0.08, respectively). In the cingulate cortex, *Propofol30* and *Medetomidine0.05* were associated with higher regional connectivity

(ReHo=0.68±0.04 and ReHo=0.67±0.06). Post hoc tests revealed that *Mediso* yielded higher ReHo than *Medetomidine0.1* in the cingulate cortex. In primary somatosensory cortex (barrel field), *Mediso* and *Isoflurane1* showed significantly higher ReHo than *Medetomidine0.1* or *Urethane1.5*.

Within the caudate-putamen, higher ReHo was observed for *Mediso* (ReHo=0.67±0.04), *Medetomidine0.1* (ReHo=0.66±0.04), *Medetomidine0.05* (ReHo=0.66±0.02) and *Urethane1.5* (ReHo=0.65±0.08). *Propofol30* yielded the highest regional connectivity in both the hippocampus and thalamus (ReHo=0.52±0.03 and ReHo=0.62±0.05, respectively). Most other groups were associated with similar regional coherence in the hippocampus. Higher regional coherence within the thalamus was observed for *Isoflurane1*, *Medetomidine0.05* and *Urethane1.5* (ReHo=0.57±0.05, ReHo=0.58±0.09 and ReHo=0.60±0.05, respectively). Post hoc analysis further revealed that *Propofol30* and *Isoflurane1* showed significantly reduced regional coherence in the caudate-putamen compared to *Mediso* or *Medetomidine0.1*. *Propofol30* also showed significantly lower regional coherence than *Medetomidine0.05* in this brain region. Post hoc analysis suggested significant between-group differences in the thalamus, although none survived FDR correction. To be consistent with ANOVA, the results before FDR correction in the thalamus are presented in Figure 3-3. *Propofol30* showed higher regional connectivity than *Isoflurane1*, *Medetomidine0.1* and *Mediso*, while *Urethane1.5* showed higher ReHo than *Medetomidine0.1*.

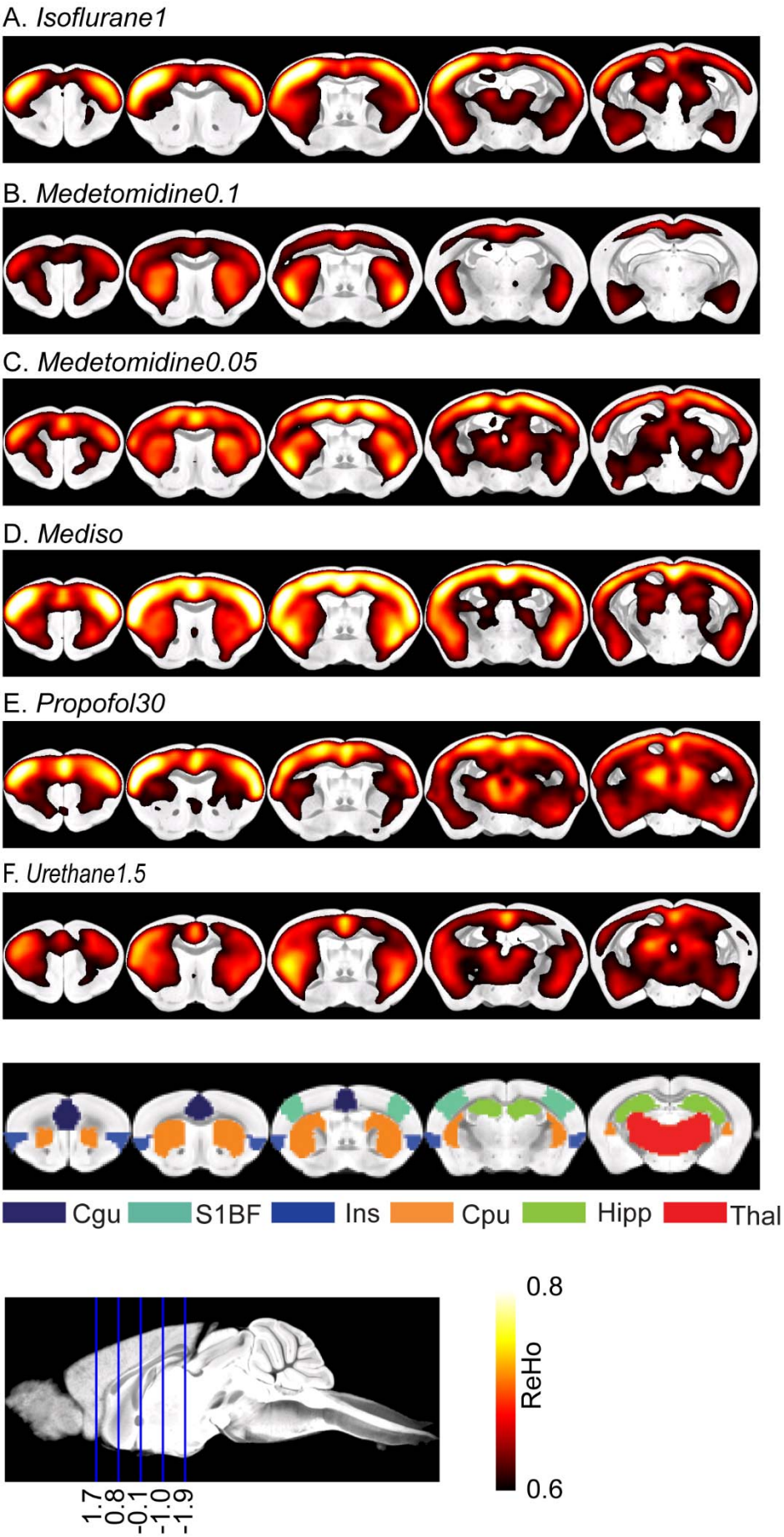
A. Isoflurane1
B. Medetomidine0.1
C. Medetomidine0.05
D. Mediso
E. Propofol30
F. Urethane1.5
Cgu
S1BF
Ins
Cpu
Hipp
Thal
0.8
ReHo
0.6
1.7
0.8
-0.1
-1.0
-1.9

Figure 3-1 Thresholded group-mean maps showing the distribution of ReHo values for *Isoflurane1* (A), *Medetomidine0.1* (B), *Medetomidine0.05* (C), *Mediso* (D), *Propofol30* (E), and *Urethane1.5* (F) groups. Marked ReHo was found in the cortex, predominantly in the *Isoflurane1*, *Medetomidine0.05*, *Mediso*, and *Propofol30* groups, encompassing the whole sensory-motor cortex, and cingulate cortex, and in the case of *Isoflurane1*, *Mediso*, and *Propofol30*, including the cortical sub-plate, such as the amygdala. Striatal ReHo was mostly found to overlap with the caudate-putamen, principally in *Medetomidine0.1, Medetomidine0.05, Mediso,* and *Urethane1.5* groups. ReHo was found to be weak in the hippocampus in all groups, whereas thalamic ReHo was highlighted in the *Propofol30* and *Urethane1.5* groups specifically. The sagittal image indicates the position of the coronal slices with values representing the position relative to Bregma in mm. ReHo values are colour coded from 0.6 to 0.8 as shown in the colour bar. An atlas with five ROIs based on the AMBMC atlas and thalamus from the functional organization of the mouse brain were overlaid on the AMBMC anatomical template. ROIs are: cingulate cortex (Cgu), primary sensory cortex of the barrel field cortex (S1BF), insular cortex (Ins), caudate-putamen (Cpu), hippocampus (Hipp), and thalamus (Thal). Animal numbers for each group were 11 in *Isoflurane1*, 6 in *Medetomidine0.05*, 13 in *Medetomidine0.1*, 8 in *Mediso*, 6 in *Propofol30*, 13 in *Urethane1*.5.

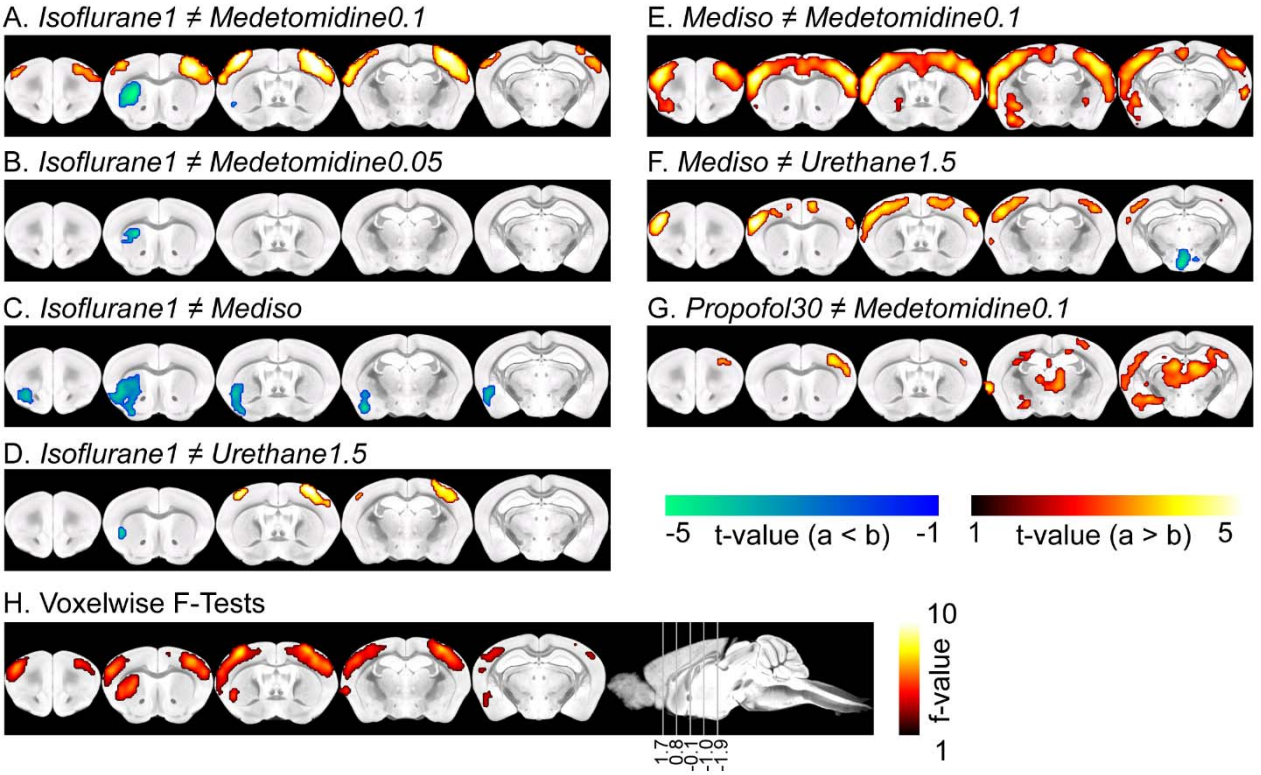

Figure 3-2 Voxelwise statistical analysis. Statistically significant increase in ReHo in the somatosensory cortex was found between *Isoflurane1* (A), *Mediso (E),* and to a lesser extent *Propofol30* (G) with respect to the *Medetomidine0.1* group. Similarly, cortical ReHo was significantly increased in the *Isoflurane1* (D) and *Mediso* (F) groups compared to *Urethane1.5*. The *Isoflurane1* group presented consistently decreased ReHo in the striatum upon comparison with *Medetomidine0.1* (A), *Medetomidine0.05 (B), Mediso* (C), and *Urethane1.5* (D) groups. Finally, portions of the hypothalamus were found to have decreased ReHo in the *Mediso* group when compared to *Urethane1.5* (F), while portions of the thalamus presented higher ReHo in the *Propofol30* group compared to *Medetomidine0.1*. (H) Voxelwise F-tests revealed the presence of global between-group differences summarizing results from unpaired t tests as described above. Image overlays

from (A) to (G) indicate colour coded t-values surviving TFCE correction (p<0.05, corrected). Image overlays of (H) indicate colour coded f-values surviving TFCE correction (p<0.05, corrected). The sagittal image indicates the position of the coronal slices with values representing the position relative to Bregma in mm. Animal numbers for each group were 11 in *Isoflurane1*, 6 in *Medetomidine0.05*, 13 in *Medetomidine0.1*, 8 in *Mediso*, 6 in *Propofol30*, 13 in *Urethane1.5*.

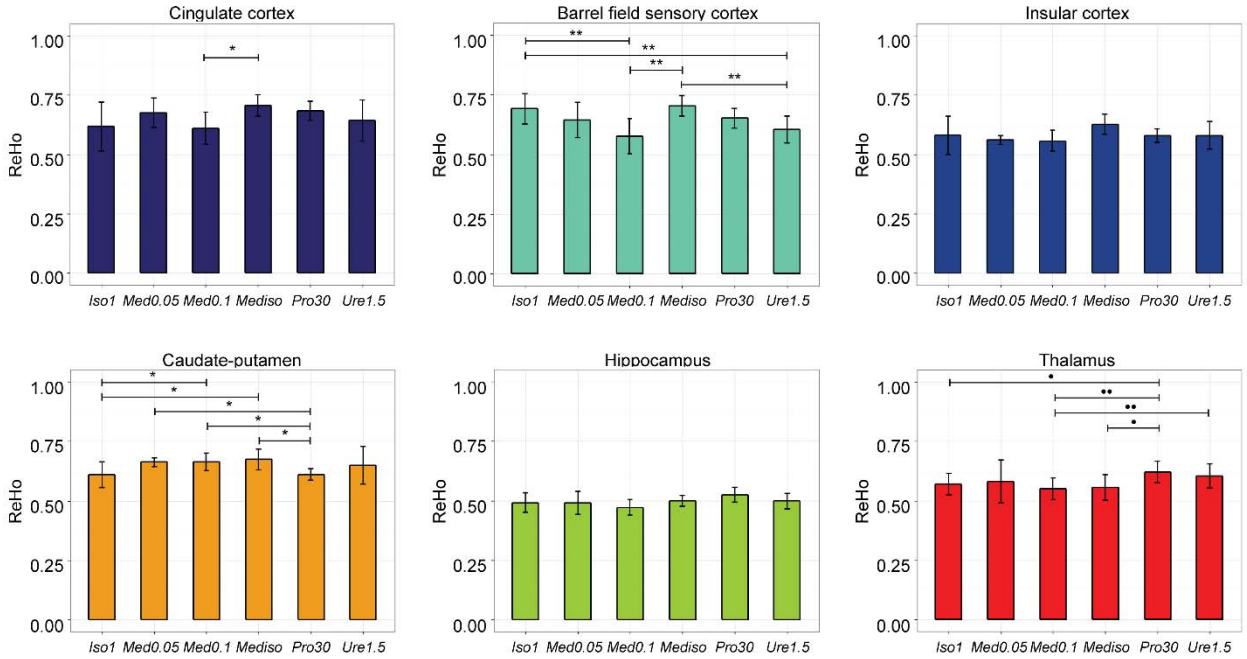

Figure 3-3 Analysis for 6 selected ROIs. Average ReHo values were extracted for each ROI. One-way ANOVA reported statistically significant differences between groups in the cingulate cortex ($F_{(5,51)}$=2.42, p=4.84×10-2), barrel field sensory cortex ($F_{(5,51)}$=7.04, p=4.52×10-5), caudate-putamen ($F_{(5,51)}$=2.51, p=4.15×10-2) and thalamus ($F_{(5,51)}$=2.43, p=4.77×10-2). Differences between pairs of groups were explored in a post-hoc analysis using unpaired two-sample t tests. In the barrel field cortex, both the *Isoflurane1* and *Mediso* groups presented higher ReHo compared to *Medetomidine0.1* and *Urethane1.5*. This was also the case between the *Mediso* and *Medetomidine0.1* groups in the cingulate cortex. In the caudate-putamen, medetomidine-based groups (*Medetomidine0.05*, *Medetomidine0.1*, *Mediso*) presented significantly increased ReHo compared to both the *Isoflurane1* and *Propofol30* groups. Between-group differences in the thalamus were revealed by the post-hoc tests, but did not survive FDR correction, and are therefore shown as uncorrected p values. Labels are: *, p<0.05; **, p<0.01, FDR corrected, •, p<0.05, uncorrected; ••, p<0.01, uncorrected. Bar plots and error bars indicate the mean ReHo across animals ± 1 SD. The group labels on the bottom of each bar plot are: *Isoflurane1* (*Iso1*), *Medetomidine0.05* (*Med0.05*), *Medetomidine0.1* (*Med0.1*), *Mediso* (*Mediso*), *Propofol30* (*Pro30*), *Urethane1.5* (*Ure1.5*). Animal numbers for each group were 11 in *Isoflurane1*, 6 in *Medetomidine0.05*, 13 in *Medetomidine0.1*, 8 in *Mediso*, 6 in *Propofol30*, 13 in *Urethane1.5*.

3.5 Discussion

The goal of this study was to characterize regional connectivity under six different and commonly applied anaesthetic regimens using mouse rs-fMRI. The results show that the strength of regional connectivity varied across brain regions irrespective of the drugs applied, suggesting common non-uniform effects of the investigated anaesthetics on local brain activity. Specifically, higher ReHo was observed in cortical regions, the caudate-putamen and some parts of the thalamus. Two-sample unpaired t-tests revealed different local activity in the primary somatosensory barrel field cortex and caudate-putamen between groups, indicating their drug-specific characteristics. Retained ReHo were observed under both relative deep and light anaesthesia in the thalamus, suggesting reasons including global synchronization between extensive neural networks and the relatively more complex structure of this region. Higher ReHo within both cortical and most subcortical regions was observed under *Mediso* indicating retained local activity across the brain under this regimen. Results revealed by our analysis provided a detailed description of the brain measured at the level of small clusters of voxels. The resultant map of local synchronization may serve to complement research on general anaesthesia and shed light on the investigated drug effects on neural activity between molecular level and large-scale imaging studies (Richiardi et al., 2015). Different anaesthetics induce anaesthesia through different targeting receptors. Some anaesthetics selectively target on specific receptors, while some impact on multiple receptor systems to a similar degree. The expression density of specific receptors varied across the brain areas, hence likely influences local connectivity yielded in different brain regions. Furthermore, this study used ReHo as an approach to tentatively investigate the local neuronal activity at a voxelwise spatial resolution (univariate) with few user interactions to minimize bias induced by individual researchers, hence reducing variability in comparisons between studies. ReHo is an attractive method when describing the brain with emphasis on focal clusters of voxels and when there is a need to extract information using univariate analytical approaches. The application of multi-scale analysis on the human brain function show that local connectivity helps to draw more sound conclusions on disease states (Cocchi et al., 2012b; Liu et al., 2014). The neighbour-to-neighbour connections are important for us to understand brain organizations (Jiang and Zuo, 2015), hence its application on mice may fill the gap of local FC between ongoing human research and studies on mouse models of brain disorders.

Local anaesthesia effects are central to our interpretation of the BOLD signal and our understanding of the underlying neuronal activity in the brain. The regionally suppressive

effects of specific regimens on brain activity have been reported by other studies (Heinke and Koelsch, 2005) and led to the detection of brain areas postulated to be important to consciousness (White and Alkire, 2003). By using different techniques, such as electroencephalogram (EEG), it has long been known that anaesthetic agents do not exert uniform effects over the whole cortical regions (Bonhomme et al., 2012). Our observations are consistent with these findings, showing that varied local synchronizations across the whole brain appear to be a common characteristic in mice, irrespective of the anaesthetic agent being used. Specifically, the retention of local connections in cortical areas, particularly somatosensory areas, was observed under all regimens. This is in agreement with previous studies using ICA and/or SBA. Research on rodent rs-fMRI repeatedly observed motor and somatosensory RSNs under anaesthesia (Hutchison et al., 2010; Lu et al., 2012; Grandjean et al., 2014b; Mechling et al., 2014; Nasrallah et al., 2014a; Sforazzini et al., 2014) comparable to those detected in awake rats (Liang et al., 2011, 2012a). Sensorimotor networks have been observed in monkeys and humans both under anaesthesia and at conscious rest (Peltier et al., 2005; Vincent et al., 2007; Martuzzi et al., 2010; van den Heuvel and Pol, 2010; Belcher et al., 2013). Together, these lines of evidence suggest that low-level somatosensory areas are likely to be less affected by anaesthetics at commonly used dosages. This may reflect elementary properties across species less influenced by anaesthetics.

Under the common observation of non-uniform local connectivity across the brain, regions yielding high ReHo were not the same between groups, suggesting the possibly drug-specific responses in some areas. Anaesthetic drugs act on neural processing through interactions with different receptors, altering neurotransmission at multiple sites in the brain. Their specific effects at the molecular level may extend to their specific effects on the brain at the level of neuronal networks (Franks, 2008; Brown et al., 2010), which might be reflected by the findings of this study from the perspective of focal clusters at the macroscale. Two-sample unpaired t-tests showed that cortical areas and the caudate-putamen are two regions that respond specifically to certain anaesthetics. Although high ReHo were observed in cortical areas under all regimens, significantly higher ReHo was also detected under *Isoflurane1*, *Mediso* and *Propofol30* compared to *Medetomidine0.1* and *Urethane1.5*. In contrast, three regimens containing medetomidine, i.e. *Mediso*, *Medetomidine0.1* and *Medetomidine0.05*, *were* associated with retained focal functional clusters in the left caudate-putamen compared to *Isoflurane1*. Although another study using halothane in mice reported the striatum as one RSN (Sforazzini et al., 2014), these between-group differences at the local level are more in line with the results of a previous large-scale SBA (Grandjean

et al., 2014b). In mice, other studies applying medetomidine alone also reported retained FC in striatum (Mechling et al., 2014; Nasrallah et al., 2014a). Although there were some discrepancies between studies comparing FC in the striatum under isoflurane and medetomidine in rats, more evidence suggest that the bilateral FC within the striatum was less compromised under medetomidine (Hutchison et al., 2010; Williams et al., 2010; Kalthoff et al., 2013), which is in agreement with the findings using ReHo in mice. Combined with previous SBA analysis (Grandjean et al., 2014b), the consistency within cortical areas and the caudate-putamen across analytical scales suggests that characteristics of interhemispheric FC patterns are promoted by the characteristics of local functional clusters, which may be an extension of agent effects at the molecular level.

An aforementioned study on mice examining FC changes as a function of anaesthetic depth using medetomidine reported preserved bilateral FC in the caudate-putamen compared to other areas at deep levels of anaesthesia, arguing that the density of α2-adrenoceptors across the brain was driving this regionally specific FC under medetomidine (Nasrallah et al., 2014a). The receptor-modulated changes of BOLD signal were previously observed in rats and mice under medetomidine and correlated well with electrophysiological measurements (Nasrallah et al., 2014b; Nasrallah et al., 2014c; Schroeter et al., 2016). This may also explain our observation of retained functional clusters revealed by ReHo under the three regimens involving medetomidine. Medetomidine shows strong affinity to α2-adrenoceptors with high specificity and selectivity (Scheinin et al., 1989). The expression density of α2-adrenoceptors is high in the thalamus, low in the striatum and medium in cortical regions (Wang et al., 1996). Unlike medetomidine, isoflurane and propofol mainly target GABAergic neurotransmission (Trapani et al., 2000; Richards, 2002). The expression of GABA(A) receptors is higher in subcortical regions, such as the striatum, compared to cortical regions. This may cause the caudate-putamen to respond more sensitively to *Isoflurane1*, producing reduced local connectivity in this region (Muller and Nistico, 1989). Medetomidine has almost no effect and affinity for GABA receptors which would further explain the retained local connectivity within the caudate-putamen in *Medetomidine0.1*, *Medetomidine0.05* and *Mediso* groups (Virtanen et al., 1988). Whereas many drugs target primarily one receptor system, *Urethane1.5* is reported to be an agent that induce anaesthesia by exerting small changes on multiple receptor systems (Hara and Harris, 2002). ROI analysis showed both cortical and subcortical regions associated with medium ReHo under *Urethane1.5* which may be partly explained by the pharmacological mechanism of this drug. One may notice that some significant results from the unpaired two-sample t tests were only observed in one hemisphere. This may due to the stringent statistical

analysis (Eklund et al., 2016) to improve false positive rates applied in this study at some cost of false negative rates. In other words, these results do not necessarily indicate unilateral effects of anaesthetics on the brain. Mean ReHo values were therefore extracted from left and right caudate-putamen as well as somatosensory cortex. Very similar strength distribution of the mean regional connectivity across anaesthetics were observed in the two regions across hemispheres, indicating that similar effects of regimens were presented in both sides of the brain.

Further investigations on several cortical and subcortical areas revealed in more detail how the local synchronization of focal clusters spread within each ROI. The cingulate cortex is involved in the default-mode network (DMN) of different species (Vincent et al., 2007; Buckner et al., 2008; Lu et al., 2012; Sforazzini et al., 2014) and is also reported to be a functional hub in humans and rodents (van den Heuvel and Sporns, 2013; D'Souza et al., 2014; Liska et al., 2015; Rubinov et al., 2015). Previous studies repeatedly reported it as an independent RSN in anaesthetized rodents (Hutchison et al., 2010; Jonckers et al., 2011; Grandjean et al., 2014b; Mechling et al., 2014; Sforazzini et al., 2014; Zerbi et al., 2015) and awake mice (Jonckers et al., 2014), but not awake rats (Becerra et al., 2011; Liang et al., 2011). ROI analysis showed that *Mediso* was associated with significantly higher regional connectivity compared to *Medetomidine0.1*, indicating that the local clusters within the cingulate cortex may respond differently to the two regimens. Due to the proximity of the cingulate cortex and some large blood vessels in the mouse brain (Dorr et al., 2007), local connectivity drawn from BOLD signals in this region might also be partially influenced by blood vessel signals. Just mentioned reports using SBA and ICA on rodents, however, indicated that the RSN within cingulate cortex showed clear anatomical specificity. This evidence implies that the regional connectivity in the cingulate cortex might also reflect local neural activity more under the examined experimental conditions. Effects of the six anaesthetic agents on neurovascular coupling, metabolism and local neural activity are further addressed later. *Mediso* yielded the highest ReHo among all the examined cortical ROIs, whereas *Medetomidine0.1* yielded the lowest. One plausible explanation may be that *Mediso* combined low levels of isoflurane and medetomidine, reducing the impact on their specific target receptor systems. *Mediso* is therefore likely to exert less specific local suppression on the brain. Observations between *Medetomidine0.1* and *Isoflurane1* as well as *Mediso* within the primary somatosensory barrel field cortex appear to support this. The somatosensory cortices play important roles in sensory information flow as well as movement planning and execution, while posterior areas include associative cortical functions (Matyas et al., 2010; Watson et al., 2011). Significantly reduced ReHo in the

primary somatosensory barrel field cortex under *Urethane1.5* in comparison to *Isoflurane1* and *Mediso* led to consideration of the pharmacological mechanism mentioned above as one plausible explanation. The insular cortex is a functional hub in mice (Liska et al., 2015). Unlike the other two cortical ROIs, no between-group differences were detected in this region. The insular cortex was observed to be part of the limbic system in a previous SBA (Grandjean et al., 2014b) and drug specificity may be less significant in this cortical region. Alternatively, the detection of its responses to different drugs may be beyond the sensitivity of both analytical methods.

In subcortical regions, the significant between-group differences obtained in the caudate-putamen based on ROI analysis were consistent with the results from voxelwise two-sample t tests in this study. No between-group differences were detected in the hippocampus at the local level, but in comparison to other areas, we observed slightly lower ReHo here for all regimens compared to other areas. The hippocampus is a small structure consisted of several smaller sub-regions (CA1, CA2, CA3, DG) that are represented by a handful of voxels individually, hence one reason for the low regional connectivity observed here may be for that each sub-structure yielded its own activity patterns. The thalamus is a common suppression site of anaesthetics and plays an important role in the distribution of sensory information flow (Nallasamy and Tsao, 2011; Hudetz, 2012). The thalamus and hippocampus have been reported to be functional hubs in mice (Liska et al., 2015). Uncorrected post hoc tests revealed significantly increased ReHo in the thalamus under *Propofol30* and *Urethane1.5* compared to *Mediso*, *Medetomidine0.1* and *Isoflurane1*, which cannot be explained by drug-specific responses alone. Previous SBA showed no significant between-group differences in the thalamus, which also indicated that this region may display few agent-specific responses (Grandjean et al., 2014b). *Medetomidine0.1* was associated with the lowest regional connectivity in the thalamus which may be due to the high density of α2-adrenoceptors in this structure. Given that the thalamus is a region comprises various nuclei which express multiple anaesthetic molecular targets non-uniformly (Arcelli et al., 1997; Watson et al., 2011; Uhrig et al., 2014), this may partly explain the mild ReHo observed under *Isoflurane1* and *Mediso* in this region. However, *Medetomidine0.05* yielded a less suppressed ReHo in the thalamus, suggesting anaesthetic dosage effects on the regional connectivity. Lower level dosages may preserve more thalamic activity, which is supported by the fact that *Propofol30* yielded the highest ReHo. Thus, the medium anaesthetic level under *Isoflurane1* and *Mediso* may also be one contributor to the corresponding mild activity in the thalamus. *Urethane1.5* induced deeper anaesthesia than observed in the other groups, but yielded high ReHo, a seemingly contradictory finding that

may be partly explained by the fact that urethane exerts modest effects on multiple receptor systems. However, one study in mice using the similar level of urethane reported depressed thalamic activity, indicating that there may also be other reasons for the retained ReHo under *Urethane1.5* (Huh and Cho, 2013). One possibility can be drawn from a previous SBA study that reported extensive FC under *Urethane1.5*, which the authors attributed to the global synchronization across the brain under deep anaesthesia (Grandjean et al., 2014b). If high levels of anaesthesia lead to widely synchronized neural activity and urethane does not specifically target a single receptor system, highly retained local synchronization revealed by ReHo within the thalamus may be a plausible outcome. This explanation may be further supported by studies on brain activations of rats under varied anaesthetic levels using rs-fMRI and EEG under isoflurane or propofol (Liu et al., 2013b; Liu et al., 2013a). Synchronized EEG signals were observed in rats under deeper anaesthetic dosages, which were associated with less specific large-scale FC patterns under deeper anaesthesia. Together with our observations, synchronization of neuronal activity under deep anaesthesia may hold higher weights on the strengthened local to long-range functional connectivity, compared to specific mechanisms of anaesthetics. Understanding different agent effects on these ROIs at a local level may help to refine our mapping of brain function in mice, provide explorative information to facilitate the selection of anaesthetics according to brain ROIs and might enable the translation of discoveries in mouse models to humans across analytical scales.

BOLD rs-fMRI is an indirect measure of neural activity and based on neurovascular coupling (Ogawa et al., 1990; D'Esposito et al., 2003). Anaesthetic regimens are known to impact on physiological parameters and neurovascular coupling mechanisms, hence influence BOLD fluctuations and confound the interpretations of fMRI experimental results (Tremoleda et al., 2012; Pan et al., 2015). Tight physiological control and monitoring have been applied in the experiment to minimize physiological confounds. In addition, cerebral blood volume (CBV) was measured during the experiment. Based on the observed long-range FC, CBV, action mode of anaesthetics and distribution density of specific receptors, Grandjean et al. concluded that contributions of CBV was minor to the rs-fMRI results (Grandjean et al., 2014a). The marginal effects of cerebrovascular parameters on BOLD signals are in agreement with other rodent studies using different agents and/or electrophysiological techniques, confirming that BOLD fMRI signals reflect neuronal activity rather than vascular (Nasrallah et al., 2014b; Nasrallah et al., 2014c; Schroeter et al., 2016). These reports suggest that contributions of vascular to regional connectivity should also

remain minor compared to the modulation of receptor systems under the anaesthetic regimens investigated.

There are, however, several limitations to the current study. First, the small sample sizes of the *Medetomidine0.05* and *Propofol30* groups may have introduced more confounds and individual variability into the results. Second, there is no awake baseline using mouse rs-fMRI technique in this study. However, as far as we are aware, the awake mouse imaging is reported to be difficult (Jonckers et al., 2014). In addition, we used carefully monitored, ventilated and paralyzed animals to minimize physiological and motion confounds. BOLD fMRI signals from awake animals would especially have severe noise from movements, which would introduce auto-correlations between voxels and artificially increase local connectivity. Repeated MR-restraint training for awake rat studies is reported to be a stressful procedure and cause long-lasting changes in physiology, behavioral responses and brain responses to pain stimuli detected by fMRI, hence may introduce confounds into the functional pattern of BOLD signals (Low et al., 2016b). Third, different anaesthesia regimens may also lead to different sources of physiological noise, or noise with different properties, rendering automatic noise classification difficult with FIX. New pipelines based on multi-echo sequences may offer unbiased methods to discriminate BOLD from non-BOLD signal based on physical properties of the signal, irrespective of the animal physiological state, leading to improved and more robust results (Kundu et al., 2012). Fourth, there are few agents with special peculiarities on the brain activity compared with most anaesthetics used in human and animals reported so far, such as ketamine, an agent observed to generate increased brain metabolism compared with the decreased metabolism under most other agents (Alkire and Miller, 2005; Heinke and Koelsch, 2005; Bonhomme et al., 2012). Hence, observations in this report may not be generalized to all anaesthetics. More experimental evidence may be required to deepen the understanding of regional connections measured by ReHo under general anaesthesia. Furthermore, many previously reported electrophysiological studies examining the correlation between electrophysiological and BOLD signals acquired EEG or somatosensory evoked potentials in somatosensory areas, but not other cortical or subcortical regions (Liu et al., 2013a; Nasrallah et al., 2014b; Nasrallah et al., 2014c). In the future, direct electrophysiological measurements from multiple regions may provide more information to validate correlations between them and regional connections drawn from BOLD rs-fMRI signals. Finally, unlike FC-based readouts that revealed large-scale brain activation confined within several functional systems, ReHo analysis generated high regional connectivity across the whole brain under all the regimens investigated. This suggests that anatomical information may be

reduced by using this method in mice. However, ReHo might provide a tentative way to capture small clusters of highly synchronized voxels and provide preliminary and complementary information on local neural activity that may not be revealed by large-scale analysis.

3.6 Summary

In summary, this study used local connections to detect regional FC on the basis of spontaneous activity under six different anaesthetic regimens using mouse rs-fMRI. The results showed consistency with several results from the previous FC analysis. Different agents produce anaesthesia by acting on different molecular targets, leading to agent-specific regional connectivity patterns. Results from regional connectivity showed that high ReHo could be observed in both cortical and subcortical areas under *Mediso* compared to other regimens indicating that it is the preferable regimen for local connectivity analysis using mouse rs-fMRI. This study provides the first initial evidence for using ReHo to probe brain FC in mice under six commonly applied anaesthetics. Given the wide use of ReHo in human studies on the one hand, and the application of transgenic mouse models of human brain diseases on the other hand, our results from this study may serve as a preliminary reference to future studies linking clinical applications to pre-clinical animal research using rs-fMRI.

Chapter 4 Effects of different anaesthetic protocols on the functional network organization in mice using resting-state fMRI

4.1 Abstract

Graph analysis has provided rich information on the architecture of functional networks in the normal and disordered brains. To further pursue the underlying mechanisms of human brain diseases, research on transgenic mouse models drives the growth of mouse rs-fMRI to translate discoveries between the two species. Network topology in mice using rs-fMRI is still largely unexplored. As a typical feature of this technique, anaesthesia facilitates experiments, but influences brain functions. It is hence crucial to understand agent impacts on the mouse brain for correct interpretations of the results. The previous regional and long-range FC analysis across agents showed agent-specific FC patterns. However, whether the agent-specific impact affects topologies of functional networks in mice is unknown. In addition, different labs adopt different regimens inducing difficulties in result comparisons. Therefore, understanding how commonly used regimens influence topological properties is necessary for understanding network organizations in mice using rs-fMRI. In this study, I examined how several graph parameters of functional integration and segregation were affected by six commonly used regimens. The findings showed that small-worldness was retained across agents, implying that the efficient information processing capability was preserved in the anaesthetized brain irrespective of the agents and dosages investigated. The significant difference in small-worldness between *Medetomidine0.1* and *Mediso* groups indicating that local topological variations drove changes of some global properties. Functional modules were generally similar across regimens, suggesting that agent-specific effects did not impact on the large-scale functional segregation in mice. However, anaesthetic dosages affected modular organizations significantly. These results shed light on the retained and changed principles governing the network organizations of the anaesthetized mouse brain, and may help translational research between mice and humans using rs-fMRI and graph theoretical analysis.

4.2 Introduction

Resting-state functional magnetic resonance imaging (rs-fMRI) is a popular and powerful translational approach to characterize whole brain activity in different species (Biswal, 2012; Pan et al., 2015). A central goal of neuroscience is to understand the brain connectivity revealing principles of how the brain operates (Friston, 2011). One approach to study connectivity is the graph theory. It has not only been widely applied in human brain research and clinical applications, but can be adapted to all kinds of neuroimaging and neurophysiological data. This feature is paving a promising avenue to examine the brain

networks with the same topological characteristics across species and modalities for neuroscientists from different fields (Fornito et al., 2016). Furthermore, graph theory has provided abundant information on the brain's functional organization in both normal and abnormal states (Park and Friston, 2013; Fornito et al., 2016). Accumulative evidence of graph analysis on human rs-fMRI research points to its potential to identify endophenotypes of brain disorders (Bullmore and Sporns, 2009a; Wang et al., 2010b; Lo et al., 2015). However, human research is not enough to pursue the underlying neurophysiological mechanisms of mental disorders. Evidence from animal studies, especially mice, show promises to disclose the underlying mechanisms of these diseases. Particularly, this species provides opportunities to investigate gene dysfunctions of human brain disorders (Rosenthal and Brown, 2007).

Although research on transgenic mice in histological, biochemical, anatomical and behavioral tests is progressing fast, rs-fMRI studies on mice remains a largely unexplored domain. This leaves an important gap between findings in mice and human rs-fMRI research. Mouse rs-fMRI is therefore receiving rising attention for translational neuroscience and basic neuroscience research. However, anaesthesia is a typical component of this technique. Awake mouse rs-fMRI was reported impracticable so far (Jonckers et al., 2014). Anaesthesia helps to keep the animal sedate and control stress-related physiological levels (Grandjean et al., 2014a). But it influences brain metabolisms and neurovascular coupling, bringing confounds into BOLD fMRI signals (Pan et al., 2015). For example, recent studies reported both consistencies and discrepancies in resting-state functional networks (RSNs) and network topologies in mice under different anaesthetics. Particularly, graph measures have only been examined under one agent in each study with different results and not yet been widely applied in this field (Jonckers et al., 2011; Guilfoyle et al., 2013; Grandjean et al., 2014b; Mechling et al., 2014; Nasrallah et al., 2014a; Sforazzini et al., 2014; Liska et al., 2015; Bardella et al., 2016). The principles governing functional network topology in mice under anaesthesia are not well-understood. Furthermore, functional connectivity (FC) patterns in rodent brains were reported to show agent-specific characteristics by several comparative studies (Williams et al., 2010; Grandjean et al., 2014b; Jonckers et al., 2014; Nasrallah et al., 2014c). Whether the agent-specific effects will influence functional network organization in mice remains unknown.

Investigating topological properties of the brain is important to understand how anaesthesia affects functional networks. Comparing these properties across agents may reveal commonly retained and specifically changed architectures of the anaesthetized mouse brain under different regimens. It may contribute to preliminary references for

comparisons between studies and help establish how functional networks is organized in the normal mouse brain for future research of transgenic mouse models. The results may facilitate translations of findings between mice and increasingly growing human rs-fMRI studies using graph theoretical measures.

This study compared integration and segregation topologies in mice using rs-fMRI under six anaesthetic regimens commonly used in rodent studies: isoflurane, two different doses of medetomidine, propofol, urethane, and a combination of medetomidine and isoflurane (Grandjean et al., 2014b). Global, local graph metrics and functional modules were applied to extract information about the network architecture. The results shed light on the retained and changed topologies governing the functional organizations of the mouse brain across these agents.

4.3 Material and methods

4.3.1 Data acquisition

Please find details of the data acquisition for this study in Chapter 2 Materials and Methods, section 2.1.1 Data acquisition.

4.3.2 Systemic physiological measurement

Please find details of the systemic physiological monitoring for this study in Chapter 2 Materials and Methods, Section 2.1.2 Systemic physiological measurement.

4.3.3 Pre-processing

Images were pre-processed as in (Grandjean et al., 2014a). Briefly, the first 10 volumes were discarded, following rigid body realignment and slice timing. All data were normalized to an in-house EPI template. Regression with global signal and six motion parameters were performed (GSR data). Data without this regression were also analyzed (UR data). Both datasets were further band pass filtered between 0.01 to 0.3 Hz. Blood vessel signals were further regressed out in this study. In the following descriptions, data with GSR and vessel signal regression were referred to as GVR data, data with only vessel signal regression were referred to as VR data. The templates and data were multiplied by a factor of 10 in voxel spacing to adapt to human imaging software. All data was registered to the MRI template using FSL FLIRT with a final resolution 1x1x1 mm^3.

4.3.4 Complex network analysis

Please find the details in Chapter 2 Materials and Methods, Section 2.4.3.c.

Increased specificity of FC patterns after applying GSR are reported in previous studies using seed-based analysis in rodents (Kalthoff et al., 2013; Grandjean et al., 2014a). In particular, Grandjean et al. (2014) using the same data without GSR reported widespread FC with less specific anatomical confinement in cortical regions under isoflurane and urethane, whereas extended FC from subcortical regions to muscle tissue under propofol (Grandjean et al., 2014a). Their results indicate that data without GSR may contain more noise masking the specificity of functional connections. Therefore, the following sections will mainly focus on results from GVR data. Results from VR data were presented in Appendix F to Appendix H.

4.4 Results

4.4.1 Measures of topological parameters

The skeleton of functional brain networks under six anaesthetics showed characteristics of small-worldness (mean $\bar{\sigma}^w \pm$ standard deviation, i.e. mean $\pm$ std: 2.40 ± 0.35, where $\bar{\sigma}^w$ was calculated by averaging over group means). When compared with corresponding null random networks, the normalized clustering coefficients of all groups were significantly greater than 1 (mean $\bar{\gamma}^w \pm$ std: 3.73 ± 0.43, where $\bar{\gamma}^w$ was calculated by averaging over group means), indicating a highly clustered local organization. The normalized characteristic path lengths of all six groups were slightly above one (mean $\bar{\lambda}^w \pm$ std: 1.58 ± 0.06, where $\bar{\lambda}^w$ was calculated by averaging over group means). After Kruskal-Wallis test, small-worldness ($p = 0.03$) and the normalized clustering coefficient ($p = 0.02$) both showed an existence of significant between-group difference. Post hoc tests further located possible significant difference between *Medetomidine0.1* and *Mediso* as shown in Figure 4-1. No significant overall difference was detected in the shortest path length L^w, the normalized shortest path length λ^w, nor the clustering coefficient C^w.

Global attributes calculated at threshold p=0.0001 revealed similar results, i.e. significant overall differences were detected in small-worldness (p=0.01) and gamma (p=0.02). Post hoc results are shown in Appendix D.

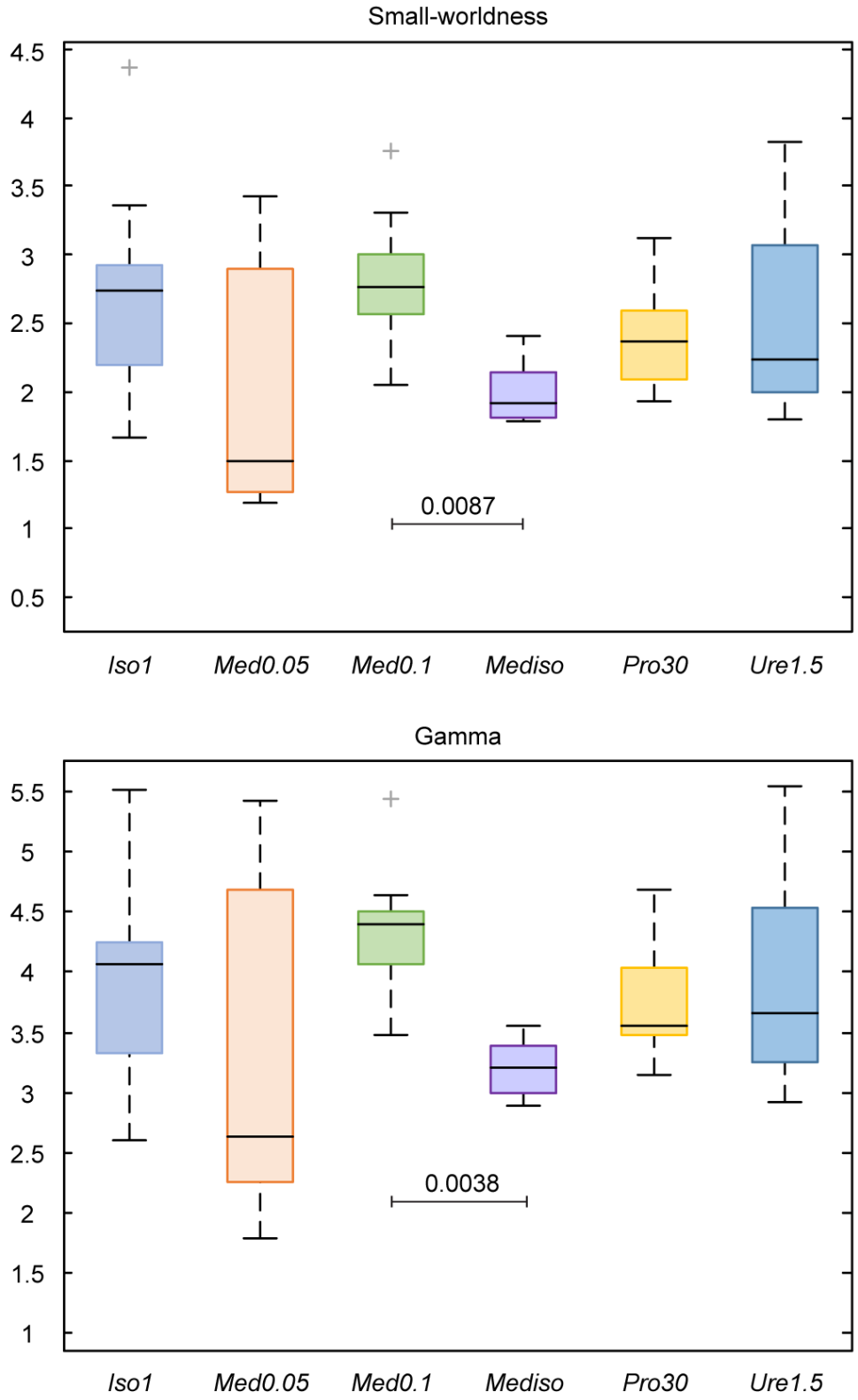

Figure 4-1 Small-worldness and normalized clustering coefficient measures for mouse functional networks under different anaesthesia protocols. Each horizontal line and above number represent the p-value of a post hoc Wilcoxon test, with FDR correction. (A) Boxplots showing median, interquartile range and range for small-worldness. There was significant difference between *Medetomidine0.1* and *Mediso*. (B) Boxplots showing median, interquartile range and range for the normalized clustering coefficient (gamma). There was significant difference between *Medetomidine0.1* and *Mediso*. *Iso1*: *Isoflurane1*. *Med0.05*: *Medetomidine0.05*. *Med0.1*: *Medetomidine0.1*. *Pro30*: *Propofol30*. *Ure1.5*: *Urethane1.5*.

4.4.2 Modules

Similar to functional networks of the human brain, there were many high-Q degenerate partitions in the functional networks of the mouse brain (Rubinov and Sporns, 2011). To search for the most stable structures, we assigned one node to a certain module if it was affiliated to it in more than 50% of the detected degenerate partitions, which was similar to the within-module connection likelihood (Rubinov and Sporns, 2011; Liska et al., 2015). The high mean Q values of the functional networks (mean Q ± std.: 0.6116±0.0344, averaged over the mean of six groups) indicated the presence of high-modularity within the intrinsic connectional architecture of the mouse brain. The mean Q values of corresponding null-networks (mean Q ± std.: 0.2042±0.0158) were significantly lower than those calculated from empirical networks (paired t-test: $p = 2.683 \times 10^{-7}$). The Q values of each group and its null-network using GVR data were listed in Appendix E. The distance (averaged VI) between the discovered partitions of each empirical network (mean VI ± std.: 0.1115±0.0447) was significantly smaller than the averaged VI of their corresponding null-networks (mean VI ± std.: 0.4188±0.0286, paired t-test: $p = 2.049 \times 10^{-5}$). This was consistent with human functional networks, i.e. smaller distances between high-Q partitions of empirical networks compared to those in random networks (Rubinov and Sporns, 2011). Group-mean VI values of the empirical networks and their corresponding null-networks were listed in Appendix E.

Different numbers of functional modules were detected in the mouse brain networks under anaesthesia: 5 modules in *Medetomidine0.1* group, 4 in *Isoflurane1*, *Mediso* and *Propofol30* groups, 3 in *Medetomidine0.05* and *Urethane1.5* groups. Although *Medetomidine0.1* contained five modules, four of them were highly consistent with the modules observed in *Isoflurane1*, *Mediso* and *Propofol30* groups, as shown in Table 4-1. The first module included agranular insular areas, anterior cingulate areas (except for *Mediso*), endopiriform nucleus, amygdala, striatum, pallidum, and nodes in prefrontal cortex, claustrum and piriform cortex. This organization was in reminiscent of the salience network (SN) of the human brain anchoring in insular cortex and cingulate cortex, and extended to subcortical areas including amygdala and striatopallidum (Seeley et al., 2007; Menon, 2015). A similar functional network was previously reported in mice using seed-based analysis by Sforazzini et al. (Sforazzini et al., 2014), therefore this module was referred to as the salience-like module. A second lateral cortical network (LCN) included only cortical areas consist of visceral area, gustatory area, primary somatosensory areas (nose, mouth, unassigned) and supplemental somatosensory areas. This organization may be related to the mouse taste system, which is dependent on olfactory sensation and visceral-gustatory

associations (Shipley and Geinisman, 1984; Watson et al., 2011). The third module included posterior parietal and temporal association areas, primary somatosensory regions, somatomotor areas, retrosplenial cortex (except for *Isoflurane1* group), visual cortex, auditory cortex and extends to some parts of the hippocampus. Small portions of amygdala were involved in this module under *Proprofol30*. Bilateral cingulate cortex and retrosplenial cortex were simultaneously allocated into this module only under *Mediso*. This modular organization was very similar to the default-mode network (DMN) previously reported in rats (Upadhyay et al., 2011a; Lu et al., 2012) and mice (Sforazzini et al., 2014; Stafford et al., 2014; Liska et al., 2015; Zerbi et al., 2015). Therefore, it was named as DMN-like module. Although several previous studies reported that cingulate and retrosplenial cortices were both presented in rodent DMN, retrosplenial cortex was only observed in the DMN-like module under *Medetomidine0.1* and *Propofol30*. In *Isoflurane1*, retrosplenial cortex and some parts of hippocampus were affiliated with the forth module. Because all the other nodes in this module under isoflurane overlapped well with nodes in the DMN-like module of the other three regimens, it was still referred to as DMN-like module. The fourth brain-stem module contained only subcortical areas within thalamus, hypothalamus and the midbrain in *Medetomidine0.1*, *Propofol30* and *Mediso*. As just mentined, retrosplenial cortex and some parts of the hippocampus were connected to the brain-stem module under isoflurane. A brainstem-cerebellum module was reported in the anatomical network of the mouse brain (Rubinov et al., 2015). A fifth module detected in the *Medetomidine0.1* group contained only four unilateral regions (left temporal association areas, left perirhinal area, left ectorhinal area and entorhinal area). However, the aforementioned four big modules showed well-preserved bilaterality across regimens.

Three functional modules were observed in the *Medetomidine0.05* and *Urethane1.5* groups with different organizations, as shown in Table 4-2 and Table 4-3. In *Medetomidine0.05* group, the first module included angular insular cortex, piriform cortex, cortical nodes of LCN, subcortical regions consisted of claustrum, endopiriform nucleus, amygdala and some parts of the striatum. This organization may be an extension of the taste system dependent the olfactory, visceral and gustatory sensations, because insular cortex is suggested to be the direct convergent area of the olfactory and visceral-gustatory sensory pathways (Shipley and Geinisman, 1984). The second module was a DMN-like module. The third module contained prefrontal cortical regions (orbital, prelimbic, infralimbic and anterior cingulate cortices), pallidum, some parts of striatum, some portions of amygdala and nodes within the brain-stem module.

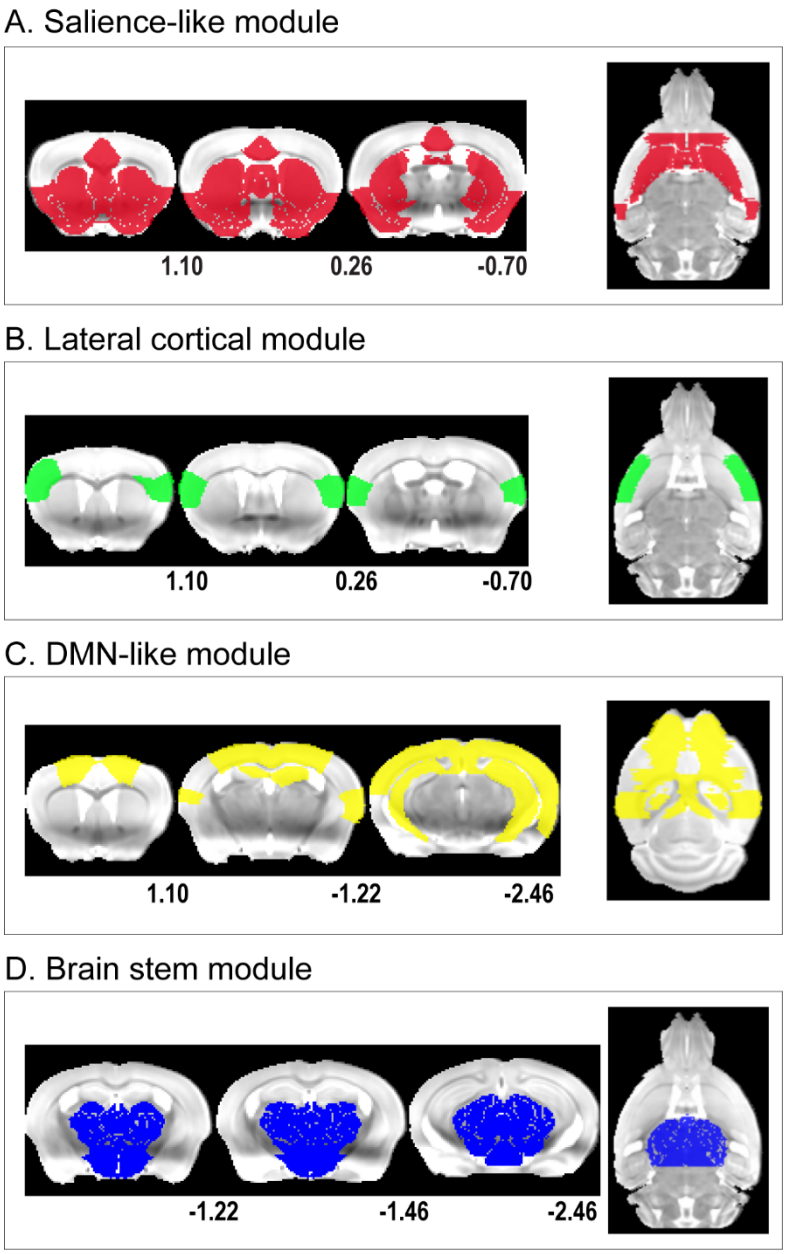

Figure 4-2 Similar functional modules were revealed across anaesthetic regimens including *Isoflurane1*, *Medetomidine0.1*, *Mediso* and *Propofol30*. Most areas within each module show good bilaterality. (A) A salience-like module resembled the salience network reported in human studies. The anterior cingulate cortex was not included in this module under *Mediso*. (B) A lateral cortical network encompassing taste-related primary somatosensory regions, supplementary somatosensory regions, visceral and gustatory areas. (C) A DMN-like module. Both anterior cingulate cortex and retrosplenial cortex were included in this module under *Mediso*. Retrosplenial cortex was not observed in this module in *Isoflurane*1 group, but other nodes overlapped very well with nodes of DMN-like module under the other three regimens. (D) A brain-stem module containing thalamus, hypothalamus, midbrain and pons. In *Isoflurane*1 group, the retrosplenial cortex was associated with this module. The horizontal slice presents an overview of each module. Distances of each coronal slice to the bregma (mm) are displayed under the slices.

Table 4-2

Unlike the split salience-like module observed in *Medetomidine0.05* group, the first module of the *Urethane1.5* group appeared to contain nodes from both the salience-like network and LCN. The DMN-like and brain-stem modules were also observed in this group. Several nodes were not reliably assigned to any module under urethane: primary somatosensory areas (left upper limb, barrel field), anterior cingulate area, left dentate gyrus and left basomedial amygdalar nucleus. The anterior cingulate cortex seemed to be a node not reliably assigned to one consistent module across regimens nor dosages, implying its dynamic functional roles in modular organizations.

Table 4-1 Consistent functional modules in *Isoflurane1*, *Medetomidine0.1*, *Mediso* and *Propofol30* groups

Modules	Common brain regions within each module	Exceptions
Salience-like module	Agranular insular areas, anterior cingulate areas, orbital areas, olfactory area, prelimbic areas, infralimbic areas, claustrum, piriform, endopiriform nucleus, amygdala, cerebral nuclei (striatum and pallidum)	Anterior cingulate areas is not allocated in this module under *Mediso* Perirhinal, ectorhinal and entorhinal areas are assigned into this module under *Isoflurane1*
Lateral cortical modules	Visceral areas, gustatory areas, primary and supplemental somatosensory areas	-
DMN-like module	Posterior parietal association areas, temporal association areas, primary somatosensory areas, somatomotor areas, visual areas, auditory areas, retrosplenial, hippocampus, perirhinal areas, ectorhinal areas, entorhinal areas	Anterior cingulate areas is merged into this module under *Mediso* Retrosplenial, perirhinal, ectorhinal and entorhinal areas are not assigned to this module under *Isoflurane1*
Brain-stem module	Thalamus, hypothalamus, midbrain, pons	Retrosplenial cortex and some parts of hippocampus are not assigned into this module under *Isoflurane1*

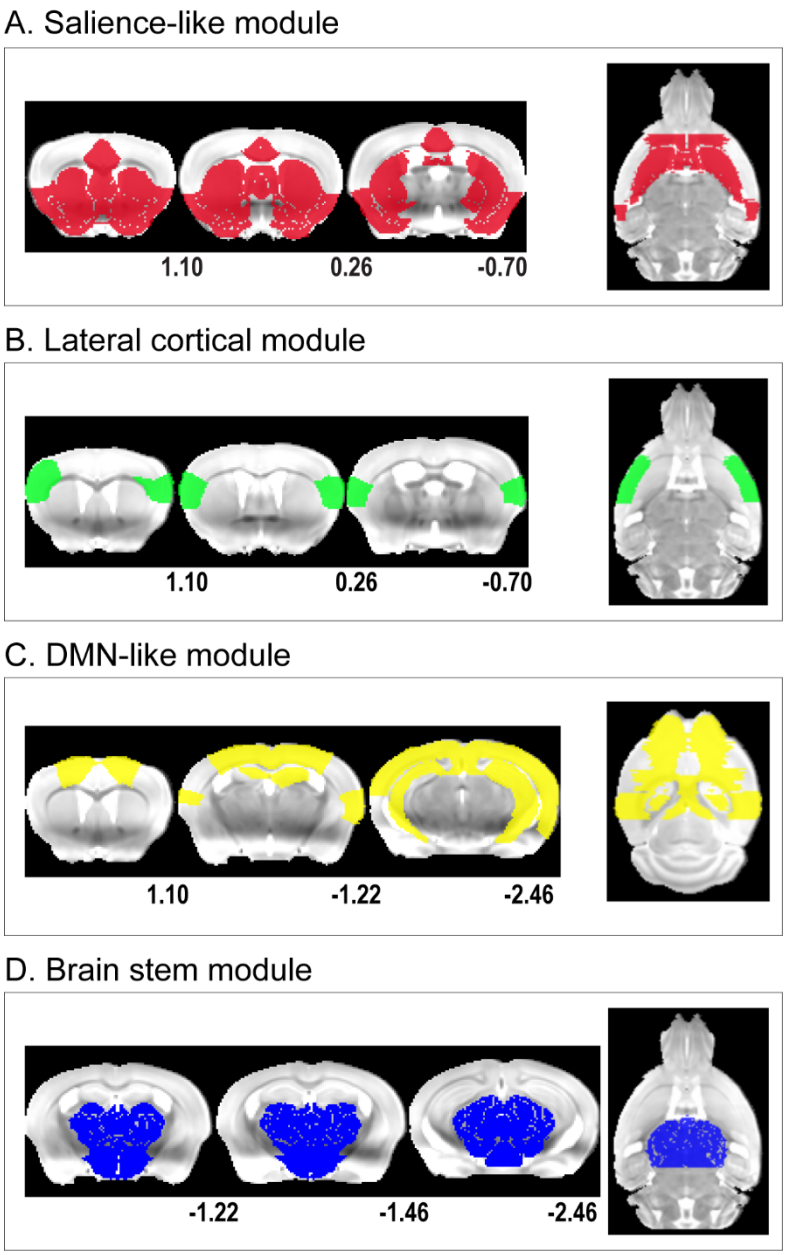

Figure 4-2 Similar functional modules were revealed across anaesthetic regimens including *Isoflurane1*, *Medetomidine0.1*, *Mediso* and *Propofol30*. Most areas within each module show good bilaterality. (A) A salience-like module resembled the salience network reported in human studies. The anterior cingulate cortex was not included in this module under *Mediso*. (B) A lateral cortical network encompassing taste-related primary somatosensory regions, supplementary somatosensory regions, visceral and gustatory areas. (C) A DMN-like module. Both anterior cingulate cortex and retrosplenial cortex were included in this module under *Mediso*. Retrosplenial cortex was not observed in this module in *Isoflurane*1 group, but other nodes overlapped very well with nodes of DMN-like module under the other three regimens. (D) A brain-stem module containing thalamus, hypothalamus, midbrain and pons. In *Isoflurane*1 group, the retrosplenial cortex was associated with this module. The horizontal slice presents an overview of each module. Distances of each coronal slice to the bregma (mm) are displayed under the slices.

Table 4-2 Brain regions within the three modules detected in the *Medetomidine0.05* group

Modules	Brain regions within each module
Module 1	Agranular insular areas, claustrum, piriform, endopiriform nucleus, amygdala, some parts of striatum, visceral areas, gustatory areas, primary and supplemental somatosensory areas
DMN-like module	Posterior parietal association areas, temporal association areas, primary somatosensory areas, somatomotor areas, retrosplenial areas, visual areas, auditory areas, perirhinal areas, ectorhinal areas, small portions of hippocampus
Module 3	Thalamus, hypothalamus, midbrain, pons, some parts of hippocampus, orbital area, olfactory area, prelimbic area, infralimbic area, anterior cingulate areas, pallidum, some parts of striatum, some parts of amygdala

A. Module 1 in *Medetomidine0.05* group

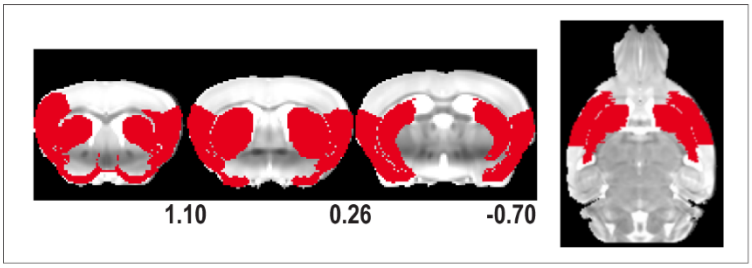

B. Module 2 (DMN-like module) in *Medetomidine0.05* group

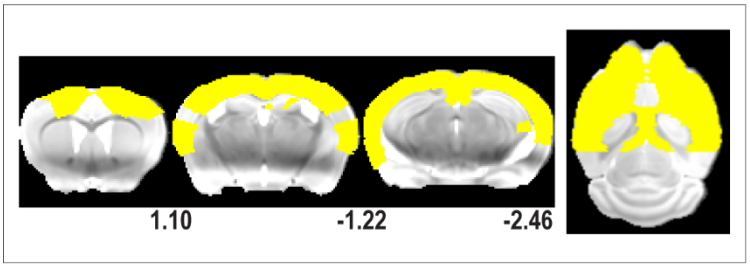

C. Module 3 in *Medetomidine0.05* group

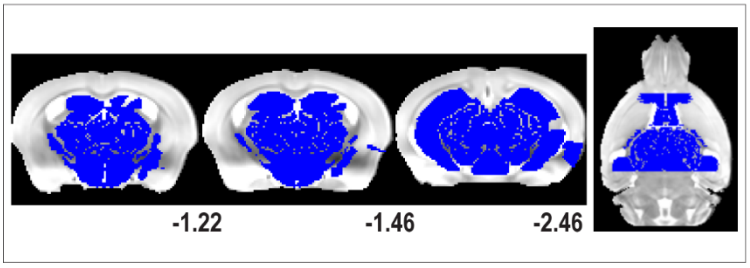

Figure 4-3 Three functional modules were revealed under *Medetomidine0.05*. (A) The first module contained agranular insular areas, piriform cortex, cortical regions of LCN and subcortical regions including claustrum, endopiriform nucleus, amygdala and some parts of striatum. (B) The second module was a DMN-like module, but with fewer nodes in the hippocampus compared to DMN-like module detected in the aforementioned four anaesthetics. (C) The third module contained prefrontal cortical regions, some parts of striatum, some parts of amygdala, some parts of hippocampus and brain stem regions (thalamus, hypothalamus, midbrain, pons). The horizontal slice presents an overview of each module. Distances of each coronal slice to the bregma (mm) are displayed under the slices.

Table 4-3 Brain regions within the three modules detected in the *Urethane1.5* group

Modules	Brain regions within each module
Module 1	Agranular insular areas, prelimbic area, orbital area, infralimbic area, olfactory area, claustrum, piriform, endopiriform nucleus, amygdala, cerebral nuclei (striatum and pallidum), visceral areas, gustatory areas, primary and supplemental somatosensory areas
DMN-like module	Posterior parietal association areas, temporal association areas, primary somatosensory areas, somatomotor areas, retrosplenial areas, visual areas, auditory areas, perirhinal areas, ectorhinal areas, hippocampus, small portions of amygdala
Brain-stem module	Thalamus, hypothalamus, midbrain, pons

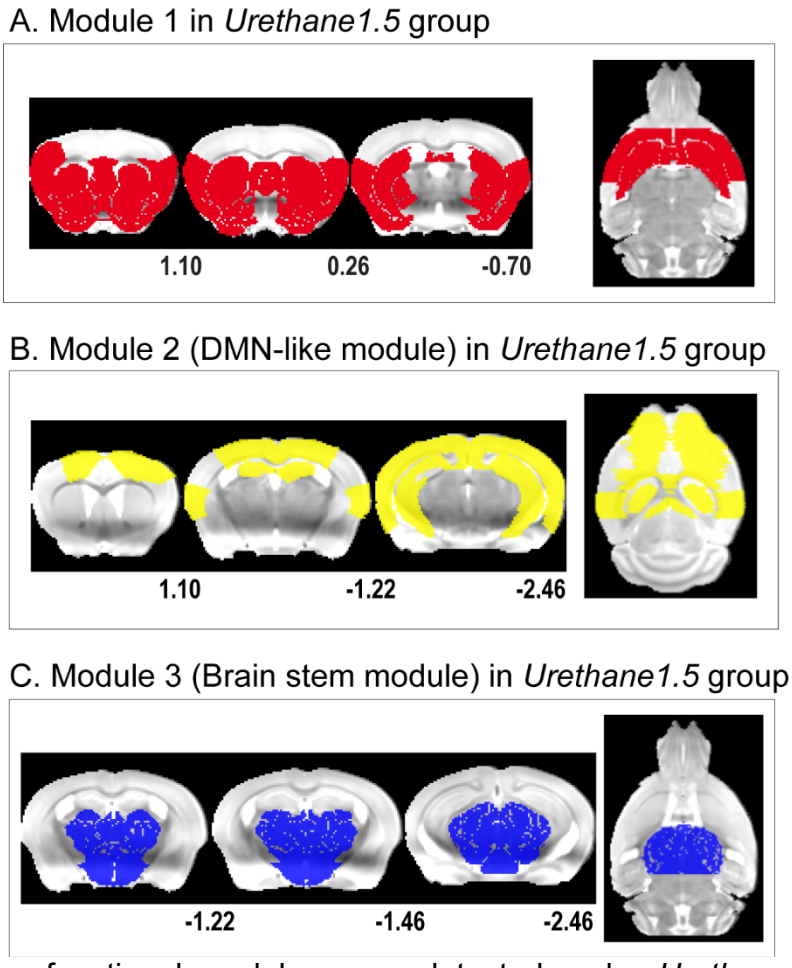

Figure 4-4 Three functional modules were detected under *Urethane1.5*. (A) The first module contained nodes from salience-like network and LCN. (B) The second module was a DMN-like module. (C) The third module was a brain stem module. The horizontal slice presents an overview of each module. Distances of each coronal slice to the bregma (mm) are displayed under the slices.

Module organizations revealed in VR data were presented in Appendix G. There were discrepancies between module structures using data with and without GSR. This was

consistent with the former study (Grandjean et al., 2014a), indicating that GSR may induce changes in the community structures.

4.5 Discussion

Characterizing the network topology may provide important insights into how the FC organization the brain possesses to support its various functional capabilities. The goal of this study was to delineate the topologies of functional brain networks in mice under six commonly used anaesthetic regimens using rs-fMRI. Results from GVR showed that small-world property was preserved under all groups. The small-world value of *Medetomidine0.1* group was significantly higher than the value of *Mediso* group, mostly driven by normalized clustering coefficients. This implies that local clustering distribution led to altered global properties. Similar module structures were observed under *Isoflurane1*, *Medetomidine0.1*, *Mediso* and *Propofol30* groups, indicating that anaesthetic-specific effects may not influence the large-scale functional segregation within the mouse brain under moderate anaesthetic depths. Different functional modules were observed in *Medetomidine0.05* and *Urethane1.5*, suggesting that anaesthetic dosages introduced changes into modular structures.

4.5.1 Significant difference in small-worldness was driven by local clustering coefficient

The mouse brain exhibited small-worldness under all six anaesthetic regimens in the study. This is in agreement with preserved small-worldness reported by rs-fMRI studies on anaesthetized and awake rats, as well as mice under medetomidine (Liang et al., 2011, 2012b; Mechling et al., 2014). These observations indicate that small-worldness is an intrinsic property of functional networks in mice. The efficient information processing afforded by small-world topology is retained in mice under light to moderate anaesthetic dosages, irrespective of the investigated agents so far. Among all the compared graph metrics, statistically significant differences were detected in the small-worldness and normalized clustering coefficient between *Medetomidine0.1* and *Mediso* groups. The normalized shortest path length of each group was very similar to each other, the different small-world values hence should be mainly driven by changed gamma values. This indicated that the distribution of local clustering coefficients varied significantly between the two regimens and influenced the global metrics. Such difference was not revealed by non-normalized average clustering coefficient C^w, it could therefore be inferred that higher clustering values were presented in *Medetomidine0.1* group after normalizing by C^w_{rand} when compared to *Mediso* group. In other words, the random models of *Medetomidine0.1* group

exhibited much smaller C^w_{rand} in comparison to C^w_{rand} of the random networks of *Mediso* group. The degree distribution is preserved in null networks, i.e. the degree of each node remains unchanged, whereas their connected partner nodes are completely random (Maslov and Sneppen, 2002). Hence, the reduction of C^w_{rand} reflected reduced density of clustered triangles during the process of randomization. One possible explanation may be that the distributions of nodes with clustered triangles around them (higher C^w_i) in the two groups were different. Indeed, the twenty nodes with the highest C^w_i under *Medetomidine0.1* were mainly within subcortical areas including claustrum and caudate-putamen, cortical regions including primary somatosensory areas (nose, mouth, unassigned), visceral and gustatory areas. The twenty nodes with the highest C^w_i under *Mediso* containing mainly cortical areas including more nodes within primary somatosensory areas, supplemental somatosensory areas, visceral and gustatory areas, as well as subcortical regions from the claustrum. This is in agreement with regional connectivity analysis in Chapter 3 and previous long-range FC analysis using the same data (Grandjean et al., 2014a): 1) retained somatosensory FC was observed across agents; 2) strong FC was observed in caudate-putamen under medetomidine; 3) stronger FC within cortical regions under *Mediso* was detected compared to *Medetomidine0.1*.

Based on these evidence, it may be that the significant difference in gamma between *Medetomidine0.1* and *Mediso* was driven by different distributions of high local clustering coefficients within the two groups, leading to changed small-world values. Retained cortical and subcortical FC was reported previously in mice under *Mediso* (Grandjean et al., 2014a). Agent-specific FC patterns were observed under medetomidine (Grandjean et al., 2014a; Nasrallah et al., 2014a). Results from graph metrics in this study were in line with the previous reports. This suggests that medetomidine-specific effects on functional network might influence some global metrics of network topology in mice. Future studies on transgenic mouse models performed under this regimen should take this information into consideration.

4.5.2 Similar modules were detected across agents

To the best of my knowledge, this is the first study investigating degenerate high-modularity partitions of the mouse functional brain networks across different agents using rs-fMRI. Similar to functional human brain networks, I observed the presence of degeneracy in the mouse functional brain networks. This suggests that the degeneracy is a feature of

functional networks in mice irrespective of the agents investigated, and a feature of functional brain networks across species. Previous module analysis in mice typically reported only one high-Q partition, highly reproducible partitions or hierarchical structure of modules under a single agent (Mechling et al., 2014; Liska et al., 2015; Bardella et al., 2016). This study considered degenerate partitions and sought for the most stable modules across a large sample of partitions representative of the whole partition space (Rubinov and Sporns, 2011). These results combined information from many degenerate solutions (Good et al., 2010) to collectively present the dynamic functional separation of the given network in a more comprehensive manner.

Four modules comprising most of the nodes in the graph as detected in *Isoflurane0.1*, *Medetomidine0.1*, *Mediso* and *Propofol30* groups showed high similarity. Although there were small differences in community affiliation of some nodes between the groups, the overall consistency suggested that anaesthetic-specific effects might not impact on large-scale functional separation of the resting-state functional networks. The first common module is a salience-like module reminiscent of the human salience network (Seeley et al., 2007). It resembles the salience-like network reported by a previous seed-based analysis on mice (Sforazzini et al., 2014). Several other nodes in prefrontal cortex were involved in this module. The strong anatomical connections in mice between infralimbic cortex, striatum and amygdala suggest that this region is critical to emotional and autonomic functions (e.g. visceral related functions). Anatomical connections between prelimbic area, striatum, amygdala and orbital frontal cortex suggest that it is important for cognitive functions (e.g. working memory). Orbital frontal areas are important for affective and motivational aspects of behaviour, as well as execution of goal-directed behaviour (Watson et al., 2011). Olfactory-related regions such as piriform cortex, endopiriform nucleus and olfactory area were also allocated into this module. These regions are inferred to be responsible for odor information processing and association. Piriform cortex and endopiriform nucleus project massively to amygdala, indicating olfactory functions and olfactory-related emotional processing (Watson et al., 2011). Based on the anatomical connectivity in mice between nodes of this module and their functional roles, this salience-like module may possess several functions including salience directed function, olfactory information processing, affective processing, motivation and reward, as well as execution of behaviour.

In *Mediso* group, the anterior cingulate cortex was not allocated into this module, but the DMN-like module. This may be due to the stronger functional connection between the anterior cingulate cortex and DMN-like network under this regimen. In salience network, the cingulate cortex is thought to play a prominent role in behaviour selection in response to the

salient stimuli. In DMN, cingulate cortex (posterior cingulate cortex in humans) is thought to play crucial roles in internally oriented cognition and regulating the attention focus (Leech and Sharp, 2014). Its heterogeneous functional roles are also reflected in its topological positions within structural and functional networks, where both human and rodent studies identified it as a hub (van den Heuvel and Sporns, 2013; D'Souza et al., 2014; Liska et al., 2015; Rubinov et al., 2015). Hubs may not always be reliably assigned into one single module by community detection methods given their multiple participation roles in different subsystems (Rubinov et al., 2015). Except for the cingulate cortex, all the other nodes of the first module under *Mediso* remained the same as the first module detected in the other groups, implying that the main functions of this module were retained across these regimens. Therefore, it was still named as salience-like module under *Mediso*. However, functional aspects related to the cingulate cortex should be absent in *Mediso* group.

In *Isoflurane1* group, perirhinal, ectorhinal and entorhinal cortices were involved into this module, whereas they were connected to the hippocampus under the other regimens. This indicated that the three nodes showed stronger functional connections with the first module under isoflurane. One possible reason may arise from the fact that isoflurane is a volatile anaesthetic agent. Perirhinal and entorhinal cortices both receive dense projections from olfactory bulb, piriform cortex and endopiriform nucleus (Herzog and Otto, 1998; Watson et al., 2011). The entorhinal cortex is thought to play a substantial role in odor memory process (Xu and Wilson, 2012). The three nodes are anatomically adjacent to each other and with dense anatomical connectivity to each other (Deacon et al., 1983; Brown and Aggleton, 2001). To achieve a near-awake resting state, the anaesthetic dosage was kept as light as possible. Hence, inhaling isoflurane might slightly enhance or preserve the functional synchronization between the three regions and olfactory related regions in this functional module. The near-awake resting state is the goal of current mouse rs-fMRI experiments to keep results comparable to awake resting state. But the unavoidable influence of agents emphasizes the proper compromise between anaesthetic depths and animals' states. This slight difference between *Isoflurane0.1* and other groups may further confirm the importance of understanding agent effects on the mouse brain for proper interpretations of results.

The second module was the lateral cortical module comprising only cortical regions related to visceral and gustatory functions and perceptions. This organization implied strong inter-connections between these cortical areas. A similar module was reported in awake rat brain containing visceral cortex, gustatory cortex, primary and supplemental somatosensory areas, but also motor cortex and insular cortex (Liang et al., 2012b). The difference may be caused by the anaesthetic depths and/or experimental procedures. But the LCN observed

in this study was more specific to the internal and external visceral-gustatory sensations, which are important for flavour perception and the taste system. Gustatory cortex influences visceral activities, such as gastrointestinal functions, cardiovascular and respiratory, to guide taste related behaviours (Krushel and van der Kooy, 1988; Chen et al., 2011; Peng et al., 2015). Visceral cortex is involved in efficient integration of these visceral sensory information and regulate visceral responses of organisms (Krushel and van der Kooy, 1988). Hence, this functional module may reflect the close functional connections between the gustatory-visceral perceptions and oral/olfactory somatosensory regions, indicating the important role of gustatory-visceral associations in food identification, selection and control of food intake in mice (de Araujo and Simon, 2009).

The third common module was the DMN-like module. It was reported by some previous rodent rs-fMRI studies with variations in the involved brain areas (Upadhyay et al., 2011b; Lu et al., 2012; Schwarz et al., 2013; Sforazzini et al., 2014; Stafford et al., 2014; Liska et al., 2015; Zerbi et al., 2015). However, anterior cingulate cortex was only assigned into the DMN-like module in *Mediso* group, which is more in line with most DMN studies. Based on results of Chapter 3 and previous long-range FC analysis (Grandjean et al., 2014b), better retained local and long-distance FC were observed in both cortical and subcortical brain regions under *Mediso*, suggesting that brain functions of the mouse were less affected by *Mediso* compared to the other regimens. Observations on this module under *Mediso* may confirm that it is a more promising regimen for studying mouse brain topology at rest. In *Isoflurane1* group, retrosplenial region was not involved in this module. However, the other nodes in it under isoflurane were the same as the other regimens, implying its fundamental functions may remain similar across groups. In awake rat, one study reported that the retrosplenial cortex was a single functional module. In contrast, it was not reported in any module under isoflurane anaesthesia (Liang et al., 2012b). These results implied that retrosplenial cortex might have dynamic roles in rodent functional networks. For example, it was reported to be a network hub in several rodent studies (D'Souza et al., 2014; Mechling et al., 2014). Overall, this module provided further evidence of the presence of a DMN-like structure in mice.

The fourth module detected across groups was a brain stem module with no cortical regions involved. This is in agreement with the absence of thalamocortical connections under corresponding regimens reported in the previous long-range FC analysis using data with GSR (Grandjean et al., 2014b). A brainstem-cerebellum module was reported in the mouse connectome (Rubinov et al., 2015), providing an anatomical substrate for the close functional connections between components within this module. Due to limitations of the

local shimming capacity of the small animal scanner, cerebellum was not included in this study. A thalamo-hypothalamo functional community was reported in awake rat (Liang et al., 2012b). Thalamus is well known for its role as the sensory information relay station to all cortical regions (except for olfactory pathways in mice). It is also increasingly recognized for playing substantial roles in higher order information regulations, sleep and arousal, memory, as well as motor control and monitoring (McCormick and Bal, 1997; Sommer, 2003; Watson et al., 2011; Saalmann and Kastner, 2015). It is proposed to be a common modulation site of several anaesthetics. Disrupted FC between thalamus and cortex is assumed to be critical for the loss of consciousness and a common feature of anaesthesia-induced unconsciousness (Alkire and Miller, 2005; Franks, 2008; Hudetz, 2012). The isolation of this module from cortical areas may be due to the disrupted synchronizations between thalamus and cortical regions. Hypothalamus is responsible for autonomic controls (Powley and Laughton, 1981; Toni et al., 2004; Mai and Paxinos, 2012). Midbrain and pons are involved in motor control, sleep regulation, hearing and vision information analysis (Margaret and Phyllis, 2009). Therefore, the brain stem module may have functions related to sensory information relay and modulation, sensory-motor modulation, sleep regulation and homeostatic controls. In *Isoflurane1* group, retrosplenial cortex and some parts of hippocampus were affiliated with this subsystem. Retrosplenial cortex is thought to play an important functional role in spatial navigation and memory when it acts with hippocampus and thalamus (Vann et al., 2009). This spatial memory circuitry (retrosplenial-hippocampus-thalamus) was reported in the fourth module as a subnetwork in mice by (Mechling et al., 2014). Hippocampus and thalamus were also reported to be allocated into the same module in both awake and isoflurane anaesthetized rats (Liang et al., 2012b). Furthermore, direct anatomical connections between retrosplenial cortex, hippocampus and thalamus are present in mammalian brain (Vann et al., 2009). Taken together, results from *Isoflurane1* group suggest that functional connections between the three regions may be less affected under isoflurane at commonly used dosages. Because all other nodes in this module revealed under *Isoflurane1* were almost the same as the brain stem module observed in the other groups, the main functions of the module should remain similar to the above mentioned functions. It is therefore still referred to as a brain stem module.

In *Medetomidine0.1* group, four nodes were grouped together as one single module: left temporal association area, left perirhinal area, left ectorhinal area and left entorhinal area. Given the close anatomical positions and connections between the four regions, this small module may have functions related to recognition and identification of the categorical natures of complex stimuli from external and internal environment, and memory associated

with these recognition functions (Purves et al., 2004). In humans, lesions in left and right temporal association cortex led to recognition deficits on different features (faces, objects, language-related materials) (Purves et al., 2004). One study on rats reported that temporal association lesion was associated with black-white reversal learning, implying that temporal association cortex in rodents may also be associated with recognition of specific properties of objects. This unilateral module may hence be related to some particular recognition abilities and related memory information processing. It might be a sub-system within the DMN-like module described above. Medetomidine is well-known for its vasoconstriction effect, which was translated into smaller magnitudes of BOLD fluctuations and delayed stimulated signals (Grandjean et al., 2014b; Schroeter et al., 2014). The long-distance cortical synchronizations between some cortical regions may be relatively weaker due to smaller signal magnitudes. GSR was reported to reveal more specific connectivity patterns (Kalthoff et al., 2013; Grandjean et al., 2014b). Taken together, one plausible explanation to the isolation of this sub-network was that there were stronger synchronizations between the four nodes, but relatively weaker synchronizations between them and their right-hemisphere counterparts or other functional correlated regions. It was not observed in modules detected in *Medetomidine0.1* group using VR data, which may support that it is a sub-module within a bigger functional community.

In summary, the mouse brain under anaesthesia presented high modularity feature. This is in line with the increasingly accepted notion that the brain is a complex system with hierarchical and modular organizations to support complex cognition and behaviour (Park and Friston, 2013). Similar functional modules were observed across agents, indicating that agent-specific effects did not significantly influence modular organizations. Cingulate cortex and retrosplenial cortex showed less consistency in the community affiliation across groups, implying their dynamic functional roles. Some differences between modules in *Isoflurane1* and other groups were observed, but did not change the main structure of the overall functional framework.

4.5.3 Anaesthetic depths influence modular organizations

In contrast to the similar four modules across agents, module organizations appeared to be influenced significantly by anaesthetic depths. Compared to the other groups, animals in *Medetomidine 0.05* and *Urethane1.5* groups were under lighter and deeper anaesthesia respectively (Grandjean et al., 2014b). Three modules were detected in *Medetomidine 0.05*, which were different from those detected in *Medetomidine 0.1*. Although a DMN-like module was observed, other modules were not similar to those described above. Cortical and

subcortical regions were mixed together under *Medetomidine 0.05*, implying stronger cortical and subcortical synchronizations under the lighter dosage. One study comparing functional communities under awake and anaesthetized rats reported similar phenomenon. They observed that functional communities under awake resting state consisted of mingled cortical and subcortical regions, whereas more communities under anaesthetized state consisted of separated cortical or subcortical regions. They concluded that cortical-subcortical communications were significantly compromised under anaesthesia (Liang et al., 2012b). The results from *Medetomidine 0.05* were in agreement with this conclusion.

Three modules were detected in *Urethane 1.5* group. Unlike the significantly reorganized communities under *Medetomidine 0.05*, functional segregations in this group were more in line with observations under other regimens. For example, the DMN-like and brain stem modules were detected. Another module contained nodes from salience-like and lateral cortical modules, i.e. salience-like and lateral cortical modules were merged into one bigger community under this regimen. At this deeper anaesthetic level, the separation from cortical and subcortical regions was observed, especially as evidenced in the brain stem module. As aforementioned, the disrupted communication between thalamus and cortical areas was a common feature of anaesthesia-induced unconsciousness. This may also explain the brain stem module observed under moderate to deeper dosages. The lateral cortical network serves mainly gustatory-visceral perceptions and oral/olfactory somatosensory information processing. Its main functions may be closely related to gustatory-visceral salience stimuli, olfactory information processing, affective processing, motivation and gustatory-visceral directed execution of behaviour, which are the main functions of the salience-like module. Hence, grouping the two together was not unexpected. The previous seed-based FC analysis on this dataset reported unspecific cortical FC in *Urethane 1.5*. They concluded that deeper anaesthesia induced global synchronizations of neuronal activity, and was significantly depressed with GSR (Grandjean et al., 2014b). EEG and rs-fMRI studies in rats under isoflurane and propofol reported a global synchronization in functional connectivity associated with EEG burst suppression as anaesthesia deepened (Austin et al., 2005; Liu et al., 2013b; Liu et al., 2013a). Hence, the merged community may be explained by the cortical synchronization masking more specific submodules in the brain.

Collectively, the modules under *Isoflurane1*, *Medetomidine0.1*, *Mediso*, *Propofol30* and *Urethane1.5* suggested that agent-specific effects of the five regimens may not influence community structures of the functional network in mice. The significantly reorganized modules under *Medetomidine 0.05* and the merged community under *Urethane1.5* indicated that anaesthetic depths affected community structures.

4.5.4 Anaesthetic effects on neurovascular coupling

Anaesthesia influences brain metabolism and neurovascular coupling, which may confound the observed topological properties. However, as discussed in Chapter 3, contributions of the vasculature under the investigated regimens to the long-range and regional connectivity are minor compared to the modulation of receptor systems. Graph analysis is usually based on long-range functional connectivity, hence the observed topological organizations should not be significantly influenced by vascular coupling.

4.5.5 GSR

GSR remains a controversial pre-processing step. To better understand influences of different anaesthetic regimens on large-scale network topologies in mice, this study performed analysis on data with and without GSR. Differences were observed, i.e. small-worldness was not detected, modules showed less consistencies across groups in VR data. These results were consistent with previous seed-based analysis using the same dataset (Grandjean et al., 2014b). Grandjean et al. reported that less specific functional networks were seen in data without GSR. This was in line with the recent conclusion that GSR can improve the specificity of positive correlations (Murphy and Fox, 2016). Graph measures were previously reported to be significantly affected by GSR in rats and humans, which supported the observations in this chapter (Murphy and Fox, 2016). Liska et al., however, did not find dramatic changes induced by GSR in the functional communities in mice. This might be due to the voxel-wise graph they used and/or different noise characteristics between datasets, since GSR contains both neural and non-neural components (Liska et al., 2015; Murphy and Fox, 2016). Furthermore, small-world property was observed in several rodent studies at awake state or under anaesthesia, indicating that it is a common feature of the rodent functioning brain (Liang et al., 2011, 2012b; Mechling et al., 2014). Collectively, these reports suggest that results from GVR data in this study may serve as a better reference for topological properties in mice.

4.5.6 Limitations of this study

There were limitations in the current study. First, there is no awake baseline using mouse rs-fMRI technique in this study. However, as far as we are aware, the awake mouse imaging is reported to be difficult (Jonckers et al., 2014). In addition, we used carefully monitored, ventilated and paralyzed animals to minimize physiological and motion confounds. BOLD fMRI signals from awake animals would especially have severe noise from movements, which would introduce auto-correlations between brain regions and artificially increase

functional connectivity. Second, the small sample sizes of the *Medetomidine0.05* and *Propofol30* groups may have introduced some confounds and individual variability into the results. However, the large-scale graph measures did not seem to be significantly affected by the small sample size.

4.5.7 Summary

The accumulative evidence on network topologies in human points to the promising avenues of applying graph metrics to understand functional organizations of the brain using rs-fMRI. The creation of transgenic mouse models of human brain diseases starts driving the need to characterize potential functional biomarkers of the abnormal brains in mice with translational techniques. In this context, mouse rs-fMRI receives increasing attention. Anaesthesia is a typical component in current mouse rs-fMRI and different labs adopted different anaesthetic protocols. The knowledge of impacts from various regimens on normal mouse brain is limited. To fill the gap, this chapter investigated how different regimens influence large-scale graph measures following the regional connectivity analysis in Chapter 3. To the best of my knowledge, this is the first study aiming at searching for large-scale topologies in mice across commonly used regimens using rs-fMRI. Findings showed that small-worldness was retained in the anaesthetized mice, but altered between *Medetomidine0.1* and *Mediso* groups. The overall functional modules were not affected by agent-specific effects. However, anaesthetic dosages impacted community organizations significantly.

Chapter 5 Functional brain network of the *DISC1* transgenic mouse model

5.1 Abstract

DISC1 has received much attention from scientists working to understand the neurobiological mechanisms of psychiatric diseases. *DISC1* transgenic mouse models have been created to perform experiment that are not possible in humans or other species. Over the past years, studies on these models have focused on histological, anatomical, biochemical and behavioural tests, but not fMRI given the challenge of applying this technique to mice. Meanwhile, fruitful discoveries have been accumulated in human (rs-)fMRI research to identify potential functional biomarkers of psychiatric diseases. Therefore, mouse rs-fMRI has been receiving increasing attention for translating findings between the two species. In this context, searching for functional phenotypes associated with *DISC1* gene is a major goal to understand how dysfunction of this gene influences the functional brain network. To achieve this aim, I investigated the functional brain network in the *αCaMKII-DN-DISC1* mouse model using rs-fMRI. Before *in vivo* rs-fMRI experiment, Y maze and fear conditioning were performed to assay the working and fear memories, respectively. Multi-scale analysis was performed. As far as I know, this is the first study investigating the effects of *DISC1* on functional brain network using mouse rs-fMRI with behavioural assays and multi-scale analytical methods. No significant differences were detected in behavioral tests, regional connectivity or most graph parameters. Mild differences in module organizations were detected. Amygdala showed stronger synchronizations with subcortical regions involved in fear learning and memory in the *DISC1* transgenic mice, whereas it was grouped with cortical regions and striatum in wild type controls. The results indicate that altered amygdala-related emotion and memory processing in transgenic mice may be associated with *DISC1* after the fear conditioning.

5.2 Introduction

Major mental disorders such as schizophrenia (SZ), bipolar disorder and major depression create a heavy social burden, and given the underlying pathology of these diseases is not well understood, they remain poorly treated (Brandon and Sawa, 2011). Several key elements are shared by SZ and affective disorders, such as abnormal neurodevelopment, glutamate dysfunction and altered grey and white matter structure (Belsham, 2001; Insel, 2010; Brandon and Sawa, 2011). Recent reports examining the genetic and molecular structure of brain disorders discovered the *DISC1* gene to be significantly associated with these disorders and plays a substantial role in influencing a range of endophenotypes underlying psychiatric disorders (Brandon and Sawa, 2011; Duff

et al., 2013). This has led to a powerful gateway for us to explore the underlying pathology and to achieve better diagnosis as well as treatments of major mental diseases. Characterising the phenotypes of *DISC1* in brain functions would provide valuable insights into the mechanism of how this gene influences the brain.

FMRI provides a powerful and translational approach to map the characteristics of brain activations. Rs-fMRI has been applied to more than 30 different kinds of brain disorders and different species (Biswal, 2012). Findings from fMRI studies on humans provide ample evidence of abnormal functional patterns in patients with mental illnesses (Mitterschiffthaler et al., 2006). Specifically, altered FC and network properties are proposed to be plausible imaging endophenotypes of psychotic disorders (Bullmore, 2012; Khadka et al., 2013). However, little is known about the direct effects of gene dysfunction, such as *DISC1* mutations, on resting-state brain activations. With the availability of *DISC1* transgenic mouse models and advanced high field small animal MRI scanner, the relationship between *DISC1* and abnormal brain activity is becoming more detectable.

The brain is a complex system with a hierarchical organization, whereby its RSN architecture can be characterised from mutiple perspectives. The most widely applied methods in human rs-fMRI studies can be classified into regional or global levels for the puporse of extracting complementary information (Zang et al., 2004; Li et al., 2009; Rubinov and Sporns, 2010; Cocchi et al., 2012b; Sporns, 2013; Liu et al., 2014). Hence, delineating functional brain networks of transgenic mice using analytical methods in parallel with those widely applied in human rs-fMRI research will provide useful and insightful information on abnormal FC associated with gene dysfunctions. This study applied multi-scale analysis on the *DISC1* mouse model, and therefore may facilitate ongoing translational studies.

Numerous *DISC1* mouse models have been generated to study the role of this gene in neuronal functions. Each model is unique due to its developmental timing of manipulation, laboratory conditions and assays used to characterize it. However, they exhibited several overlapping histological, anatomical, neurochemical and behavioural phenotypes associated with SZ or other mood disorders (Kelly and Brandon, 2011; Cash-Padgett and Jaaro-Peled, 2013). In this study, the *αCaMKII-DN-DISC1* mouse model was used. This model was generated by inserting a C-terminal truncated human DISC1 under the αCaMKII promoter in a pure C57BL/6 background. A dorminant-negative form of DISC1 is expressed under the αCaMKII promoter. The *αCaMKII-DN-DISC1* mice display several abnormalities that recapitulate findings from at least a subset of human schizophrenia patients. Enlargement of lateral ventricles, especially on the left side, were observed in juvenile mice (at 6-week old), however, this abnormality disappeared at 3-month old. Behavioural

analyses performed between 3 to 8 months revealed altered behavioural characteristics in *αCaMKII-DN-DISC1* mice compared to wild type control: these include hyperactivity, disturbance in sensorimotor gating, abnormal olfactory-associated behaviour and an anhedonia/depression-like deficit (Hikida et al., 2007). These observations suggest a link between the genetic mutation and associated phenotypic changes. One study demonstrated that gene-environmental interactions in this mouse model result in deficits of short-term object recognition and hippocampus-dependent fear memories, which have also been associated with SZ patients (Ibi et al., 2010). However, tests such as fear conditioning were not performed to characterize the effects of *DISC1* alone using this model. Abnormal emotions are significant features of major mental illnesses (Tremeau, 2006; Levenson et al., 2014) and fear is a well-studied emotion. It is therefore important to investigate how *DISC1* influences fear-related emotion and memory processing in the brain using transgenic mice. Characterizing the influence of *DISC1* alone without environment factors using mouse rs-fMRI remains an important research gap. Filling this gap will contribute to the translation of findings in animals to human patients suffering from the major mental illness from not only a behavioural perspective, but also from the perspective of the functional brain network.

This study aimed to determine how DISC1 influences the functional brain network using mouse rs-fMRI. The *αCaMKII-DN-DISC1* transgenic mouse model and their wild type littermates were first sent to Y maze and fear conditioning, then went through *in vivo* fMRI scanning. Regional connectivity, ICA and graph analysis were performed. The results may shed light on the impact of DISC1 on FC and network topologies in the mouse brain, and hence may help bridge findings between mice and humans using rs-fMRI to understand major mental disorders.

5.3 Materials and methods

5.3.1 Animals, behavioral experiment and MRI

Eleven heterozygous *αCaMKII-DN-DISC1* transgenic male mice (Tg) and ten littermate wild type male controls (Wt) were included in the experiment. Please find detailed descriptions in Chapter 2 Materials and Methods, Section 2.3.1.

5.3.2 Preprocessing

Slightly different pre-processing pipelines were applied to the topological analysis compared to ReHo and ICA analysis on Tg and Wt mice. Original spatial resolution was used for ReHo and ICA because of the much fewer time and computational resources required. For the construction of the adjacency matrix, higher spatial resolution was used

for the topological analysis to register EPI images to the anatomical template and Allen Mouse Brain Atlas.

5.3.2.a Pre-processing for regional connectivity and ICA

Pre-processing was performed using Statistical Parametric Mapping (SPM8, Wellcome Trust Centre for Neuroimaging, UK), MATLAB R2014a (The MathWorks, USA), FSL and Data Processing Assistant for Resting-State fMRI (DPARSF) (Chao-Gan and Yu-Feng, 2010) with the following pipeline. The first 10 time points were discarded, following realignment with 6 rigid body parameters and registration to a reference animal's mean EPI template using FLIRT and FNIRT. A brain mask was created based on the EPI template and applied to all data before further processing. Spatial smoothing was done with a Gaussian kernel of full width at half maximum = 1.5 voxel size. After detrend, movement traces and ventricle signals were regressed. Because the global signal is still disputable, data with and without the global signal regression (GSR) were both analysed. Finally, images were temporally filtered between 0.01 to 0.1Hz. Data without GSR would be referred to as MV data, while data with GSR would be referred to as MVG data.

No spatial smoothing was performed before ReHo calculation to reduce the introduction of artificial regional coherence influencing its reliability (Zuo et al., 2013). Other pre-processing steps were the same as described above.

5.3.2.b Pre-processing for graph analysis

Pre-processing was performed using Statistical Parametric Mapping (SPM8, Wellcome Trust Centre for Neuroimaging, UK), MATLAB R2014a (The MathWorks, USA), FSL and Data Processing Assistant for Resting-State fMRI (DPARSF) (Chao-Gan and Yu-Feng, 2010) with the following pipeline. The first 10 time points were discarded, following realignment with 6 rigid body parameters. A brain mask was created based on the EPI template and applied to all data before further processing. The anatomical template used for normalization was provided by the Australian Mouse Brain Mapping Consortium (AMBMC, http://www.imaging.org.au/AMBMC/AMBMC). All EPI images were normalized using FLIRT to a down-sampled version of this template. Spatial smoothing was done with a Gaussian kernel of full width at half maximum = 1.5 voxel size. After detrending, movement traces and ventricle signals were regressed. Because the global signal is still disputable, data with and without the global signal regression (GSR) were both analysed. Finally, images were temporally filtered between 0.01 to 0.1Hz. Data without GSR would be referred to as MV data, while data with GSR would be referred to as MVG data.

5.3.3 Post-processing

5.3.3.a Regional homogeneity analysis on the Tg and Wt mice

Please find details of ReHo calculation in Chapter 2 Materials and Methods, Section 2.4.3.a.

Voxel-wise statistics were performed using FSL, t-tests were performed within and between Tg and Wt groups. Image overlays indicate corrected $p<0.05$ for two sample unpaired t-test and one-sample t-test, threshold-free cluster enhancement correction (TFCE).

5.3.3.b ICA on the Tg and Wt mice

Please find detailed procedures of ICA and corresponding statistics in Chapter 2 Materials and Methods, Section 2.4.3.b.

5.3.3.c Graph analysis on the Tg and Wt mice

Please find detailed graph analytical methods and corresponding statistics in Chapter 2 Materials and Methods, 2.4.3.d.

5.4 Results

5.4.1 Behavioural tests

There was no statistically significant differences in the scores recorded from Y maze tests between Tg group and Wt group ($t_{(19)}=0.62$, $p=0.54$) indicating intact working memory. No statistically significant difference was detected in scores from contextual test after fear conditioning between the two groups ($t_{(19)}=0.91$, $p=0.37$) nor in the scores from the cue test between the two groups ($t_{(19)}=-1.70$, $p=0.10$). These results may suggest that no abnormal fear response and associative learning were observed in Tg mice in this study. Figure 5-1 shows bar plots presenting results from the three behavior assays.

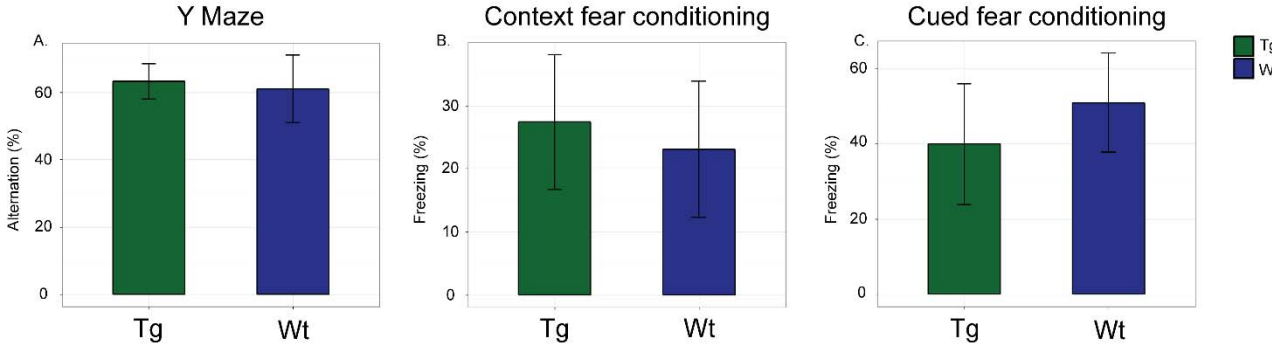

Figure 5-1 Behaviour assessment revealed no significant differences between Tg and Wt mice. (A) Results of Y maze paradigm. No significant difference was observed between Tg and Wt mice, two sample t-test $p = 0.54$. (B) Results of the test on the memory for the context after fear conditioning. No significant difference was detected in scores recorded from the context test, two sample t-test $p = 0.37$. (C) Results of the test on the memory for the cue after fear conditioning. No significant difference was detected in scores recorded from the cue test, two sample t-test $p = 0.10$. All results were showed as mean ± 1 SD over each group.

5.4.2 ReHo analysis

5.4.2.a ReHo analysis on MVG data

ReHo analysis reflected the strength of local connectivity between one voxel and its nearest neighbours. The distributions of ReHo in the brain of both Tg and Wt groups using MVG data were presented in group-mean maps for visual inspection as shown in Figure 5-2 (A). Both groups were associated with high ReHo across the entire brain. Somatosensory areas and thalamus yielded slightly higher ReHo compared to other brain structures. Results from one-sample t-test yielded similar patterns, therefore data not shown.

No between-group differences were revealed by two-sample t-test.

5.4.2.b ReHo analysis on MV data

ReHo results from MV data were presented in Figure 5-2 (B) and are very similar to results from MVG data. Values of local connectivity in MV data were higher than those in MVG data, thus yielded brighter images under the same colour coding range.

No between-group differences were revealed by two-sample t-test at local level.

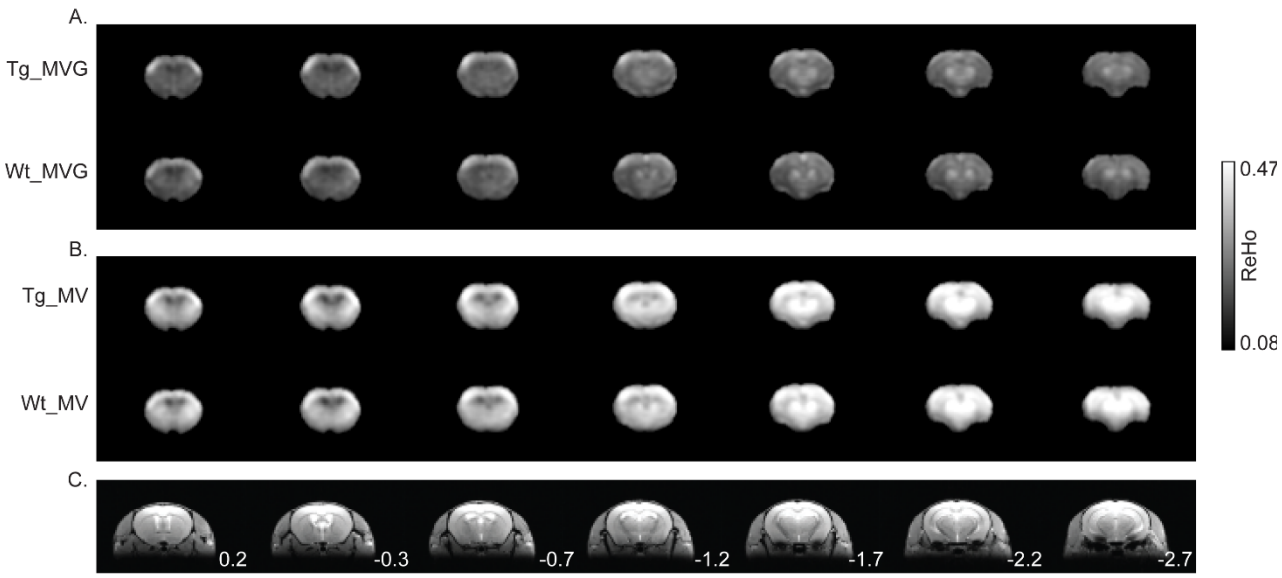

Figure 5-2 Group-mean maps of Tg and Wt mice calculated from both MVG and MV data showing the ReHo distribution. High ReHo values are observed across the whole brain. Cortical areas and thalamus show slightly higher ReHo in comparison to other areas. ReHo

values are colour coded for each voxel, as shown in the colour bar on the right side. (A) Group-mean maps from MVG data with group label on the left side. (B) Group-mean maps from MV data with group label on the left side. (C) Anatomical template of the selected coronal slices showing structural information of each slice. Distances (mm) relative to bregma are shown on the right bottom of the image.

5.4.3 Functional brain networks revealed by ICA

ICA analysis on MVG data revealed 11 components with clear anatomical confinements which are consistent with segregated functional systems in the mouse brain. Most RSNs revealed by the combined ICA on one mixed group and the separate ICA on each of the two groups showed high similarity. Functional brain networks are primary/secondary somatosensory cortex (S1/S2), primary/secondary motor cortex (M1/M2), cingulate/retrosplenial cortex (Cgu/RSD), piriform cortex (Pir, extending to some parts of insular cortex and amygdala), hippocampus (Hipp), thalamus (Thal), hypothalamus (HypoThal) and pons (extending to some parts of the midbrain). Figure 5-3 shows results from the combined ICA approach. No statistically significant between-group differences were detected by two-sample t test on the shared RSNs.

5.4.3.a ICA on MVG data

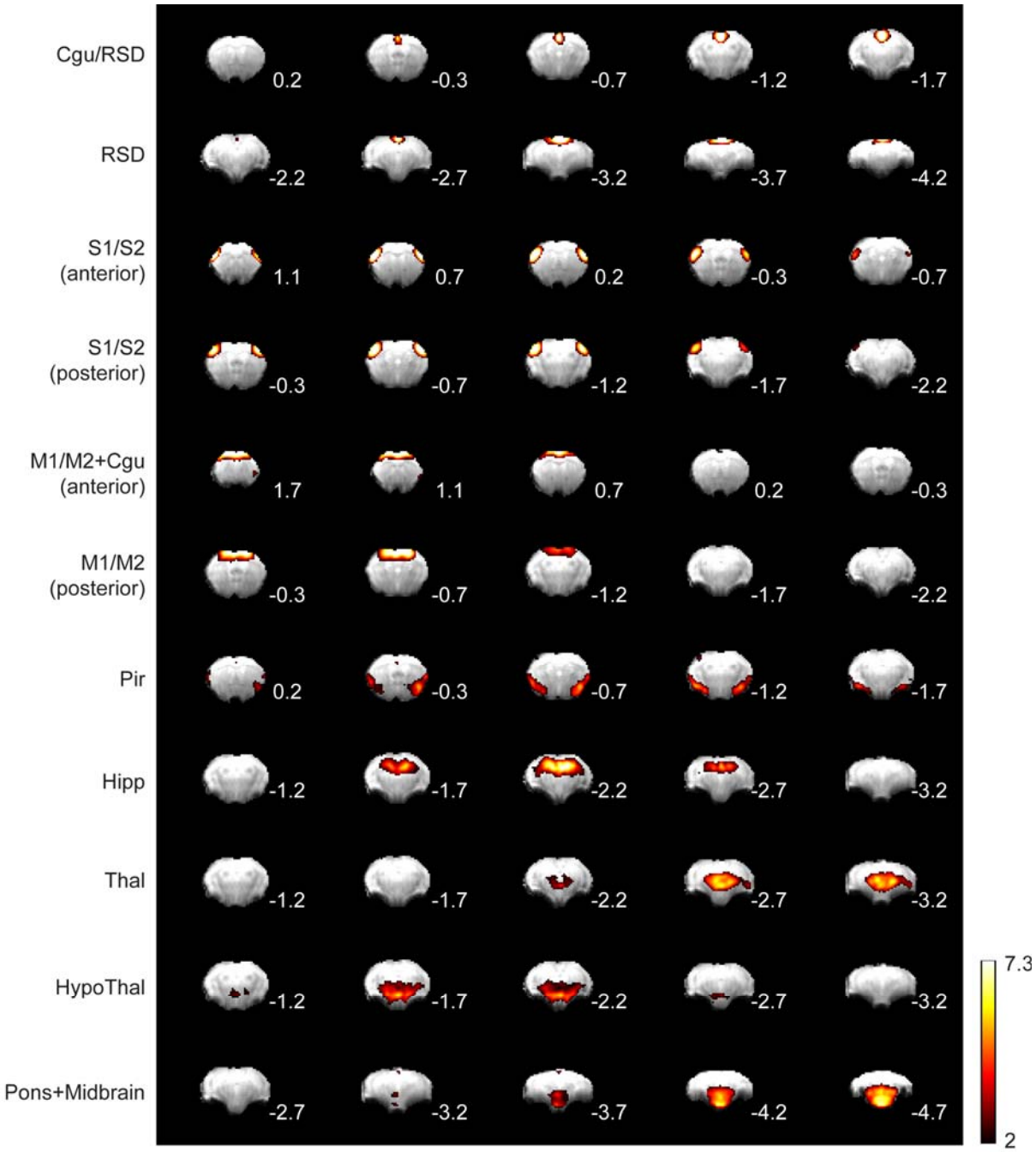

Figure 5-3 The combined ICA and separate ICA approaches revealed highly consistent RSNs in both Tg and Wt groups using MV data. Eleven RSNs detected by the combined ICA approach are shown. Each row showed the representative coronal slices of one identified component, with distinct pattern and clear anatomical confinement. This is in agreement with segregated functional systems of the mouse brain. Corresponding RSN names are listed on the left side. Image overlays indicate $|Z| > 2$ (equivalent to p<0.05, uncorrected). These results are very similar to functional clusters thresholded at p<=0.05 (FWE-corrected) for one-sample t-test (data not shown). Colour bar shows the range of values in the maps. Distances (mm) relative to bregma are shown on the right bottom of each coronal slice. Cgu/RSD: cingulate/retrosplenial cortex. RSD: retrosplenial cortex. S1/S2: primary/secondary somatosensory cortex. M1/M2: primary/secondary motor cortex. Pir: piriform cortex. Hipp: hippocampus. Thal: thalamus. HypoThal: hypothalamus.

5.4.3.b ICA on MV data

Similar RSNs were detected by ICA using data without GSR, as shown in Appendix I. No significant between-group differences were revealed by two-sample t test.

Among the shared RSNs, however, the separate ICA approach revealed that the piriform cortex was only detected in Tg group, as shown in Figure 5-4. At IC=50, piriform cortex was split into left and right functional clusters. A complete piriform cortex with bilateral patterns was observed at some other numbers of IC tested. No reliable nor clearly confined piriform cortex was seen in the Wt group. This subtle difference was reminiscent of the abnormal olfaction reported in the original study that established this *DISC1* mouse model (Hikida et al., 2007). However, similar results were observed in results of separate ICA on data with GSR. Therefore, I concluded that no reliable between-group differences in RSNs were discovered by ICA approaches.

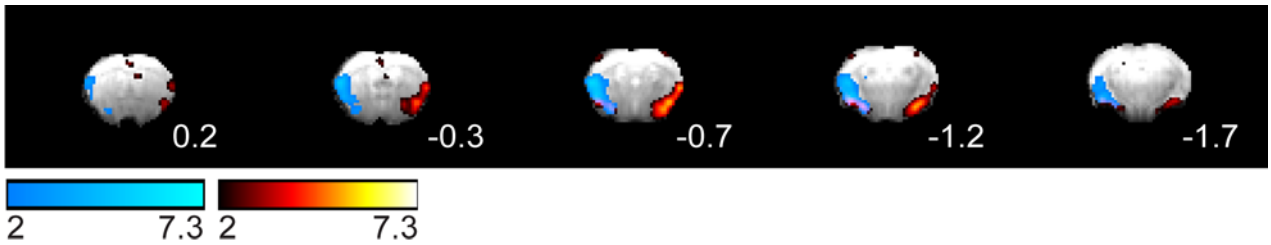

Figure 5-4 The piriform cortex was only observed in Tg group under separate ICA approach using MV data. At IC=50, the piriform cortex was split into left and right functional clusters as indicated by different colours. A complete bilateral piriform cortex could be observed at some other IC numbers. Image overlays indicate $|Z| > 2$ (equivalent to p<0.05, uncorrected). These results are consistent with functional clusters survived at p<=0.05 (FWE-corrected) for one-sample t-test (data not shown). Colour bars show the range of values in the maps. Distances (mm) relative to bregma are shown on the right bottom of the image.

5.4.4 Network topology revealed by graph analysis

5.4.4.a Similar global and nodal properties were observed in Tg and Wt mice

Analysis of MVG data revealed that the brain networks of Tg and Wt mice showed small-worldness ($\sigma > 1$) at all connection densities (Figure 5-5 (A)). In both groups, the normalized clustering coefficient was greater than 1 (gamma > 1) indicating higher clustering coefficient than expected in the random network (Figure 5-5 (B)). The normalized characteristic path length was approximately equal to 1 (lambda ≈ 1) suggesting that the average shortest path length was almost the same as expected in the random network (Figure 5-5 (C)). No between-group differences were identified in the global parameters investigated (σ :

p=0.49±0.26; C: *p*=0.39±0.20; gamma: *p*=0.41±0.27; L: *p*=0.26±0.13; lambda: *p*=0.27±0.12. All values were presented as mean±std. over all connection densities). Investigations of nodal parameters using MVG data revealed that there were several brain regions yielding statistically significant between-group differences in nodal global efficiency at some connection densities, however, none of the significant results were consistently observed across more than 50% of the densities investigated (Appendix J).

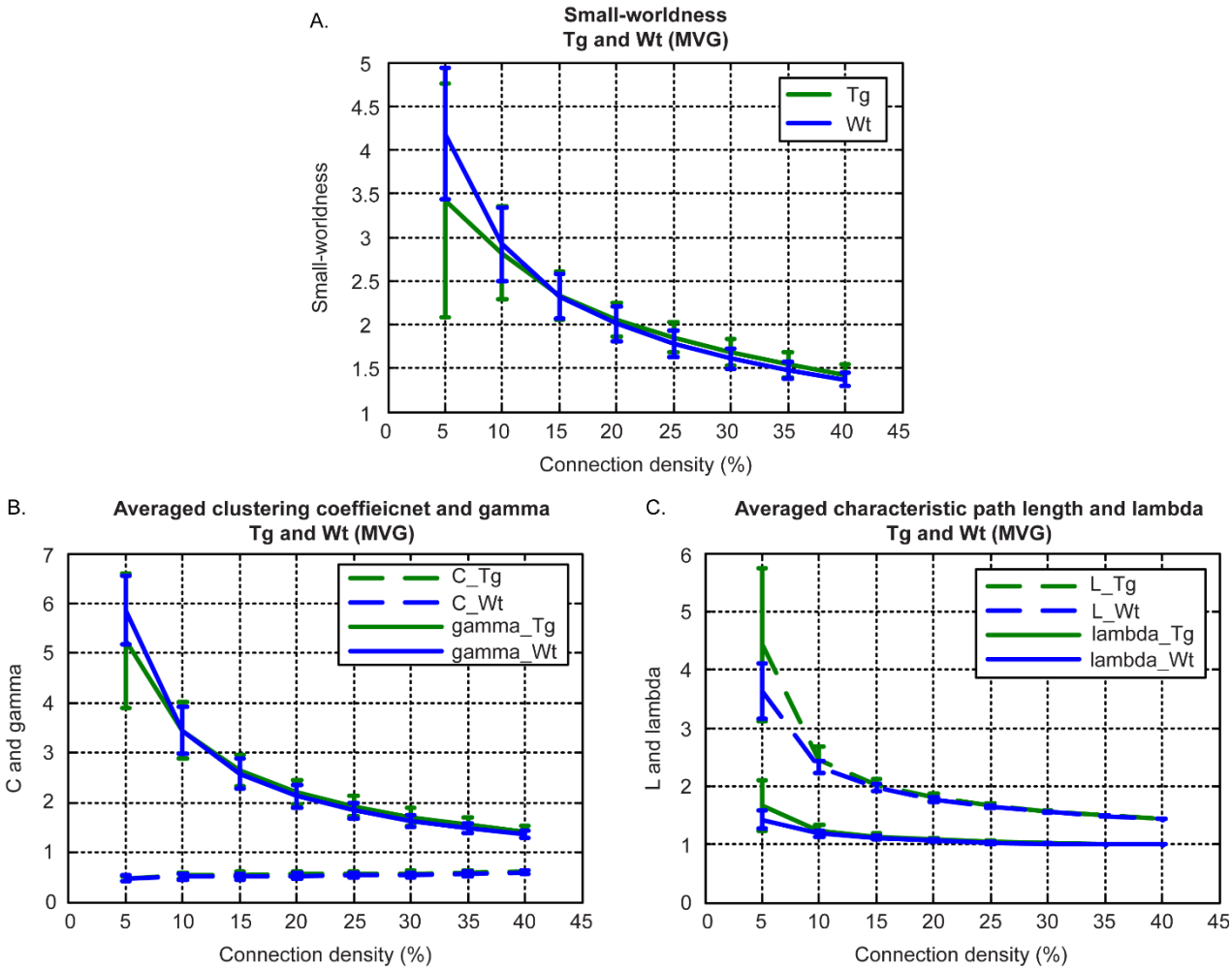

Figure 5-5 Global network attributes of the functional brain network in mice revealed in MVG data. No statistically significant between-group differences were found in the five measures and eight connection densities investigated. (A) Small-worldness. Both Tg and Wt mice showed small-worldness under all connection densities. No statistically significant differences were observed (*p*=0.49±0.26, mean±std. across all connectivity densities). (B) Averaged clustering coefficient and the normalized clustering coefficient (gamma). No statistically significant differences were observed (*p*=0.39±0.20 and *p*=0.41±0.27, respectively). (C) Averaged shortest path length and the normalized characteristic path length (lambda). No significant differences were detected (*p*=0.26±0.13 and *p*=0.27±0.12, respectively). All results were averaged over each group and error bars represent standard deviation.

Analysis on MV data revealed similar results with slight differences at higher connection densities. The functional brain network of both Tg and Wt mice showed small-worldness (

$\sigma > 1$) at sparse connection densities, but started approaching unity at higher densities (Appendix K (A)). Gamma was above one at sparse densities suggesting higher clustering coefficient than expected in the random network. As evidenced in small-worldness, gamma was approaching one at higher connection densities (Appendix K (B)). The normalized shortest path length was approximately equal to the unity (lambda ≈ 1) suggesting that the average shortest path length was almost the same as expected in the random network (Appendix K (C)). No between-group differences were identified in the global parameters investigated (σ: p=0.73±0.05; C: p=0.66±0.21; gamma: p=0.51±0.10; L: p=0.41±0.19; lambda: p=0.60±0.24. All values were presented as mean ± std. over all connection densities). No statistically significant between-group differences were detected in nodal clustering coefficient nor nodal global efficiency.

5.4.4.b Different functional module organizations between Tg and Wt mice

A large ensemble of high-Q degenerate partitions were detected in the mouse functional networks. The averaged Q of Tg and Wt groups calculated from GVR data were much higher (mean Q ± std.: 0.5554±0.0038 and 0.4915±0.0038, respectively) than the averaged Q values of their corresponding null-networks (mean Q ± std.: 0.1584±0.0035 and 0.1552±0.0027, respectively). The mean distance (VI) of discovered high-Q partitions of Tg and Wt mice (mean VI ± std.: 0.0762±0.0471 and 0.0948±0.0471, respectively) were much lower than VI of the corresponding null-networks (mean VI ± std.: 0.4952±0.0549 and 0.5242±0.0501, respectively). These parameters suggested the presence of high-modularity within the intrinsic functional networks in mice.

Three and four communities were revealed in Tg and Wt mice, respectively. While there was significant overlaps between the overall module structures of the two groups, some differences were discovered (Table 5-1 and Table 5-2). In Wt mice, the first module contained insular cortex, anterior cingulate area, prefrontal regions (prelimbic, orbital, olfactory and infralimbic areas), visceral area, primary and supplemental somatosensory areas, somatomotor area, gustatory area, and subcortical areas including claustrum, endopiriform nucleus, amygdala, striatum and pallidum. This module is almost the same as the first functional module observed in Tg mice, except for that amygdala was not included in this module of Tg group. The second module of Wt mice consisted of posterior parietal and temporal association area, posterior primary somatosensory area, perirhinal and ectorhinal areas, auditory, and subcortical regions containing hippocampus, thalamus, hypothalamus and some parts of the midbrain. This organization is very similar to the second module of Tg mice, except that amygdala and striatum-like amygdalar nuclei were

allocated into this module in the Tg group. The third module in Wt mice was small and mainly contained visual area and retrosplenial area. The fourth module consisted of posterior subcortical areas including retrohippocampal region, midbrain and pons. The third community of Tg mice contained nodes from the third and the fourth modules detected in Wt mice.

In summary, amygdala was allocated into a different module in Tg group implying altered functional connections between amygdala and brain regions in the first and second modular organization. Visual cortex and retrosplenial cortex formed a single module in the Wt group, suggested close functional connections between the two areas in mice that may reflect the dense reciprocal connections of retrosplenial cortex with visual cortex (Vann et al., 2009; Todd and Bucci, 2015). Strong functional connections between the two regions were reported in another study on modular structure in mice (Bardella et al., 2016).

Table 5-1 Consistent modules detected in the Tg group using MVG data

Modules	Brain regions within each module
Module 1	Agranular insular area, anterior cingulate area, prelimbic area, orbital area, olfactory area, infralimbic area, somatomotor area, entorhinal area, piriform cortex, claustrum, endopiriform nucleus, striatum, pallidum, visceral area, primary and supplemental somatosensory area, gustatory area
Module 2	Posterior parietal association area, primary somatosensory area (unassigned), temporal association area, perirhinal area, ectorhinal area, auditory area, hippocampus, amygdalar, striatum-like amygdalar nuclei, thalamus, hypothalamus, some parts of the midbrain
Module 3	Visual area, retrosplenial area, retrohippocampal region, midbrain, pons

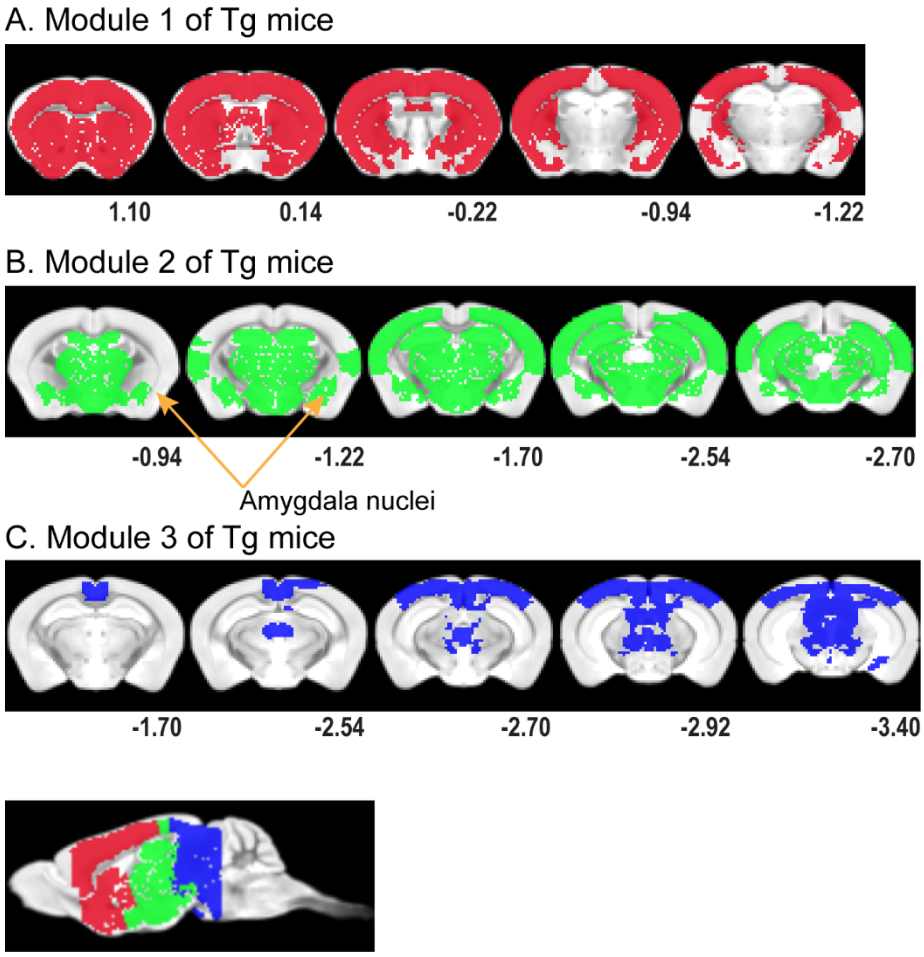

Figure 5-6 Three **f**unctional modules were detected in Tg group using MVG data. (A) The first module includes anterior cortical and subcortical regions. (B) The second module contains association areas, posterior somatosensory areas, hippocampus, amygdala and brain stem regions (thalamus, hypothalamus, some parts of the midbrain). (C) The third module consists of retrosplenial cortex, visual cortex, midbrain and pons. The orange arrows point to amygdala nuclei that are included in another functional module in Wt mice. The sagittal slice shows an overview of the three modules. Distances to bregma of each coronal slice is shown under the bottom of the images.

Table 5-2 Consistent modules detected in the Wt group using MVG data

Modules	Brain regions within each module
Module 1	Agranular insular area, anterior cingulate area, prelimbic area, orbital area, olfactory area, infralimbic area, somatomotor area, perirhinal area L, entorhinal area, piriform cortex, claustrum, endopiriform nucleus, amygdalar, striatum, pallidum, visceral area, primary and supplemental somatosensory area, gustatory area
Module 2	Posterior parietal association area, primary somatosensory area (unassigned), temporal association area, perirhinal area R, ectorhinal area, auditory area, hippocampus, lateral amygdalar nucleus R, thalamus, hypothalamus, some parts of the midbrain
Module 3	Visual area, retrosplenial area, posterior amygdalar nucleus R
Module 4	Retrohippocampal region, midbrain, pons

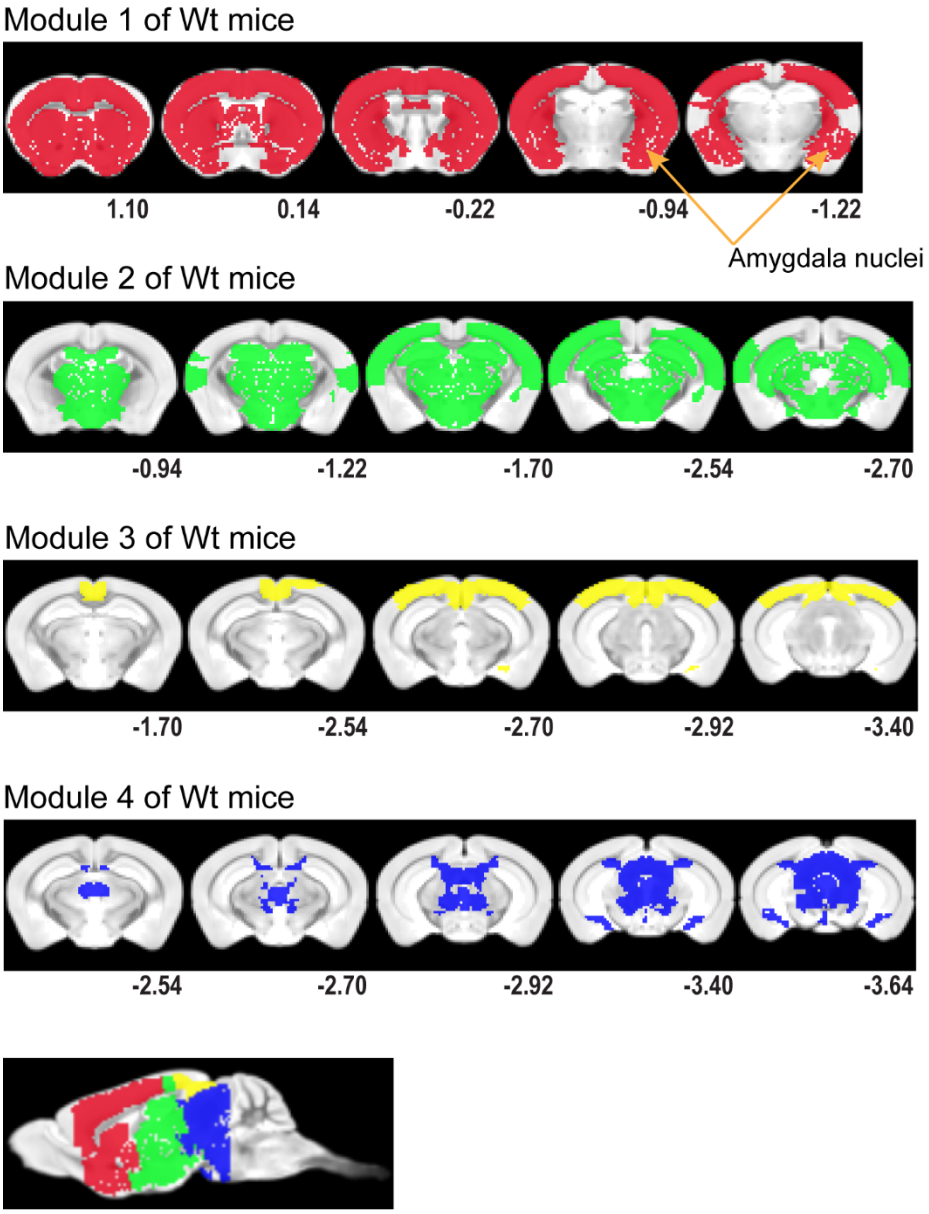

Figure 5-7 Four functional modules are detected in Wt mice using MVG data. (A) The first module contains mainly the anterior cortical and subcortical regions including amygdala, as well as entorhinal area. This module is very similar to the first functional module in Tg mice, except that amygdala is affiliated with the second module in Tg group. (B) The second module contains association areas, posterior somatosensory areas, auditory, hippocampus and brain stem regions (thalamus, hypothalamus, some parts of medbrain). Except for the absence of amygdala, this module is very similar to the second module detected in Tg group. (C) The third module includes mainly the retrosplenial and visual cortices, suggesting strong functional connections between the two regions. (D) The fourth module consists of retrohippocampal region and brain stem areas (midbrain, pons). The sagittal slice shows an overview of the three modules. Distances to bregma of each coronal slice is shown under the bottom of the images.

Module analysis on MV data revealed that the mouse brain of both Tg and Wt groups can be partitioned into three functional modules with subtly different organizations. Similar to observations in GVR, the averaged Q of Tg and Wt mice (mean ± std.: 0.0364±0.0006 and

0.0226±0.0002, respectively) were much higher than Q values of the null models (mean ± std.: 0.0065±0.0003 and 0.0043±0.0003, respectively). The average VI of Tg and Wt mice (mean VI ± std.: 0.1377±0.0643 and 0.1400±0.0612, respectively) were lower than their corresponding VI values of null networks (mean VI ± std.: 0.4726±0.0512 and 0.4365±0.0519, respectively). The parameters indicated the presence of high-modularity within functional networks in mice using MV data.

The modular organizations of Tg mice revealed in MV data are almost the same as described above in MVG data. The communities of Wt mice discovered in MV data were similar to those described above, except that the retrosplenial and visual regions were allocated into the second module, therefore forming a DMN-like network. The right posterior amygdala nucleus was assigned into the module containing retrohippocampal area, midbrain and pons. Because of several reasons, such as the non-deterministic nature of the modularity-based algorithms used (Good et al., 2010; Rubinov and Sporns, 2011), the structural differences between high-Q degenerate partitions, and the majority of amygdala nuclei were consistently grouped together across these partitions, the functional connections between the right posterior amygdala and retrosplenial-visual module may not strongly imply biological meanings for this module. Therefore, the following discussions focused on the main parts of each module. Detailed regions of all modular structures are shown in Appendix L and Appendix M.

In summary, similar module organizations were detected in Tg and Wt mice using both MV and MVG data. Amygdala showed altered module affiliation between the two groups. GSR introduced some changes in module structures in Wt mice.

5.5 Discussion

The goal of this study was to investigate the potential associations between FC and *DISC1* gene using the heterozygous *αCaMKII-DN-DISC1* transgenic mouse model, mouse rs-fMRI and regional-to-global analytical methods. To test if there were abnormalities in the working memory and emotional processing associated with DISC1, Y maze and fear conditioning behavioral tests were performed before *in vivo* rs-fMRI studies, respectively. No statistically significant between-group differences were observed in behavior assays, RSNs detected by ICA, regional connectivity, regional nor global graph parameters. However, differences were discovered in functional modules between the two groups. Amygdala was involved in a different module in Tg mice compared to the Wt mice.

5.5.1 Behavioural tests revealed no significant between-group differences

No abnormal behavioral phenotypes were observed in Y maze assay in Tg mice which is in agreement with the results reported by the group that generated this mouse model (Hikida et al., 2007). This suggests that there may be no impaired function of working memory in the Tg group. No abnormal behavioral phenotypes were observed in contextual nor cued memory tests after fear conditioning. To the best of my knowledge, this is the first fear conditioning tests have not been carried out on this mouse model to date. But Y maze and fear conditioning may not provide enough information on the behavioral characteristics of the Tg mice due to the absence of a wide array of behavioral assays.

5.5.2 Regional connectivity showed no difference as detected by ReHo analysis

The local connectivity patterns in both groups were very similar. High ReHo values were observed across the whole brain. Cortical and thalamus yielded slightly higher local connections. These results were consistent with ReHo patterns described in WT mice under isoflurane in Chapter 3. No differences were detected between Tg and Wt mice, implying that there may be no abnormal changes in regional FC. GSR reduced ReHo values, but did not introduce dramatic changes in their spatial distributions. This was consistent with results from human studies using ReHo (Maximo et al., 2013; Qing et al., 2015). The global signal may mainly reflect fluctuations shared by voxels across wider spatial distances (Murphy et al., 2009), therefore the less affected ReHo spatial distribution may be due to the regional coherence shared by a few closely clustered voxels that hold less weight in the global signal.

5.5.3 RSNs revealed by two ICA approaches showed no differences

Two ICA approaches were applied to detect the shared and different RSNs in the two groups. Results from the two approaches showed high consistency. Eleven commonly observed RSNs were revealed by the combined ICA in both Tg and Wt mice with no between-group differences detected. Interestingly, the separate ICA on MV data showed that piriform cortex was only observed in Tg mice, but not Wt mice. A separate ICA approach was applied to maximize potential differences and obtain ‘best fit’ estimations of the RSNs in each group (Cocchi et al., 2012a). This subtle difference was reminiscent of the abnormal olfaction of this mouse model reported previously (Hikida et al., 2007). Piriform cortex is one of the first cortical regions processing olfactory information in mammals and critical for initial odour perception (Robertson et al., 2006; Bekkers and Suzuki, 2013). Abnormal olfaction is observed in Schizophrenia (SZ) patients (Turetsky et al., 2009). However, this difference was not replicated by separate ICA on MVG data. Hikida et al. (2007) attributed the abnormal olfactory behaviour of this *DISC1* mouse model to either a problem in olfaction or poor

motivation. Based on the presence of the piriform cortex in results of Wt mice using MVG data and results of combined ICA on MV data, this difference was not strong enough to imply altered functional connectivity of the piriform RSN in Tg mice. Hence, results from ICA analysis implied that there were similar RSNs in both groups, but no differences in large-scale functional networks in the Tg group compared with the Wt group.

5.5.4 Network topology revealed by graph analysis showed differences in functional modules

5.5.4.a Similar global and nodal topologies were observed in Tg and Wt mice

The mouse brain exhibits small-worldness under isoflurane anaesthesia, a property indicating the simultaneous presence of distributed and specialized information processing (Bassett and Bullmore, 2006; Sporns and Honey, 2006). The presence of small-worldness characteristic in Tg mice is in agreement with the preserved small-world topology in human psychiatric patients including Schizophrenia (SZ) patients (Li et al., 2012a). The small-world network in Wt mice is in agreement with the results from WT mice under isoflurane in Chapter 4. Preserved small-worldness was reported by several previous studies on rats using rs-fMRI under anaesthesia or at awake state, as well as mice under medetomidine anaesthesia (Liang et al., 2011, 2012b; Mechling et al., 2014). There were no statistically significant differences between the two groups in all the compared graph parameters, collectively demonstrating that the functional network of Tg mice was topologically organized under similar governing principles to Wt mice. Disrupted small-world networks with altered nodal parameters (nodal clustering coefficients and efficiency) were reported in some studies of human SZ patients (Li et al., 2012a), but the local metrics of this *DSIC1* mouse model did not exhibit these alterations. As mentioned above, the behavioural phenotypes appeared to be consistent with the unchanged topology in Tg mice, suggesting that there were no significant effects of DISC1 on network organizations measured by these parameters in this model under isoflurane anaesthesia.

5.5.4.b Altered functional modules were detected in brain networks of Tg mice

This is the first study investigating degenerate high-modularity partitions of the functional brain network in the *DISC1* mouse model using rs-fMRI. Similar to functional human brain networks (Rubinov and Sporns, 2011), I observed degeneracy in the functional brain networks of the Tg and Wt mice. This is in agreement with the degeneracy observed in WT mice in Chapter 4, confirming that degeneracy may be a feature of functional brain networks in mice, and across species. The single gene investigated did not appear to influence this

intrinsic feature. Previous module analysis in WT mice typically reported only one high-Q partition, highly reproducible partitions or hierarchical structure of modules under a single anaesthetic agent (Mechling et al., 2014; Liska et al., 2015; Bardella et al., 2016). This study considered degenerate partitions and sought for the overlapping modules across a large sample of partitions representative of the whole partition space (Rubinov and Sporns, 2011), i.e. combined information from many degenerate solutions (Good et al., 2010), to collectively present the dynamic functional separation of the given network in a more comprehensive manner.

Except for the affiliation of amygdala, the overall modular organizations between the two groups showed similarity. In the Wt group, the first module mainly contained anterior cortical and subcortical regions. It is a module combining nodes from the salience-like module and lateral cortical module observed in Chapter 4. The differences between this module and the corresponding module in the *Isoflurane1* group in Chapter 4 may be due to the deeper anaesthetic level and free breathing paradigm used in this study. This module also resembles the frontal module reported in awake rats (Liang et al., 2012b). Several sub-systems may exist in this module, i.e. salience-like network (insular cortex, anterior cingulate cortex, striatum with extending to pallidum) (Seeley et al., 2007; Sforazzini et al., 2014), the cortical visceral-gustatory system and regions related to olfaction (olfactory areas, piriform cortex, endopiriform nucleus, entorhinal area). Furthermore, somatomotor area and prefrontal regions were affiliated with this functional community.

Insular cortex communicates with amygdala, regions in the prefrontal cortex and the olfactory cortex, and plays significant roles in affection, cognition and homeostatic systems (Uddin, 2016). The strong anatomical connections in mice between infralimibic cortex, striatum and amygdala suggest that this module is critical to emotional and autonomic functions (e.g. visceral related functions). Anatomical connections between prelimbic area, striatum, amygdala and orbital frontal cortex suggest that it is also important to cognitive functions (e.g. working memory). Another prefrontal cortex region affiliated with this module is the orbital area, with strong connections to sensory areas, insular area, amygdala and striatum. Orbital frontal areas are important in affective and motivational aspects of behaviour, as well as execution of goal-directed behaviour (Watson et al., 2011). Olfactory-related regions such as piriform cortex, endopiriform nucleus and olfactory area are inferred to be responsible for odor information processing and association. Piriform cortex and endopiriform nucleus project massively to amygdala, indicating interactions between olfactory functions, olfactory-related emotional processing and odor memory (Watson et al., 2011). Claustrum is a small region densely connected to almost all brain regions, therefore

regarded as an important multisensory integration centre (Crick and Koch, 2005). Gustatory cortex encodes different taste information in the brain and interacts with other brain regions to influence visceral activities to guide taste related behaviours (Krushel and van der Kooy, 1988; Chen et al., 2011; Peng et al., 2015). Visceral cortex is involved in the efficient integration of visceral sensory information and regulate visceral responses of organisms (Krushel and van der Kooy, 1988).

Based on the anatomical connectivity in mice between nodes of this module and their functional roles, the first module detected in the Wt group may possess several functions including salience directed function, olfactory information processing, affective processing, motivation and rewarding, gustatory-visceral associations, and behaviour selection directed by these external and internal sensory clues.

In Tg mice, however, amygdala was not allocated into this extensive community. From the observations on all WT mice in Chapter 4, amygdala was consistently grouped with many nodes of the first module as described above. This is similar to observations on anaesthetized rats (Liang et al., 2012b; D'Souza et al., 2014) and anaesthetized mice (Mechling et al., 2014). It was also grouped with prefrontal cortex and insular cortex in one study of awake rats (Liang et al., 2011). These results suggested that the communications between amygdala complex and nodes within the first module might be more detectable or more synchronized under normal states. The amygdala is connected to many brain regions including prefrontal cortex (prelimbic, infralimbic and anterior cingulate), sensory cortex (auditory, visual, somatosensory, gustatory, visceral and olfactory cortical areas), striatum, hippocampus, thalamus and hypothalamus. It associates different sensory modalities for emotional processing and memory processing (e.g., retrieving and storage), hence influences physiology and behaviour (Sah et al., 2003; LeDoux, 2007; Watson et al., 2011). In WT mice, the closer functional correlation between amygdala, the cortex and striatum compared to hippocampus, thalamus and hypothalamus suggested that sensory-, attention- and motivation-related aspects of emotional processing may be more retained at rest. In Tg mice, however, the functional correlations between amygdala and hippocampus, thalamus and hypothalamus appeared to be stronger, which will be discussed as follows.

In the Wt group, the second functional module contains hippocampus, thalamus, hypothalamus, some regions in the midbrain and several posterior cortical regions. A hypothalamo-thalamo-hippocampal module and a posterior module were detected in the anaesthetized rat brain (Liang et al., 2012b). The second module revealed in this study resembles a combination of the two. The hippocampal-hypothalamic subnetwork was previously reported in the anatomical brain network in mice (Rubinov et al., 2015).

Hippocampus is a crucial region for memory, spatial navigation, and interactions between emotion and memory (Scoville and Milner, 1957; Burgess et al., 2002; Phelps, 2004; Moser et al., 2008). Hippocampal-anterior thalamic pathways were reported to be important to human episodic and rodent event memory (Aggleton et al., 2010). Thalamus is well-known for its role as the sensory information relay station to all cortical regions (except for olfactory pathways in mice), playing substantial roles in higher order information regulations (McCormick and Bal, 1997; Sommer, 2003; Watson et al., 2011; Saalmann and Kastner, 2015) and is proposed to be a common modulation site of several anaesthetics. Disrupted FC between thalamus and cortex is assumed to be critical for the loss of consciousness and a common feature of anaesthesia-induced unconsciousness (Alkire and Miller, 2005; Franks, 2008; Hudetz, 2012). In this module, only several posterior cortical regions were involved, implying that functional connections between thalamus and the majority of cortical areas were disrupted. Hypothalamus is responsible for autonomic controls (homeostatic and metabolic controls) crucial for the organism's survival, behaviours, sleep and involved in emotion modulation (Powley and Laughton, 1981; Toni et al., 2004; Mai and Paxinos, 2012). Midbrain is involved in motor control, sleep regulation, hearing and visual information processing (Margaret and Phyllis, 2009). Cortical regions within this module are responsible for auditory and somatosensory information processing, higher order information processing on complex external and internal stimuli as well as recognition on the nature of these stimuli (Purves et al., 2004). Based on the functional roles of nodes and sub-circuitries in this community, this module is likely to serve memory functions, various sensory information relay and processing, sensory-motor modulation, sleep regulation and homeostatic controls.

The second module of the Tg group consisted of the above mentioned brain regions, but also amygdala. This implied that functional correlations between amygdala and some nodes in this module were enhanced in this group. Amygdala is a critical brain structure for emotion and emotional learning (Gallagher and Chiba, 1996), and it responds particularly to fearful stimuli. Studies on humans and animals indicated that fear conditioning is dependent on amygdala (LeDoux, 1998; Dalgleish, 2004). All mice were sent to fear conditioning before *in vivo* fMRI scanning, hence the altered allocation of amygdala in modular organizations may be related to the fear emotion, learning and expression. Most subcortical areas involved in the second functional module of Tg mice are important structures for the emotional brain system, such as amygdala, hippocampus, hypothalamus, thalamus, and some regions in the brainstem (e.g. ventral tegmental area) (Dalgleish, 2004). In addition, hippocampus and amygdala are viewed as two critical structures to the contextual fear conditioning (LeDoux, 2003). Emotion and memory closely interact with each other. Recent research evidence

shows that amygdala has roles in both the modulation of memory-related processing in hippocampus, and the storage of information related to emotional memory (especially fear induced events) (Richter-Levin, 2004). Thalamo-amygdala route sends rough sensory information to the amygdala for rapid and unconscious danger evaluation and fear responses. This route is essential for the survival of organisms. In human, activated amygdala showed strongest functional relations with subcortical areas than cortical areas, such as the thalamus during the fear conditioning experiment. It emphasized the important role of the thalamo-amygdala circuitry in fear responses (LeDoux, 2003). Anatomical connections between amygdala, hypothalamus and some regions in the midbrain allow emotional modulations on physiological states and bodily actions induced by fear (LeDoux, 2003; Sah et al., 2003). Taken together, the synchronization between amygdala and these subcortical areas in Tg mice may indicate the strengthened FC between them after fear conditioning, which might be associated with DISC1.

Altered behaviours in contextual fear conditioning in *DISC1* transgenic mice have been previously reported in another mouse model (Kuroda et al., 2011). Although the abnormal behaviours were not observed in this study using the heterozygous *αCaMKII-DN-DISC1* model, the changed allocation of amygdala in functional modules might provide clues to the effects of *DISC1* on the functional brain network associated with fear processing. Deficits in emotion processing and abnormal amygdala functions are significant symptoms in SZ patients (Shayegan and Stahl, 2005; Pankow et al., 2013; Mukherjee et al., 2014). Altered community organizations were reported in SZ patients and proposed to be potential biomarkers of aberrant development and the topological marker of this disorder (Yu et al., 2012). The altered module affiliation of amygdala in Tg mice implied changed modular organizations, hence is in line with these human clinical findings. The overall community structures were similar between Tg and Wt mice, one plausible reason may arise from the mild effects of the single gene on brain functions.

The third module in Wt mice mainly consisted of visual and retrosplenial areas. These close functional connections may reflect the dense reciprocal connections of retrosplenial cortex with visual cortex (Vann et al., 2009; Todd and Bucci, 2015). Retrosplenial cortex is thought to carry an important functional role in spatial navigation that usually requires visuospatial information and strategies (Vann et al., 2009; Hindley et al., 2014). Strong functional connections between the two regions were reported in another module study in mice (Bardella et al., 2016). The forth module in Wt mice contained midbrain, pons and parahippocampal regions. Midbrain and pons are involved in motor control, sleep regulation, hearing and visual information processing (Margaret and Phyllis, 2009). Parahippocampal

regions (subiculum complex) are important for the medial temporal memory system and interact with a wide range of cortical and subcortical regions. However, their functional roles are not well-understood. Their functions may be related to spatial navigation, motivation and memory processing (O'Mara et al., 2001; Witter, 2006). Anatomical projections from subiculum to brain stem suggest that it may play a role in motivated behaviours by passing highly processed information to the hypothalamus and brain stem (Kohler, 1990). Taken together, this module may serve functions including motor control and monitoring, sleep, memory and motivated behaviours.

In contrast, the third module in the Tg group was the combination of the third and the fourth modules detected in the Wt group, implying stronger synchronizations between these regions in Tg mice. Retrosplenial cortex, visual cortex and subiculum complex are all related to spatial navigation and information processing. Retrosplenial cortex and parahippocampal regions are not only anatomically connected, but their functions are very similar (Sugar et al., 2011). This functional module may therefore serve functions including not only motor control and monitoring, sleep, motivated behaviours, but spatial navigation and visuospatial memory.

GSR did not induce dramatic changes into the community structures of both groups. Consistent modular organizations revealed by data with and without GSR was previously reported by another mouse rs-fMRI study (Liska et al., 2015). In Wt mice, visual and retrosplenial cortices were merged into the second module revealed by MVG data. This bigger module was consistent with observations on *Isoflurane 1* group in Chapter 4. Retrosplenial cortex may have dynamic roles in rodent functional networks. For example, it was reported to be the topological hub in some previous rodent studies (D'Souza et al., 2014; Mechling et al., 2014). Based on their community affiliations across anaesthetic regimens in Chapter 4, the small module consisting of visual and retrosplenial cortices observed in the Wt group using MVG data may be due to effects of GSR. Increased specific functional connectivity patterns after applying GSR were reported in previous studies using seed-based analysis in rodents (Kalthoff et al., 2013; Grandjean et al., 2014b). This indicated that GSR may reveal potential sub-modules within a large functional community. Hierarchical modularity is an important property of the brain and is plausible given the multiscale nature of neuronal systems (Park and Friston, 2013). Given the close anatomical connections between visual and retrosplenial cortices, their close spatial positions and functional correlations, it is possible that the two areas formed a sub-community that could be detected after GSR. In Tg mice, the two areas were consistently connected to the module containing parahippocampal region, midbrain and pons in data with and without GSR.

Retrosplenial cortex and parahippocampal areas were reported to be necessary for normal acquisition of conditioned fear (Corcoran et al., 2011; Robinson and Bucci, 2012). The enhanced synchronizations between retrosplenial cortex and nodes in this module might also be due to an outcome following the fear conditioning. Visual cortex is very close to retrosplenial region and subiculum complex. It is involved in visuospatial memory and information processing. Pons receives visual information directly from visual cortex to guide movements (e.g., eye movements) (Sparks, 2002; Margaret and Phyllis, 2009). Hence, the increased synchronization between visual cortex and nodes in this module may imply enhanced relations between visuospatial information processing and visually determined movements. The fear learning on associations between contextual signals and fear response might be altered in Tg mice. This observation was reminiscent of the abnormal visual processing and visually related movements reported in SZ patients (Abel et al., 1992; Butler et al., 2008; King et al., 2016). However, as evidenced in Chapter 4, agent-specific effects did not influence the overall community structures. But some differences including community affiliation of retrosplenial cortex was observed in the *Isoflurane1* group, i.e. it was connected to brain stem regions in this group. Collectively, the more plausible explanation on this may be the dynamic roles of retrosplenial cortex in WT mice. Hence, the changed affiliation of retrosplenial cortex and visual cortex detected in Tg mice might also be a result of the dynamic hub roles of retrosplenial region.

In summary, network topological analysis revealed that small-worldness was retained in Tg and Wt mice. No differences in global parameters were detected. Similar modular organizations were observed in the two groups, but amygdala was connected to different functional communities implying altered emotional processing after fear conditioning. Visual cortex and retrosplenial cortex were allocated into a module containing parahippocampal regions, midbrain and pons in the Tg group, indicating potentially changed visual motion and spatial information processing. The two differences detected in modules of Tg mice were reminiscent of amygdala dysfunctions and abnormal visual motion processing observed in SZ patients. Therefore, the changed modular organizations in Tg mice might be associated with effects of DISC1 on functional brain networks. However, the second difference may also be explained by the dynamic functional roles of retrosplenial cortex.

5.5.5 Anaesthetic effects on FC in the *DISC1* mouse model

Result interpretations of mouse rs-fMRI signals should take effects of anaesthesia on neurovascular coupling into consideration. Although no cerebrovascular parameters were measured in this experiment, contributions of the vasculature under isoflurane are minor as

discussed in Chapter 3. FC properties of both Tg and Wt mice revealed in this study should reflect neural activity.

5.5.6 Limitations of this study

There were several limitations in this study. First, the absence of a wide spectrum of behavioural assays on the mouse model may not provide enough behavioural phenotypes for further assessments on animals' states. Second, although some differences in functional modules were detected in Tg group, they were not supported by findings of behaviour tests on both cued and contextual fear memory. Hence, interpretations of the results based on the associations between the effects of DISC1 and functional modules must be made with caution. Differences in module organizations may, however, serve as clues for further analysis and research. Third, differences between modules in Wt mice and WT mice of *Isoflurane1* in Chapter 4 were observed. This may be due to different experimental pipelines applied in the two studies (free-breathing vs ventilation, animal handling), different local shimming strategies, anaesthetic dosages, and/or possibly different coverage of the brain. It may be further supported by discrepancies between module studies on rodents across studies (Becerra et al., 2011; Liang et al., 2011, 2012b; D'Souza et al., 2014; Mechling et al., 2014; Liska et al., 2015; Bardella et al., 2016). However, the results observed from both datasets were from the collective information on a large ensemble of degenerate partitions aiming to present modular structures in a more comprehensive manner. Hence, they may serve as preliminary references for the ongoing brain network studies of mice using rs-fMRI. Fourth, there was no awake baseline in this study. However, as far as we are aware, the awake mouse imaging is reported to be difficult (Jonckers et al., 2014). In addition, all animals were carefully handled, monitored, and maintained to minimize physiological and motion confounds. BOLD fMRI signals from awake animals would especially suffer from severe noise due to movements, which would introduce auto-correlations between close brain regions and artificially increase functional connectivity between them. Fifth, isoflurane was applied to perform the experiment. It is the most commonly used inhalation agent for laboratory animal studies as described in Chapter 1. It yielded some specific regional to long-range FC in results from Chapter 3 and a seed-based analysis (Grandjean et al., 2014b). However, global graph parameters and modules may not be affected by agent-specific impacts based on observations in Chapter 4. Sixth, the anaesthetic depth used in this study was slightly above moderate. Furthermore, observations provided by this chapter were from only one *DISC1* transgenic mouse model. To fully understand impacts of this risk gene on functional brain networks in mice may require more studies on multiple *DISC1*

mouse models in future. Finally, timing is a critical factor for brain development and manifestations of gene dysfunctions (Cash-Padgett and Jaaro-Peled, 2013). Although the time points of behavioral and *in vivo* rs-fMRI experiment were strictly designed according to the original paper, more precise time points may be helpful for future studies. This is still a relatively new mouse model (Hikida et al., 2007)..

5.5.7 Summary

This chapter investigated associations between the effects of *DISC1* gene and functional brain networks using mouse rs-fMRI. The brain is a hierarchical modular system with multiscale nature. Different methodologies are developed to probe the characteristics of brain networks at various scales in human rs-fMRI community with fruitful results from both healthy and psychotic subjects. To be parallel to human studies, I applied commonly used analytical methods to capture information of FC and network topologies in Tg and Wt mice across scales. *DISC1* is a well-known gene for the major mental illness where abnormal emotion is one of the common characteristics (Manderscheid et al., 2010; Levenson et al., 2014). In addition, fear is a well-studied emotion. Animals were hence sent to fear conditioning before *in vivo* rs-fMRI scanning. To the best of my knowledge, this is the first study on effects of *DISC1* gene alone on the functional brain network using the heterozygous *αCaMKII-DN-DISC1* model, rs-fMRI and multiscale methodologies.

Findings from the investigations showed that there were no significant differences in regional connectivity, RSNs and most topological parameters between the Tg and Wt groups. These results were consistent with the behavioral tests. Functional module analysis revealed altered community affiliations of the amygdala, implying strengthened synchronization between this region and several subcortical areas involved in the emotional processing. Originally, Hikida et al. (2007) reported that the physiological and behavioral differences in the *αCaMKII-DN-DISC1* model were significant but subtle. Hence, additional environmental factors may be required for full manifestation of disease characteristics of the mouse model (Hikida et al., 2007). Results in this chapter indicated that some significant but subtle differences were detected by modular analysis, but not cued or contextual fear memory tests. This implies the absence of the link between function and behavior. One explanation may be that some changes associated with effects of *DISC1* on amygdala-related functions were introduced by fear conditioning, but not strong enough to be detectable by corresponding behavioral assays. Therefore, full manifestations of behavior, structure and functional phenotypes caused by the disruption of this single genetic factor may need strong environmental interruptions (e.g., stressors, insults). It also implies that rs-

fMRI may be a sensitive tool capturing mild changes in brain functions. Results of this chapter may contribute to our understanding of effects of *DISC1* alone on the FC in mice using rs-fMRI.

Chapter 6 General discussion

Overview

The goal of this thesis is to investigate functional brain network in the wild type and *DISC1* transgenic mouse model using rs-fMRI. Accumulative evidence from human rs-fMRI studies shows the power and potentials of rs-fMRI to reveal intrinsic characteristics of the normal brains and identify endophenotypes of abnormal brains. These progresses are accompanied by the development of various analytical methods for functional connectivity and network topology. The brain is a complex system with hierarchical nature of neural circuits, hence different methods provide complementary information on the brain's functional characteristics. Meanwhile, transgenic mouse models of human brain disorders are created to study phenotypes of gene dysfunctions. Particularly, a well-known *DISC1* gene is assumed to play substantial roles in major mental illnesses. Several *DISC1* mouse models are created. To translate findings between mice and humans, mouse rs-fMRI starts to receive increasing attention given the translational nature of the technique. Specifically, the functional phenotypes of *DISC1* in mice mapped by rs-fMRI has not been explored. Since mouse rs-fMRI is a growing but relatively new research field, knowledge accumulation in this field is still limited. Anaesthesia is a typical component of this technique. It helps to keep the animal still, maintain stable physiology and minimize motion and physiological artefacts. However, these advantages come with the cost of confounding effects from agents on BOLD signals. Therefore, understanding effects of gene dysfunctions on the abnormal mouse brain initially requires the understanding of how anaesthetics affect the normal mouse brain. Furthermore, different labs adopted different regimens bringing difficulties for result comparisons. Collectively, the need of functional imaging on transgenic mouse models using rs-fMRI and current limited knowledge of anaesthetic impacts on the FC in mice point to the necessity of understanding how different regimens influence the functional brain network in the mouse brain.

In this context, the thesis investigated effects of six different and commonly used anaesthetic regimens on FC characteristics in the wild type mice, using a multi-scale analysis to draw information about the brain from different perspectives (Chapter 3 and Chapter 4). Next, this research investigated effects of *DISC1* on the *αCaMKII-DN-DISC1* mouse model under one of the investigated regimens (0). To achieve this goal, I established experimental pipelines for mouse rs-fMRI data acquisition at UQ. After the pipeline validation (Section 2.2), data from the *αCaMKII-DN-DISC1* mouse model and its wild type littermate controls were acquired. Based on the experimental and analytical results, I am able to

answer the following questions with the novel findings and contributions to the field described as follows:

1. What is the regional connectivity in mice under different anaesthetic agents?

I observed high local coherence in most brain areas in mice across the six regimens. The primary somatosensory cortex and caudate-putamen showed agent-specific properties. Lower local coherence in the cingulate cortex was observed under medetomidine, particularly when compared to the combination of medetomidine and isoflurane. The thalamus was associated with retained local coherence across anaesthetic depths and multiple nuclei. Collectively, these results show that anaesthesia through different molecular targets promote agent-specific regional connectivity.

Because anaesthesia does not influence the brain uniformly as a whole, mapping regional synchronization provides information on the functioning brain from a local perspective. ReHo is widely applied in human rs-fMRI studies, our results show its sensitivity to extract information on varied neuronal activity under different agents in mice. These results, therefore, will inform future rs-fMRI studies on mice and the type of anaesthetic agent used, and will help to bridge observations between this burgeoning research field and ongoing human research across analytical scales.

2. How do different anaesthetic agents influence the large-scale network topologies?

I found out that small-worldness was retained in the anaesthetized mouse brain irrespective of the agents and dosages investigated. A significant difference in small-worldness between *Medetomidine0.1* and *Mediso* was detected, mainly driven by changed local clustering coefficient. This result implied that local alterations influenced the global topology. The overall functional modules were not affected by agent-specific effects, indicating a similar large-scale functional segregation in mice under moderate anaesthesia. However, anaesthetic depths affected functional modules implying that the functional segregation was affected by dosages significantly.

These results contribute to build preliminary references to the topology of the mouse functional network under commonly used agents, hence facilitate comparisons between different studies. They may serve as initial references to the growing research using transgenic mouse models. These results will also help bridge findings between mice and human research using graph theoretical analysis and rs-fMRI.

3. How does *DISC1* influence the functional network of the mouse brain mapped by rs-fMRI?

I found that there were no significant differences between the transgenic and wild type mice in behavioural tests, local connectivity patterns, large-scale RSNs and most graph parameters examined. Commonly observed RSNs were detected in both groups. Mild

differences in functional modules were detected. Amygdala was grouped with several subcortical regions involved in emotional processing in the transgenic mice, but with cortical and striatal regions in wild type mice. It implied that amygdala-related emotion processing in the *DISC1* mice may be altered after fear conditioning.

Searching for potential associations between *DISC1* and functional brain network in mice using rs-fMRI has not been explored previously. Attempts to fill this gap will contribute to our understanding on how the dysfunction of this single gene is manifested in FC in mice. The results suggest that its impacts on functional networks were mild. Amygdala-related emotional functions might be more vulnerable in the *αCaMKII-DN-DISC1* mouse model. Emotional deficits are significant symptoms of patients suffering from major mental illnesses. These results might imply a potential association between *DISC1* and amygdala functions. Furthermore, Schizophrenia is a complex disease due to multiple genetic and environmental factors. Consistent with the significant but subtle behavioural abnormalities reported in the original paper, mild changes in modules indicated that stronger environmental interruptions may be helpful to detect stronger effects of *DISC1* dysfunctions (Hikida et al., 2007). This may also suggest that mouse rs-fMRI is a technique sensitive to subtle changes of the brain functions.

All experiments performed in this thesis were under general anaesthesia, which alters the brain metabolism and neurovascular coupling. This raises concerns on effects of vasculature on the observed FC distributions and topologies in mice. As detailed in Chapter 3, however, the contribution of vascular effects on BOLD signals in mice under the investigated regimens were marginal. Hence, FC patterns and its topology in this thesis should reflect neural activity rather than vascular noise. Another issue raised by the usage of anaesthesia is that how comparable anaesthetic states in animals are to human resting states. Researchers make efforts to keep anaesthetic states in mouse rs-fMRI under light to moderate levels. This is to maintain the brain activity as similar to the awake states as possible, whereas minimizing movement and physiological noise during the experiment. As detailed in the later section, awake mouse rs-fMRI is not reliable yet, therefore cannot be used as “grand truth” or “reliable baseline”. In addition, resting-state networks (RSNs) and topological properties in mice reported by previous reports and this thesis showed significant correspondence with several RSNs measured by analogous techniques in awake (light anaesthetized) rats, monkeys and human studies (Vincent et al., 2007; Hutchison et al., 2011; Liang et al., 2012b; Grandjean et al., 2014a; Mechling et al., 2014; Nasrallah et al., 2014a; Sforazzini et al., 2014). These evidence suggest that results from mouse-rs-fMRI are comparable to many homologous RSNs in humans.

6.1 Influences of commonly used anaesthetic regimens on local to global FC characteristics

The usage of anaesthesia brings confounds into the identification and interpretations of meaningful BOLD signals in mice, especially might confound meaningful fluctuations in BOLD signals related to gene dysfunctions. By analysing local FC using ReHo and global topology using graph theory, this study showed that agent-specific effects on FC may originate from local FC properties. Functional modules were generally similar across agents, but significantly influenced by anaesthetic depths. Discrepancies in modular organizations have been observed in previous rodent studies under one anaesthesia agent (Liang et al., 2011, 2012b; D'Souza et al., 2014; Mechling et al., 2014; Bardella et al., 2016). Based on the observations presented here, one plausible explanation may be that there were other variables contributing to the differences between studies, such as different experimental pipelines, parcellation schemes, anaesthesia depths and/or detection algorithms (Liska et al., 2015; Bardella et al., 2016). The algorithm for community detection applied in the present study was the first to investigate degenerate partitions in mice. Results combined information from a large ensemble of detected degenerate candidates, hence provided a more comprehensive picture of the functional segregation compared to most previous studies reporting only one degenerate partition.

6.2 Associations between *DISC1* and changed FC in mice

Further understanding of the underlying mechanisms of major mental disorders requires investigations of animal models. Mouse rs-fMRI provides a translational and powerful tool to map how FC changes associated with specific gene dysfunctions. The current study provided the first evidence on how FC altered in one *DISC1* mouse model. Based on the understanding of how different agents influence functional brain network in mice and the available experimental conditions, we investigated this question by using the *αCaMKII-DN-DISC1* mouse model under isoflurane. Y maze and fear conditioning were performed before in *vivo* rs-fMRI. As evidenced in Chapter 4, agent-specific effects appeared to not influence the overall community structures. But some differences including community affiliation of retrosplenial cortex was observed in the *Isoflurane1* group. One plausible explanation on this may be the dynamic roles of retrosplenial cortex in WT mice. Hence, the changed affiliation of retrosplenial cortex and visual cortex detected in Tg mice might also be a result of the dynamic hub roles of retrosplenial region. To be conservative, the changed modular affiliation of amygdala hence appeared to be more associated with *DISC1* after fear conditioning.

Some differences in functional modules were observed in the Wt mice and WT mice under isoflurane in the thesis. Because the anaesthetic dosages applied to the free-breathing Wt mice was 1.2%, which was deeper than the light level of 1% isoflurane applied to the ventilated WT mice, one possible reason led to the differences may be the different anaesthetic dosages. Based on discussions and observations in Chapter 4, other variables that might also be contributing to the differences were breathing modality, local shimming strategies and animal handling procedures.

6.3 Limitations of the thesis

One limitation commonly shared by current mouse rs-fMRI studies is the absence of awake baseline in mice. However, as far as we are aware, the awake mouse imaging is reported to be difficult (Jonckers et al., 2014). In addition, all animals were carefully handled, ventilated (Chapter 3 and Chapter 4, but not in 0), monitored, and maintained to minimize physiological and motion confounds. BOLD fMRI signals from awake animals would especially have severe noise from movements, which would introduce auto-correlations between close brain regions and artificially increase FC between them. Furthermore, current awake mouse rs-fMRI is not feasible. Repeated restraint training for awake rat fMRI studies is reported to be a stressful procedure and can cause long-lasting changes in physiology, behavioral responses and brain responses to pain stimuli detected by fMRI, and may, therefore, introduce confounds into the functional pattern of BOLD signals (Upadhyay et al., 2011b; Henckens et al., 2015; Low et al., 2016b). In addition, briefly repeated an anaesthesia is commonly involved in MRI-acclimation training, which may result in cellular and hormonal changes (Low et al., 2016b). The long-lasting effects of repeated brief anaesthesia is not well-understood. Although Bergmann et al. (2016) reported that there was no abnormal breathing rate (as an indicator of stress levels) in the trained awake rats and that body temperature was maintained, direct physiological recordings were not reported (Bergmann et al., 2016). Jonkers et al. (2014) reported that oxygen saturation could not be performed in awake mice due to the encumbrance of this measurement. Hence, physiological verification of the awake rodents during fMRI experiment appeared to be difficult.

Second, GSR introduced different effects in studies presented in the thesis. Dramatic changes or few changes before and after GSR were reported across human and rodent studies. Murphy and Fox concluded that there is no gold standard to identify a single “right” way, but different processing approaches tend to provide complementary insights about the functional organizations of the brain (Murphy and Fox, 2016). Observations in this research

are in line with previous findings and support the conclusion. They show the complexity of GSR. Third, a wide spectrum of behavioral assays of the *αCaMKII-DN-DISC1* mouse model may be performed to further establish the states of transgenic mice in future research. Fourth, the topological study in Chapter 4 were performed with fewer slices covering the mouse brain due to limitations of the local shimming. This is a common limitation in most mouse rs-fMRI studies using ParaVision 5. However, the previous literatures and results reported in this research showed that basic FC characteristics were retained in the data covering the major bulk of the mouse brain. Finally, isoflurane is not the most ideal agent for cstudying mice. For example, caudate-putamen was not detected as a single RSN in Tg and Wt mice. This is in agreement with a formerly published study (Grandjean et al., 2014b). *Mediso* may be a more promising regimen for mouse rs-fMRI research.

6.4 Future work and conclusion

The future work on mouse rs-fMRI may take the results presented in the current study into considerations for the choice of anaesthetics according to the scientific questions and finding interpretations. More comparative work on other variables influencing the functional network in mice may be needed for establishing comprehensive references for the ongoing research, e.g. different MRI parameters, handling procedures, free-breathing and ventilation, anaesthetic dosages and shimming strategies. The future work on correlations between *DISC1* and functional network properties in mice may take the findings reported in the thesis into consideration for result comparisons, the choice of region-of-interest, experimental design (e.g., adding strong environmental factors), the choice of anaesthetic regimens and choices of the analytical pipelines.

In conclusion, this research investigated the functional network of the wild type and *DISC1* mouse model using rs-fMRI. The findings are the first to establish initial references to regional connectivity and the topology of the functional network in mice under six different anaesthetic regimens. Particularly, this work provides new insights into how agent-specific effects were manifested in the functional properties from a multiscale perspective. In addition, findings in the *DISC1* mouse model are the first to establish potential associations between this gene alone and changed properties of the functional brain network in mice using rs-fMRI. Specifically, this work provides clues on amygdala-related functions in this mouse model. Furthermore, results discussed in this thesis shed light on multiple directions for future research, including: 1) beyond anaesthesia, comparative studies on other variables affecting functional connectivity in mice may be necessary to deepen our understanding on mouse rs-fMRI; 2) investigating dysfunctions of *DISC1* using this mouse

model with strong environmental interruptions. Efforts on searching for translationally functional phenotypes using mouse rs-fMRI will need more work to solve the remaining issues of this technique and unanswered questions.

Bibliography

Abel LA, Levin S, Holzman PS (1992) Abnormalities of smooth pursuit and saccadic control in schizophrenia and affective disorders. Vision Res 32:1009-1014.

Achard S, Bullmore E (2007) Efficiency and cost of economical brain functional networks. PLoS Comput Biol 3:e17.

Aggleton JP, O'Mara SM, Vann SD, Wright NF, Tsanov M, Erichsen JT (2010) Hippocampal-anterior thalamic pathways for memory: uncovering a network of direct and indirect actions. Eur J Neurosci 31:2292-2307.

Alkire MT, Miller J (2005) General anesthesia and the neural correlates of consciousness. Boundaries of Consciousness: Neurobiology and Neuropathology 150:229-244.

Ambrosino S, Bos DJ, van Raalten TR, Kobussen NA, van Belle J, Oranje B, Durston S (2014) Functional connectivity during cognitive control in children with autism spectrum disorder: an independent component analysis. J Neural Transm (Vienna) 121:1145-1155.

Arcelli P, Frassoni C, Regondi MC, De Biasi S, Spreafico R (1997) GABAergic neurons in mammalian thalamus: a marker of thalamic complexity? Brain Res Bull 42:27-37.

Attwell D, Buchan AM, Charpak S, Lauritzen M, MacVicar BA, Newman EA (2010) Glial and neuronal control of brain blood flow. Nature 468:232-243.

Austin VC, Blamire AM, Allers KA, Sharp T, Styles P, Matthews PM, Sibson NR (2005) Confounding effects of anesthesia on functional activation in rodent brain: a study of halothane and alpha-chloralose anesthesia. Neuroimage 24:92-100.

Ballesteros KA, Sikorski A, Orfila JE, Martinez JL, Jr. (2012) Effects of inhaled anesthetic isoflurane on long-term potentiation of CA3 pyramidal cell afferents in vivo. Int J Gen Med 5:935-942.

Baltes C, Bosshard S, Mueggler T, Ratering D, Rudin M (2011) Increased blood oxygen level-dependent (BOLD) sensitivity in the mouse somatosensory cortex during electrical forepaw stimulation using a cryogenic radiofrequency probe. NMR Biomed 24:439-446.

Bandettini PA (2012) Twenty years of functional MRI: the science and the stories. Neuroimage 62:575-588.

Bardella G, Bifone A, Gabrielli A, Gozzi A, Squartini T (2016) Hierarchical organization of functional connectivity in the mouse brain: a complex network approach. Scientific Reports 6:32060.

Bassett DS, Bullmore E (2006) Small-world brain networks. Neuroscientist 12:512-523.

Becerra L, Pendse G, Chang PC, Bishop J, Borsook D (2011) Robust reproducible resting state networks in the awake rodent brain. PLoS ONE 6:e25701.

Beckmann CF, DeLuca M, Devlin JT, Smith SM (2005) Investigations into resting-state connectivity using independent component analysis. Philosophical Transactions of the Royal Society B-Biological Sciences 360:1001-1013.

Bedell MA, Jenkins NA, Copeland NG (1997) Mouse models of human disease. Part I: techniques and resources for genetic analysis in mice. Genes Dev 11:1-10.

Bekkers JM, Suzuki N (2013) Neurons and circuits for odor processing in the piriform cortex. Trends Neurosci 36:429-438.

Belcher AM, Yen CC, Stepp H, Gu H, Lu H, Yang Y, Silva AC, Stein EA (2013) Large-scale brain networks in the awake, truly resting marmoset monkey. J Neurosci 33:16796-16804.

Belsham B (2001) Glutamate and its role in psychiatric illness. Hum Psychopharmacol 16:139-146.

Bennett CM, Miller MB (2010) How reliable are the results from functional magnetic resonance imaging? Year in Cognitive Neuroscience 2010 1191:133-155.

Benveniste H, Blackband SJ (2006) Translational neuroscience and magnetic-resonance microscopy. Lancet Neurol 5:536-544.

Bergmann E, Zur G, Bershadsky G, Kahn I (2016) The Organization of Mouse and Human Cortico-Hippocampal Networks Estimated by Intrinsic Functional Connectivity. Cereb Cortex.

Biswal B, Yetkin FZ, Haughton VM, Hyde JS (1995) Functional connectivity in the motor cortex of resting human brain using echo-planar MRI. Magn Reson Med 34:537-541.

Biswal BB (2012) Resting state fMRI: A personal history. Neuroimage 62:938-944.

Blondel VD, Guillaume JL, Lambiotte R, Lefebvre E (2008) Fast unfolding of communities in large networks. Journal of Statistical Mechanics-Theory and Experiment.

Bonhomme V, Boveroux P, Brichant JF, Laureys S, Boly M (2012) Neural correlates of consciousness during general anesthesia using functional magnetic resonance imaging (fMRI). Arch Ital Biol 150:155-163.

Bosshard SC, Baltes C, Wyss MT, Mueggler T, Weber B, Rudin M (2010) Assessment of brain responses to innocuous and noxious electrical forepaw stimulation in mice using BOLD fMRI. Pain 151:655-663.

Boveroux P, Vanhaudenhuyse A, Bruno MA, Noirhomme Q, Lauwick S, Luxen A, Degueldre C, Plenevaux A, Schnakers C, Phillips C, Brichant JF, Bonhomme V, Maquet P, Greicius MD, Leureys S, Boly M (2010) Breakdown of within- and between-network

Resting State Functional Magnetic Resonance Imaging Connectivity during Propofol-induced Loss of Consciousness. Anesthesiology 113:1038-1053.

Brandon NJ, Sawa A (2011) Linking neurodevelopmental and synaptic theories of mental illness through DISC1. Nat Rev Neurosci 12:707-722.

Brown EN, Lydic R, Schiff ND (2010) General anesthesia, sleep, and coma. N Engl J Med 363:2638-2650.

Brown MW, Aggleton JP (2001) Recognition memory: What are the roles of the perirhinal cortex and hippocampus? Nat Rev Neurosci 2:51-61.

Buckner RL, Andrews-Hanna JR, Schacter DL (2008) The brain's default network: anatomy, function, and relevance to disease. Ann N Y Acad Sci 1124:1-38.

Bullmore E (2012) Functional network endophenotypes of psychotic disorders. Biol Psychiatry 71:844-845.

Bullmore E, Sporns O (2009a) Complex brain networks: graph theoretical analysis of structural and functional systems. Nat Rev Neurosci 10:186-198.

Bullmore E, Sporns O (2009b) Complex brain networks: graph theoretical analysis of structural and functional systems. Nat Rev Neurosci 10:186-198.

Bullmore ET, Bassett DS (2011) Brain graphs: graphical models of the human brain connectome. Annu Rev Clin Psychol 7:113-140.

Burgess N, Maguire EA, O'Keefe J (2002) The human hippocampus and spatial and episodic memory. Neuron 35:625-641.

Butler PD, Silverstein SM, Dakin SC (2008) Visual Perception and Its Impairment in Schizophrenia. Biol Psychiatry 64:40-47.

Butts CT (2009) Revisiting the foundations of network analysis. Science 325:414-416.

Calhoun VD, Liu J, Adali T (2009) A review of group ICA for fMRI data and ICA for joint inference of imaging, genetic, and ERP data. Neuroimage 45:S163-172.

Calhoun VD, Adali T, Pearlson GD, Pekar JJ (2001) A method for making group inferences from functional MRI data using independent component analysis. Hum Brain Mapp 14:140-151.

Cao QJ, Zang YF, Sun L, Sui MQ, Long XY, Zou QH, Wang YF (2006) Abnormal neural activity in children with attention deficit hyperactivity disorder: a resting-state functional magnetic resonance imaging study. Neuroreport 17:1033-1036.

Cash-Padgett T, Jaaro-Peled H (2013) DISC1 mouse models as a tool to decipher gene-environment interactions in psychiatric disorders. Front Behav Neurosci 7:113.

Chao-Gan Y, Yu-Feng Z (2010) DPARSF: A MATLAB Toolbox for "Pipeline" Data Analysis of Resting-State fMRI. Front Syst Neurosci 4:13.

Chen X, Gabitto M, Peng Y, Ryba NJ, Zuker CS (2011) A gustotopic map of taste qualities in the mammalian brain. Science 333:1262-1266.

Chen XJ, Kovacevic N, Lobaugh NJ, Sled JG, Henkelman RM, Henderson JT (2006) Neuroanatomical differences between mouse strains as shown by high-resolution 3D MRI. Neuroimage 29:99-105.

Chubb JE, Bradshaw NJ, Soares DC, Porteous DJ, Millar JK (2008) The DISC locus in psychiatric illness. Mol Psychiatry 13:36-64.

Cocchi L, Harrison BJ, Pujol J, Harding IH, Fornito A, Pantelis C, Yucel M (2012a) Functional alterations of large-scale brain networks related to cognitive control in obsessive-compulsive disorder. Hum Brain Mapp 33:1089-1106.

Cocchi L, Bramati IE, Zalesky A, Furukawa E, Fontenelle LF, Moll J, Tripp G, Mattos P (2012b) Altered functional brain connectivity in a non-clinical sample of young adults with attention-deficit/hyperactivity disorder. J Neurosci 32:17753-17761.

Corcoran KA, Donnan MD, Tronson NC, Guzmán YF, Gao C, Jovasevic V, Guedea AL, Radulovic J (2011) NMDA Receptors in Retrosplenial Cortex Are Necessary for Retrieval of Recent and Remote Context Fear Memory. The Journal of Neuroscience 31:11655-11659.

Cordes D, Haughton VM, Arfanakis K, Wendt GJ, Turski PA, Moritz CH, Quigley MA, Meyerand ME (2000) Mapping functionally related regions of brain with functional connectivity MR imaging. American Journal of Neuroradiology 21:1636-1644.

Crick FC, Koch C (2005) What is the function of the claustrum? Philosophical Transactions of the Royal Society B-Biological Sciences 360:1271-1279.

D'Esposito M, Deouell LY, Gazzaley A (2003) Alterations in the BOLD fMRI signal with ageing and disease: a challenge for neuroimaging. Nat Rev Neurosci 4:863-872.

D'Souza DV, Jonckers E, Bruns A, Kunnecke B, von Kienlin M, Van der Linden A, Mueggler T, Verhoye M (2014) Preserved modular network organization in the sedated rat brain. PLoS ONE 9:e106156.

Dalgleish T (2004) The emotional brain. Nat Rev Neurosci 5:583-589.

Damoiseaux JS, Rombouts SA, Barkhof F, Scheltens P, Stam CJ, Smith SM, Beckmann CF (2006) Consistent resting-state networks across healthy subjects. Proc Natl Acad Sci U S A 103:13848-13853.

de Araujo IE, Simon SA (2009) The gustatory cortex and multisensory integration. Int J Obes 33 Suppl 2:S34-43.

De Luca M, Beckmann CF, De Stefano N, Matthews PM, Smith SM (2006) fMRI resting state networks define distinct modes of long-distance interactions in the human brain. Neuroimage 29:1359-1367.

Deacon TW, Eichenbaum H, Rosenberg P, Eckmann KW (1983) Afferent connections of the perirhinal cortex in the rat. J Comp Neurol 220:168-190.

Dean K, Murray RM (2005) Environmental risk factors for psychosis. Dialogues Clin Neurosci 7:69-80.

Dember WN, Fowler H (1958) Spontaneous alternation behavior. Psychol Bull 55:412-428.

Dorr A, Sled JG, Kabani N (2007) Three-dimensional cerebral vasculature of the CBA mouse brain: a magnetic resonance imaging and micro computed tomography study. Neuroimage 35:1409-1423.

Dorr AE, Lerch JP, Spring S, Kabani N, Henkelman RM (2008) High resolution three-dimensional brain atlas using an average magnetic resonance image of 40 adult C57Bl/6J mice. Neuroimage 42:60-69.

Duff BJ, Macritchie KA, Moorhead TW, Lawrie SM, Blackwood DH (2013) Human brain imaging studies of DISC1 in schizophrenia, bipolar disorder and depression: a systematic review. Schizophr Res 147:1-13.

Eklund A, Nichols TE, Knutsson H (2016) Cluster failure: Why fMRI inferences for spatial extent have inflated false-positive rates. Proc Natl Acad Sci U S A 113:7900-7905.

Fiset P, Paus T, Daloze T, Plourde G, Meuret P, Bonhomme V, Hajj-Ali N, Backman SB, Evans AC (1999) Brain mechanisms of propofol-induced loss of consciousness in humans: a positron emission tomographic study. J Neurosci 19:5506-5513.

Fodale V, La Monaca E (2008) Propofol infusion syndrome: an overview of a perplexing disease. Drug Saf 31:293-303.

Fornito A, Zalesky A, Bullmore E (2016) Fundamentals of brain network analysis. U.S.A.: Academic Press.

Fox MD, Raichle ME (2007) Spontaneous fluctuations in brain activity observed with functional magnetic resonance imaging. Nat Rev Neurosci 8:700-711.

Fox MD, Snyder AZ, Vincent JL, Corbetta M, Van Essen DC, Raichle ME (2005) The human brain is intrinsically organized into dynamic, anticorrelated functional networks. Proc Natl Acad Sci U S A 102:9673-9678.

Fox PT (2012) The coupling controversy. Neuroimage 62:594-601.

Franklin KBJ, Paxinos G (2007) The mouse brain in stereotaxic coordinates, 3rd Edition. Academic Press, San Diego: Elsevier Academic Press.

Franks NP (2008) General anaesthesia: From molecular targets to neuronal pathways of sleep and arousal. Nature Reviews Neuroscience 9:370-386.

Friston KJ (2011) Functional and effective connectivity: a review. Brain Connect 1:13-36.

Friston KJ (2012) What does functional MRI measure? Two complementary perspectives. Trends in Cognitive Sciences 16:491-492.

Fukuda M, Vazquez AL, Zong X, Kim S-G (2013) Effects of the α(2)-adrenergic receptor agonist dexmedetomidine on neurovascular responses in somatosensory cortex. The European journal of neuroscience 37:80-95.

Fulton B, Goa KL (1996) Propofol - A pharmacoeconomic appraisal of its use in day case surgery. Pharmacoeconomics 9:168-178.

Gallagher M, Chiba AA (1996) The amygdala and emotion. Curr Opin Neurobiol 6:221-227.

Giannelli M, Diciotti S, Tessa C, Mascalchi M (2010) Characterization of Nyquist ghost in EPI-fMRI acquisition sequences implemented on two clinical 1.5 T MR scanner systems: effect of readout bandwidth and echo spacing. J Appl Clin Med Phys 11:170-180.

Girvan M, Newman ME (2002) Community structure in social and biological networks. Proc Natl Acad Sci U S A 99:7821-7826.

Gomez-Sintes R, Kvajo M, Gogos JA, Lucas JJ (2014) Mice with a naturally occurring DISC1 mutation display a broad spectrum of behaviors associated to psychiatric disorders. Front Behav Neurosci 8:253.

Good BH, de Montjoye YA, Clauset A (2010) Performance of modularity maximization in practical contexts. Phys Rev E Stat Nonlin Soft Matter Phys 81:046106.

Gotts SJ, Saad ZS, Jo HJ, Wallace GL, Cox RW, Martin A (2013) The perils of global signal regression for group comparisons: a case study of Autism Spectrum Disorders. Front Hum Neurosci 7:356.

Grandjean J, Schroeter A, Batata I, Rudin M (2014a) Optimization of anesthesia protocol for resting-state fMRI in mice based on differential effects of anesthetics on functional connectivity patterns. Neuroimage 102, Part 2:838-847.

Grandjean J, Schroeter A, Batata I, Rudin M (2014b) Optimization of anesthesia protocol for resting-state fMRI in mice based on differential effects of anesthetics on functional connectivity patterns. Neuroimage 102 Pt 2:838-847.

Grandjean J, Derungs R, Kulic L, Welt T, Henkelman M, Nitsch RM, Rudin M (2016) Complex interplay between brain function and structure during cerebral amyloidosis in APP transgenic mouse strains revealed by multi-parametric MRI comparison. Neuroimage 134:1-11.

Grandjean J, Schroeter A, He P, Tanadini M, Keist R, Krstic D, Konietzko U, Klohs J, Nitsch RM, Rudin M (2014c) Early alterations in functional connectivity and white matter structure in a transgenic mouse model of cerebral amyloidosis. J Neurosci 34:13780-13789.

Greicius MD, Krasnow B, Reiss AL, Menon V (2003) Functional connectivity in the resting brain: A network analysis of the default mode hypothesis. Proc Natl Acad Sci U S A 100:253-258.

Guilfoyle DN, Gerum SV, Sanchez JL, Balla A, Sershen H, Javitt DC, Hoptman MJ (2013) Functional connectivity fMRI in mouse brain at 7T using isoflurane. J Neurosci Methods 214:144-148.

Gusnard DA, Raichle ME, Raichle ME (2001) Searching for a baseline: functional imaging and the resting human brain. Nature reviews Neuroscience 2:685-694.

Haberl MG, Zerbi V, Veltien A, Ginger M, Heerschap A, Frick A (2015) Structural-functional connectivity deficits of neocortical circuits in the Fmr1 (-/y) mouse model of autism. Sci Adv 1:e1500775.

Haensel JX, Spain A, Martin C (2015) A systematic review of physiological methods in rodent pharmacological MRI studies. Psychopharmacology (Berl) 232:489-499.

Hampson M, Olson IR, Leung HC, Skudlarski P, Gore JC (2004) Changes in functional connectivity of human MT/V5 with visual motion input. Neuroreport 15:1315-1319.

Hara K, Harris RA (2002) The anesthetic mechanism of urethane: the effects on neurotransmitter-gated ion channels. Anesth Analg 94:313-318, table of contents.

Harper A (2010) Mouse models of neurological disorders--a comparison of heritable and acquired traits. Biochim Biophys Acta 1802:785-795.

Hayasaka S, Laurienti PJ (2010) Comparison of characteristics between region-and voxel-based network analyses in resting-state fMRI data. Neuroimage 50:499-508.

He Y, Wang L, Zang YF, Tian LX, Zhang XQ, Li KC, Jiang TZ (2007) Regional coherence changes in the early stages of Alzheimer's disease: A combined structural and resting-state functional MRI study. Neuroimage 35:488-500.

Heinke W, Koelsch S (2005) The effects of anesthetics on brain activity and cognitive function. Current Opinion in Anesthesiology 18:625-631.

Henckens MJAG, van der Marel K, van der Toorn A, Pillai AG, Fernández G, Dijkhuizen RM, Joëls M (2015) Stress-induced alterations in large-scale functional networks of the rodent brain. Neuroimage 105:312-322.

Herzog C, Otto T (1998) Contributions of anterior perirhinal cortex to olfactory and contextual fear conditioning. Neuroreport 9:1855-1859.

Hikida T, Jaaro-Peled H, Seshadri S, Oishi K, Hookway C, Kong S, Wu D, Xue R, Andrade M, Tankou S, Mori S, Gallagher M, Ishizuka K, Pletnikov M, Kida S, Sawa A (2007) Dominant-negative DISC1 transgenic mice display schizophrenia-associated phenotypes detected by measures translatable to humans. Proc Natl Acad Sci U S A 104:14501-14506.

Himberg J, Hyvarinen A, Esposito F (2004) Validating the independent components of neuroimaging time series via clustering and visualization. Neuroimage 22:1214-1222.

Hindley EL, Nelson AJD, Aggleton JP, Vann SD (2014) The rat retrosplenial cortex is required when visual cues are used flexibly to determine location. Behav Brain Res 263:98-107.

Hudetz AG (2012) General anesthesia and human brain connectivity. Brain Connect 2:291-302.

Huettel SA, Song AW, McCarthy G (2009) Functional magnetic resonance imaging, 2nd Edition. U.S.A.: Sinauer Associates.

Huh Y, Cho J (2013) Urethane anesthesia depresses activities of thalamocortical neurons and alters its response to nociception in terms of dual firing modes. Front Behav Neurosci 7:141.

Humphries MD, Gurney K (2008) Network 'small-world-ness': a quantitative method for determining canonical network equivalence. PLoS ONE 3:e0002051.

Hutchison RM, Mirsattari SM, Jones CK, Gati JS, Leung LS (2010) Functional networks in the anesthetized rat brain revealed by independent component analysis of resting-state FMRI. J Neurophysiol 103:3398-3406.

Hutchison RM, Leung LS, Mirsattari SM, Gati JS, Menon RS, Everling S (2011) Resting-state networks in the macaque at 7 T. Neuroimage 56:1546-1555.

Hyman SE (2000) The genetics of mental illness: implications for practice. Bull World Health Organ 78:455-463.

Ibi D, Nagai T, Koike H, Kitahara Y, Mizoguchi H, Niwa M, Jaaro-Peled H, Nitta A, Yoneda Y, Nabeshima T, Sawa A, Yamada K (2010) Combined effect of neonatal immune activation and mutant DISC1 on phenotypic changes in adulthood. Behav Brain Res 206:32-37.

Insel TR (2010) Rethinking schizophrenia. Nature 468:187-193.

Ishizuka K, Paek M, Kamiya A, Sawa A (2006) A review of Disrupted-In-Schizophrenia-1 (DISC1): neurodevelopment, cognition, and mental conditions. Biol Psychiatry 59:1189-1197.

Jaaro-Peled H, Niwa M, Foss CA, Murai R, de Los Reyes S, Kamiya A, Mateo Y, O'Donnell P, Cascella NG, Nabeshima T, Guilarte TR, Pomper MG, Sawa A (2013) Subcortical dopaminergic deficits in a DISC1 mutant model: a study in direct reference to human molecular brain imaging. Hum Mol Genet 22:1574-1580.

Janke AL, Ullmann J, Kurniawan N, Paxinos G, Keller M, Yang Z, Richards K, Egan G, Petrou S, Galloway G, Reutens D (2012) 15μm average mouse models in Waxholm space from 16.4T 30μm images. In: 20th Annual ISMRM Scientific Meeting and Exhibition. Melbourne, Australia.

Jiang L, Zuo XN (2015) Regional Homogeneity: A Multimodal, Multiscale Neuroimaging Marker of the Human Connectome. Neuroscientist.

Johnstone M, Thomson PA, Hall J, McIntosh AM, Lawrie SM, Porteous DJ (2011) DISC1 in schizophrenia: genetic mouse models and human genomic imaging. Schizophr Bull 37:14-20.

Jonckers E, Van Audekerke J, De Visscher G, Van der Linden A, Verhoye M (2011) Functional connectivity fMRI of the rodent brain: comparison of functional connectivity networks in rat and mouse. PLoS ONE 6:e18876.

Jonckers E, Shah D, Hamaide J, Verhoye M, Van der Linden A (2015) The power of using functional fMRI on small rodents to study brain pharmacology and disease. Frontiers in Pharmacology 6.

Jonckers E, Delgado y Palacios R, Shah D, Guglielmetti C, Verhoye M, Van der Linden A (2014) Different anesthesia regimes modulate the functional connectivity outcome in mice. Magn Reson Med 72:1103-1112.

Kalthoff D, Po C, Wiedermann D, Hoehn M (2013) Reliability and spatial specificity of rat brain sensorimotor functional connectivity networks are superior under sedation compared with general anesthesia. NMR Biomed 26:638-650.

Kelly M, Brandon N (2011) Taking a bird's eye view on a mouse model review: a comparison of findings from mouse models targeting DISC1 or DISC1-interacting proteins. Future Neurology:6(5):661–677.

Khadka S, Meda SA, Stevens MC, Glahn DC, Calhoun VD, Sweeney JA, Tamminga CA, Keshavan MS, O'Neil K, Schretlen D, Pearlson GD (2013) Is Aberrant Functional Connectivity A Psychosis Endophenotype? A Resting State Functional Magnetic Resonance Imaging Study. Biol Psychiatry 74:458-466.

King DJ, Hodgekins J, Chouinard PA, Chouinard VA, Sperandio I (2016) A review of abnormalities in the perception of visual illusions in schizophrenia. Psychon Bull Rev.

Kohler C (1990) Subicular projections to the hypothalamus and brainstem: some novel aspects revealed in the rat by the anterograde Phaseolus vulgaris leukoagglutinin (PHA-L) tracing method. Prog Brain Res 83:59-69.

Krushel LA, van der Kooy D (1988) Visceral cortex: integration of the mucosal senses with limbic information in the rat agranular insular cortex. J Comp Neurol 270:39-54, 62-33.

Kundu P, Inati SJ, Evans JW, Luh WM, Bandettini PA (2012) Differentiating BOLD and non-BOLD signals in fMRI time series using multi-echo EPI. Neuroimage 60:1759-1770.

Kuroda K et al. (2011) Behavioral alterations associated with targeted disruption of exons 2 and 3 of the Disc1 gene in the mouse. Hum Mol Genet 20:4666-4683.

Kwong KK, Belliveau JW, Chesler DA, Goldberg IE, Weisskoff RM, Poncelet BP, Kennedy DN, Hoppel BE, Cohen MS, Turner R, et al. (1992) Dynamic magnetic resonance imaging of human brain activity during primary sensory stimulation. Proc Natl Acad Sci U S A 89:5675-5679.

Latora V, Marchiori M (2001) Efficient behavior of small-world networks. Phys Rev Lett 87:198701.

LeDoux J (1998) Fear and the brain: Where have we been, and where are we going? Biol Psychiatry 44:1229-1238.

LeDoux J (2003) The emotional brain, fear, and the amygdala. Cell Mol Neurobiol 23:727-738.

LeDoux J (2007) The amygdala. Curr Biol 17:R868-874.

Lee MH, Smyser CD, Shimony JS (2013) Resting-state fMRI: a review of methods and clinical applications. AJNR Am J Neuroradiol 34:1866-1872.

Leech R, Sharp DJ (2014) The role of the posterior cingulate cortex in cognition and disease. Brain 137:12-32.

Leung C, Jia Z (2016) Mouse Genetic Models of Human Brain Disorders. Front Genet 7:40.

Levenson RW, Sturm VE, Haase CM (2014) Emotional and behavioral symptoms in neurodegenerative disease: A model for studying the neural bases of psychopathology. Annual review of clinical psychology 10:581-606.

Li K, Guo L, Nie J, Li G, Liu T (2009) Review of methods for functional brain connectivity detection using fMRI. Comput Med Imaging Graph 33:131-139.

Li M, Chen Z, Li T (2012a) Small-world brain networks in schizophrenia. Shanghai Arch Psychiatry 24:322-327.

Li S, Eloyan A, Joel S, Mostofsky S, Pekar J, Bassett SS, Caffo B (2012b) Analysis of group ICA-based connectivity measures from fMRI: application to Alzheimer's disease. PLoS ONE 7:e49340.

Liang Z, King J, Zhang N (2011) Uncovering intrinsic connectional architecture of functional networks in awake rat brain. J Neurosci 31:3776-3783.

Liang Z, King J, Zhang N (2012a) Anticorrelated resting-state functional connectivity in awake rat brain. Neuroimage 59:1190-1199.

Liang Z, King J, Zhang N (2012b) Intrinsic organization of the anesthetized brain. J Neurosci 32:10183-10191.

Liska A, Galbusera A, Schwarz AJ, Gozzi A (2015) Functional connectivity hubs of the mouse brain. Neuroimage 115:281-291.

Liu H, Liu Z, Liang M, Hao Y, Tan L, Kuang F, Yi Y, Xu L, Jiang T (2006) Decreased regional homogeneity in schizophrenia: a resting state functional magnetic resonance imaging study. Neuroreport 17:19-22.

Liu X, Zhu XH, Zhang Y, Chen W (2013a) The Change of Functional Connectivity Specificity in Rats Under Various Anesthesia Levels and its Neural Origin. Brain Topogr 26:363-377.

Liu X, Pillay S, Li R, Vizuete JA, Pechman KR, Schmainda KM, Hudetz AG (2013b) Multiphasic modification of intrinsic functional connectivity of the rat brain during increasing levels of propofol. Neuroimage 83:581-592.

Liu Y, Yu C, Zhang X, Liu J, Duan Y, Alexander-Bloch AF, Liu B, Jiang T, Bullmore E (2014) Impaired long distance functional connectivity and weighted network architecture in Alzheimer's disease. Cereb Cortex 24:1422-1435.

Lo C-YZ, Su T-W, Huang C-C, Hung C-C, Chen W-L, Lan T-H, Lin C-P, Bullmore ET (2015) Randomization and resilience of brain functional networks as systems-level endophenotypes of schizophrenia. Proc Natl Acad Sci U S A 112:9123-9128.

Long XY, Zuo XN, Kiviniemi V, Yang Y, Zou QH, Zhu CZ, Jiang TZ, Yang H, Gong QY, Wang L, Li KC, Xie S, Zang YF (2008) Default mode network as revealed with multiple methods for resting-state functional MRI analysis. J Neurosci Methods 171:349-355.

Low LA, Bauer LC, Klaunberg BA (2016a) Comparing the Effects of Isoflurane and Alpha Chloralose upon Mouse Physiology. PLoS ONE 11:e0154936.

Low LA, Bauer LC, Pitcher MH, Bushnell MC (2016b) Restraint training for awake functional brain scanning of rodents can cause long-lasting changes in pain and stress responses. Pain 157:1761-1772.

Lowe MJ, Mock BJ, Sorenson JA (1998) Functional connectivity in single and multislice echoplanar imaging using resting-state fluctuations. Neuroimage 7:119-132.

Lu H, Zou Q, Gu H, Raichle ME, Stein EA, Yang Y (2012) Rat brains also have a default mode network. Proc Natl Acad Sci U S A 109:3979-3984.

Luo C, Qiu C, Guo Z, Fang J, Li Q, Lei X, Xia Y, Lai Y, Gong Q, Zhou D, Yao D (2011) Disrupted functional brain connectivity in partial epilepsy: a resting-state fMRI study. PLoS ONE 7:e28196.

Lynall ME, Bassett DS, Kerwin R, McKenna PJ, Kitzbichler M, Muller U, Bullmore E (2010) Functional connectivity and brain networks in schizophrenia. J Neurosci 30:9477-9487.

Ma L, Wang B, Chen X, Xiong J (2007) Detecting functional connectivity in the resting brain: a comparison between ICA and CCA. Magn Reson Imaging 25:47-56.

Ma S, Correa NM, Li XL, Eichele T, Calhoun VD, Adali T (2011) Automatic identification of functional clusters in FMRI data using spatial dependence. IEEE Trans Biomed Eng 58:3406-3417.

Ma Y, Hof PR, Grant SC, Blackband SJ, Bennett R, Slatest L, McGuigan MD, Benveniste H (2005) A three-dimensional digital atlas database of the adult C57BL/6J mouse brain by magnetic resonance microscopy. Neuroscience 135:1203-1215.

MacDonald AA, Naci L, MacDonald PA, Owen AM (2015) Anesthesia and neuroimaging: investigating the neural correlates of unconsciousness. Trends Cogn Sci 19:100-107.

Mai JK, Paxinos G (2012) The human nervous system: Amsterdam ; Boston : Elsevier Academic Press.

Manderscheid RW, Ryff CD, Freeman EJ, McKnight-Eily LR, Dhingra S, Strine TW (2010) Evolving Definitions of Mental Illness and Wellness. Prev Chronic Dis 7:A19.

Mannell MV, Franco AR, Calhoun VD, Canive JM, Thoma RJ, Mayer AR (2010) Resting state and task-induced deactivation: A methodological comparison in patients with schizophrenia and healthy controls. Hum Brain Mapp 31:424-437.

Margaret S, Phyllis E (2009) Child Neuropsychology: Assessment and Interventions for Neurodevelopmental Disorders, 2nd ed. Edition: New York ; London : Springer.

Martuzzi R, Ramani R, Qiu M, Rajeevan N, Constable RT (2010) Functional connectivity and alterations in baseline brain state in humans. Neuroimage 49:823-834.

Maslov S, Sneppen K (2002) Specificity and stability in topology of protein networks. Science 296:910-913.

Matyas F, Sreenivasan V, Marbach F, Wacongne C, Barsy B, Mateo C, Aronoff R, Petersen CC (2010) Motor control by sensory cortex. Science 330:1240-1243.

Maximo JO, Keown CL, Nair A, Muller RA (2013) Approaches to local connectivity in autism using resting state functional connectivity MRI. Frontiers in Human Neuroscience 7.

McCormick DA, Bal T (1997) Sleep and arousal: thalamocortical mechanisms. Annu Rev Neurosci 20:185-215.

McKeown MJ, Hansen LK, Sejnowsk TJ (2003) Independent component analysis of functional MRI: what is signal and what is noise? Curr Opin Neurobiol 13:620-629.

Mechling AE, Hubner NS, Lee HL, Hennig J, von Elverfeldt D, Harsan LA (2014) Fine-grained mapping of mouse brain functional connectivity with resting-state fMRI. Neuroimage 96:203-215.

Menon V (2015) Salience Network A2 - Toga, Arthur W. In: Brain Mapping, pp 597-611. Waltham: Academic Press.

Mitterschiffthaler MT, Ettinger U, Mehta MA, Mataix-Cols D, Williams SC (2006) Applications of functional magnetic resonance imaging in psychiatry. J Magn Reson Imaging 23:851-861.

Moser EI, Kropff E, Moser MB (2008) Place cells, grid cells, and the brain's spatial representation system. Annu Rev Neurosci 31:69-89.

Mueggler T, Sturchler-Pierrat C, Baumann D, Rausch M, Staufenbiel M, Rudin M (2002) Compromised hemodynamic response in amyloid precursor protein transgenic mice. J Neurosci 22:7218-7224.

Mueggler T, Baltes C, Bosshard S, Princz-Kranz FL, Ratering D, Razoux F, Sydekum E, Rudin M (2012) FMRI in Mice: Functional Phenotyping of Transgenic Mouse Lines Based on Hemodynamic Readouts. In: Neural Metabolism In Vivo: Advances in Neurobiology 4 (Choi I-Y, Gruetter R, eds), pp 593-621. New York, United States: Springer.

Muir WJ, Pickard BS, Blackwood DH (2008) Disrupted-in-Schizophrenia-1. Curr Psychiatry Rep 10:140-147.

Mukherjee P, Whalley HC, McKirdy JW, Sprengelmeyer R, Young AW, McIntosh AM, Lawrie SM, Hall J (2014) Altered Amygdala Connectivity Within the Social Brain in Schizophrenia. Schizophr Bull 40:152-160.

Muller EE, Nistico G (1989) Brain messengers and the pituitary. San Diego, California, USA: Academic Press, Inc.

Murphy K, Fox MD (2016) Towards a consensus regarding global signal regression for resting state functional connectivity MRI. Neuroimage.

Murphy K, Birn RM, Handwerker DA, Jones TB, Bandettini PA (2009) The impact of global signal regression on resting state correlations: Are anti-correlated networks introduced? Neuroimage 44:893-905.

Nair G, Duong TQ (2004) Echo-planar BOLD fMRI of mice on a narrow-bore 9.4 T magnet. Magn Reson Med 52:430-434.

Nallasamy N, Tsao DY (2011) Functional connectivity in the brain: effects of anesthesia. Neuroscientist 17:94-106.

Narayan S, Nakajima K, Sawa A (2013) DISC1: a key lead in studying cortical development and associated brain disorders. Neuroscientist 19:451-464.

Nasrallah FA, Tay HC, Chuang KH (2013) Detection of functional connectivity in the resting mouse brain. NeuroImage.

Nasrallah FA, Tay HC, Chuang KH (2014a) Detection of functional connectivity in the resting mouse brain. Neuroimage 86:417-424.

Nasrallah FA, Lew SK, Low ASM, Chuang KH (2014b) Neural correlate of resting-state functional connectivity under alpha 2 adrenergic receptor agonist, medetomidine. Neuroimage 84:27-34.

Nasrallah FA, Low SMA, Lew SK, Chen K, Chuang KH (2014c) Pharmacological insight into neurotransmission origins of resting-state functional connectivity: alpha 2-adrenergic agonist vs antagonist. Neuroimage 103:364-373.

Newman MEJ (2003) The structure and function of complex networks. Siam Review 45:167-256.

Newman MEJ (2006) Modularity and community structure in networks. Proc Natl Acad Sci U S A 103:8577-8582.

Niwa M, Jaaro-Peled H, Tankou S, Seshadri S, Hikida T, Matsumoto Y, Cascella NG, Kano S-i, Ozaki N, Nabeshima T, Sawa A (2013a) Adolescent Stress–Induced Epigenetic Control of Dopaminergic Neurons via Glucocorticoids. Science 339:335-339.

Niwa M, Jaaro-Peled H, Tankou S, Seshadri S, Hikida T, Matsumoto Y, Cascella NG, Kano S, Ozaki N, Nabeshima T, Sawa A (2013b) Adolescent stress-induced epigenetic control of dopaminergic neurons via glucocorticoids. Science 339:335-339.

O'Mara SM, Commins S, Anderson M, Gigg J (2001) The subiculum: a review of form, physiology and function. Prog Neurobiol 64:129-155.

Ogawa S (2012) Finding the BOLD effect in brain images. Neuroimage 62:608-609.

Ogawa S, Lee TM, Kay AR, Tank DW (1990) Brain magnetic resonance imaging with contrast dependent on blood oxygenation. Proc Natl Acad Sci U S A 87:9868-9872.

Oh SW et al. (2014) A mesoscale connectome of the mouse brain. Nature 508:207-214.

Onnela JP, Saramaki J, Kertesz J, Kaski K (2005) Intensity and coherence of motifs in weighted complex networks. Phys Rev E Stat Nonlin Soft Matter Phys 71:065103.

Paakki JJ, Rahko J, Long X, Moilanen I, Tervonen O, Nikkinen J, Starck T, Remes J, Hurtig T, Haapsamo H, Jussila K, Kuusikko-Gauffin S, Mattila ML, Zang Y, Kiviniemi V (2010) Alterations in regional homogeneity of resting-state brain activity in autism spectrum disorders. Brain Res 1321:169-179.

Pan WJ, Billings JC, Grooms JK, Shakil S, Keilholz SD (2015) Considerations for resting state functional MRI and functional connectivity studies in rodents. Front Neurosci 9:269.

Pankow A, Friedel E, Sterzer P, Seiferth N, Walter H, Heinz A, Schlagenhauf F (2013) Altered amygdala activation in schizophrenia patients during emotion processing. Schizophr Res 150:101-106.

Park HJ, Friston K (2013) Structural and functional brain networks: from connections to cognition. Science 342:1238411.

Parrish TB, Gitelman DR, LaBar KS, Mesulam MM (2000) Impact of signal-to-noise on functional MRI. Magn Reson Med 44:925-932.

Pattwell SS, Bath KG, Casey BJ, Ninan I, Lee FS (2011) Selective early-acquired fear memories undergo temporary suppression during adolescence. Proc Natl Acad Sci U S A 108:1182-1187.

Pauling L, Coryell CD (1936) The Magnetic Properties and Structure of Hemoglobin, Oxyhemoglobin and Carbonmonoxyhemoglobin. Proc Natl Acad Sci U S A 22:210-216.

Peltier SJ, Kerssens C, Hamann SB, Sebel PS, Byas-Smith M, Hu X (2005) Functional connectivity changes with concentration of sevoflurane anesthesia. Neuroreport 16:285-288.

Peng Y, Gillis-Smith S, Jin H, Trankner D, Ryba NJ, Zuker CS (2015) Sweet and bitter taste in the brain of awake behaving animals. Nature 527:512-515.

Petrinovic MM, Hankov G, Schroeter A, Bruns A, Rudin M, von Kienlin M, Kunnecke B, Mueggler T (2016) A novel anesthesia regime enables neurofunctional studies and imaging genetics across mouse strains. Sci Rep 6:24523.

Phelps EA (2004) Human emotion and memory: interactions of the amygdala and hippocampal complex. Curr Opin Neurobiol 14:198-202.

Pletnikov MV, Ayhan Y, Xu Y, Nikolskaia O, Ovanesov M, Huang H, Mori S, Moran TH, Ross CA (2008) Enlargement of the lateral ventricles in mutant DISC1 transgenic mice. Mol Psychiatry 13:115.

Power JD, Schlaggar BL, Lessov-Schlaggar CN, Petersen SE (2013) Evidence for Hubs in Human Functional Brain Networks. Neuron 79:798-813.

Power JD, Barnes KA, Snyder AZ, Schlaggar BL, Petersen SE (2012) Spurious but systematic correlations in functional connectivity MRI networks arise from subject motion. Neuroimage 59:2142-2154.

Power JD, Cohen AL, Nelson SM, Wig GS, Barnes KA, Church JA, Vogel AC, Laumann TO, Miezin FM, Schlaggar BL, Petersen SE (2011) Functional network organization of the human brain. Neuron 72:665-678.

Powley TL, Laughton W (1981) Neural pathways involved in the hypothalamic integration of autonomic responses. Diabetologia 20 Suppl:378-387.

Purves D, G.J. A, D. F, W.C. H, O. LAMJ, S.M. W (2004) Neuroscience, 3rd ed.. Edition: Sunderland, Mass. : Sinauer Associates.

Qing Z, Dong ZY, Li SF, Zang YF, Liu DQ (2015) Global signal regression has complex effects on regional homogeneity of resting state fMRI signal. Magn Reson Imaging 33:1306-1313.

Richard EF (2008) Anesthesia and analgesia in laboratory animals, 2nd ed. Edition. Amsterdam ; London: Academic.

Richards CD (2002) Anaesthetic modulation of synaptic transmission in the mammalian CNS. Br J Anaesth 89:79-90.

Richards K, Watson C, Buckley RF, Kurniawan ND, Yang Z, Keller MD, Beare R, Bartlett PF, Egan GF, Galloway GJ, Paxinos G, Petrou S, Reutens DC (2011) Segmentation of the mouse hippocampal formation in magnetic resonance images. NeuroImage 58:732-740.

Richiardi J et al. (2015) BRAIN NETWORKS. Correlated gene expression supports synchronous activity in brain networks. Science 348:1241-1244.

Richter-Levin G (2004) The amygdala, the hippocampus, and emotional modulation of memory. Neuroscientist 10:31-39.

Robertson GS, Hori SE, Powell KJ (2006) Schizophrenia: an integrative approach to modelling a complex disorder. J Psychiatry Neurosci 31:157-167.

Robinson S, Bucci DJ (2012) Fear conditioning is disrupted by damage to the postsubiculum. Hippocampus 22:1481-1491.

Rosazza C, Minati L, Ghielmetti F, Mandelli ML, Bruzzone MG (2012) Functional connectivity during resting-state functional MR imaging: study of the correspondence between independent component analysis and region-of-interest-based methods. AJNR Am J Neuroradiol 33:180-187.

Rosenthal N, Brown S (2007) The mouse ascending: perspectives for human-disease models. Nat Cell Biol 9:993-999.

Rubinov M, Sporns O (2010) Complex network measures of brain connectivity: uses and interpretations. Neuroimage 52:1059-1069.

Rubinov M, Sporns O (2011) Weight-conserving characterization of complex functional brain networks. Neuroimage 56:2068-2079.

Rubinov M, Ypma RJ, Watson C, Bullmore ET (2015) Wiring cost and topological participation of the mouse brain connectome. Proc Natl Acad Sci U S A 112:10032-10037.

Saad ZS, Reynolds RC, Jo HJ, Gotts SJ, Chen G, Martin A, Cox RW (2013) Correcting brain-wide correlation differences in resting-state FMRI. Brain Connect 3:339-352.

Saalmann YB, Kastner S (2015) The cognitive thalamus. Front Syst Neurosci 9:39.

Sah P, Faber ES, Lopez De Armentia M, Power J (2003) The amygdaloid complex: anatomy and physiology. Physiol Rev 83:803-834.

Salimi-Khorshidi G, Douaud G, Beckmann CF, Glasser MF, Griffanti L, Smith SM (2014) Automatic denoising of functional MRI data: combining independent component analysis and hierarchical fusion of classifiers. Neuroimage 90:449-468.

Salvador R, Suckling J, Coleman MR, Pickard JD, Menon D, Bullmore E (2005) Neurophysiological architecture of functional magnetic resonance images of human brain. Cereb Cortex 15:1332-1342.

Saramaki J, Kivela M, Onnela JP, Kaski K, Kertesz J (2007) Generalizations of the clustering coefficient to weighted complex networks. Phys Rev E Stat Nonlin Soft Matter Phys 75:027105.

Scheinin H, Virtanen R, MacDonald E, Lammintausta R, Scheinin M (1989) Medetomidine--a novel alpha 2-adrenoceptor agonist: a review of its pharmacodynamic effects. Prog Neuropsychopharmacol Biol Psychiatry 13:635-651.

Scholvinck ML, Maier A, Ye FQ, Duyn JH, Leopold DA (2010) Neural basis of global resting-state fMRI activity. Proc Natl Acad Sci U S A 107:10238-10243.

Schroeter A, Schlegel F, Seuwen A, Grandjean J, Rudin M (2014) Specificity of stimulus-evoked fMRI responses in the mouse: the influence of systemic physiological changes associated with innocuous stimulation under four different anesthetics. Neuroimage 94:372-384.

Schroeter A, Grandjean J, Schlegel F, Saab BJ, Rudin M (2016) Contributions of structural connectivity and cerebrovascular parameters to functional magnetic resonance

imaging signals in mice at rest and during sensory paw stimulation. J Cereb Blood Flow Metab.

Schwarz AJ, Gass N, Sartorius A, Zheng L, Spedding M, Schenker E, Risterucci C, Meyer-Lindenberg A, Weber-Fahr W (2013) The low-frequency blood oxygenation level-dependent functional connectivity signature of the hippocampal-prefrontal network in the rat brain. Neuroscience 228:243-258.

Scoville WB, Milner B (1957) Loss of recent memory after bilateral hippocampal lesions. J Neurol Neurosurg Psychiatry 20:11-21.

Seeley WW, Menon V, Schatzberg AF, Keller J, Glover GH, Kenna H, Reiss AL, Greicius MD (2007) Dissociable intrinsic connectivity networks for salience processing and executive control. J Neurosci 27:2349-2356.

Sforazzini F, Schwarz AJ, Galbusera A, Bifone A, Gozzi A (2014) Distributed BOLD and CBV-weighted resting-state networks in the mouse brain. Neuroimage 87:403-415.

Sforazzini F, Bertero A, Dodero L, David G, Galbusera A, Scattoni ML, Pasqualetti M, Gozzi A (2016) Altered functional connectivity networks in acallosal and socially impaired BTBR mice. Brain Struct Funct 221:941-954.

Shah D, Blockx I, Keliris GA, Kara F, Jonckers E, Verhoye M, Van der Linden A (2016a) Cholinergic and serotonergic modulations differentially affect large-scale functional networks in the mouse brain. Brain Struct Funct 221:3067-3079.

Shah D, Jonckers E, Praet J, Vanhoutte G, Delgado YPR, Bigot C, D'Souza DV, Verhoye M, Van der Linden A (2013) Resting state FMRI reveals diminished functional connectivity in a mouse model of amyloidosis. PLoS ONE 8:e84241.

Shah D, Blockx I, Guns PJ, De Deyn PP, Van Dam D, Jonckers E, Delgado YPR, Verhoye M, Van der Linden A (2015) Acute modulation of the cholinergic system in the mouse brain detected by pharmacological resting-state functional MRI. Neuroimage 109:151-159.

Shah D, Praet J, Latif Hernandez A, Hofling C, Anckaerts C, Bard F, Morawski M, Detrez JR, Prinsen E, Villa A, De Vos WH, Maggi A, D'Hooge R, Balschun D, Rossner S, Verhoye M, Van der Linden A (2016b) Early pathologic amyloid induces hypersynchrony of BOLD resting-state networks in transgenic mice and provides an early therapeutic window before amyloid plaque deposition. Alzheimers Dement 12:964-976.

Shayegan DK, Stahl SM (2005) Emotion processing, the amygdala, and outcome in schizophrenia. Prog Neuropsychopharmacol Biol Psychiatry 29:840-845.

Shen HH (2015) Core Concept: Resting-state connectivity. Proc Natl Acad Sci U S A 112:14115-14116.

Shen SB, Lang B, Nakamoto C, Zhang F, Pu J, Kuan SL, Chatzi C, He S, Mackie I, Brandon NJ, Marquis KL, Day M, Hurko O, McCaig CD, Riedel G, St Clair D (2008) Schizophrenia-Related Neural and Behavioral Phenotypes in Transgenic Mice Expressing Truncated Disc1. J Neurosci 28:10893-10904.

Shipley MT, Geinisman Y (1984) Anatomical evidence for convergence of olfactory, gustatory, and visceral afferent pathways in mouse cerebral cortex. Brain Res Bull 12:221-226.

Shulman RG, Rothman DL, Behar KL, Hyder F (2004) Energetic basis of brain activity: implications for neuroimaging. Trends Neurosci 27:489-495.

Sinclair MD (2003) A review of the physiological effects of alpha2-agonists related to the clinical use of medetomidine in small animal practice. Can Vet J 44:885-897.

Sladky R, Friston KJ, Trostl J, Cunnington R, Moser E, Windischberger C (2011) Slice-timing effects and their correction in functional MRI. Neuroimage 58:588-594.

Smith SM, Nichols TE (2009) Threshold-free cluster enhancement: addressing problems of smoothing, threshold dependence and localisation in cluster inference. Neuroimage 44:83-98.

Soares DC, Carlyle BC, Bradshaw NJ, Porteous DJ (2011) DISC1: Structure, Function, and Therapeutic Potential for Major Mental Illness. ACS Chemical Neuroscience 2:609-632.

Sommer MA (2003) The role of the thalamus in motor control. Curr Opin Neurobiol 13:663-670.

Song XX, Yu BW (2015) Anesthetic effects of propofol in the healthy human brain: functional imaging evidence. J Anesth 29:279-288.

Sparks DL (2002) The brainstem control of saccadic eye movements. Nat Rev Neurosci 3:952-964.

Sporns O (2011) Networks of the brain. Cambridge, MA, USA MIT Press

Sporns O (2013) Structure and function of complex brain networks. Dialogues Clin Neurosci 15:247-262.

Sporns O, Honey CJ (2006) Small worlds inside big brains. Proc Natl Acad Sci U S A 103:19219-19220.

Stafford JM, Jarrett BR, Miranda-Dominguez O, Mills BD, Cain N, Mihalas S, Lahvis GP, Lattal KM, Mitchell SH, David SV, Fryer JD, Nigg JT, Fair DA (2014) Large-scale

topology and the default mode network in the mouse connectome. Proc Natl Acad Sci U S A 111:18745-18750.

Sugar J, Witter MP, van Strien NM, Cappaert NL (2011) The retrosplenial cortex: intrinsic connectivity and connections with the (para)hippocampal region in the rat. An interactive connectome. Front Neuroinform 5:7.

Sun Y, Danila B, Josic K, Bassler KE (2009) Improved community structure detection using a modified fine-tuning strategy. Epl 86.

Tanabe J, Miller D, Tregellas J, Freedman R, Meyer FG (2002) Comparison of detrending methods for optimal fMRI preprocessing. Neuroimage 15:902-907.

Telesford QK, Joyce KE, Hayasaka S, Burdette JH, Laurienti PJ (2011) The ubiquity of small-world networks. Brain Connect 1:367-375.

Todd TP, Bucci DJ (2015) Retrosplenial Cortex and Long-Term Memory: Molecules to Behavior. Neural Plast.

Tohka J, Foerde K, Aron AR, Tom SM, Toga AW, Poldrack RA (2008) Automatic independent component labeling for artifact removal in fMRI. Neuroimage 39:1227-1245.

Toni R, Malaguti A, Benfenati F, Martini L (2004) The human hypothalamus: a morpho-functional perspective. J Endocrinol Invest 27:73-94.

Trapani G, Altomare C, Sanna E, Biggio G, Liso G (2000) Propofol in anesthesia. mechanism of action, structure-activity relationships, and drug delivery. Curr Med Chem 7:249-271.

Tremeau F (2006) A review of emotion deficits in schizophrenia. Dialogues Clin Neurosci 8:59-70.

Tremoleda JL, Kerton A, Gsell W (2012) Anaesthesia and physiological monitoring during in vivo imaging of laboratory rodents: considerations on experimental outcomes and animal welfare. EJNMMI Res 2:44.

Triantafyllou C, Hoge RD, Krueger G, Wiggins CJ, Potthast A, Wiggins GC, Wald LL (2005) Comparison of physiological noise at 1.5 T, 3 T and 7 T and optimization of fMRI acquisition parameters. Neuroimage 26:243-250.

Tsuang MT, Bar JL, Stone WS, Faraone SV (2004) Gene-environment interactions in mental disorders. World Psychiatry 3:73-83.

Tu Y, Yu T, Fu XY, Xie P, Lu S, Huang XQ, Gong QY (2011) Altered thalamocortical functional connectivity by propofol anesthesia in rats. Pharmacology 88:322-326.

Turetsky BI, Hahn CG, Borgmann-Winter K, Moberg PJ (2009) Scents and nonsense: olfactory dysfunction in schizophrenia. Schizophr Bull 35:1117-1131.

Uddin LQ (2016) Salience network of the human brain. London, United Kingdom: Academic Press is an imprint of Elsevier.

Uehara T, Yamasaki T, Okamoto T, Koike T, Kan S, Miyauchi S, Kira J, Tobimatsu S (2014) Efficiency of a "small-world" brain network depends on consciousness level: a resting-state FMRI study. Cereb Cortex 24:1529-1539.

Uhrig L, Dehaene S, Jarraya B (2014) Cerebral mechanisms of general anesthesia. Ann Fr Anesth Reanim 33:72-82.

Ullmann JF, Watson C, Janke AL, Kurniawan ND, Reutens DC (2013) A segmentation protocol and MRI atlas of the C57BL/6J mouse neocortex. Neuroimage 78:196-203.

Ullmann JFP, Watson C, Janke AL, Kurniawan ND, Paxinos G, Reutens DC (2014) An MRI atlas of the mouse basal ganglia. Brain Struct Funct 219:1343-1353.

Upadhyay J, Baker SJ, Chandran P, Miller L, Lee Y, Marek GJ, Sakoglu U, Chin CL, Luo F, Fox GB, Day M (2011a) Default-Mode-Like Network Activation in Awake Rodents. PLoS ONE 6.

Upadhyay J, Baker SJ, Chandran P, Miller L, Lee Y, Marek GJ, Sakoglu U, Chin CL, Luo F, Fox GB, Day M (2011b) Default-mode-like network activation in awake rodents. PLoS ONE 6:e27839.

van den Heuvel M, Mandl R, Hulshoff Pol H (2008) Normalized cut group clustering of resting-state FMRI data. PLoS ONE 3:e2001.

van den Heuvel MP, Pol HEH (2010) Exploring the brain network: A review on resting-state fMRI functional connectivity. Eur Neuropsychopharmacol 20:519-534.

van den Heuvel MP, Sporns O (2013) Network hubs in the human brain. Trends Cogn Sci 17:683-696.

Vann SD, Aggleton JP, Maguire EA (2009) What does the retrosplenial cortex do? Nature Reviews Neuroscience 10:792-U750.

Vincent JL, Patel GH, Fox MD, Snyder AZ, Baker JT, Van Essen DC, Zempel JM, Snyder LH, Corbetta M, Raichle ME (2007) Intrinsic functional architecture in the anaesthetized monkey brain. Nature 447:83-U84.

Virtanen R, Savola JM, Saano V, Nyman L (1988) Characterization of the selectivity, specificity and potency of medetomidine as an alpha 2-adrenoceptor agonist. Eur J Pharmacol 150:9-14.

Wang J, Zuo X, He Y (2010a) Graph-based network analysis of resting-state functional MRI. Front Syst Neurosci 4:16.

Wang J, Zuo X, He Y (2010b) Graph-based network analysis of resting-state functional MRI. Frontiers in Systems Neuroscience 4.

Wang R, Macmillan LB, Fremeau RT, Jr., Magnuson MA, Lindner J, Limbird LE (1996) Expression of alpha 2-adrenergic receptor subtypes in the mouse brain: evaluation of spatial and temporal information imparted by 3 kb of 5' regulatory sequence for the alpha 2A AR-receptor gene in transgenic animals. Neuroscience 74:199-218.

Watson C, Paxinos G, Puelles L (2011) The mouse nervous system. San Diego, United States: Burlington : Elsevier Science.

Watts DJ, Strogatz SH (1998) Collective dynamics of 'small-world' networks. Nature 393:440-442.

Weber R, Ramos-Cabrer P, Wiedermann D, van Camp N, Hoehn M (2006) A fully noninvasive and robust experimental protocol for longitudinal fMRI studies in the rat. Neuroimage 29:1303-1310.

Welvaert M, Rosseel Y (2013) On the definition of signal-to-noise ratio and contrast-to-noise ratio for FMRI data. PLoS ONE 8:e77089.

White NS, Alkire MT (2003) Impaired thalamocortical connectivity in humans during general-anesthetic-induced unconsciousness. Neuroimage 19:402-411.

Williams KA, Magnuson M, Majeed W, LaConte SM, Peltier SJ, Hu XP, Keilholz SD (2010) Comparison of alpha-chloralose, medetomidine and isoflurane anesthesia for functional connectivity mapping in the rat. Magn Reson Imaging 28:995-1003.

Witter MP (2006) Connections of the subiculum of the rat: Topography in relation to columnar and laminar organization. Behav Brain Res 174:251-264.

Wu T, Long XY, Zang YF, Wang L, Hallett M, Li KC, Chan P (2009) Regional Homogeneity Changes in Patients With Parkinson's Disease. Hum Brain Mapp 30:1502-1510.

Xiong JH, Parsons LM, Gao JH, Fox PT (1999) Interregional connectivity to primary motor cortex revealed using MRI resting state images. Hum Brain Mapp 8:151-156.

Xu W, Wilson DA (2012) Odor-evoked activity in the mouse lateral entorhinal cortex. Neuroscience 223:12-20.

Yu Q, Allen EA, Sui J, Arbabshirani MR, Pearlson G, Calhoun VD (2012) Brain connectivity networks in schizophrenia underlying resting state functional magnetic resonance imaging. Curr Top Med Chem 12:2415-2425.

Yuan Y, Zhang Z, Bai F, Yu H, Shi Y, Qian Y, Liu W, You J, Zhang X, Liu Z (2008) Abnormal neural activity in the patients with remitted geriatric depression: a resting-state functional magnetic resonance imaging study. J Affect Disord 111:145-152.

Zang Y, Jiang T, Lu Y, He Y, Tian L (2004) Regional homogeneity approach to fMRI data analysis. Neuroimage 22:394-400.

Zerbi V, Grandjean J, Rudin M, Wenderoth N (2015) Mapping the mouse brain with rs-fMRI: An optimized pipeline for functional network identification. Neuroimage 123:11-21.

Zerbi V, Wiesmann M, Emmerzaal TL, Jansen D, Van Beek M, Mutsaers MP, Beckmann CF, Heerschap A, Kiliaan AJ (2014) Resting-state functional connectivity changes in aging apoE4 and apoE-KO mice. J Neurosci 34:13963-13975.

Zhan Y, Paolicelli RC, Sforazzini F, Weinhard L, Bolasco G, Pagani F, Vyssotski AL, Bifone A, Gozzi A, Ragozzino D, Gross CT (2014) Deficient neuron-microglia signaling results in impaired functional brain connectivity and social behavior. Nat Neurosci 17:400-406.

Zhen ZL, Tian J, Qin W, Zhang H (2007) Partial correlation mapping of brain functional connectivity with resting state fMRI - art. no. 651112. Medical Imaging 2007: Physiology, Function, and Structure from Medical Images 6511:51112-51112.

Zhurakovskaya E, Paasonen J, Shatillo A, Lipponen A, Salo R, Aliev R, Tanila H, Grohn O (2016) Global Functional Connectivity Differences between Sleep-Like States in Urethane Anesthetized Rats Measured by fMRI. PLoS ONE 11.

Zuo XN, Ehmke R, Mennes M, Imperati D, Castellanos FX, Sporns O, Milham MP (2012) Network Centrality in the Human Functional Connectome. Cereb Cortex 22:1862-1875.

Zuo XN, Xu T, Jiang L, Yang Z, Cao XY, He Y, Zang YF, Castellanos FX, Milham MP (2013) Toward reliable characterization of functional homogeneity in the human brain: preprocessing, scan duration, imaging resolution and computational space. Neuroimage 65:374-386.

Appendices

Appendix A Table S1 FIX classification

Number of components

Categories	*Iso1*	*Med0.1*	*Med0.05*	*Mediso*	*Pro30*	*Ure1.5*
Signal	6.45±3.47	12.23±6.43	15.33±3.20	16.75±5.09	6.166±3.12	3.38±3.50
Motion	5.81±1.53	5.53±0.77	7.00±7.37	3.87±1.12	5.16±1.47	6.69±1.70
Vascular	11.09±3.30	4.76±1.48	4.33±1.63	5.62±2.13	6.83±1.16	8.69±1.93
Acquisition	9.90±5.33	9.15±4.68	4.16±6.04	4.12±3.09	9.00±4.56	8.07±4.76
Outside	5.36±2.46	10.30±3.61	6.33±9.07	1.12±1.35	2.66±1.63	2.00±2.04
Unclassified	46.18±14.32	38.69±10.20	67.66±21.46	82.87±13.53	92.83±10.41	91.23±14.82

Classified as signal

Categories	*Iso1*	*Med0.1*	*Med0.05*	*Mediso*	*Pro30*	*Ure1.5*
Signal	100.00±0.00	97.87±4.11	100.00±0.00	98.36±3.17	100.00±0.00	96.36±8.44
Motion	0.00±0.00	1.09±3.96	0.00±0.00	0.00±0.00	3.08±5.10	3.73±7.76
Vascular	7.84±13.69	5.00±12.58	16.66±27.88	6.25±17.67	2.08±5.10	5.30±7.18
Acquisition	13.26±20.54	24.42±33.94	20.00±44.72	34.16±39.91	18.05±19.83	14.33±27.86
Outside	87.04±19.47	93.13±14.26	100.00±0.00	100.00±0.00	93.33±16.32	91.11±26.66
Unclassified	96.56±6.00	96.51±4.33	99.32±2.56	98.04±3.01	98.54±1.90	96.93±6.76

Classified as noise

Categories	*Iso1*	*Med0.1*	*Med0.05*	*Mediso*	*Pro30*	*Ure1.5*
Signal	0.00±0.00	0.00±0.00	0.00±0.00	0.00±0.00	0.00±0.00	0.00±0.00
Motion	98.98±3.35	97.80±7.92	100.00±0.00	91.87±11.31	93.75±15.30	93.58±11.71
Vascular	78.91±16.97	82.17±30.10	66.66±51.63	77.60±35.70	97.91±5.10	82.57±26.08
Acquisition	66.23±40.20	62.68±36.46	74.75±42.57	50.00±42.01	59.25±35.03	56.33±39.71
Outside	5.05±11.50	0.48±1.73	0.00±0.00	0.00±0.00	0.00±0.00	6.66±20.00
Unclassified	1.17±1.82	0.46±1.15	0.17±0.45	0.78±1.12	0.35±0.54	0.52±1.34

Classified as unknown

	Iso1	*Med0.1*	*Med0.05*	*Mediso*	*Pro30*	*Ure1.5*
Signal	0.00±0.00	2.12±4.11	0.00±0.00	1.63±3.17	0.00±0.00	3.70±8.44
Motion	1.01±3.35	1.09±3.96	0.00±0.00	8.12±11.31	4.16±10.20	2.67±5.08
Vascular	13.23±11.10	12.82±27.97	16.66±27.88	16.14±21.87	0.00±0.00	12.12±27.34
Acquisition	20.49±26.33	12.88±14.34	5.25±8.67	15.83±17.79	22.68±15.72	29.32±34.87
Outside	7.90±13.65	6.38±12.70	0.00±0.00	0.00±0.00	6.66±16.32	2.22±6.66
Unclassified	1.37±3.10	3.01±3.58	1.04±1.35	1.17±1.98	1.10±1.40	2.53±5.48

Independent component extracted using Melodic were classified using FIX and compared to hand classification. Components were manually sorted into 'signal' for components with a plausible BOLD origin, 'motion' for movement-related artefacts, 'vascular' for components overlapping with major blood vessels, 'acquisition' for acquisition related artefact such as spikes, 'outside' for components principally found in tissues outside the brain, and 'unclassified' for ambiguous components.

Appendix B Unthresholded group-mean ReHo maps

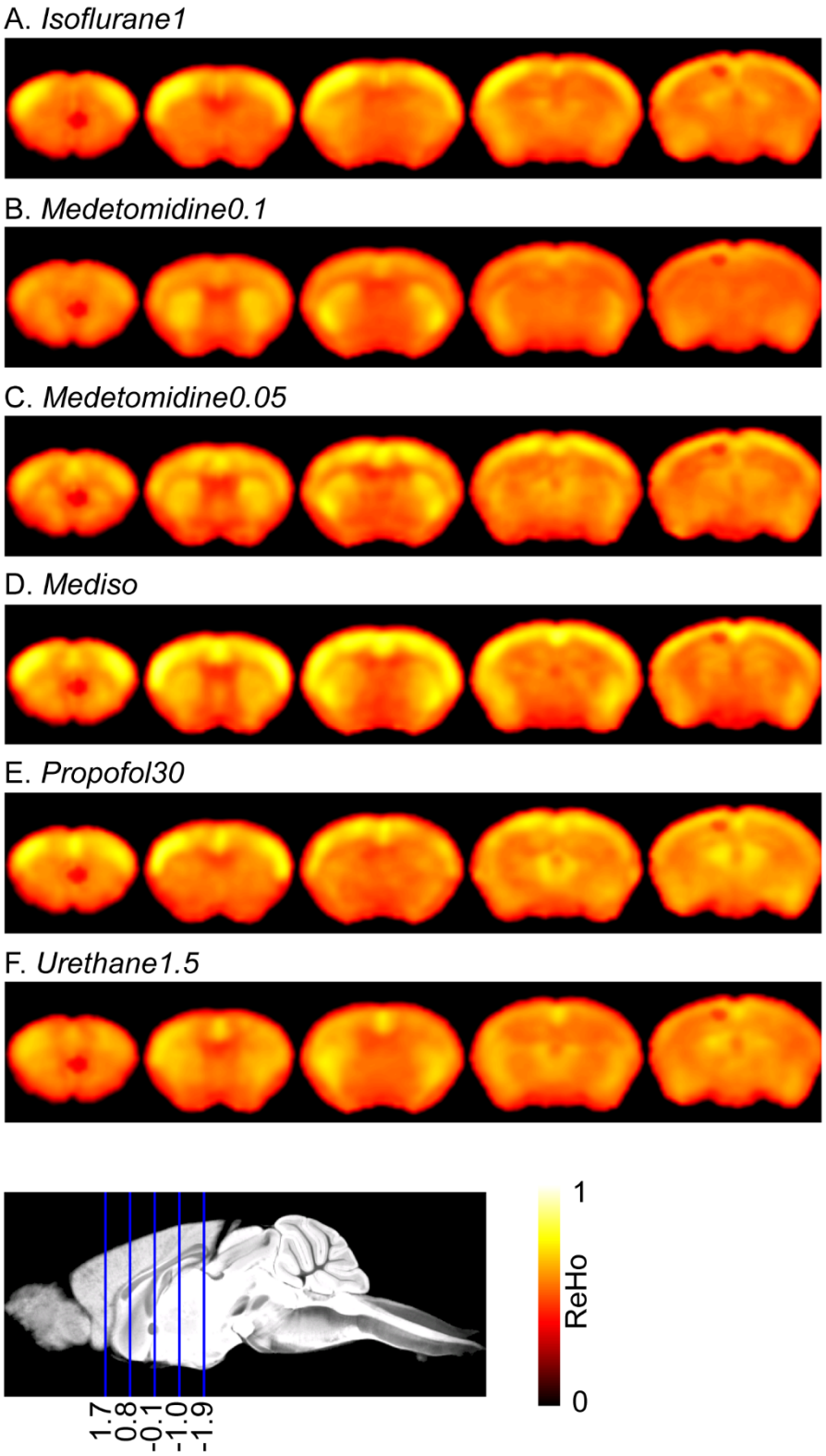

Unthresholded group-mean maps overlaid onto five representative coronal slices showing the distribution of ReHo values in each group. (A) *Isoflurane1*. (B) *Medetomidine0.1*. (C) *Medetomidine0.05*. (D) *Mediso*. (E) *Propofol30*. (F) *Urethane1.5*. ReHo values are colour coded from 0 to 1 as shown in the colour bar. Sagittal image on the bottom indicates the position of the coronal slices indicated by blue lines with values representing the position relative to Bregma in mm.

Appendix C Average ReHo values were extracted from left and right caudate-putamen and barrel field sensory cortex

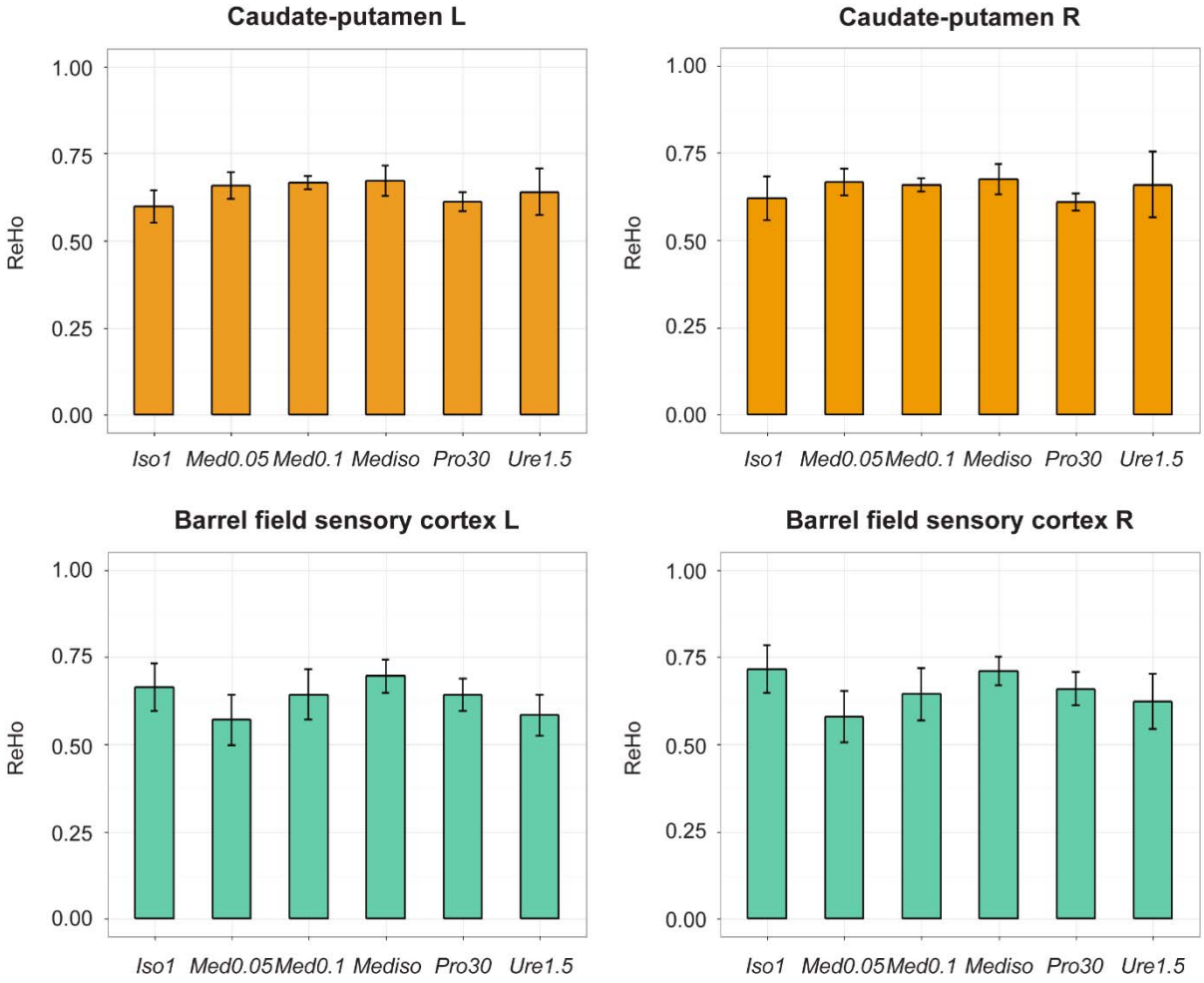

Average ReHo values were extracted from left and right caudate-putamen and barrel field sensory cortex. Bar plots and error bars indicate the mean ReHo across animals ± 1 standard deviation (SD). The distributions of the strength of the local connectivity across regimens in the left caudate-putamen are very similar to the strength distributions in the right caudate-putamen. This bilateral distribution of local connectivity strength is also observed in the barrel field sensory cortex. These results suggest that the same anaesthetic effects are presented in both hemispheres. The group labels on the bottom of each bar plot are: *Isoflurane1* (*Iso1*), *Medetomidine0.05* (*Med0.05*), *Medetomidine0.1* (*Med0.1*), *Mediso* (*Mediso*), *Propofol30* (*Pro30*), *Urethane1.5* (*Ure1.5*). L: left. R: right. Animal numbers for each group were 11 in *Isoflurane1*, 6 in *Medetomidine0.05*, 13 in *Medetomidine0.1*, 8 in *Mediso*, 6 in *Propofol30*, 13 in *Urethane1.*5.

Appendix D Global network parameters using GVR data at threshold p=0.0001 revealed significant differences between *Medetomidine0.1* and *Mediso* in small-worldness and gamma (normalized clustering coefficient)

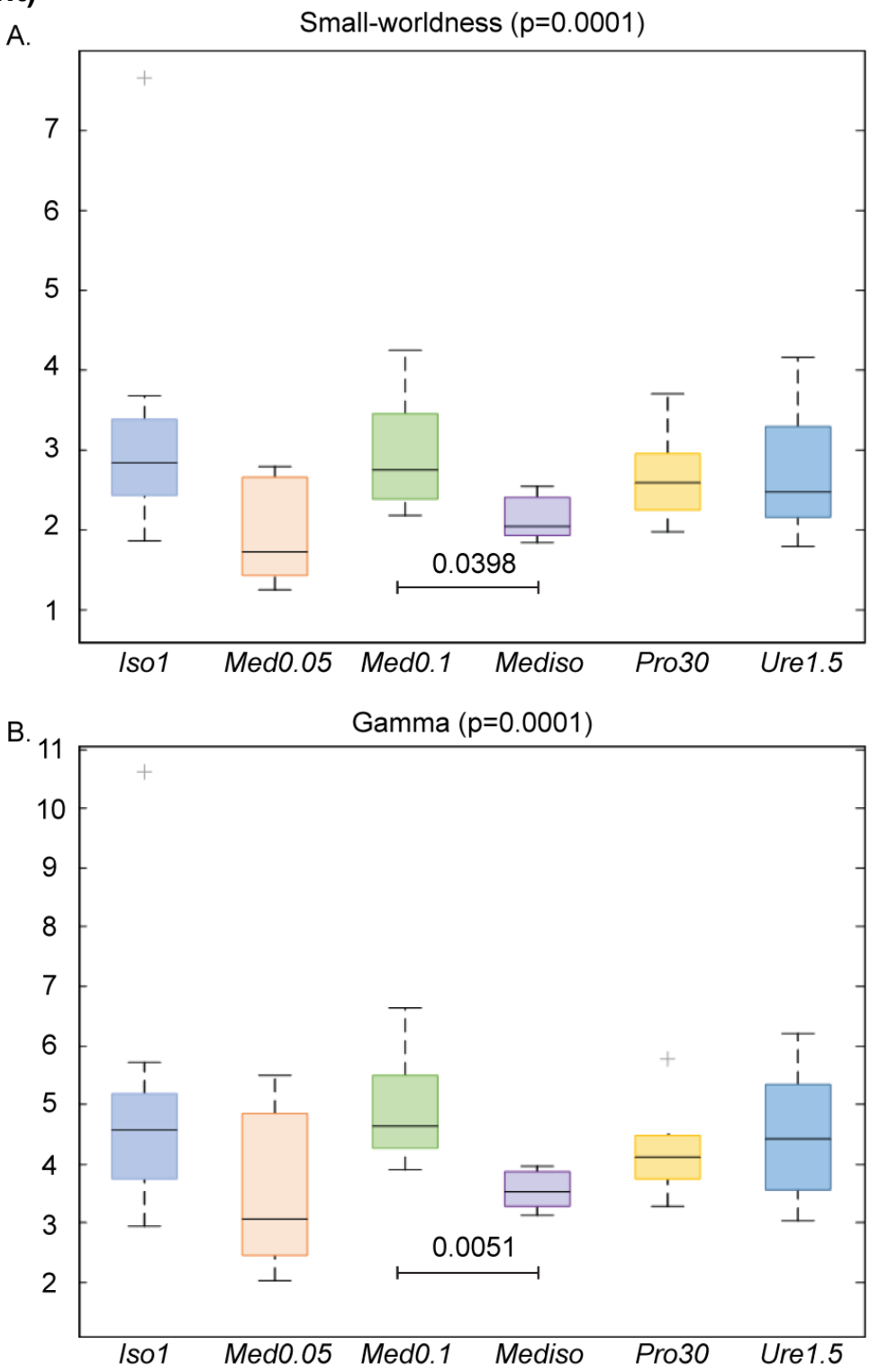

Small-worldness and normalized clustering coefficient measures for mouse functional networks under different anaesthesia protocols at threshold p=0.0001. Each horizontal line and above number represent the p-value of a post hoc Wilcoxon test, with FDR correction. (A) Boxplots showing median, interquartile range and range for small-worldness. There was significant difference between *Medetomidine0.1* and *Mediso*. (B) Boxplots showing median, interquartile range and range for the normalized clutering coefficient (gamma). There was

significant difference between *Medetomidine0.1* and *Mediso*. *Iso1*: *Isoflurane1*. *Med0.05*: *Medetomidine0.05*. *Med0.1*: *Medetomidine0.1*. *Pro30*: *Propofol30*. *Ure1.5*: *Urethane1.5*.

Appendix E Modularity Q and VI of functional brain networks and their corresponding null-networks in mice using GVR data

Table E-1 Modularity Q of each group and its corresponding null network calculated from GVR data, averaged over all degenerate partitions.

Anaesthesia regimens	Modularity Q of each group (mean ± std)	Modularity Q of the corresponding null networks (mean ± std)
Isoflurane1	0.5934±0.0029	0.2048±0.0037
Medetomidine0.1	0.6290±0.0047	0.2242±0.0044
Medetomidine0.05	0.5531±0.0018	0.1773±0.0031
Mediso	0.6330±0.0024	0.2039±0.0027
Proprofol30	0.6490±0.0002	0.2005±0.0036
Urethrane1.5	0.6119± 0.0045	0.2145±0.0038

Table E-2 Distance (VI) between degenerate partitions of each empirical network and their corresponding null networks

Anaesthesia regimens	VI of distinct degenerate partitions of each network (mean ± std)	VI of distinct degenerate partitions of the corresponding null networks (mean ± std)
Isoflurane1	0.1267±0.0598	0.4055±0.0670
Medetomidine0.1	0.1265±0.0550	0.3887±0.0623
Medetomidine0.05	0.1536±0.0623	0.4591±0.0629
Mediso	0.0558±0.0261	0.3927±0.0720
Proprofol30	0.0557±0.0290	0.4454±0.0676
Urethrane1.5	0.1506±0.0566	0.4215±0.0642

Appendix F Measures of global topology using VR data

Brain networks constructed from VR data did not show small-world property at both thresholds (mean $\bar{\sigma}^w$ ± std.: 0.94±0.02, values calculated at p=0.0001 were 0.93±0.02). Normalized clustering coefficients were not significantly greater than 1 (mean $\bar{\gamma}^w$ ± std: 1.01±0.01) indicating that the highly clustered structures were not prevalence compared to random networks. Normalized shortest path length was around 1 (mean $\bar{\lambda}^w$ ± std: 1.08± 0.03). No significant between-group differences were detected in the other global parameters. Calculation at threshold p=0.0001 revealed similar results, therefore data were not shown.

Appendix G Module organizations revealed in VR data

Different modular structures were revealed by analysis on data without global signal regression, indicating the influence of GSR on community detection. The average Q over discovered degenerate partitions from empirical networks (mean Q ± std.: 0.0482±0.0078, averaged over the mean Q values of six groups) were significantly higher than the averaged Q of the degenerate partitions of null networks (mean Q ± std.: 0.0105±0.0022, paired t-test: $p = 1.759 \times 10^{-5}$). The averaged VI of six empirical network (mean VI ± std.: 0.1206±0.0214) was significantly lower than the corresponding VI of the null-networks (mean Q ± std.: 0.4543±0.0241, paired t-test: $p = 4.8227 \times 10^{-7}$). The Q and VI calculated from VR data suggest strong modular structures within the functional network in mice. The Q and VI values of each group were presented in Appendix H.

Three functional modules were detected in the *Isoflurane1* group. The salience-like and brain-stem module with connections to retrosplenial cortex as well as hippocampus were both observed. The third module contained nodes from LCN and DMN-like modules discovered under isoflurane using GVR data. Three modules were also observed in *Medetomidine0.1* group, including a DMN-like module extending to small portions of striatum, a brain-stem module and one large module consisting of nodes from the salience-like and LCN modules discovered under this regimen in GVR data. Similar to *Medetomidine0.1*, the DMN-like and brain-stem modules were detected in *Mediso* group. One large module contained nodes from salience-like and LCN modules was revealed. But another module under *Mediso* included nodes within prefrontal cortex, some parts of striatum and pallidum. In *Propofol30* group, similar community structures were discovered to those observed using GVR data. Modular organizations in *Medetomidine0.05* group revealed by data without GSR were different from those detected in the same group in the GVR data. In *Urethane1.5*, four modules were discovered. The DMN-like and brain-stem modules were observed, which was consistent with the result from GVR analysis. The large module containing nodes from salience-like and LCN modules under this regimen using GVR data, however, was split into two communities. One community included the prefrontal cortex regions and subcortical regions containing some parts of amygdala, striatum and pallidum, which was similar to the prefrontal-cerebral nuclei (striatum and pallidum) module observed under *Mediso*. The other community contained the rest of the nodes within the merged salience-like and LCN modules. The detailed brain regions involved in functional module organizations of each group were listed in Table G-1 to G-6.

Table G-1 Brain regions in the detected modules in *Isoflurane1* group.

Modules in *Isoflurane1* group	Brain region in each module
Salience-like module	Agranular insular areas, anterior cingulate areas, prelimbic areas, orbital areas, olfactory area, infralimbic areas, piriform cortex, claustrum, endopiriform nucleus, amygdala, striatum, pallidum, perirhinal areas, ectorhinal areas, entorhinal areas
Module 2	Posterior parietal association areas, temporal association areas, visceral areas, primary and supplemental somatosensory areas, gustatory areas, visual areas, somatomotor areas, auditory areas
Brain-stem like module	Retrosplenial areas, hippocampus, thalamus, hypothalamus, midbrain, pons

Table G-2 Brain regions in the detected modules in *Medetomidine0.1* group.

Modules in *Medetomidine0.1* group	Brain region in each module
M1	Agranular insular areas, orbital areas, olfactory area, infralimbic areas, piriform cortex, claustrum, endopiriform nucleus, amygdala, striatum, pallidum, visceral areas, primary and supplemental somatosensory areas, gustatory areas
DMN-like module	Posterior parietal association areas, primary somatosensory areas, temporal association areas, visual areas, anterior cingulate areas, retrosplenial areas, perirhinal areas, somatomotor areas, ectorhinal areas, auditory areas, hippocampus, small portions of amygdala, small portions of striatum
Brain-stem module	Thalamus, hypothalamus, midbrain, pons, prelimbic area

Table G-3 Brain regions in the detected modules in *Mediso* group.

Modules in *Mediso* group	Brain region in each module
M1	Agranular insular areas, piriform cortex, claustrum, endopiriform nucleus, amygdala, some parts of striatum, visceral areas, primary and supplemental somatosensory areas, gustatory areas,
DMN-like module	Posterior parietal association areas, primary somatosensory areas, temporal association areas, visual areas, anterior cingulate areas, retrosplenial areas, perirhinal areas, somatomotor areas, ectorhinal areas, auditory areas, entorhinal areas
M3	Prelimbic areas, orbital areas, olfactory area, infralimbic areas, some parts of striatum (nucleus accumbens, olfactory tubercle), pallidum
Brain-stem like module	Thalamus, hypothalamus, midbrain, pons, hippocampus, small portions of amygdala, small portions of striatum

Table G-4 Brain regions in the detected modules in *Pro30* group.

Modules in *Pro30* group	Brain region in each module
Salience-like module	Agranular insular areas, anterior cingulate area, prelimbic area, orbital area, olfactory area, infralimbic area, claustrum, endopiriform nucleus, striatum, pallidum

Lateral cortical module	visceral areas, primary and supplemental somatosensory areas, gustatory areas
DMN-like module	Posterior parietal association areas, primary somatosensory areas, temporal association areas, visual areas, retrosplenial areas, perirhinal areas, somatomotor areas, ectorhinal areas, auditory areas, entorhinal areas, hippocampus, piriform cortex, amygdalar
Brain-stem module	Thalamus, hypothalamus, midbrain, pons

Table G-5 Brain regions in the detected modules in *Medetomidine0.05* group.

Modules in *Medetomidine0.05* group	Brain region in each module
M1	Agranular insular areas, anterior cingulate areas, prelimbic areas, orbital areas, olfactory area, infralimbic areas, hippocampus (Field CA2, entorhinal areas), piriform cortex, claustrum, endopiriform nucleus, amygdala, striatum, pallidum, hypothalamus, small portions of midbrain (lateral terminal nucleus of the accessory optic tract)
M2	Posterior parietal association areas, temporal association areas, visual areas, somatomotor areas, perirhinal area, ectorhinal areas, auditory areas perirhinal areas, visceral areas, primary and supplemental somatosensory areas, gustatory area,
M3	Thalamus, midbrain, pons, retrosplenial areas, hippocampus, posterior amygdalar nucleus

Table G-6 Brain regions in the detected modules in *Ure1.5* group.

Modules in *Ure1.5* group	Brain region in each module
M1	Agranular insular areas, anterior cingulate areas, prelimbic areas, orbital area, claustrum, endopiriform nucleus, some parts of amygdala, some parts of striatum, visceral areas, primary and supplemental somatosensory areas, gustatory areas
DMN-like module	Posterior parietal association areas, primary somatosensory areas, temporal association areas, visual areas, retrosplenial areas, perirhinal areas, ectorhinal areas, auditory areas, hippocampus, entorhinal area
M3	Olfactory area, infralimbic areas, piriform cortex L, some parts of amygdala, striatum, pallidum
Brain-stem module	Thalamus, hypothalamus, midbrain, pons

Appendix H Modularity Q and VI of functional brain networks and their corresponding null-networks in mice using VR data

Table H-1 Modularity Q of each group and its corresponding null network calculated from VR data, averaged over all degenerate partitions.

Anaesthesia agents	Modularity Q of each group (mean ± std)	Modularity Q of the corresponding null networks (mean ± std)

Isoflurane1	0.0530±0.0005	0.0114±0.0006
Medetomidine0.1	0.0370±0.0004	0.0079±0.0004
Medetomidine0.05	0.0583±0.0007	0.0131±0.0005
Mediso	0.0495±0.0003	0.0105±0.0005
Proprofol30	0.0505±0.0003	0.0122±0.0004
Urethrane1.5	0.0412±0.0001	0.0080±0.0004

Table H-2 Distance (VI) between degenerate partitions of each empirical network and their corresponding null networks calculated from VR data

Anaesthesia agents	VI of distinct degenerate partitions of each network (mean ± std)	VI of distinct degenerate partitions of the corresponding null networks (mean ± std)
Isoflurane1	0.1187±0.0602	0.4766±0.0586
Medetomidine0.1	0.1368±0.0567	0.4432±0.0614
Medetomidine0.05	0.1294±0.0497	0.4884±0.0514
Mediso	0.1142±0.0502	0.4279±0.0664
Proprofol30	0.0824±0.0405	0.4337±0.0579
Urethrane1.5	0.1419±0.0619	0.4558±0.0546

Appendix I RSNs shared by Tg and Wt groups detected by ICA using MV data

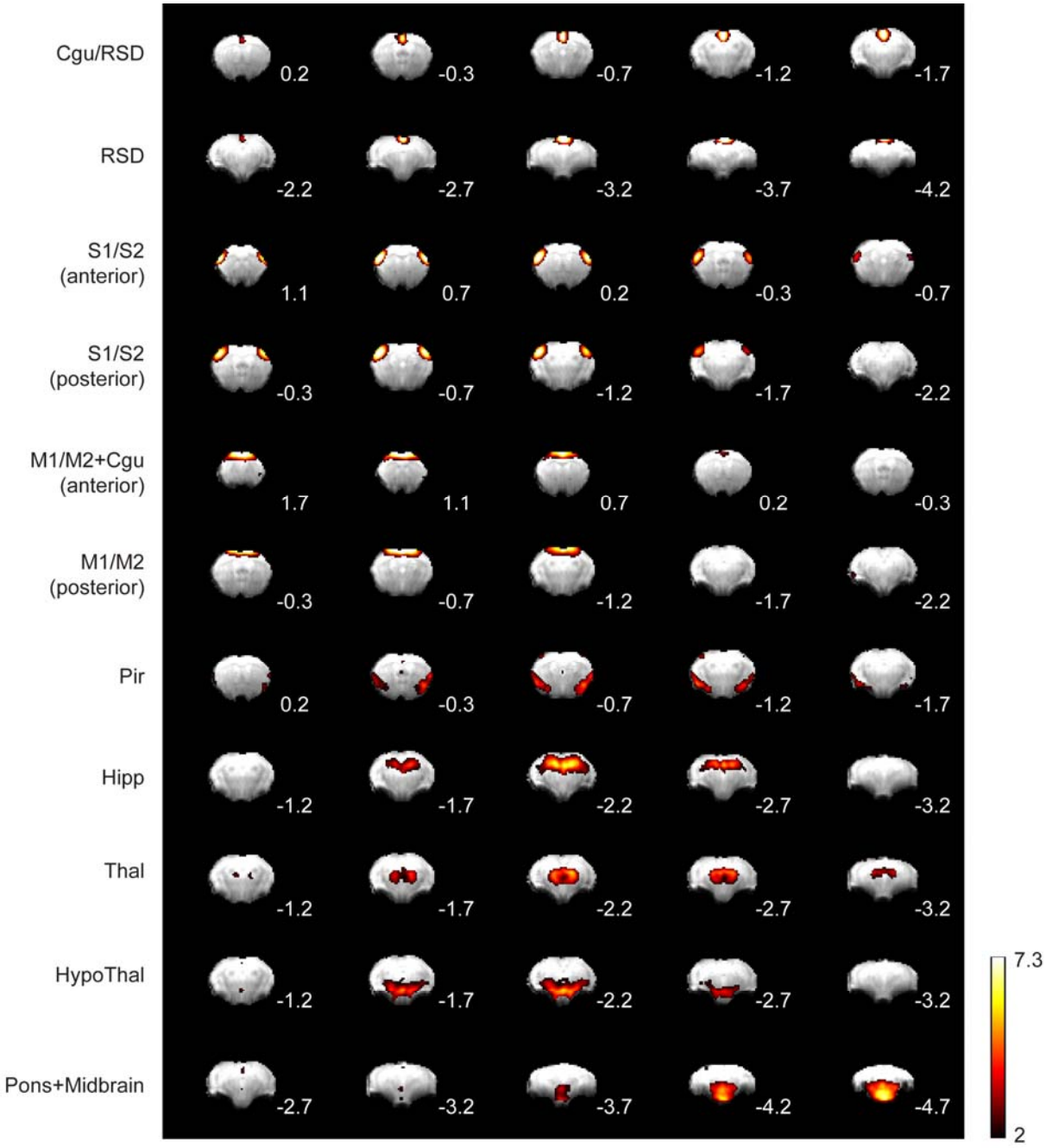

The combined ICA and separate ICA approaches revealed highly consistent RSNs in both Tg and Wt groups using MV data. Eleven RSNs detected by the combined ICA approach are shown. Each row showed the representative coronal slices of one identified component, with distinct pattern and clear anatomical confinement. This is in agreement with segregated functional systems of the mouse brain. Corresponding RSN names are listed on the left side. Image overlays indicate $|Z| > 2$ (equivalent to $p<0.05$, uncorrected). These results are very similar to functional clusters thresholded at p<=0.05 (FWE-corrected) for one-sample t-test (data not shown). Colour bar shows the range of values in the maps. Distances (mm) relative to bregma are shown on the right bottom of each coronal slice. Cgu/RSD: cingulate/retrosplenial cortex. RSD: retrosplenial cortex. S1/S2: primary/secondary somatosensory cortex. M1/M2: primary/secondary motor cortex. Pir: piriform cortex. Hipp: hippocampus. Thal: thalamus. HypoThal: hypothalamus.

Appendix J Brain regions yielded statistically significant between-group results in nodal clustering coefficient and nodal global efficiency in MVG data

Connection density (%)	Nodal global efficiency	Nodal clustering coefficient
5	Nucleus accumbens R (Tg<Wt)	-
10	-	-
15	Inferior colliculus L (Tg<Wt)	-
20	Lateral septal complex R (Tg<Wt) Hypothalamus R (Tg<Wt) Inferior colliculus L (Tg<Wt)	-
25	Hypothalamus R (Tg<Wt) Inferior colliculus L (Tg<Wt)	-
30	Hypothalamus R (Tg<Wt) Inferior colliculus L (Tg<Wt) Trochlear nucleus L (Tg<Wt)	-
35	Nucleus of the brachium of the inferior colliculus L (Tg>Wt)	-
40	Hypothalamus R (Tg<Wt)	-

The symbol “>” and “<” represent stronger and weaker than, respectively. L: left. R: right.

Appendix K Global network attributes of the functional brain network in *DISC1* mice using MV data.

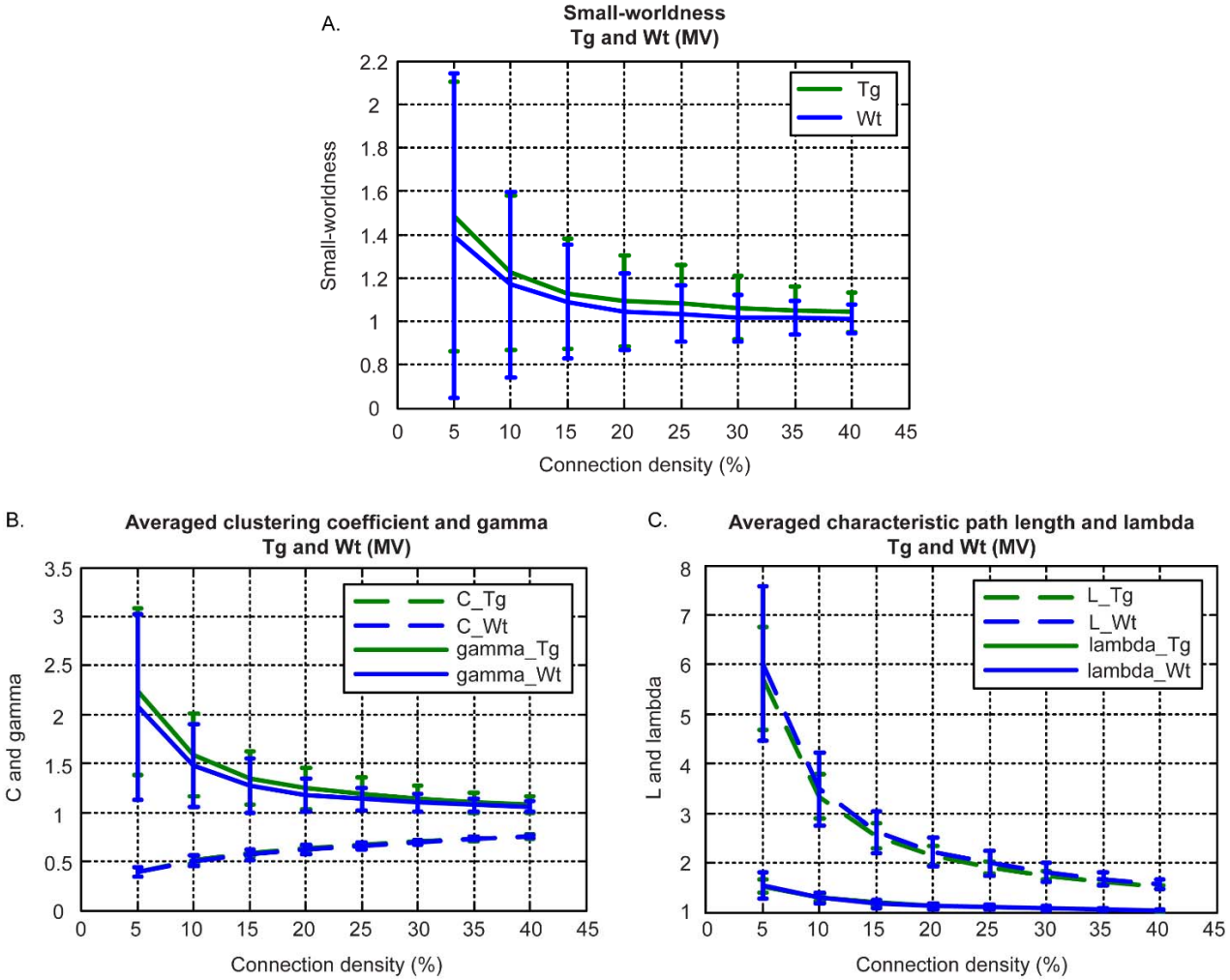

Global network attributes of the functional brain network in mice revealed in MV data. No statistically significant between-group differences were found in the five measurements. (A) Small-worldness. Both Tg and Wt mice showed small-world property under sparse connection densities. σ started to approach 1 at higher connection densities. No statistically significant differences were observed (p=0.73±0.05, mean±std. across all connection densities) (B) Averaged clustering coefficient and the normalized clustering coefficient (gamma). No significant differences were detected (p=0.66±0.21 and p=0.51±0.10, respectively). (C) Averaged shortest path length and the normalized characteristic path length (lambda). No significant differences were detected (p=0.41±0.19 and p=0.60±0.24, respectively). All results were averaged over each group and error bars represent standard deviation.

Appendix L Modules detected in the Tg group using MV data

Modules	Brain regions within each module
Module 1	Agranular insular areas, anterior cingulate areas, prelimbic areas, orbital area, olfactory area, infralimbic area, somatomotor area, entorhinal area, piriform cortex, claustrum, endopiriform nucleus, striatum, pallidum, visceral areas, primary and supplemental somatosensory area, gustatory area

Module 2	Posterior parietal association areas, primary somatosensory area (unassigned), temporal association areas, perirhinal area, ectorhinal area, auditory area, hippocampus, amygdala, striatum-like amygdala nuclei, thalamus, hypothalamus, some parts of midbrain
Module 3	Visual area, retrosplenial area, retrohippocampal region (except for subiculum), midbrain, pons

Appendix M Modules detected in the Wt group using MV data

Modules	Brain regions within each module
Module 1	Agranular insular areas, anterior cingulate areas, prelimbic areas, orbital area, olfactory area, infralimbic area, perirhinal area L, somatomotor area, entorhinal area, ectorhinal area L, piriform cortex, claustrum, endopiriform nucleus, amygdalar, striatum, pallidum, visceral areas, primary and supplemental somatosensory area, gustatory area
Module 2	Posterior parietal association areas, primary somatosensory area (unassigned), temporal association areas, visual areas, retrosplenial area, perirhinal area R, ectorhinal area R, auditory area, hippocampus, thalamus, hypothalamus, pretectal region of the midbrain
Module 3	retrohippocampal region (except for subiculum), posterior amygdalar nucleus R, midbrain, pons